Deciphering the pneumococcal cell cycle

Gallay, Clément

DOI:
10.33612/diss.127737312

Deciphering the pneumococcal cell cycle

Identification and characterization of new genes involved in growth and replication

Clément Gallay

Deciphering the pneumococcal cell cycle

Identification and characterization of new genes involved in growth and replication

The research presented in this thesis was carried out in the laboratory of Molecular Genetics of the Groningen Biomolecular and Biotechnology Institute (GBB), Faculty of Science and Engineering, University of Groningen, The Netherlands and in the laboratory of Systems and Synthetic Microbiology of the Department of Fundamental Microbiology (DMF), Faculty of Biology and Medicine, University of Lausanne, Switzerland.

Printing of this thesis was financially supported by the Groningen Graduate School of Science and the University of Groningen.

Printed by Ridderprint BV, the Netherlands

Cover designed by Matheus Guimarães da Silva (impactamidia.ch)

ISBN (book): 978-94-034-2745-4
ISBN (ebook): 978-94-034-2746-1

university of groningen

Deciphering the pneumococcal cell cycle

Identification and characterization of new genes
involved in growth and replication

PhD thesis

to obtain the degree of PhD at the
University of Groningen
on the authority of the
Rector Magnificus Prof. C. Wijmenga
and in accordance with
the decision by the College of Deans.

This thesis will be defended in public on

Friday 26 June 2020 at 14.30 hours

by

Clément François Jean Gallay

born on 20 February 1990
in Lyon, France

Supervisors

Prof. J.-W. Veening
Prof. O.P. Kuipers

Assessment Committee

Prof. T. den Blaauwen
Prof. D.-J. Scheffers
Prof. P. Viollier

Table of Contents

GENERAL INTRODUCTION

Humans easily adopt an anthropocentric view of the world (Arenson and Coley, 2018) and tend to forget that, in numbers, bacteria clearly dominate our planet. Bacteria are everywhere, it is even estimated that our body contains as many bacteria as human cells (Sender *et al*., 2016). Despite their importance, a PubMed (NCBI) search for "bacteria" returned approximately 2.2 million publications over the last 100 years, while a "cancer" query returned nearly 5.2 million publications. Our modern view of cell biology, which established the basis for cancer immunology research, originates from early works on bacteria. The notion of the bacterial cell cycle therefore emerged a long time ago and it is important to place all events in time so that we may have a deeper understanding of it (Fig. 1).

A very brief history of the cell (cycle)

The first description of cells was made by Robert Hooke in 1665 when observing "dead" cells, forming the structure of cork. A few years later, in 1674, Antonie van Leeuwenhoek observed the first living cells as he discovered microbes, presumably bacteria. In 1838, Matthias Schleiden and Theodore Schwann stated that cells are part of the living (leading to the cell theory). Although Hugo von Mohl proposed in 1846 from his observations that new cells generate from division, the well-established theory at the time was still that microorganisms arise by spontaneous generation. In the late 1850s, Louis Pasteur advanced the germ theory of disease (based on Schwann's previous work), implying that microbes do not appear spontaneously.

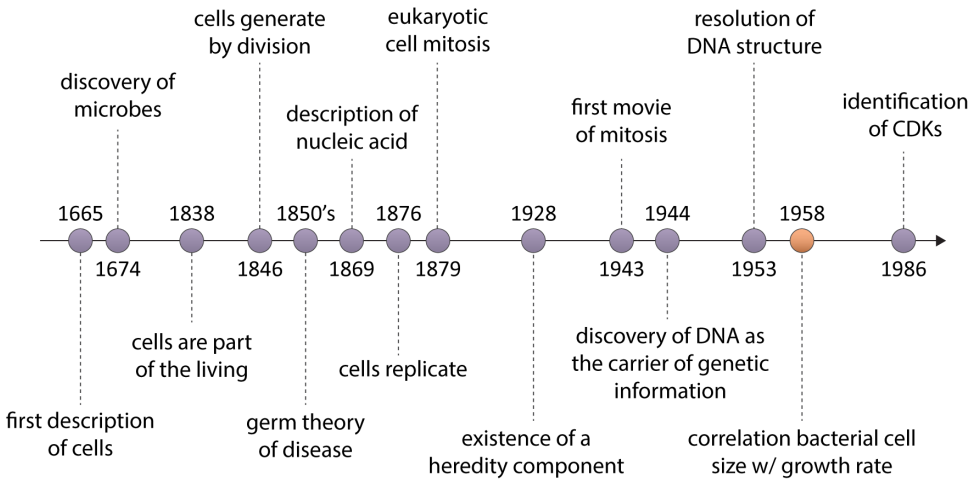

Figure 1. Timeline of the main discoveries about cell cycle.

However, Pasteur could never prove his theory. It is only in 1876 that Robert Koch could cultivate *Bacillus anthracis* and therefore postulate that microorganisms can cause disease after being grown in laboratory and injected to animals, proving Pasteur's assumptions (This is refered as Koch's postulates). Cells are therefore not arising from lifeless matter but are instead replicating from a mother cell. In 1879, Walter Flemming described for the first time the eukaryotic cell mitosis (that was filmed using time-lapse phase contrast microscopy only in 1943). Although at the time it was obvious that cell division occurs, it was not known what type of molecule was shared between daughter cells and what the heredity factor was. While trying to identify the fundamental components of leukocytes, Friedrich Miescher isolated a compound from the nucleus in 1869 (Dahm, 2008), but could not determine its composition (he assumed it was used as phosphate storage). It was only 50 years later, in 1928, that Frederick Griffith demonstrated through his well-renowned experiment, the existence of a chemical component that could transform one non-virulent *Streptococcus pneumoniae* strain into a virulent one. But it was later in 1944 that Avery, MacLeod and McCarty (Avery *et al*., 1944) discovered that DNA was responsible for transformation, and not proteins (Hershey and Chase, 1952). Elucidation of the molecular structure of DNA by Rosalind Franklin and Maurice Wilkins, and at the same time by James Watson and Francis Crick, in 1953 finally provided advanced information about how genetic information is carried between cells. Using that knowledge, Alma Howard and Stephen Pelc could propose in 1953 the existence of four distinct periods in the eukaryotic cell cycle: cell division, cell growth (G1), DNA replication (S) and a second cell growth (G2) (Dubrovsky and Ivanov, 2003). Not only we knew that cells were able to divide, but there was evidence that cells are following a precise cycle. In 1986, Russell and Nurse identified the cyclin-dependent kinases (CDK) that were able to tightly control the cell cycle (Russell and Nurse, 1986).

Mechanisms of bacterial DNA replication control

The main goal for a cell is to become two cells. To do this, cells need to duplicate their genetic material. Eukaryotic cells contain several chromosomes (*e.g.* 14 chromosomes for *Saccharomyces cerevisiae*, 46 for *Homo sapiens*, *etc*.). Bacteria can contain from one to a few chromosomes and each of them carries at least a single origin of replication (*oriC*). This origin contains specific DNA sequences that can be targeted specifically, with variable affinities, by the replication initiator protein DnaA (Katayama *et al*., 2010; Mott and Berger, 2007). DnaA is an AAA+ ATPase, like some proteins from the eukaryotic origin-recognition complex (ORC), which is responsible for recruitment of the different replisome proteins and for DNA strand opening to

initiate the bacterial cell cycle (Fuller *et al.*, 1984; Skarstad and Katayama, 2013). DnaA is composed of four distinct domains: domain I can bind the helicase responsible for DNA strand opening; domain II is a linker; domain III forms the ATPase domain; and domain IV is the DNA binding domain responsible for *oriC* recognition via three specific elements, a DnaA signature sequence targeting DnaA boxes, a "basic loop" crucial for DNA binding and the so-called DnaA-trio (Fig. 2a) (Blaesing *et al.*, 2002; Richardson *et al.*, 2016). DnaA can bind both ATP and ADP and the binding influences whether it will bind low- or high-affinity sites at *oriC*. ATP binding was also shown to facilitate DnaA oligomerization at the origin. Once DnaA is bound to the DnaA-boxes at *oriC*, it will recruit the helicase DnaB (Fig. 2b), which will be loaded by DnaC (both proteins named respectively DnaC and DnaI in *B. subtilis*). Later, the primase

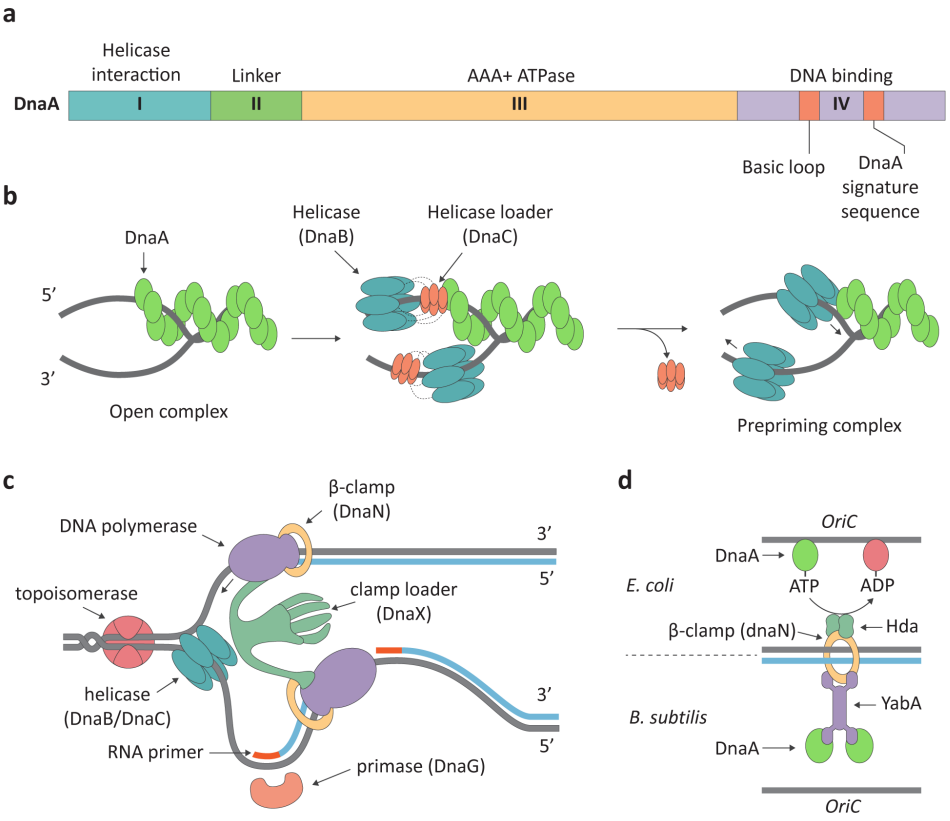

Figure 2. DNA replication control in bacteria.

(**a**) schematic representation of the DNA regulator protein DnaA, indicating the 4 domains I to IV. (**b**) initiation of DNA replication; DnaA proteins (green) can bind regions near the origin of replication, where it recruits the helicase DnaB, assisted by DnaC; once the complex is formed, DnaC is released and the different proteins of the replisome (**c**) can assemble. (**d**) in *E. coli* (up), the main replication regulation is exerted by HdA, promoting dissociation of ATP to ADP, thus reducing the pool of ATP needed by DnaA to be active; and in *B. subtilis* (down), YabA sequesters DnaA away from *oriC*. (a) and (b) adapted from Katayama *et al.* 2010.

DnaG and the polymerase β-clamp DnaN are recruited (also additionally DnaD and DnaB for *B. subtilis*), and eventually all the other proteins of the replication machinery (Fig. 2c) (Jameson and Wilkinson, 2017). The replication machinery mechanism works as follows: as the topoisomerase relaxes DNA supercoils, the helicase separates the double stranded DNA (dsDNA) while the primase adds small RNA primers that are recognized by a DNA polymerase, which is held onto the DNA by the β-clamp DnaN, and stabilized by a clamp loader (composed of different sub-units, including DnaX). A new strand will be created in both directions (always in 5′ to 3′ direction) opposite of *oriC* until the replisome reaches the terminus region, where replication stops, or until two replication forks meet each other.

Several regulatory systems controlling DNA replication initiation exist (Fig. 2d). In *E. coli*, four major mechanisms are present to reduce DnaA activity. 1) origin sequestration by SeqA binding to the newly synthesized hemi-methylated *oriC* sequence (Lu *et al*., 1994); 2) reduction of DnaA expression by a negative feedback loop; 3) titration of DnaA by replication of the *datA* locus that can bind with high affinity DnaA proteins; and 4) regulatory inactivation of DnaA system (RIDA). The latter system is the major mechanism of initiation control in *E. coli*. It is mediated by the protein Hda (DnaA paralog) able to bind the loaded β-clamp. Interaction of Hda with ATP-DnaA promotes ATP hydrolysis, therefore leading to accumulation of inactive ADP-DnaA (Fig. 2d up). The only conserved mechanism in *B. subtilis* is the DnaA negative feedback loop. However, it also uses other strategies such as: 1) *oriC* binding by SirA in sporulating cells; 2) binding of Soj (ParA) to DnaA complexed to *oriC*; and 3) DnaA sequestration and oligomerization prevention by YabA. Although YabA and *E. coli* Hda do not share sequence similarity, they are considered functional homologs. Indeed, YabA will exert its control on DnaA by binding both DnaA and the β-clamp DnaN, therefore limiting the number of DnaA molecules available at the origin, thus providing a control of DNA replication initiation linked to replication progression (Fig. 2d down).

Under ideal conditions, replication occurs without interruptions. Yet, it is frequent for the replication complex to be prematurely ejected from the replication site. The replication machinery therefore needs to be reassembled in the absence of specific recognition sequences such as *oriC*. To do so, bacteria use "DNA replication restart" pathways able to recognize specific DNA structures of the stalled replication fork (Windgassen *et al*., 2018a). The helicase PriA is the principle component of this complex as it can recognize specific structures of the DNA replication forks and interact with DNA in complex with ssDNA-binding proteins (SSBs) to further recruit the replication helicase (*E. coli* DnaB / *B. subtilis* DnaC) (Windgassen *et al*., 2018b). In *E. coli*, this complex also involves the proteins PriB, PriC and DnaT; while in *B. subtilis* it involves DnaD, DnaB (unrelated to *E. coli* DnaB) and DnaI (homolog of

E. coli DnaC) (Bruand *et al*., 2004). Although some of these proteins are involved in DnaA-mediated replication initiation, DnaA does not participate into DNA replication restart. As DNA replication progresses, both the old and the new DNA strands need to be separated into the future daughter cells. Soon after replication initiation, the replicated origins move toward the future division sites (Dewachter *et al*., 2018; Hajduk *et al*., 2016). This process in most bacteria occurs while DNA replication and cell growth operate. Chromosome segregation involves the MukEBF complex in *E. coli*; and both SMC (Structural Maintenance of the Chromosome) condensing complex and ParABS system in *B. subtilis*. The MukEBF complex is related to SMC and promotes *oriC* region separation as well as DNA decatenation (Nicolas *et al*., 2014). It is however not known what drives chromosome segregation in *E. coli*, as no active "motor" has been identified. It was proposed that entropic forces could drive segregation, but they appear to be insufficient (Di Ventura *et al*., 2014). The ParABS system in *B. subtilis* on the other hand is an active partitioning system. ParA (Soj) is a Walker-type ATPase accumulating at the cell poles, that can bind DNA non-specifically in its ATP-bound form (Wang and Rudner, 2014) and ParB (Spo0J) is able to bind *parS* sites located around *oriC*. Interaction of the ParB/*parS* complex with ATP-ParA promotes ATP hydrolysis and release of ADP-ParA from the nucleoid, "forcing" ParB/*parS* to interact with a further ATP-ParA and thus creating an active motion of the nucleoid. SMC is also important as it helps to resolve the origins, allowing the ParABS system to segregate the free origins.

Synchronization of the bacterial cell cycle

DNA replication and chromosome segregation need to be properly coordinated with cell growth and cell division. Otherwise cells risk to have too much DNA compared to their cell volume, resulting in accumulation of most translated proteins, or chromosome cutting if cell division occurs too fast. In eukaryotes these processes are coordinated by checkpoint pathways (Harashima *et al*., 2013). In bacteria, they occur simultaneously when growing under propitious conditions. Although it was suspected by the end of the 1800's that bacterial growth is influenced by different nutrient sources (Schaechter, 2015), it was only later that a clear correlation between nutrient and growth could be observed by Alfred Hershey (Hershey, 1939) and Jacques Monod (Monod, 1949). Another important observation in 1958 was that cell size correlated with growth rate (Kjeldgaard *et al*., 1958; Schaechter *et al*., 1958). These publications led to a tremendous amount of work to try to unravel how bacteria control their cell cycle. The earliest proposed model of chromosome cycle in *Escherichia coli* was that the time between initiation of DNA replication and termination was constant, implying that the timing of DNA replication initiation

was limiting (Cooper and Helmstetter, 1968). It was therefore proposed that cells initiate DNA replication at constant volume (Donachie, 1968). Two different models emerged afterwards: at a slow growth rate, DNA replication initiation occurs when a critical mass (initiation mass) is reached and cells will subsequently divide after a time that is growth rate dependent, when they reach a fixed size (sizer model) (Wallden *et al*., 2016; Zheng *et al*., 2016); on the other hand, at a fast growth rate, cells will initiate DNA replication independently from their original size and grow to a constant size, adding a fixed volume between birth and division (adder model) (Campos *et al*., 2014; Taheri-Araghi *et al*., 2015; Wold *et al*., 1994). However, recently Si and co-workers demonstrated that cell-size homeostasis is in fact driven by cell division, and not replication initiation, and that both processes are independently controlled (Si *et al*., 2019). More importantly, they observed that both *E. coli* and *B. subtilis* follow a division adder, thus ruling out the sizer model. The adder division observed can be explained by accumulation of a fixed number of initiators and precursors that are required for cell division, and balanced biosynthesis of these precursors.

The main question that remains is how bacteria can control cell division and DNA replication events at the molecular level in order to keep an adder phenotype. So far, no existence of a cell size sensor has been reported. Also, once cell division occurred, it is also not known what the trigger is to initiate a new round of DNA replication. It was proposed that the accumulation of an activator could fulfill this role and the best candidate was the protein DnaA. It was thought that accumulation of DnaA in its active ATP-bound form could trigger early initiation (Løbner-Olesen *et al*., 1989; Pierucci *et al*., 1989). This was later discredited when increasing amounts of ATP-DnaA did not correlate with time of initiation, although DnaA is crucial for DNA replication initiation as it is a limiting factor (Flåtten *et al*., 2015). Absolute amount of DNA was also not able to trigger replication on its own (Huls *et al*., 2018). Correlation between cell size and DNA replication initiation was proved in *B. subtilis*, as changes in DNA replication altered cell size (Hill *et al*., 2012) but the converse was not true. In *E. coli* however, altering cell size was able to influence DNA replication initiation, suggesting that the regulatory factors are not conserved between both organisms. It also seems that more than one regulatory system is present in *B. subtilis*, as DNA replication initiation could still be controlled by perturbing the medium composition in a strain able to initiate DNA replication independently from DnaA (swapping *oriC* for *oriN,* a RepN-dependent origin of replication) (Murray, 2016; Murray and Koh, 2014).

Once the cell has satisfied its growth and DNA replication initiation requirements, it can duplicate its DNA until completion. Cell division and DNA replication are intimately linked, as impacting DNA replication directly affects cell division of *B. subtilis* (Moriya *et al*., 2010). It was shown in *E. coli* that, after chromosome reorganization at

the center of the cells, the terminus region associates with the protein MatP, which itself interacts with the division site via ZapA/B (see below paragraph *A conserved machinery for bacterial cell division*) (Espéli *et al*., 2012; Männik *et al*., 2016). It was proposed that this interaction (together with FtsK) could be the ''sensor'' for completion of DNA replication and chromosome re-organization and thus a direct link between DNA replication and cell division (Kleckner *et al*., 2018). This simple model could therefore explain how cells "sense" the state of DNA replication, and "translate" this signal into instruction for the divisome via ZapA/B. This hypothetical model can, however, not be transposed to Firmicutes, as they lack homologs of MatP and no complex associated with the terminus has been identified. It is important to note that most cell cycle coordination models were proposed for rod-shaped bacteria able to perform multifork replication, such as *E. coli* and *B. subtilis*.

A conserved machinery for bacterial cell division

The vast majority of prokaryotes, except a very few (Erickson and Osawa, 2010), use the tubulin homolog FtsZ as major scaffold protein for cytokinesis (Bi and Lutkenhaus, 1991; Lutkenhaus *et al*., 2012). FtsZ can "polymerize" at the middle of the cell by interaction with the membrane-associated protein FtsA and promote assembly of the whole division machinery (Du and Lutkenhaus, 2017; Errington *et al*., 2003). Its innate movement of "treadmilling" via a GTP-ase activity was also shown to contribute to membrane bending and therefore to help septum constriction (Bisson-Filho *et al*., 2017; Nguyen *et al*., 2019; Yang *et al*., 2017). Bacteria developed different strategies to direct FtsZ assembly at mid-cell, but for the scope of this thesis, only the mechanisms of *E. coli* and *B. subtilis* will be described. These model bacteria belong to different phyla (Proteobacteria and Firmicutes respectively) and therefore have a different cell wall organization: *E. coli* possesses an outer membrane and a thin peptidoglycan layer, while *B. subtilis* has a thick peptidoglycan layer and no second membrane. Although they are evolutionarily very distant (billions of years), they share a very similar cell shape, and both use a variant of the MinCD system to localize FtsZ at mid-cell (Fig. 3a). In *E. coli*, MinE oscillates between the cell poles and prevents the accumulation of MinC and MinD that can inhibit FtsZ polymerization, thus creating an "inhibition-free" zone at mid-cell where the Z-ring can be formed (Bisicchia *et al*., 2013). *B. subtilis* lacks MinE and MinCD are not oscillating but are instead tethered at the poles (Marston *et al*., 1998). The Min system is however not conserved among all bacteria as, for instance, *Streptococcus pneumoniae, Staphylococcus aureus, Caulobacter crescentus* and many others use alternative systems. Another conserved mechanism to help FtsZ's mid-cell localization, and in the meantime to prevent "cutting" of the chromosome during cell division, is the nucleoid occlusion system (Noc) (Wu and Errington, 2012). SlmA in

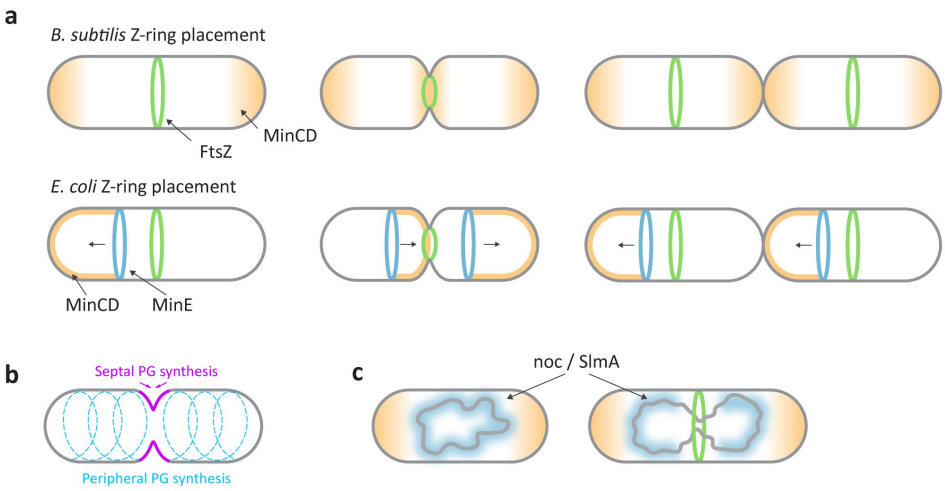

Figure 3. Division site selection and cell wall synthesis.

(**a**) both *E. coli* and *B. subtilis* use a variant of the Min system to promote FtsZ assembly at mid-cell, but MinCD in *B. subtilis* (up) is tethered at the cell poles, while it oscillates in *E. coli* (down). (**b**) schematic representation of Septal and peripheral peptidoglycan (PG) synthesis in these two model bacteria. (**c**) the nucleoid occlusion system (noc / SlmA) located over the nucleoid prevents assembly of FtsZ, preventing cutting of the chromosome.

E. coli and Noc in *B. subtilis* have DNA-binding domains that recognize specific motifs on the chromosome and can inhibit FtsZ polymerization (Fig. 3c). Recent work on *S. aureus* also showed that Noc, besides a role in cell division regulation, could directly control DNA replication initiation in a DnaA dependent manner (Pang *et al.*, 2017). Two important regulators of the Z-ring are ZapA and ZapB, forming an FtsZ-independent structure at midcell and that are thought to stabilize the FtsZ ring and coordinate DNA replication with cell division (Buss *et al.*, 2017). Once the Z-ring is formed, several proteins will be recruited to form the divisome. Among them are ABC-transporter proteins to coordinate peptidoglycan synthesis with cell division (FtsE/FtsX), the DNA translocase FtsK assisting chromosome segregation and the FtsQ/FtsB/FtsL complex. The role of FtsQ/FtsB/FtsL (DivIB/DivIC/FtsL in *B. subtilis*) is not fully understood, but it was suggested to be a scaffold for the assembly of the divisome (Choi *et al.*, 2018). Importantly, also found at the divisome are several proteins involved in peptidoglycan synthesis (see below). Besides the nearly 30 proteins of the divisome, it cannot be excluded that other unknown division proteins are also present.

Cell wall and teichoic acids biosynthesis in bacteria

The cell wall is the primary protection from external stress and provides structural support to the cell. The main component of the cell wall is the peptidoglycan (murein), built of long cross-linked glycan chains composed of *N*-acetylglucosamine (GlcNac) and *N*-acetylmuramic acid (MurNac) subunits linked by β-1,4 glycosidic bonds. These subunits also possess a pentapeptide on the C-3 carbon of MurNac composed of two amino acids, one dibasic amino acid (*meso*-diamoinopimelic acid, *m*-A_2pm, for most Gram-negative bacteria and L-lysine for most Gram-positives) and two D-alanine ($[L\text{-}Ala]_1\text{-}[D\text{-}Glu]_2\text{-}[m\text{-}A_2pm]_3\text{-}[D\text{-}Ala]_4\text{-}[D\text{-}Ala]_5$ for *E. coli* and *B. subtilis*). The glycan chain is synthesized by transglycosylation (TG) during which the last MurNac from the nascent peptidoglycan is linked to the C-4 carbon of GlcNac. The chains are later cross-linked together via the peptide chains by transpeptidation (TP) during which the $[D\text{-}Ala]_4$ from one chain is linked to the dibasic amino acid of the other chain. Peptidoglycan synthesis occurs in three different stages. First, the precursor UDP-MurNac is synthesized in the cytoplasm. Then, the precursor is linked to undecaprenyl phosphate by MraY to form so-called lipid I. The glycosyltransferase MurG then transfers GlcNac from UDP-GlcNac onto the C-4 carbon of lipid I. The formed product, called lipid II, is then translocated across the membrane by the flippase MurJ (Sham *et al*., 2014). Finally, lipid II is polymerized by transglycosylases and crosslinked by transpeptidases to form a mature peptidoglycan (Qiao *et al*., 2017). TG and TP reactions are catalyzed by penicillin-binding proteins (PBPs) and the SEDS (shape, elongation, division and sporulation) family of proteins (Meeske *et al*., 2016). Class A PBPs are bifunctional and catalyze TG and TP reactions, while class B PBPs are transpeptidases (Sassine *et al*., 2017; Sobhanifar *et al*., 2013). SEDS proteins (such as FtsW and RodA) are also peptidoglycan polymerases. Rod-shaped bacteria like *E. coli* or *B. subtilis* possess two separate peptidoglycan biosynthesis machineries: one for elongation (peripheral PG synthesis) and one for septum formation (septal PG synthesis). The septal PG machinery is mainly organized by FtsZ, while the PG elongation complex is organized by the protein MreB, a homolog of the eukaryotic actin (Billaudeau *et al*., 2017) able to bind the membrane and form large assemblies moving around the cell (Daniel and Errington, 2003; Domínguez-Escobar *et al*., 2011) (Fig. 3b). Beside the difference in types of PBPs present in each complex, the peripheral PG synthesis machinery involves the glycosyltransferase RodA (Emami *et al*., 2017), while the septal synthesis complex requires the glycosyltransferase FtsW (Harry *et al*., 2006; Taguchi *et al*., 2019). It is however unclear whether FtsW also acts as a flippase of lipid II.

Other major cell wall compounds of most Gram-positive bacteria are the PG-linked glycol polymers called teichoic acids (TAs) (Neuhaus and Baddiley, 2003). They can be either lipoteichoic acids (LTAs), when anchored in the plasma membrane,

or wall teichoic acids (WTAs) when covalently bound to the PG layer (Rajagopal and Walker, 2017). TAs play many various roles and it is not yet fully understood what their exact function is. They are involved in cell morphology and cell division (Atilano *et al*., 2010), in antibiotic resistance (Brown *et al*., 2012), in host adhesion and colonization (Weidenmaier *et al*., 2005), metal homeostasis (Errington and Wu, 2017), *etc*. The structures of LTAs and WTAs are highly variable between bacterial species. In *B. subtilis* for instance, LTAs are composed of a polyglycerol-phosphate chain anchored to a glycolipid in the membrane, while WTAs are mainly composed of glycerol-phosphate or ribitol-phosphate repeats and coupled through a disaccharide to the PG. Interestingly, although LTAs and WTAs are usually synthesized by different biosynthetic pathways, it is thought that those of *S. pneumoniae* are assembled using the same enzymes, as they appear to be structurally identical (Denapaite *et al*., 2012; Rajagopal and Walker, 2017). In the case of *S. pneumoniae*, TA biosynthesis involves at least 16 different genes and the pathway has been precisely described, although a few genes still have unknown functions (Denapaite *et al*., 2012). Furthermore, choline-binding proteins (CBPs) can bind TAs located at the surface of the bacterium via their phosphorylcholine (exclusively found in *S. pneumoniae*). These CBPs have been implicated in adherence and colonization of the pneumococcus (Rosenow *et al*., 1997) and therefore directly link TAs with a role in virulence.

Streptococcus pneumoniae, a pathogen unlike any other

Streptococcus pneumoniae (or commonly referred to as pneumococcus) is a major opportunistic human pathogen colonizing the upper respiratory tract (Weiser *et al*., 2018). Under certain circumstances, it can cause otitis media, pneumonia, sepsis and meningitis; and has therefore been classified as one of the '12 priority pathogens' by the World Health Organization (https://www.who.int/medicines/publications/WHO-PPL-Short_Summary_25Feb- ET_NM_WHO.pdf). Importantly, *S. pneumoniae* strains resistant to multiple antibiotics began to appear several years ago (Cornick and Bentley, 2012). Spontaneous resistance is largely due to the high genome plasticity of the pneumococcus because of its natural competence for genetic transformation. Briefly, cells produce a competence stimulating peptide (CSP) and export it via ComAB. Cells can then sense CSP via the histidine-kinase ComD, which will promote phosphorylation of ComE, leading to the activation of competence genes (*comAB, comCDE, ComX*$_{1,2}$) in order to further uptake and integrate DNA fragments if present in the environment (Straume *et al*., 2015).

The high virulence of *S. pneumoniae* comes from the fact that it possesses a full armada of virulence factors for host infection, in particular the presence of a polysaccharide capsule which facilitates escape from the immune system.

This capsule, synthesized by several proteins from the *cps* operon, also plays a major role in cell morphology as deletion of the *cps* genes will abrogate chain formation in *S. pneumoniae* and lead instead to the formation of short diplococci. Over 90 different capsular types (serotypes) have been described, and the main measure to fight against this pathogen, besides antibiotics, is vaccines targeting the capsular polysaccharides. However, only a small portion of the serotypes can be targeted at once and it is therefore urgent to identify new potential drug targets. In this thesis, we mainly used the pathogenic serotype 2 strain D39 (our laboratory variant is named D39V), isolated from a patient more than 100 years ago (Lanie *et al.*, 2007; Slager *et al.*, 2018); the avirulent, capsule-less strain R6 derived from D39 (Hoskins *et al.*, 2001); and the virulent serotype 4 strain TIGR4 (Tettelin *et al.*, 2001).

Although *S. pneumoniae* is evolutionarily closer to *B. subtilis* than *E. coli* (Gupta, 2000; Tatusov *et al.*, 1996), it does not share most of the cell division mechanisms previously described for the two other model bacteria. Indeed, unlike *E. coli* or *B. subtilis*, *S. pneumoniae* does not have any homolog of MreB, and its lateral peptidoglycan biosynthesis is coupled to septal synthesis (Fig. 4a). Interestingly, it also lacks homologs of a nucleoid occlusion system, as well as homologs of the

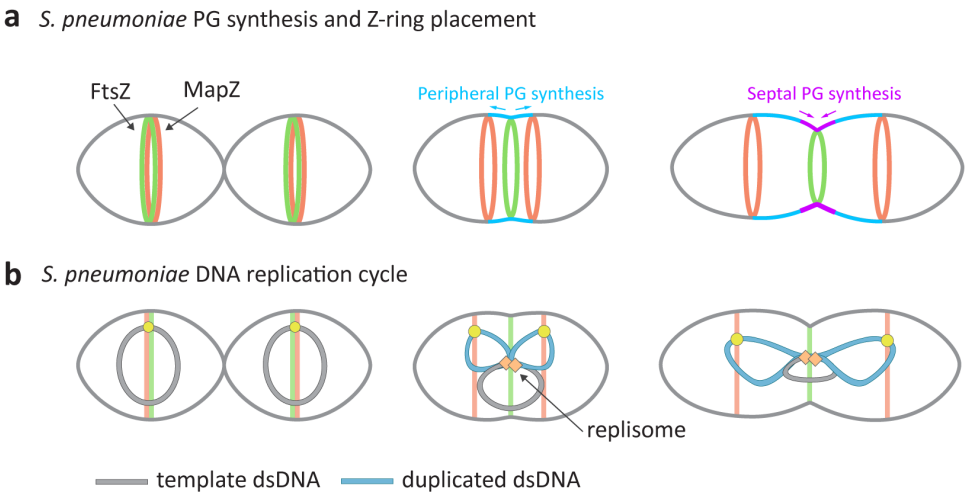

Figure 4. *Streptococcus pneumoniae*'s cell division and cell cycle model.

(**a**) *S. pneumoniae* lacks homologs of the MinCDE system and instead uses the protein MapZ, following the nascent peptidoglycan, to guide FtsZ assembly at mid-cell. (**b**) in *S. pneumoniae*, initiation of DNA replication occurs at mid-cell, shortly after the origins or replication are pushed apart from mid-cell with a dynamics similar to that of MapZ. FtsZ (green) stays at the septum until DNA replication is terminated and re-localizes at the new septum when a new round of DNA replication can start.

MinCDE system. Instead, the future division site where FtsZ assembles is determined by the mid-cell-anchored protein Z (MapZ), which is able to interact with the nascent peptidoglycan (Fig. 4a) (Fleurie *et al.*, 2014; Holečková *et al.*, 2014; Manuse *et al.*, 2016). As the peripheral PG is formed at mid-cell, the MapZ rings are pushed apart from old cell equator until they eventually define both future division sites. MapZ can interact with FtsZ and it was proposed that it acts as a beacon for FtsZ polymerization at mid-cell. However, in cells in which *mapZ* was deleted, FtsZ was still able to form rings although the angle of these rings were clearly impacted (van Raaphorst *et al.*, 2017). It was also reported that the intracellular domain of MapZ can accelerate FtsZ polymerization (Feng *et al.*, 2019). MapZ is therefore crucial for proper Z-ring maturation, orientation and precision.

S. pneumoniae carries a single chromosome and it does not perform multifork replication (no case has ever been reported yet). It was shown that localization and timing of the origin of replication *oriC* correlates with that of MapZ (van Raaphorst *et al.*, 2017) and that *oriC* localization is not dependent on MapZ. However, chromosome segregation and thus o*riC* localization defects, drastically affect MapZ and FtsZ localization. It was also shown that DNA replication takes place in the vicinity of mid-cell and that termination correlates with localization of FtsZ at the new division site (Fig. 4b). Therefore, there is a close relationship between DNA segregation and cell division in *S. pneumoniae*.

As *S. pneumoniae* lacks homologs of several proteins described for *E. coli* and / or *B. subtilis* (*e.g.* MatP, ParA, MinECD, Soj, Noc), it seems to have developed different mechanisms to control its cell cycle and cell shape.

Thesis outline

Most of our knowledge about pneumococcal cell morphology, cell division and cell cycle control come from analogies with mechanisms at play in *B. subtilis*. However, it appears that *S. pneumoniae* has evolved differently, and even though most fundamental processes are still shared with *B. subtilis*, the presence of unique regulators (*e.g.* MapZ) indicates that new control factors still need to be unraveled to further understand its division process. A better understanding of how the pneumococcus grows and divides can reveal fundamental knowledge in order to fight against this major pathogen. In that respect in **Chapter 2**, we aimed to identify new proteins involved in essential pathways using clustered regularly interspaced short palindromic repeats interference (CRISPRi) phenotyping. We successfully identified two new genes, SPV_1416 and SPV_1417 (respectively MurT and GatD), both essential for peptidoglycan synthesis. We also showed that SPV_1198 and SPV_1197 (that

we renamed TarP and TarQ respectively) are responsible for teichoic acid precursor polymerization. And finally, we identified ClpX as responsible for ClpP-dependent repression of competence. Several genes of unknown function were also identified in this screening, as they showed major defects upon inactivation. Among them, we focused on SPV_0476 (that we renamed CcrZ) and described in **Chapter 3** that CcrZ is a completely novel regulator of DNA replication initiation in *S. pneumoniae, B. subtilis* and *S. aureus* and that it coordinates cell division with DNA replication. We showed that CcrZ interacts with the divisome and that it activates DNA replication in a DnaA-dependent manner. Finally, we focused on the pAp phosphatase PapP (SPD_1153) as inactivation of PapP was previously shown to reduce virulence of *S. pneumoniae* (Cron *et al*., 2011) and *papP* silencing by CRISPRi in **Chapter 2** showed clear growth defects. In **Chapter 4**, we showed that PapP plays a direct role in lipid metabolism in *S. pneumoniae* TIGR4, and that its deletion impacts lipid biosynthesis. Interestingly, this change in membrane composition impaired pneumococcal cell division dynamics and morphology.

References

Arenson, M., and Coley, J.D. (2018). Anthropocentric by Default? Attribution of Familiar and Novel Properties to Living Things. Cogn. Sci. *42*, 253–285.

Atilano, M.L., Pereira, P.M., Yates, J., Reed, P., Veiga, H., Pinho, M.G., and Filipe, S.R. (2010). Teichoic acids are temporal and spatial regulators of peptidoglycan cross-linking in *Staphylococcus aureus*. Proc. Natl. Acad. Sci. U. S. A. *107*, 18991–18996.

Avery, O.T., Macleod, C.M., and McCarty, M. (1944). Studies on the chemical nature of the substance inducing transformation of pneumococcal types : induction of transformation by a desoxyribonucleic acid fraction isolated from pneumococcus type III. J. Exp. Med. *79*, 137–158.

Bi, E., and Lutkenhaus, J. (1991). FtsZ ring structure associated with division in *Escherichia coli*. Nature *354*, 161–164.

Billaudeau, C., Chastanet, A., Yao, Z., Cornilleau, C., Mirouze, N., Fromion, V., and Carballido-López, R. (2017). Contrasting mechanisms of growth in two model rod-shaped bacteria. Nat. Commun. *8*, 15370.

Bisicchia, P., Arumugam, S., Schwille, P., and Sherratt, D. (2013). MinC, MinD, and MinE drive counter-oscillation of early-cell-division proteins prior to *Escherichia coli* septum formation. MBio *4*, e00856-13.

Bisson-Filho, A.W., Hsu, Y.-P., Squyres, G.R., Kuru, E., Wu, F., Jukes, C., Sun, Y., Dekker, C., Holden, S., VanNieuwenhze, M.S., *et al*. (2017). Treadmilling by FtsZ filaments drives peptidoglycan synthesis and bacterial cell division. Science (80-.). *355*, 739–743.

Blaesing, F., Weigel, C., Welzeck, M., and Messer, W. (2002). Analysis of the DNA-binding domain of *Escherichia coli* DnaA protein. Mol. Microbiol. *36*, 557–569.

Brown, S., Xia, G., Luhachack, L.G., Campbell, J., Meredith, T.C., Chen, C., Winstel, V., Gekeler, C., Irazoqui, J.E., Peschel, A., *et al*. (2012). Methicillin resistance in *Staphylococcus aureus* requires glycosylated wall teichoic acids. Proc. Natl. Acad. Sci. U. S. A. *109*, 18909–18914.

Bruand, C., Velten, M., McGovern, S., Marsin, S., Sérèna, C., Ehrlich, S.D., and Polard, P. (2004). Functional interplay between the *Bacillus subtilis* DnaD and DnaB proteins essential for initiation and re-initiation of DNA replication. Mol. Microbiol. *55*, 1138–1150.

Buss, J.A., Peters, N.T., Xiao, J., and Bernhardt, T.G. (2017). ZapA and ZapB form an FtsZ-independent structure at midcell. Mol. Microbiol. *104*, 652–663.

Campos, M., Surovtsev, I.V., Kato, S., Paintdakhi, A., Beltran, B., Ebmeier, S.E., and Jacobs-Wagner, C. (2014). A Constant Size Extension Drives Bacterial Cell Size Homeostasis. Cell *159*, 1433–1446.

Choi, Y., Kim, J., Yoon, H.-J., Jin, K.S., Ryu, S., and Lee, H.H. (2018). Structural Insights into the FtsQ/FtsB/FtsL Complex, a Key Component of the Divisome. Sci. Rep. *8*, 18061.

Cooper, S., and Helmstetter, C.E. (1968). Chromosome replication and the division cycle of *Escherichia coli* Br. J. Mol. Biol. *31*, 519–540.

Cornick, J.E., and Bentley, S.D. (2012). *Streptococcus pneumoniae*: the evolution of antimicrobial resistance to beta-lactams, fluoroquinolones and macrolides. Microbes Infect. *14*, 573–583.

Cron, L.E., Stol, K., Burghout, P., van Selm, S., Simonetti, E.R., Bootsma, H.J., and Hermans, P.W.M. (2011). Two DHH Subfamily 1 Proteins Contribute to Pneumococcal Virulence and Confer Protection against Pneumococcal Disease. Infect. Immun. *79*, 3697–3710.

Dahm, R. (2008). Discovering DNA: Friedrich Miescher and the early years of nucleic acid research. Hum. Genet. *122*, 565–581.

Daniel, R.A., and Errington, J. (2003). Control of Cell Morphogenesis in Bacteria: Two Distinct Ways to Make a Rod-Shaped Cell. Cell *113*, 767–776.

Denapaite, D., Brückner, R., Hakenbeck, R., and Vollmer, W. (2012). Biosynthesis of Teichoic Acids in *Streptococcus pneumoniae* and Closely Related Species: Lessons from Genomes. Microb. Drug Resist. *18*, 344–358.

Dewachter, L., Verstraeten, N., Fauvart, M., and Michiels, J. (2018). An integrative view of cell cycle control in *Escherichia coli*. FEMS Microbiol. Rev. *42*, 116–136.

Domínguez-Escobar, J., Chastanet, A., Crevenna, A.H., Fromion, V., Wedlich-Söldner, R., and Carballido-López, R. (2011). Processive Movement of MreB-Associated Cell Wall Biosynthetic Complexes in Bacteria. Science (80-.). *333*, 225–228.

Donachie, W.D. (1968). Relationship between cell size and time of initiation of DNA replication. Nature *219*, 1077–1079.

Du, S., and Lutkenhaus, J. (2017). Assembly and activation of the *Escherichia coli* divisome. Mol. Microbiol. *105*, 177–187.

Dubrovsky, J.G., and Ivanov, V.B. (2003). Celebrating 50 years of the cell cycle. Nature *426*, 759–759.

Emami, K., Guyet, A., Kawai, Y., Devi, J., Wu, L.J., Allenby, N., Daniel, R.A., and Errington, J. (2017). RodA as the missing glycosyltransferase in *Bacillus subtilis* and antibiotic discovery for the peptidoglycan polymerase pathway. Nat. Microbiol. *2*, 16253.

Erickson, H.P., and Osawa, M. (2010). Cell division without FtsZ, a variety of redundant mechanisms. Mol. Microbiol. *78*, 267–270.

Errington, J., and Wu, L.J. (2017). Cell Cycle Machinery in *Bacillus subtilis*. Subcell. Biochem. *84*, 67–101.

Errington, J., Daniel, R.A., and Scheffers, D.-J. (2003). Cytokinesis in Bacteria. Microbiol. Mol. Biol. Rev. *67*, 52.

Espéli, O., Borne, R., Dupaigne, P., Thiel, A., Gigant, E., Mercier, R., and Boccard, F. (2012). A MatP-divisome interaction coordinates chromosome segregation with cell division in *E. coli*. EMBO J. *31*, 3198–3211.

Feng, Z., Zhang, J., Xu, D., Jiang, Y.-L., Zhou, C.-Z., and Chen, Y. (2019). Multi-functional regulator MapZ controls both positioning and timing of FtsZ polymerization. Biochem. J. BCJ20190138.

Flåtten, I., Fossum-Raunehaug, S., Taipale, R., Martinsen, S., and Skarstad, K. (2015). The DnaA Protein Is Not the Limiting Factor for Initiation of Replication in *Escherichia coli*. PLOS Genet. *11*, e1005276.

Fleurie, A., Lesterlin, C., Manuse, S., Zhao, C., Cluzel, C., Lavergne, J.-P., Franz-Wachtel, M., Macek, B., Combet, C., Kuru, E., *et al*. (2014). MapZ marks the division sites and positions FtsZ rings in *Streptococcus pneumoniae*. Nature *516*, 259–262.

Fuller, R.S., Funnell, B.E., and Kornberg, A. (1984). The dnaA protein complex with the *E. coli* chromosomal replication origin (oriC) and other DNA sites. Cell *38*, 889–900.

Gupta, R.S. (2000). The phylogeny of proteobacteria: relationships to other eubacterial phyla and eukaryotes. FEMS Microbiol. Rev. *24*, 367–402.

Hajduk, I. V., Rodrigues, C.D.A., and Harry, E.J. (2016). Connecting the dots of the bacterial cell cycle: Coordinating chromosome replication and segregation with cell division. Semin. Cell Dev. Biol. *53*, 2–9.

Harashima, H., Dissmeyer, N., and Schnittger, A. (2013). Cell cycle control across the eukaryotic kingdom. Trends Cell Biol. *23*, 345–356.

Harry, E., Monahan, L., and Thompson, L. (2006). Bacterial Cell Division: The Mechanism and Its Precison. Int. Rev. Cytol. *253*, 27–94.

Hershey, A.D. (1939). Factors Limiting Bacterial Growth: IV. The Age of the Parent Culture and the Rate of Growth of Transplants of *Escherichia coli*. J. Bacteriol. *37*, 285–299.

Hershey, A.D., and Chase, M. (1952). Independent functions of viral protein and nucleic acid in growth of bacteriophage. J. Gen. Physiol. *36*, 39–56.

Hill, N.S., Kadoya, R., Chattoraj, D.K., and Levin, P.A. (2012). Cell Size and the Initiation of DNA Replication in Bacteria. PLoS Genet. *8*, e1002549.

Holečková, N., Doubravová, L., Massidda, O., Molle, V., Buriánková, K., Benada, O., Kofroňová, O., Ulrych, A., and Branny, P. (2014). LocZ is a new cell division protein involved in proper septum placement in *Streptococcus pneumoniae*. MBio *6*, e01700-14.

Hoskins, J., Alborn, W.E., Arnold, J., Blaszczak, L.C., Burgett, S., DeHoff, B.S., Estrem, S.T., Fritz, L., Fu, D.J., Fuller, W., *et al*. (2001). Genome of the bacterium *Streptococcus pneumoniae* strain R6. J. Bacteriol. *183*, 5709–5717.

Huls, P.G., Vischer, N.O.E., and Woldringh, C.L. (2018). Different Amounts of DNA in Newborn Cells of *Escherichia coli* Preclude a Role for the Chromosome in Size Control According to the "Adder" Model. Front. Microbiol. *9*, 664.

Jameson, K.H., and Wilkinson, A.J. (2017). Control of Initiation of DNA Replication in *Bacillus subtilis* and *Escherichia coli*. Genes (Basel). *8*.

Katayama, T., Ozaki, S., Keyamura, K., and Fujimitsu, K. (2010). Regulation of the replication cycle: conserved and diverse regulatory systems for DnaA and oriC. Nat. Rev. Microbiol. *8*, 163–170.

Kjeldgaard, N.O., MaalOe, O., and Schaechter, M. (1958). The Transition Between Different Physiological States During Balanced Growth of Salmonella typhimurium. J. Gen. Microbiol. *19*, 607–616.

Kleckner, N.E., Chatzi, K., White, M.A., Fisher, J.K., and Stouf, M. (2018). Coordination of Growth, Chromosome Replication/Segregation, and Cell Division in *E. coli*. Front. Microbiol. *9*, 1469.

Lanie, J.A., Ng, W.-L., Kazmierczak, K.M., Andrzejewski, T.M., Davidsen, T.M., Wayne, K.J., Tettelin, H., Glass, J.I., and Winkler, M.E. (2007). Genome sequence of Avery's virulent serotype 2 strain D39 of *Streptococcus pneumoniae* and comparison with that of unencapsulated laboratory strain R6. J. Bacteriol. *189*, 38–51.

Løbner-Olesen, A., Skarstad, K., Hansen, F.G., von Meyenburg, K., and Boye, E. (1989). The DnaA protein determines the initiation mass of *Escherichia coli* K-12. Cell *57*, 881–889.

Lu, M., Campbell, J.L., Boye, E., and Kleckner, N. (1994). SeqA: A negative modulator of replication initiation in *E. coli*. Cell *77*, 413–426.

Lutkenhaus, J., Pichoff, S., and Du, S. (2012). Bacterial cytokinesis: from Z ring to divisome. Cytoskeleton (Hoboken). *69*, 778–790.

Männik, J., Castillo, D.E., Yang, D., Siopsis, G., and Männik, J. (2016). The role of MatP, ZapA and ZapB in chromosomal organization and dynamics in *Escherichia coli*. Nucleic Acids Res. *44*, 1216–1226.

Manuse, S., Jean, N.L., Guinot, M., Lavergne, J.-P., Laguri, C., Bougault, C.M., VanNieuwenhze, M.S., Grangeasse, C., and Simorre, J.-P. (2016). Structure–function analysis of the extracellular domain of the pneumococcal cell division site positioning protein MapZ. Nat. Commun. 2016 7 *7*, 12071.

Marston, A.L., Thomaides, H.B., Edwards, D.H., Sharpe, M.E., and Errington, J. (1998). Polar localization of the MinD protein of *Bacillus subtilis* and its role in selection of the mid-cell division site. Genes Dev. *12*, 3419–3430.

Meeske, A.J., Riley, E.P., Robins, W.P., Uehara, T., Mekalanos, J.J., Kahne, D., Walker, S., Kruse, A.C., Bernhardt, T.G., and Rudner, D.Z. (2016). SEDS proteins are a widespread family of bacterial cell wall polymerases. Nature *537*, 634–638.

Monod, J. (1949). The Growth of Bacterial Cultures. Annu. Rev. Microbiol. *3*, 371–394.

Moriya, S., Rashid, R.A., Rodrigues, C.D.A., and Harry, E.J. (2010). Influence of the nucleoid and the early stages of DNA replication on positioning the division site in *Bacillus subtilis*. Mol. Microbiol. *76*, 634–647.

Mott, M.L., and Berger, J.M. (2007). DNA replication initiation: mechanisms and regulation in bacteria. Nat. Rev. Microbiol. *5*, 343–354.

Murray, H. (2016). Connecting chromosome replication with cell growth in bacteria. Curr. Opin. Microbiol. *34*, 13–17.

Murray, H., and Koh, A. (2014). Multiple Regulatory Systems Coordinate DNA Replication with Cell Growth in *Bacillus subtilis*. PLoS Genet. *10*, e1004731.

Neuhaus, F.C., and Baddiley, J. (2003). A continuum of anionic charge: structures and functions of D-alanyl-teichoic acids in gram-positive bacteria. Microbiol. Mol. Biol. Rev. *67*, 686–723.

Nguyen, L.T., Oikonomou, C.M., Ding, H.J., Kaplan, M., Yao, Q., Chang, Y.-W., Beeby, M., and Jensen, G.J. (2019). Simulations suggest a constrictive force is required for Gram-negative bacterial cell division. Nat. Commun. *10*, 1259.

Nicolas, E., Upton, A.L., Uphoff, S., Henry, O., Badrinarayanan, A., and Sherratt, D. (2014). The SMC complex MukBEF recruits topoisomerase IV to the origin of replication region in live *Escherichia coli*. MBio *5*, e01001-13.

Pang, T., Wang, X., Lim, H.C., Bernhardt, T.G., and Rudner, D.Z. (2017). The nucleoid occlusion factor Noc controls DNA replication initiation in *Staphylococcus aureus*. PLoS Genet. *13*, e1006908.

Pierucci, O., Rickert, M., and Helmstetter, C.E. (1989). DnaA protein overproduction abolishes cell cycle specificity of DNA replication from oriC in *Escherichia coli*. J. Bacteriol. *171*, 3760–3766.

Qiao, Y., Srisuknimit, V., Rubino, F., Schaefer, K., Ruiz, N., Walker, S., and Kahne, D. (2017). Lipid II overproduction allows direct assay of transpeptidase inhibition by β-lactams. Nat. Chem. Biol. *13*, 793–798.

van Raaphorst, R., Kjos, M., and Veening, J.-W. (2017). Chromosome segregation drives division site selection in*Streptococcus pneumoniae*. Proc. Natl. Acad. Sci. U. S. A. *114*, E5959–E5968.

Rajagopal, M., and Walker, S. (2017). Envelope Structures of Gram-Positive Bacteria. Curr. Top. Microbiol. Immunol. *404*, 1.

Richardson, T.T., Harran, O., and Murray, H. (2016). The bacterial DnaA-trio replication origin element specifies single-stranded DNA initiator binding. Nature *534*, 412–416.

Rosenow, C., Ryan, P., Weiser, J.N., Johnson, S., Fontan, P., Ortqvist, A., and Masure, H.R. (1997). Contribution of novel choline-binding proteins to adherence, colonization and immunogenicity of *Streptococcus pneumoniae*. Mol. Microbiol. *25*, 819–829.

Russell, P., and Nurse, P. (1986). Schizosaccharomyces pombe and saccharomyces cerevisiae: A look at yeasts divided. Cell *45*, 781–782.

Sassine, J., Xu, M., Sidiq, K.R., Emmins, R., Errington, J., and Daniel, R.A. (2017). Functional redundancy of division specific penicillin-binding proteins in *Bacillus subtilis*. Mol. Microbiol. *106*, 304–318.

Schaechter, M. (2015). A brief history of bacterial growth physiology. Front. Microbiol. *6*, 289.

Schaechter, M., MaalOe, O., and Kjeldgaard, N.O. (1958). Dependency on Medium and Temperature of Cell Size and Chemical Composition during Balanced Growth of Salmonella typhimurium. J. Gen. Microbiol. *19*, 592–606.

Sender, R., Fuchs, S., and Milo, R. (2016). Revised Estimates for the Number of Human and Bacteria Cells in the Body. PLOS Biol. *14*, e1002533.

Sham, L.-T., Butler, E.K., Lebar, M.D., Kahne, D., Bernhardt, T.G., and Ruiz, N. (2014). Bacterial cell wall. MurJ is the flippase of lipid-linked precursors for peptidoglycan biogenesis. Science *345*, 220–222.

Si, F., Le Treut, G., Sauls, J.T., Vadia, S., Levin, P.A., and Jun, S. (2019). Mechanistic Origin of Cell-Size Control and Homeostasis in Bacteria. Curr. Biol. *29*, 1760-1770.e7.

Skarstad, K., and Katayama, T. (2013). Regulating DNA replication in bacteria. Cold Spring Harb. Perspect. Biol. *5*, a012922.

Slager, J., Aprianto, R., and Veening, J.-W. (2018). Deep genome annotation of the opportunistic human pathogen *Streptococcus pneumoniae* D39. Nucleic Acids Res. 46, 9971–9989.

Sobhanifar, S., King, D.T., and Strynadka, N.C. (2013). Fortifying the wall: synthesis, regulation and degradation of bacterial peptidoglycan. Curr. Opin. Struct. Biol. *23*, 695–703.

Straume, D., Stamsås, G.A., and Håvarstein, L.S. (2015). Natural transformation and genome evolution in *Streptococcus pneumoniae*. Infect. Genet. Evol. *33*, 371–380.

Taguchi, A., Welsh, M.A., Marmont, L.S., Lee, W., Sjodt, M., Kruse, A.C., Kahne, D., Bernhardt, T.G., and Walker, S. (2019). FtsW is a peptidoglycan polymerase that is functional only in complex with its cognate penicillin-binding protein. Nat. Microbiol. *4*, 587–594.

Taheri-Araghi, S., Bradde, S., Sauls, J.T., Hill, N.S., Levin, P.A., Paulsson, J., Vergassola, M., and Jun, S. (2015). Cell-size control and homeostasis in bacteria. Curr. Biol. *25*, 385–391.

Tatusov, R.L., Mushegian, A.R., Bork, P., Brown, N.P., Hayes, W.S., Borodovsky, M., Rudd, K.E., and Koonin, E. V. (1996). Metabolism and evolution of Haemophilus influenzae deduced from a whole-genome comparison with *Escherichia coli*. Curr. Biol. *6*, 279–291.

Tettelin, H., Nelson, K.E., Paulsen, I.T., Eisen, J.A., Read, T.D., Peterson, S., Heidelberg, J., DeBoy, R.T., Haft, D.H., Dodson, R.J., *et al*. (2001). Complete genome sequence of a virulent isolate of *Streptococcus pneumoniae*. Science *293*, 498–506.

Di Ventura, B., Knecht, B., Andreas, H., Godinez, W.J., Fritsche, M., Rohr, K., Nickel, W., Heermann, D.W., and Sourjik, V. (2014). Chromosome segregation by the *Escherichia coli* Min system. Mol. Syst. Biol. *9*, 686–686.

Wallden, M., Fange, D., Lundius, E.G., Baltekin, Ö., and Elf, J. (2016). The Synchronization of Replication and Division Cycles in Individual *E. coli* Cells. Cell *166*, 729–739.

Wang, X., and Rudner, D.Z. (2014). Spatial organization of bacterial chromosomes. Curr. Opin. Microbiol. *22*, 66–72.

Weidenmaier, C., Peschel, A., Xiong, Y., Kristian, S.A., Dietz, K., Yeaman, M.R., and Bayer, A.S. (2005). Lack of Wall Teichoic Acids in *Staphylococcus aureus* Leads to Reduced Interactions with Endothelial Cells and to Attenuated Virulence in a Rabbit Model of Endocarditis. J. Infect. Dis. *191*, 1771–1777.

Weiser, J.N., Ferreira, D.M., and Paton, J.C. (2018). *Streptococcus pneumoniae*: transmission, colonization and invasion. Nat. Rev. Microbiol. *16*, 355–367.

Windgassen, T.A., Wessel, S.R., Bhattacharyya, B., and Keck, J.L. (2018a). Mechanisms of bacterial DNA replication restart. Nucleic Acids Res. *46*, 504–519.

Windgassen, T.A., Leroux, M., Satyshur, K.A., Sandler, S.J., and Keck, J.L. (2018b). Structure-specific DNA replication-fork recognition directs helicase and replication restart activities of the PriA helicase. Proc. Natl. Acad. Sci. U. S. A. *115*, E9075–E9084.

Wold, S., Skarstad, K., Steen, H.B., Stokke, T., and Boye, E. (1994). The initiation mass for DNA replication in *Escherichia coli* K-12 is dependent on growth rate. EMBO J. *13*, 2097–2102.

Wu, L.J., and Errington, J. (2012). Nucleoid occlusion and bacterial cell division. Nat. Rev. Microbiol. *10*, 8–12.

Yang, X., Lyu, Z., Miguel, A., McQuillen, R., Huang, K.C., and Xiao, J. (2017). GTPase activity-coupled treadmilling of the bacterial tubulin FtsZ organizes septal cell wall synthesis. Science *355*, 744–747.

Zheng, H., Ho, P.-Y., Jiang, M., Tang, B., Liu, W., Li, D., Yu, X., Kleckner, N.E., Amir, A., and Liu, C. (2016). Interrogating the *Escherichia coli* cell cycle by cell dimension perturbations. Proc. Natl. Acad. Sci. U. S. A. *113*, 15000–15005.

2

HIGH-THROUGHPUT CRISPRI PHENOTYPING IDENTIFIES NEW ESSENTIAL GENES IN *STREPTOCOCCUS PNEUMONIAE*

Xue Liu, Clement Gallay, Morten Kjos, Arnau Domenech, Jelle Slager, Sebastiaan P. van Kessel, Kèvin Knoops, Robin A. Sorg, Jing-Ren Zhang and Jan-Willem Veening

Published in Molecular Systems Biology (2017) 13(5), 931. DOI 10.15252/msb.20167449.

This chapter was also part of the PhD thesis of Xue Liu.

C.G. aided in research design, constructed the strains and performed microscopy and immunoblot analysis to chracterize GatD, MurT, Tarp and TarQ, analyzed the data and co-wrote the paper.

Abstract

Genome-wide screens have discovered a large set of essential genes in the opportunistic human pathogen *Streptococcus pneumoniae*. However, the functions of many essential genes are still unknown, hampering vaccine development and drug discovery. Based on results from transposon-sequencing (Tn-seq), we refined the list of essential genes in *S. pneumoniae serotype* 2 strain D39. Next, we created a knockdown library targeting 348 potentially essential genes by CRISPR interference (CRISPRi) and show a growth phenotype for 254 of them (73%). Using high-content microscopy screening, we searched for essential genes of unknown function with clear phenotypes in cell morphology upon CRISPRi-based depletion. We show that SPD_1416 and SPD_1417 (renamed to MurT and GatD, respectively) are essential for peptidoglycan synthesis, and that SPD_1198 and SPD_1197 (renamed to TarP and TarQ, respectively) are responsible for the polymerization of teichoic acid (TA) precursors. This knowledge enabled us to reconstruct the unique pneumococcal TA biosynthetic pathway. CRISPRi was also employed to unravel the role of the essential Clp-proteolytic system in regulation of competence development and we show that ClpX is the essential ATPase responsible for ClpP-dependent repression of competence. The CRISPRi library provides a valuable tool for characterization of pneumococcal genes and pathways and revealed several promising antibiotic targets.

Introduction

Streptococcus pneumoniae (pneumococcus) is a major cause of community-acquired pneumonia, meningitis and acute otitis media and, despite the introduction of several vaccines, remains one of the leading bacterial causes of mortality worldwide (Prina *et al.*, 2015). The main antibiotics used to treat pneumococcal infections belong to the beta-lactam class, such as amino-penicillins (amoxicillin, ampicillin) and cephalosporines (cefotaxime). These antibiotics target the penicillin binding proteins (PBPs), which are responsible for the synthesis of peptidoglycan (PG) that plays a role in the maintenance of cell integrity, cell division and anchoring of surface proteins (Kocaoglu *et al.*, 2015; Sham *et al.*, 2012). The pneumococcal cell wall furthermore consists of teichoic acids (TA), which are anionic glycopolymers that are either anchored to the membrane (lipo TA) or covalently attached to PG (wall TA) and are essential for maintaining cell shape (Brown *et al.*, 2013; Massidda *et al.*, 2013). Unfortunately, resistance to most beta-lactam antibiotics remains alarmingly high. For example, penicillin non-susceptible pneumococcal strains colonizing the nasopharynx of children remains above 40% in the United States (Kaur *et al.*, 2016), despite the effect of the pneumococcal conjugate vaccines. Furthermore, multidrug resistance in *S. pneumoniae* is prevalent and antibiotic resistance determinants and virulence factors can readily transfer between strains via competence-dependent horizontal gene transfer (Chewapreecha *et al.*, 2014; Johnston *et al.*, 2014; Kim *et al.*, 2016). For these reasons, it is crucial to understand how competence is regulated and to identify and characterize new essential genes and pathways. Interestingly, not all proteins within the pneumococcal PG and TA biosynthesis pathways are known (Massidda *et al.*, 2013), leaving room for discovery of new potential antibiotic targets. For instance, not all enzymes in the biosynthetic route to lipid II, the precursor of PG, are known and annotated in *S. pneumoniae*. The pneumococcal TA biosynthetic pathway is even more enigmatic and it is unknown which genes code for the enzymes responsible for polymerizing TA precursors (Denapaite *et al.*, 2012).

Several studies using targeted gene knockout and depletion/overexpression techniques as well as transposon sequencing (Tn-seq), have aimed to identify the core pneumococcal genome (Mobegi *et al.*, 2014; Song *et al.*, 2005; Thanassi *et al.*, 2002; van Opijnen *et al.*, 2009; van Opijnen & Camilli, 2012; Verhagen *et al.*, 2014; Zomer *et al.*, 2012). These genome-wide studies revealed a core genome of around 400 genes essential for growth either in vitro or in vivo. Most of the essential pneumococcal genes can be assigned to a functional category on basis of sequence homology or experimental evidence. However, per the most recent gene annotation of the commonly used *S. pneumoniae* strain D39 (NCBI, CP000410.1, updated on 31-JAN-2015), approximately one third of the essential genes belong to the category of 'function unknown' or 'hypothetical' and it is likely that several unknown cell wall

synthesis genes, such as the TA polymerase, are present within this category.

To facilitate the high-throughput study of essential genes in *S. pneumoniae* on a genome-wide scale, we established CRISPRi (clustered regularly interspaced short palindromic repeats interference) for this organism. CRISPRi is based on expression of a nuclease-inactive *Streptococcus pyogenes* Cas9 (dCas9), which, together with expression of a single-guide RNA (sgRNA) targets the gene of interest (Bikard *et al.*, 2013; Peters *et al.*, 2016; Qi *et al.*, 2013). When targeting the non-template strand of a gene by complementary base-pairing of the sgRNA with the target DNA, the dCas9-sgRNA-DNA complex acts as a roadblock for RNA polymerase (RNAP) and thereby represses transcription of the target genes (Peters *et al.*, 2016; Qi *et al.*, 2013) (Fig. 1A). Note that *S. pneumoniae* does not contain an endogenous CRISPR/Cas system, consistent with interference with natural transformation and thereby lateral gene transfer that is crucial for pneumococcal host adaptation (Bikard *et al.*, 2012).

Using Tn-seq and CRISPRi, we refined the list of genes that are either essential for viability or for fitness in *S. pneumoniae* strain D39 (Avery *et al.*, 1944). To identify new genes involved in pneumococcal cell envelope homeostasis, we screened for essential genes of unknown function (as annotated in NCBI), with a clear morphological defect upon CRISPRi-based depletion. This identified SPD_1416 and SPD_1417 as essential peptidoglycan synthesis proteins (renamed to MurT and GatD, respectively) and SPD_1198 and SPD_1197 as essential proteins responsible for precursor polymerization in TA biosynthesis (hereafter called TarP and TarQ, respectively). Finally, we demonstrate the use of CRISPRi to unravel gene regulatory networks and show that ClpX is the ATPase subunit that acts together with the ClpP protease as a repressor for competence development.

Results

Identification of potentially essential genes in S. pneumoniae strain D39

While several previous studies have identified many pneumococcal genes that are likely to be essential, the precise contribution to pneumococcal biology has remained to be defined for most of these genes. Here, we aim to characterize the functions of these proteins in the commonly used *S. pneumoniae* serotype 2 strain D39 by the CRISPRi approach. Therefore, we performed Tn-seq on *S. pneumoniae* D39 grown in C+Y medium at 37ºC, our standard laboratory condition (see Materials and Methods). We included all genes that we found to be essential in our Tn-seq study, and added extra genes that were found to be essential by previous Tn-seq studies with a serotype 4 strain TIGR4 (van Opijnen *et al.*, 2009; van Opijnen & Camilli, 2012) in the CRISPRi library (see below). Finally, 391 potentially essential genes were selected, and the genes are listed in Dataset EV1.

CRISPRi enables tunable repression of gene transcription in S. pneumoniae

To develop the CRISPR interference system, we first engineered the commonly used LacI-based isopropyl β-D-1-thiogalactopyranoside (IPTG)-inducible system for *S. pneumoniae* (see Materials and Methods). The *dcas9* gene was placed under control of this new IPTG-inducible promoter, named $P_{lac'}$ and was integrated into the chromosome via double crossover (Fig. 1A and B). To confirm the reliability of the CRISPRi system, we tested it in a reporter strain expressing firefly luciferase (*luc*), in which an sgRNA targeting *luc* was placed under the constitutive *P3* promoter (Sorg *et al.*, 2015) and integrated at a non-essential locus (Fig. 1B). To obtain high efficiency of transcriptional repression, we used the optimized sgRNA sequence as reported previously (Chen *et al.*, 2013) (Fig. EV1A).

Induction of dCas9 with 1 mM IPTG resulted in quick reduction of luciferase activity; approximately 30-fold repression of luciferase expression was obtained within 2 hours without substantial impact on bacterial growth (Fig. 1C). Furthermore, the level of repression was tunable by using different concentrations of IPTG (Fig. 1C). To test the precision of CRISPRi in *S. pneumoniae*, we determined the transcriptome of the sgRNA*luc* strain (Strain XL28) by RNA-Seq in the presence or absence of IPTG. The data was analyzed using Rockhopper (McClure *et al.*, 2013) and T-REx (de Jong *et al.*, 2015). The RNA-Seq data showed that expression of dCas9 was stringently repressed by LacI without IPTG, and was upregulated ~600 fold upon addition of 1 mM IPTG after 2.5 hours. Upon dCas9 induction, the *luc* gene was significantly repressed (~84 fold) (Fig. 1D). Our RNA-Seq data showed that the genes (*spd_0424*, *spd_0425*, *lacE-1, lacG-1, lacF-1*) that are downstream of *luc*, which was driven by a strong constitutive promoter without terminator, were significantly repressed as

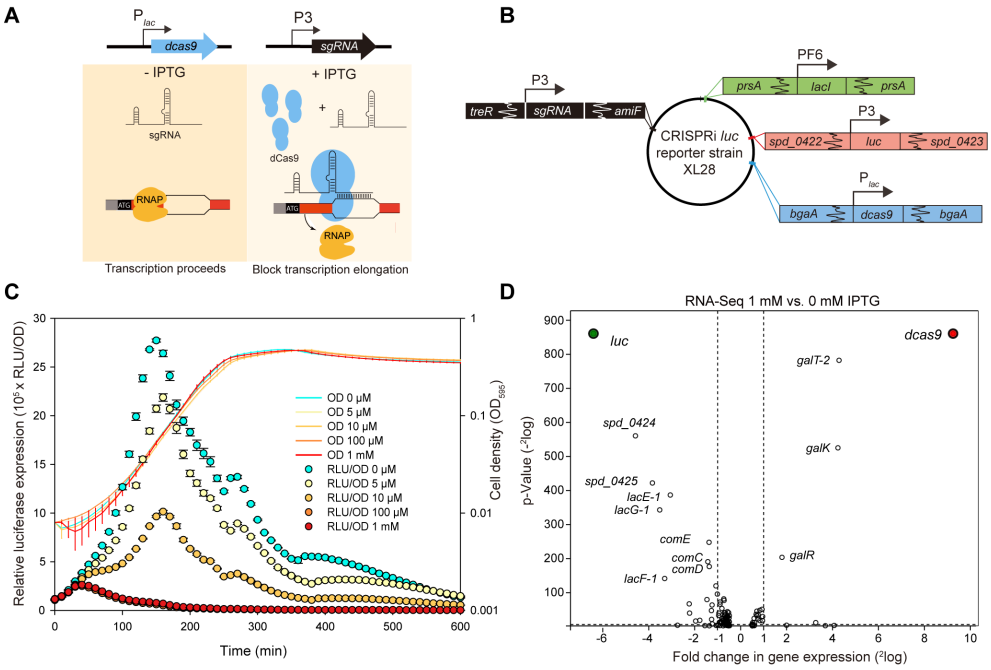

Figure 1. An IPTG-inducible CRISPRi system for tunable repression of gene expression in *S. pneumoniae*.

(**A**) *dcas9* and sgRNA sequences were chromosomally integrated at two different loci and expression was driven by an IPTG-inducible promoter (P_{lac}) and a constitutive promoter (*P3*), respectively. With addition of IPTG, dCas9 is expressed and guided to the target site by constitutively expressed sgRNA. Binding of dCas9 to the 5′ end of the coding sequence of its target gene blocks transcription elongation. In the absence of IPTG, expression of dCas9 is tightly repressed, and transcription of the target gene can proceed smoothly. (**B**) Genetic map of CRISPRi *luc* reporter strain XL28. To allow IPTG-inducible expression, the *lacI* gene, driven by the constitutive *PF6* promoter, was inserted at the non-essential *prsA* locus; *luc*, encoding firefly luciferase, driven by the constitutive *P3* promoter was inserted into the intergenic sequence between gene loci *spd_0422* and *spd_0423*; *dcas9* driven by the IPTG-inducible P_{lac} promoter was inserted into the *bgaA* locus; sgRNA-*luc* driven by the constitutive *P3* promoter was inserted into the CEP locus (between *treR* and *amiF*). (**C**) The CRISPRi system was tested in the luc reporter strain XL28. Expression of dCas9 was induced by addition of different concentrations of IPTG. Cell density (OD_{595}) and luciferase activity (shown as RLU/OD) of the bacterial cultures were measured every 10 minutes. The value represents averages of three replicates with SEM. (**D**) RNA-Seq confirms the specificity of the CRISPRi system in *S. pneumoniae*. RNA sequencing was performed on the *luc* reporter strain XL28 (panel B) with or without 1 mM IPTG. The *dcas9* and *luc* genes are highlighted. Data were analyzed with T-REx and plotted as a Volcano plot. *P*-value equals 0.05 is represented by the horizontal dotted line. Two vertical dotted lines mark the 2-fold changes.

well (Appendix Fig. S1A). This confirms the reported polar effect of CRISPRi (Qi *et al.*, 2013). In addition, induction of dCas9 in the sgRNA-deficient strain XL29 (Fig. EV1B) led to no repression of the target gene (Fig. EV1C). By comparing strains with or without sgRNA*luc*, we found that repression in our CRISPRi system is stringently dependent on expression of both dCas9 and the sgRNA, and detected no basal level repression (Fig. EV1C). Furthermore, we compared the transcriptome of *luc* reporter

strains with sgRNA*luc* (strain XL28) and without sgRNA*luc* (strain XL29) both grown in the presence of 1 mM IPTG. This showed that *galT-2, galK* and *galR* were upregulated in both strains indicating that these genes are activated in response to the inducer IPTG and not by the CRISPRi system itself (Dataset EV2). We also noted a slight repression of several competence genes in both XL28 and XL29 with 1 mM IPTG (Dataset EV2). Since this repression does not rely on the presence of a functional CRISPRi system, we anticipate that these changes are due to the noisy character of the competence system (Aprianto *et al.*, 2016; Prudhomme *et al.*, 2016). Taken together, the IPTG-inducible CRISPRi system is highly specific.

Construction and growth analysis of the CRISPRi library

We next used the CRISPRi system to construct an expression knock-down library of pneumococcal essential genes. An sgRNA to each of the 391 potentially essential genes was designed as described previously (Larson *et al.*, 2013) (Dataset EV3). Based on the sgRNA*luc* plasmid (Fig. 2A), we tested two different cloning strategies to introduce the unique 20-nt base-pairing region for each gene: infusion cloning and inverse PCR (Irwin *et al.*, 2012; Larson *et al.*, 2013; Ochman *et al.*, 1988) (Fig. EV2A). For infusion cloning, we synthesized two complementary primers consisting of the 20-nt base-pairing region flanked by 15-nt overlap sequences. The two complementary primers were then annealed to form a duplex DNA fragment and cloned into the vector by the infusion reaction, followed by direct transformation into *S. pneumoniae* D39. With inverse PCR, we used a phosphorylated universal primer, together with a gene specific primer to fuse the 20-nt base pairing region into the vector by PCR, followed by blunt-end ligation and direct transformation into *S. pneumoniae* D39 strain DCI23. We compared the efficiency of the two methods by creating sgRNA strains targeting the known essential gene *folA* (*spd_1401*). Depletion of *folA* causes a clear growth defect which could thus be used to test the functionality of sgRNA*folA* in transformants. We found that 79 % of the transformants produced by infusion cloning had a growth defect upon dCas9 induction with IPTG (38 out of 48 colonies), whereas 26 % of the transformants generated by inverse PCR showed a phenotype (12/46). Sequencing validated that transformants with a growth defect contained the correct sgRNA sequence. Considering the convenience and efficiency, we adopted the infusion cloning strategy for sgRNA cloning in this study. All sgRNA constructs were sequence verified, and we considered them genetically functional when the sgRNA did not contain more than 1 mismatch to the designed sgRNA and no mismatches in the first 14-nt prior to the PAM. Using this approach, after a single round of cloning and sequencing, we successfully constructed 348 unique sgRNA strains (see Materials and Methods). Note that we are still in the process of constructing the remaining 43 sgRNA strains, the failure of which is likely caused by technical reasons (*e.g.*, incorrect oligonucleotides, poor oligo annealing, low transformation, *etc*.).

To examine the effects of CRISPRi-based gene silencing, growth was assayed both in the presence and absence of 1 mM IPTG for 18 hours in real-time by microtiterplate assays. Two types of growth phenotypes were defined and identified: a growth defect and increased lysis (Figs EV2B-E). As shown in Fig. 2B, CRISPRi-based repression of transcription led to a growth defect in 230 genes, 48 genes showed increased lysis, including 24 that demonstrated both a growth defect and increased lysis, and 94 genes showed no defect (see Dataset EV1). In total, 254 out of 348 target genes (about 73%) repressed by CRISPRi showed growth phenotypes. Comparing the optical densities between the uninduced and induced cells at the time point at which

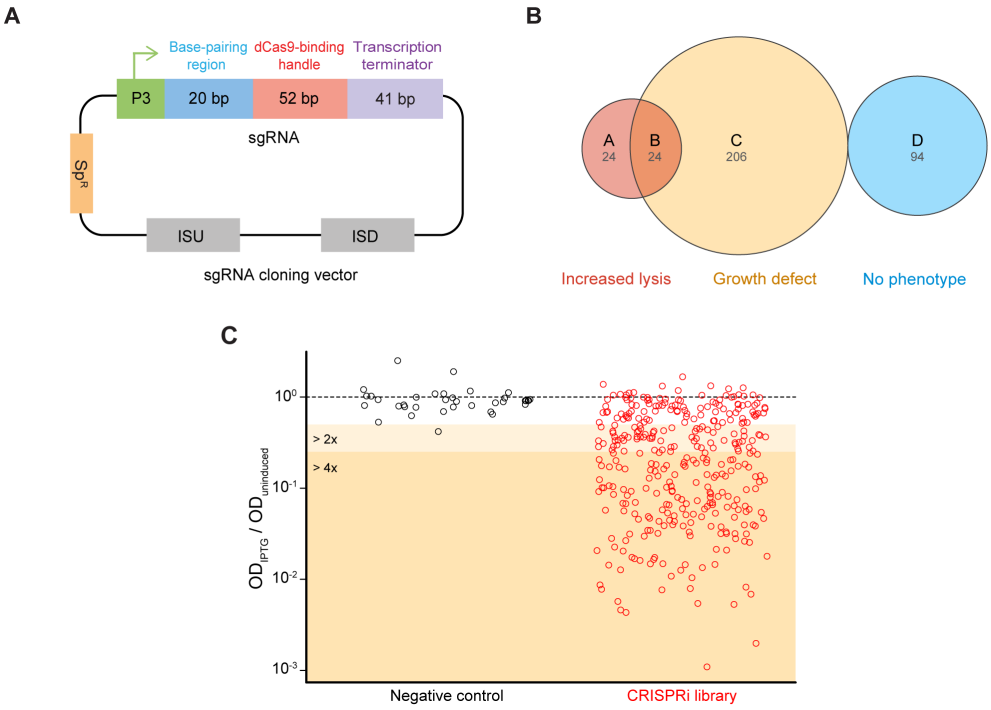

Figure 2. Construction and growth analysis of the CRISPRi library.

(**A**) The plasmid map of the sgRNA cloning vector (pPEPX-*P3*-sgRNA*luc*). The sgRNA expression vector is a *S. pneumoniae* integration vector. It contains a constitutive *P3* promoter, a spectinomycin-selectable marker (Sp^R), two homology sequences (ISU and ISD) for double crossover integration at the CEP locus (Sorg *et al.*, 2015), and the sgRNA sequence. The sgRNA chimera contains a base-pairing region (blue), dCas9-binding handle (red) and the *S. pyogenes* transcription terminator (purple). (**B**) and (**C**) Growth analysis of the whole library. (**B**) Classification of the 348 genes targeted by the CRISPRi library according to growth analysis. Criteria for determination of a growth defect and increased lysis is demonstrated in Fig. EV2B-E. (**C**) Comparison of the OD_{595} of IPTG-induced cells (OD_{IPTG}) to the OD_{595} of uninduced cells ($OD_{uninduced}$) at a timepoint. The timepoint at which uninduced cells have an Optical Density (595 nm) closest to 0.1 was selected for the plotting. Y-axis represents the value of OD_{IPTG} divided by $OD_{uninduced}$. The red data points in the dark orange area (174/348 strains) correspond to strains displaying a strong growth defect (more than 4-fold); points in the light orange area demonstrate a moderate growth defect of 2- to 4-fold (71/348 strains). The same type of analysis was performed on 36 negative control strains, shown as the black data points.

uninduced cells reached an OD_{595} of ~0.1, 174 genes repressed by CRISPRi displayed a more than 4-fold growth defect, and 254 genes showed a more than 2-fold growth defect (Fig. 2C). To further validate the specificity of the CRISPRi system, CRISPRi strains targeting 8 genes identified as essential and 8 genes as dispensable by Tn-seq were included in the growth analysis. The selected dispensable genes are present as a monocistron or are in an operon with other non-essential genes. As shown in Fig. EV3A, no apparent growth defects could be observed when these non-essential genes were targeted by CRISPRi while repression of essential genes led to strong growth defects (Fig. EV3B).

It should be noted that CRISPRi repression of dispensable genes that are cotranscribed with essential genes can lead to growth phenotypes (Appendix Fig. S1), which is due to polar effect of CRISPRi system (Qi *et al.*, 2013). Thus, some of the genes may be targeted multiple times in the CRISPRi library (in case of more than one essential gene within the operon). We also observed that after a lag phase, most CRISPRi knockdowns with growth phenotypes eventually grow out to the same final OD (Figure EV4A). Re-culturing these cells showed the absence of sensitivity to IPTG, indicative of the presence of suppressor mutations (Fig. EV4A). Indeed, by sequencing the two key elements of the CRISPRi system, the sgRNA and *dcas9*, we found that most of the suppressor strains contain loss-of-function mutation in the dcas9 coding sequence (Fig. EV4B). This is similar to observations made for the CRISPRi system in *Bacillus subtilis* (Zhao *et al.*, 2016).

Phenotyping pneumococcal genes by combined CRISPRi and high-content microscopy

To test whether CRISPRi was able to place genes in a functional category and thereby allow us to identify previously uncharacterized genes with a function in cell envelope homeostasis, we first analyzed the effects of CRISPRi-based repression on cell morphology using 68 genes. These genes were selected as they represent different functional pathways and have been identified as essential or crucial for normal pneumococcal growth by Tn-seq studies (van Opijnen *et al.*, 2009; van Opijnen & Camilli, 2012) and by displaying strong growth phenotypes in our CRISPRi assay (Fig. 2B-C). The selected genes have been associated with capsule synthesis (3 genes), transcription (4 genes), cell division (6 genes), translation (7 genes), teichoic acid biosynthesis (9 genes), cell membrane synthesis (11 genes), chromosome biology (14 genes), and peptidoglycan synthesis (14 genes) (Table 1). High-content microscopy of the CRISPRi knockdowns showed a good correlation between reported gene function and observed phenotype. The common features of the morphological changes caused by CRISPRi repression of genes belonging to the same functional categories are summarized in Table 1. Growth analysis and microscopy phenotyping

of a representative gene of each pathway, CRISPRi repression of which showed typical morphological changes of its pathway, were included in Fig. 3. Morphological changes of CRISPRi repression of the other genes of the pathways are shown in Appendix Fig. S2-S9. For instance, compared with the control strain (Fig. 3, XL28), repression of transcription of genes involved in chromosome biology caused, as expected, appearance of anucleate cells or cells with aberrant chromosomes (Fig. 3, dnaA; Appendix Fig. S2). Cells with repression of genes involved in transcription showed a significant growth defect, no obvious morphological changes were observed (Fig. 3, *rpoC*; Appendix Fig. S3). Repression of genes involved in translation showed heterogeneous cell shapes and condensed nucleoids (Fig. 3, infC; Appendix Fig. S4), in line with our previous observations (Sorg & Veening, 2015) and observations made in *E. coli* showing that inhibition of protein synthesis by antibiotics leads to nucleoid condensation (Morgan *et al.*, 1967; Roggiani & Goulian, 2015; Zusman *et al.*, 1973).

In *S. pneumoniae*, the fatty acid biosynthesis genes are all located in a single cluster (Lu & Rock, 2006) (Appendix Fig. S5A), and two promoters in front of *fabT* and *fabK* are regulated by the transcriptional repressor FabT (Jerga & Rock, 2009). It was shown that *fabT* and *fabH* are cotranscribed (Lu & Rock, 2006), but the transcription pattern of the other genes is still unknown, which makes functional study of these genes with CRISPRi very difficult due to polar effect of the block of transcription elongation (Qi *et al.*, 2013). Nevertheless, repression of transcription of genes involved in cell membrane synthesis caused diverse patterns of morphological changes: repression of *fabH, acpP, fabK*, *fabD* and *fabG* led to a spotty nile red pattern and irregular cell shapes including more pointy cells (Fig. 3, *fabK*; Appendix Fig. S5B), as was shown previously (Kuipers *et al.*, 2016); repression of *fabF, accB, fabZ* and *accD* led to chaining of cells, heterogeneous cell sizes and irregular cell shapes; repression of *acpS* resulted in elongated and enlarged cells, whereas repression of *cdsA* caused cell rounding with heterogeneous cell sizes (Appendix Fig. S5B).

When transcription of genes involved in cell division was repressed, we observed cells with irregular shapes and heterogeneous sizes (Appendix Fig. S6). Interestingly, repression of *ftsZ* and *ftsL* caused similar morphological changes (Fig. 3, *ftsZ*; Appendix Fig. S6), consistent with the reported function of FtsL on regulating FtsZ ring (Z-ring) dynamics in *B. subtilis* (Kawai & Ogasawara, 2006). Cells with repression of *ezrA* formed twisting chains, and contained multiple septa, some of which formed at cell poles instead of midcell. Indeed, it was reported that *B. subtilis* EzrA can modulate the frequency and position of the Z-ring formation (Chung *et al.*, 2004). Repression of genes involved in capsule synthesis caused aggregation of cells (Appendix Fig. S7), which may be due to the reduction of the negatively charged capsule that can provide a repelling electrostatic force preventing cell aggregation (Li *et al.*, 2013).

Table 1. Cellular pathways selected for CRISPRi phenotyping.

Pathway	Phenotype	Gene[a]
Chromosome replication	Anucleate cells; Longer chains; Uneven distribution of chromosomes; heterogeneous cell size	***dnaA (SPD_0001)*** *dnaN* (*SPD_0002*) *gyrB* (*SPD_0709*) *parE* (*SPD_0746*) *parC* (*SPD_0748*) *dnaX* (*SPD_0760*) *ftsK* (*SPD_0774*) *dnaG* (*SPD_0957*) *xerS* (*SPD_1023*) *gyrA* (*SPD_1077*) *dnaI* (*SPD_1521*) *priA* (*SPD_1546*) *parB* (*SPD_2069*) *dnaC* (*SPD_2030*)
Transcription	No strong morphological phenotype	*rpoA* (*SPD_0218*) *rpoD* (*SPD_0958*) ***rpoC (SPD_1758)*** *rpoB* (*SPD_1759*)
Translation	Condensed nucleoids; Short cells; Heterogeneous cell size	*rpsJ* (*SPD_0192*) *rplD* (*SPD_0194*) *rplV* (*SPD_0198*) *rpsC* (*SPD_0199*) *efp* (*SPD_0395*) ***infC (SPD_0847)*** *tsf* (*SPD_2041*)
Cell membrane biosynthesis	Spotty membrane staining; Irregular cell shape; Heterogeneous cell size	*cdsA* (*SPD_0244*) *fabH* (*SPD_0380*) *acpP* (*SPD_0381*) ***fabK (SPD_0382)*** *fabD* (*SPD_0383*) *fabG* (*SPD_0384*) *fabF* (*SPD_0385*) *accB* (*SPD_0386*) *fabZ* (*SPD_0387*) *accD* (*SPD_0389*) *acpS* (*SPD_1509*)

Table 1. Continued

Pathway	Phenotype	Gene[a]
Cell division	Exploding cells; Heterogeneous cell size; Defective septa; Twisting chains	*ftsL (SPD_0305)* *gpsB (SPD_0339)* *ftsE (SPD_0659)* *ftsX (SPD_0660)* *ezrA (SPD_0710)* ***ftsZ (SPD_1479)***
Capsule synthesis	Cell aggregation; Heterogeneous cell size	*cps2E* (*SPD_0319*) *cps2I* (*SPD_0324*) *cps2L* (*SPD_0328*)
Peptidoglycan biosynthesis	Heterogeneous cell size; Coccus-to-rod transition; Round cells; Elongated cells; Enlarged cells: Defective septa	*uppS* (*SPD_0243*) ***pbp2X (SPD_0306)*** *mraY* (*SPD_0307*) *uppP* (*SPD_0417*) *murD* (*SPD_0598*) *murG* (*SPD_0599*) *rodA* (*SPD_0706*) *glmU* (*SPD_0874*) *ftsW* (*SPD_0952*) *murE* (*SPD_1359*) *murF* (*SPD_1483*) *ddl* (*SPD_1484*) *alr* (*SPD_1508*) *murI* (*SPD_1661*)
Techoic acid biosynthesis	Longer chains; Elongated cells; Enlarged cells; Heterogeneous cell size; Defective septa	*SPD_0099* *licC* (*SPD_1123*) *licB* (*SPD_1124*) *licA* (*SPD_1125*) *tarJ* (*SPD_1126*) *tarI* (*SPD_1127*) *SPD_1200* ***licD3 (SPD_1201)*** *SPD_1620*

[a] The genes highlighted in bold were included in Fig. 3.

Repression of transcription of genes involved in cell wall synthesis caused different phenotypes, depending on which step in peptidoglycan synthesis was interrupted. *S. pneumoniae* is oval-shaped, and it displays both septal and peripheral growth (Massidda *et al.*, 2013; Pinho *et al.*, 2013). Peptidoglycan synthesis of *S. pneumoniae* starts from formation of UDP-MurNAc-pentapeptides. Repression of expression of genes playing roles in these very first steps, including *glmU, alr, ddl, murI, murC, murD, murE,* and *murF*, will block both septal and peripheral peptidoglycan synthesis. Consistent with this prediction, we observed severe changes in cell shape and size, including heterogeneous cell sizes, exploding cells, defective septa, round cells and cells demonstrating a coccus-to-rod transition (Appendix Fig. S8). MraY and MurG play roles in formation of lipid II, and they are thus also involved in both peripheral and septal peptidoglycan synthesis. CRISPRi strains repressing *mraY* or *murG* led to a mix of elongated cells and short cells (Appendix Fig. S8). FtsW and RodA are members of SEDS (shape, elongation, division and sporulation) proteins (Meeske *et al.*, 2016), and were first identified in *E. coli* (Ikeda *et al.*, 1989). Inactivation of FtsW in *E. coli* blocks cell division without an effect on cell elongation (Khattar *et al.*, 1994), and FtsW is suggested to act as a lipid II flippase (Mohammadi *et al.*, 2011). FtsW of *S. pneumoniae* was believed to have a conserved function with *E. coli* (Maggi *et al.*, 2008), and is co-localized with septal HMW (high molecular weight) PBPs (Morlot *et al.*, 2004), and is thus predicted to be involved in septal peptidoglycan synthesis. By morphological analysis, we provided experimental evidence to support this prediction: FtsW and Pbp2X are responsible for septal peptidoglycan synthesis, and elongated cells and coccus-to-rod transition were observed with CRISPRi repression of *ftsW* or *pbp2X* (Fig. 3, *pbp2X*; Appendix Fig. S8, *ftsW*). RodA of *S. pneumoniae* shows 26 % identity with RodA of *E. coli* (Noirclerc-Savoye *et al.*, 2003), which is required for cell elongation. Studies of RodA in *B. subtilis* also support its function on elongation of the lateral wall (Henriques *et al.*, 1998; Meeske *et al.*, 2016). RodA of *S. pneumoniae* was predicted to be a lipid II flippase responsible for peripheral peptidoglycan synthesis (Massidda *et al.*, 2013). *S. pneumoniae* cells with repressed *rodA* expression by CRISPRi are consistently shorter (Appendix Fig. S8), indicating a defect in cell elongation.

Repression of genes involved in teichoic acid (TA) biosynthesis led to morphological changes, including formation of longer chains and cells of heterogeneous sizes, mostly enlarged or elongated (Fig. 3, *licD3*; Appendix Fig. S9). Growth of *S. pneumoniae* depends on exogenous choline, which is an essential molecule for the synthesis of pneumococcal TA, and the chaining phenotype caused by repression of genes involved in TA synthesis is in line with *S. pneumoniae* growing in medium without choline (Damjanovic *et al.*, 2007).

In summary, by morphological analysis of CRISPRi strains for repression of transcription of genes with known function from different pathways, we established links between genotypes and phenotypes. Importantly, repression of transcription of genes known to be involved in cell envelope homeostasis such as *ftsZ, ftsL, ftsW, rodA, pbp2X, glmU, murC, murF, tarI, tarJ, licA, licB, licC* and *licD3*, caused severe changes in cell shape and size, including heterogeneous cell size, ballooning cells, defective septa, short cells, round cells, cells in chains and cells demonstrating a coccus-to-rod transition. These observations provide a useful platform for the functional identification of hypothetical genes, especially genes involved in cell envelope homeostasis.

Functional verification and annotation of pcsB (spd_2043), vicR (spd_1085), divIC (spd_0008) and rafX (spd_1672)

We next analyzed 44 strains in the CRISPRi library that target genes that are annotated as hypothetical in the *S. pneumoniae* D39 genome in the NCBI database (CP000410.1, updated on 31-JAN-2015). From this approach, we were able to verify the function and annotate several genes, whose function had been studied in pneumococci before but have not been properly annotated in the D39 genome. For example, repression of genes (*spd_0008, spd_1085* and *spd_2043*) led to significant growth defects and cell shape and cell size changes (Appendix Fig. S11A and B). Knocking down *spd_2043* and *spd_1085* led to almost the same morphological changes, which included irregular cell shape, heterogeneous cell sizes, and appearance of ballooned cells, suggesting that these two genes might be functionally associated and play roles in peptidoglycan synthesis or cell division. By literature mining and BLAST searches, we recognized *spd_1085* as *vicR* and *spd_2043* as *pcsB* (Ng *et al.*, 2003). Consistent with the observed phenotypes in the CRISPRi strains, *pcsB* was shown to be essential for cell wall separation and its expression relies on the response regulator encoded by *vicR* (Bartual *et al.*, 2014; Ng *et al.*, 2003; Reinscheid *et al.*, 2001; Sham *et al.*, 2011). Similarly, the morphological changes suggested a potential role of SPD_0008 in cell wall synthesis or cell division.In line with this, SPD_0008 was identified as DivIC, which was reported to form a trimeric complex with DivIB and FtsL and colocalized at division sites of *S. pneumoniae* strain R6 (Noirclerc-Savoye *et al.*, 2005).

CRISPRi knockdown strain targeting *spd_1672* showed no significant growth defect at exponential phase, but cells lysed quicker in the stationary phase (Appendix Fig. S11C). Microscopy showed that bacterial cells with CRISPRi-repressed *spd_1672* formed significantly longer chains (Appendix Fig. S11D). Chained cells displayed irregular shapes and heterogeneous cell sizes. These phenotypes are very similar to the morphological changes caused by repression of genes involved in the biosynthesis of teichoic acid (Appendix Fig. S9). Actually, *spd_1672* has been studied

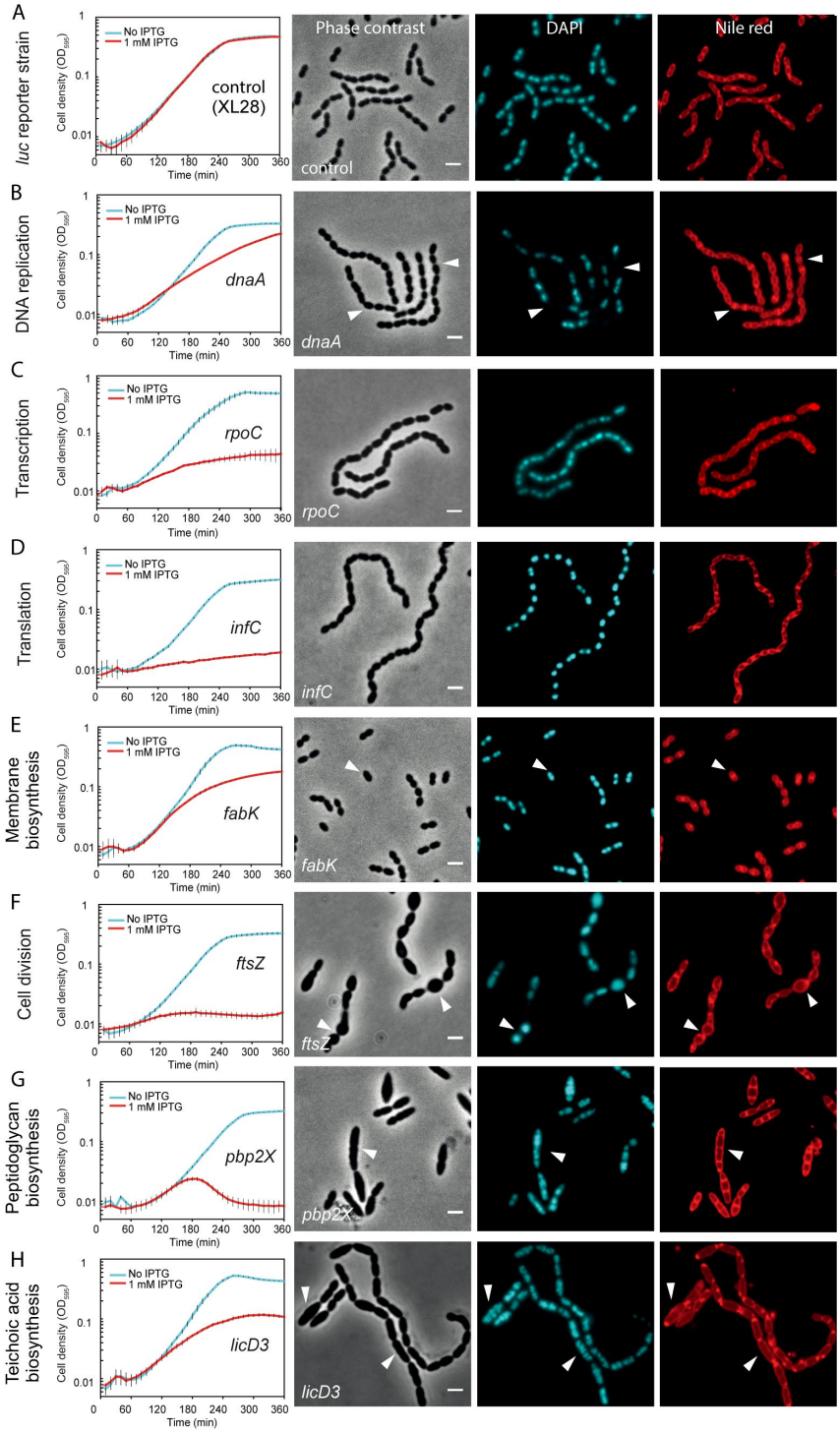
A
luc reporter strain
control (XL28)
No IPTG
1 mM IPTG
Cell density (OD600)
Time (min)
Phase contrast
DAPI
Nile red
control
B
DNA replication
dnaA
C
Transcription
rpoC
D
Translation
infC
E
Membrane biosynthesis
fabK
F
Cell division
ftsZ
G
Peptidoglycan biosynthesis
pbp2X
H
Teichoic acid biosynthesis
licD3

Figure 3. Growth profiles and morphological changes of CRISPRi strains with sgRNA targeting genes of different functional pathways

(**A**-**H**) Growth of S. *pneumoniae* strains was performed in C+Y medium with (red) or without (cyan) 1 mM IPTG. Cell densities were measured every 10 min. The values represent averages of three replicates with SEM. Morphological changes were examined by fluorescence microscopy, and representative micrographs are shown. Phase contrast, DAPI staining, and Nile red staining are displayed. Scale bars = 2 μm. *Streptococcus pneumoniae* D39 reporter strain XL28 expresses firefly luciferase (*luc*) from a constitutive promoter and contains an sgRNA targeting the *luc* gene, and serves as a control strain without growth defects. White arrows point to specific (morphological) changes. For *dnaA*, arrows point to anucleate cells (**B**); *fabK*, non-uniform, spotty membrane staining (**E**); *ftsZ*, ballooning cells (**F**); *pbp2X*, elongated cells (**G**); *licD3*, elongated and enlarged cells (**H**) Repression of a transcription-related gene, *rpoC*, no strong morphological changes were observed (**C**); a translation-related gene, *infC*, led to generally condensed chromosomes as shown in the DAPI staining image (**D**) One gene of each pathway was presented in this figure. Additional information related to this figure can be found in Table 1 and Appendix Figs S2–S9, which show microscopy images of more genes of each pathway.

in *S. pneumoniae* R6 and was shown to contribute to the biosynthesis of wall teichoic acid and was named *rafX* (Wu *et al.*, 2014). The reported *spd_1672* knockout strain of *S. pneumoniae* R6 also displayed a reduced stationary phase with similar cell shape and cell size defects. Inconsistent with our study, longer chains were not observed by TEM (Transmission Electron Microscopy) imaging in the Wu *et al.* study. To exclude the possible polar effect of CRISPRi repression, we made a *spd_1672* knockout in *S. pneumoniae* D39, and the *spd_1672* knockout strain also showed longer chains. Thus, the mismatch in phenotypes between the studies may be due to the different genetic background of *S. pneumoniae* D39 and R6, or may be caused by the process of sample preparation for TEM examination.

Annotation and characterization of chromosome replication genes dnaB (spd_1522), dnaD (spd_1405) and yabA (spd_0827)

High-content microscopy screening of the CRISPRi library showed that repression of *spd_1405*, *spd_1522* and *spd_0827* led to significant growth defects and generation of anucleate cells (Appendix Fig. S10). Appearance of anucleate cells is an important sign of a defect in chromosome biology, thus suggesting that these three genes are involved in chromosome replication or segregation. SPD_0827 shows 33 % identity with initiation control protein YabA of *B. subtilis*, which interacts with DnaN and DnaA, and acts as a negative regulator of replication initiation (Goranov *et al.*, 2009; Noirot-Gros *et al.*, 2002). We thus named SPD_0827 to YabA. To test the function of *yabA* in *S. pneumoniae*, a deletion mutant was made by erythromycin marker replacement. The *yabA* deletion (Δ*yabA*) showed a significantly reduced growth rate compared to the wild type (Appendix Fig. S12A), and displayed longer chains with frequent anucleate cells (Appendix Fig. S12C). To test whether *S. pneumoniae* YabA is also a negative regulator of initiation of DNA replication, we determined the *oriC*-*ter* ratio using real-time quantitative PCR (qPCR). As shown in Appendix Fig. S12D, the

oriC-ter ratio was significantly higher in Δ*yabA* indicative of over-initiation, strongly suggesting a similar function as *B. subtilis* YabA.

When making a list of known genes involved in pneumococcal chromosome biology (Table 1), we noticed that *dnaB* and *dnaD*, two known bacterial DNA replication proteins (Briggs *et al.*, 2012; Smits *et al.*, 2011), were not annotated in *S. pneumoniae* D39. BlastP analyses showed that *spd_1405* and *spd_1522* might be coding for DnaD and DnaB, respectively. SPD_1405 showed 30 % identity with DnaD of *B. subtilis*, and thus we named *spd_1405* to *dnaD*. SPD_1522 has 389 amino acids (aa), and the N-terminal 1-149 aa-long domain showed 19.8 % identity with domain I of DnaB of *B. subtilis*, whereas aa 206-379 showed 45.7 % identity with domain II. DnaB of *B. subtilis* (472 aa) is longer than SPD_1522 of *S. pneumoniae* D39 (389 aa), because the former contains a degenerated middle DDBH2 domain (Briggs *et al.*, 2012). Additionally, the arrangement of the neighboring genes of *S. pneumoniae dnaB* (*spd_1522*), *dnaI* and *nrdR* is the same in *B. subtilis*. Based on these observations, we named *spd_1522* to *dnaB*.

It was reported that DnaD and DnaB are recruited to the chromosome by DnaA and play important roles in chromosome replication initiation in *B. subtilis* (Smits *et al.*, 2011). To test the function of *S. pneumoniae* DnaD and DnaB, we constructed Zn^{2+}-inducible depletion strains (*P_{Zn}-dnaD; P_{Zn}-dnaB*), because efforts to make deletion mutants failed. In the absence of 0.1 mM Zn^{2+}, the depletion strains showed significant growth defects (Appendix Fig. S12A), confirming their essentiality. If DnaB and DnaD indeed play a role in replication initiation, repression of them should lead to a decrease in the *oriC-ter* ratio. Indeed, the *oriC-ter* ratio of cells in absence of Zn^{2+} was significantly lower than in the presence of Zn^{2+} (Appendix Fig. S12D). Together, we identified and annotated *yabA*, *dnaD* and *dnaB* and confirmed their function in pneumococcal DNA replication.

SPD_1416 and SPD_1417 are involved in peptidoglycan precursor synthesis

We found that CRISPRi strains with sgRNA targeting hypothetical genes *spd_1416* or *spd_1417* showed significant growth retardation and morphological abnormality, such as heterogeneous cell size and elongated and enlarged cells with multiple incomplete septa (Appendix Fig. S10). These manifestations mirrored what we observed upon inhibiting the expression of genes known to be involved in peptidoglycan (PG) synthesis (Appendix Fig. S8). Consistent with the essentiality of these two genes as suggested by Tn-seq, we were unable to obtain deletion mutants of *spd_1416* or *spd_1417* after multiple attempts. To confirm that these genes are essential for pneumococcal growth, we constructed merodiploid strains of *spd_1416* and *spd_1417* by inserting a second copy of each gene fused to *gfp* (encoding a monomeric superfolder GFP) at their N-terminus (referred as *gfp-*

spd_1416 or *gfp-spd_1417*) or C-terminus (referred as *spd_1416-gfp* or *spd_1417-gfp*). These gfp-fusions were integrated at the ectopic *bgaA* locus under the control of the zinc-inducible promoter, P_{Zn}. In the presence of Zn^{2+}, we could delete the native *spd_1416* or *spd_1417* gene by allelic replacement in the P_{Zn}*-gfp-spd_1417* or P_{Zn}*-gfp-spd_1416* genetic background. When transforming in the P_{Zn}*-spd_1417-gfp* genetic background, we did not obtain erythromycin resistant colonies, indicating that the C-terminal GFP fusion of SPD_1417 is not functional. Note that we could not replace *spd_1416* or *spd_1417* in the wild type in the presence of Zn^{2+}. While both the *spd_1416* and *spd_1417* mutants behaved normally in the presence of Zn^{2+}, severe growth retardation was observed in the absence of Zn^{2+} (Fig. 4A). Together, these lines of evidence demonstrate that both *spd_1416* and *spd_1417* are essential genes.

Morphological analysis by light microscopy of bacterial cells upon depletion of *gfp-spd_1416* or *gfp-spd_1417* confirmed the morphological changes as observed in the CRISPRi knockdowns (Fig. 4B). The *gfp-spd_1416* or *gfp-spd_1417* cells were further analyzed using freeze-substitution electron microscopy (Fig. 4C). This showed the presence of elongated cells and the frequent formation of multiple septa per cell, in contrast to wild type D39 cells which showed the typical diplococcal shape. Note that the mild sample preparation used in our freeze-substitution EM protocol also preserved the capsule, which can be readily lost during traditional EM sample preparation (Hammerschmidt *et al.*, 2005). BlastP analysis shows that SPD_1416 contains a Mur-ligase domain with 36 % sequence identity with MurT of *Staphylococcus aureus*, whereas SPD_1417 possesses a glutamine amidotransferase domain with 40 % sequence identity with GatD of *S. aureus*. MurT and GatD, two proteins involved in staphylococcal cell wall synthesis (Figueiredo *et al.*, 2012; Munch *et al.*, 2012), form a complex to perform the amidation of the D-glutamic acid in the stem peptide of PG. It was previously reported that recombinant MurT/GatD of *S. pneumoniae* R6, purified from *Escherichia coli*, indeed can amidate glutamate lipid II into iso-glutamine lipid II *in vitro* (Zapun *et al.*, 2013). Therefore, we named *spd_1416* to *murT* and *spd_1417* to *gatD*. It is interesting to note that while MurT or GatD depletion strains in *S. aureus* showed reduced growth, cells exhibited normal cell morphologies (Figueiredo *et al.*, 2012), in contrast to the strong morphological defects observed in *S. pneumoniae* D39.

MurT and GatD contain no membrane domain or signal peptide, and are thus predicted to be cytoplasmic proteins. However, fluorescence microcopy of the N-terminal GFP fused to MurT or GatD showed that they are partially membrane localized (Fig. 4D). In-gel fluorescence imaging showed that GFP-MurT and GFP-GatD were correctly expressed without any detectable proteolytic cleavage (Appendix Fig. S13). Since *in vitro* assays demonstrated that glutamate lipid II, which is anchored to the membrane by the bactoprenol hydrocarbon chain of lipid II, is a substrate of the

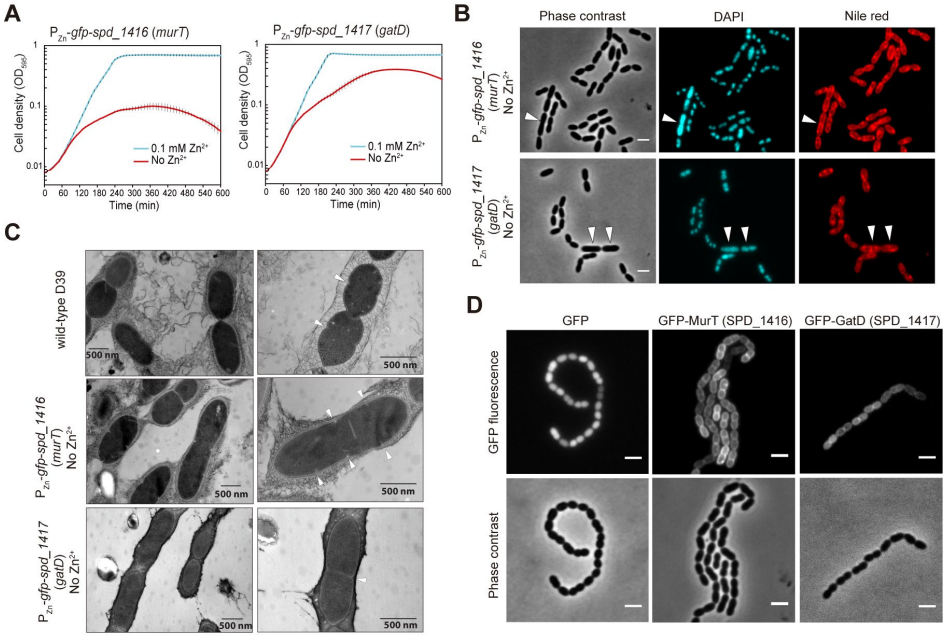

Figure 4. Identification of peptidoglycan synthesis genes *spd_1416* (*murT*) and *spd_1417* (*gatD*).

(**A**) Growth curves of depletion strains P_{Zn}-*gfp-spd_1416* (*murT*) and P_{Zn}-*gfp-spd_1417* (*gatD*), in C+Y medium with (cyan) or without (red) 0.1 mM Zn^{2+}. The value represents averages of three replicates with SEM. (**B**) Microscopy of cells from panel A after incubating in C+Y medium without Zn^{2+} for 2.5 hours. Representative micrographs of phase contrast, DAPI, and nile red are shown. Scale bar = 2 µm. White arrows point to elongated and enlarged cells. (**C**) Electron micrographs of the same samples as in panel (**B**) and wild-type *S. pneumoniae* D39 as reference. Note that depletion of *spd_1416* or *spd_1417* resulted in elongated cells. Septa are pointed with white arrows. (**D**) Localization of GFP-MurT and GFP-GatD. Micrographs of GFP signal (upper panel) and phase contrast (lower panel) are shown. Scale bar = 2 µm. *S. pneumoniae* D39 with free GFP showing cytoplasmic localization was included as reference.

MurT/GatD amidotransferase complex, it is reasonable to assume that membrane localization of MurT or GatD is caused by recruitment to the membrane-bound substrate. Indeed, amidation of the glutamic acid at position 2 of the peptide chain most likely occurs after formation of lipid-linked PG precursors (Rajagopal & Walker, 2016).

CRISPRi revealed novel pneumococcal genes involved in teichoic acid biosynthesis

CRISPRi-based repression of hypothetical essential genes *spd_1197* and *spd_1198* led to significant growth defects and microscopy revealed chained cells with abnormal shape and size (Appendix Fig. S10). Some of the cells were elongated and enlarged. These phenotypes are consistent with the typical morphological changes caused by repression of genes in teichoic acid (TA) biosynthesis (Appendix Fig. S9). In accordance with this, analysis of the genetic context of *spd_1197* and *spd_1198* showed that they

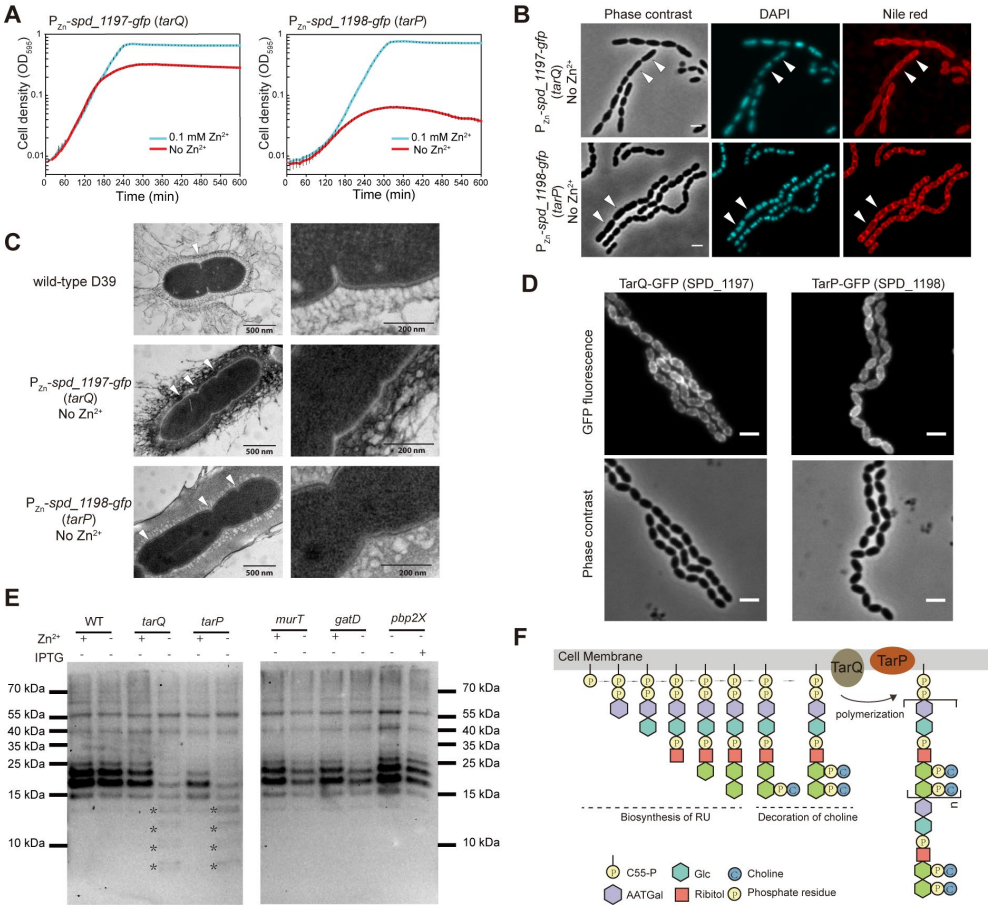

Figure 5. Newly identified genes of the teichoic acid biosynthesis pathway: *spd_1198* (*tarP*) and *spd_1197* (*tarQ*) are involved in precursor polymerization.

(**A**) Growth curves of depletion strains P_{Zn}-*spd_1197-gfp* (*tarQ*) and P_{Zn}-*spd_1198-gfp* (*tarP*) in C+Y medium with (cyan) or without (red) 0.1 mM Zn^{2+}. The value represents averages of three replicates with SEM. (**B**) Microscopy of strains as in panel (**A**) after incubation in C+Y medium without Zn^{2+} for 2.5 hours. Representative micrographs are shown. Scale bar = 2 µm. White arrows point to elongated and enlarged cells. Note that depletion of *spd_1197* or *spd_1198* led to long-chain formation of cells. (**C**) Electron micrographs of the same samples as in panel (**B**) with wild-type *S. pneumoniae* D39 as reference. Arrowheads point to the septa of cells. (**D**) Localization of TarQ-GFP, TarP-GFP, with C-terminal fused monomeric GFP. GFP signal (upper panel) and phase contrast (lower panel) are shown. Scale bar = 2 µm. (**E**) Western blotting to detect phosphorylcholine-containing molecules of *S. pneumoniae*. Whole cell lysates were separated with SDS-PAGE, and phosphorylcholine containing molecules were detected by phosphorylcholine antibody TEPC-15. Smaller bands caused by depletion of *tarQ* (*spd_1197*) or *tarP* (*spd_1198*) are indicated by asterisks. Note that for *tarQ, tarP, murT*, and *gatD*, Zn^{2+} inducible strains were used, and for *pbp2X*, a CRISPRi strain was used. (**F**) Model for TarP/TarQ function in precursor polymerization of the teichoic acid biosynthesis pathway in *S. pneumoniae*. Steps of biosynthesis of repeat units (RU), decoration of RU with choline and polymerization of the precursor are shown.

are in the *lic3* region, which was predicted to be a pneumococcal TA gene cluster (Denapaite *et al.*, 2012; Kharat *et al.*, 2008). Similar to the approach described above, we generated Zn^{2+}-inducible C-terminal GFP fusions to SPD_1197 and SPD_1198, integrated these ectopically at the *bgaA* locus and then deleted the native *spd_1197* or *spd_1198* genes in the presence of Zn^{2+}. Plate reader assays showed strong growth impairment in the absence of Zn^{2+} (Fig. 5A), suggesting their essentiality. In line with this, we were unable to replace these genes with an erythromycin resistance marker in the wild-type background in either the absence or presence of Zn^{2+}. Consistent with the phenotypes of the CRISPRi screen, the zinc-depletion strains showed similar morphological defects with cells in chains and elongated or enlarged cell shape and size (Fig. 5B). EM analysis of depleted cells also revealed uneven distribution of multiple septa within a single cell, increased extracellular material and a rough cell surface (Fig. 5C).

SPD_1198 contains 11 predicted transmembrane (TM) helices while SPD_1197 has 2 predicted TM segments with a C-terminal extracytoplasmic tail. In-gel fluorescence showed that SPD_1197-GFP was mainly produced as a full-length product. The SPD_1198-GFP fusion, however, showed clear signs of protein degradation (Appendix Fig. S13). Nevertheless, we performed fluorescence microscopy to determine their localizations. In agreement with the prediction, SPD_1197-GFP and SPD_1198-GFP are clearly localized to the membrane (Fig. 5D).

Phosphorylcholine is an essential component of pneumococcal TA and for this reason a phosphorylcholine antibody is frequently used to detect *S. pneumoniae* TA (Vollmer & Tomasz, 2001; Wu *et al.*, 2014). To explore whether SPD_1197 and SPD_1198 indeed play a role in TA synthesis, we performed Western blotting to detect phosphorylcholine-decorated TA using whole cell lysates (Fig. 5E). Cells of strains P_{Zn}- *spd_1197-gfp* and P_{Zn} -*spd_1198-gfp* were grown in the presence or absence of 0.1 mM Zn^{2+}. As controls, we depleted expression of three genes involved in PG synthesis (*murT*, *gatD*, and *pbp2x*). As shown in Fig. 5E, Zn^{2+} did not influence TA synthesis of the *S. pneumoniae* D39 wild-type (WT) strain, and the four main TA bands are clearly visible, migrating in the range between 15 and 25 kDa consistent with previous reports (Wu *et al.*, 2014).In contrast, cells depleted for SPD_1197 or SPD_1198 displayed a different pattern and the 4 main bands around 15 kDa and 25 kDa were missing or much weaker, while multiple bands with a size smaller than 15 kDa appeared. TA of *S. pneumoniae*, including wall teichoic acid (WTA) and membrane-anchored lipoteichoic acid (LTA), are polymers with identical repeating units (RU) (Fischer *et al.*, 1993). Addition of one RU can lead to about a 1.3 kDa increase in molecular weight (Gisch *et al.*, 2013). Interestingly, the weight interval between the extra smaller bands from bacterial cells with depleted SPD_1197 or SPD_1198 seemed to match the molecular weight of the RU, suggesting that SPD_1197 and

SPD_1198 play a role in TA precursor polymerization. Although repression of the genes associated with peptidoglycan synthesis (*murT*, *gatD* and *pbp2x*) made the 4 main TA bands weaker, the pattern of the TA bands was not changed. Likely, the reduction of the TA of these three strains is due to the reduction of peptidoglycan, which constitutes the anchor for wall TA. Additionally, a CRISPRi strain targeting tarI of the *lic1* locus, which is involved in an early step of TA precursor synthesis, was included as a control. Note that *tarI* is cotranscribed with the other 4 genes of the *lic1* locus, including *tarJ*, *licA*, *licB* and *licC*. Likely, CRISPRi knockdown of *tarI* will repress transcription of the entire *lic1* locus, and thus block the synthesis of TA precursors. In line with this, we observed a reduction in the total amount of teichoic acid chains when tarI was repressed by CRISPRi (Appendix Fig. S14).

The TA chains of *S. pneumoniae* are thought to be polymerized before they are transported to the outside of the membrane by the flippase TacF (Damjanovic *et al.*, 2007), and so far it is not known which protein(s) function(s) as TA polymerase (Denapaite *et al.*, 2012). In line with SPD_1198 being the TA polymerase, homology analysis shows that it contains a predicted polymerase domain. The large cytoplasmic part of SPD_1197 may aid in the assembly of the TA biosynthetic machinery by protein-protein interactions (Denapaite *et al.*, 2012). Together, we here show that SPD_1197 and SPD_1198 are essential for growth and we suggest that they are responsible for polymerization of TA chains (Fig. 5F). Consistent with the nomenclature used for genes involved in TA biosynthesis, we named *spd_1198 tarP* (for teichoic acid ribitol polymerase) and *spd_1197 tarQ* (in operon with *tarP*, sequential alphabetical order). Whether TarP and TarQ interact and function as a complex remains to be determined.

The essential ATPase ClpX and the protease ClpP repress competence development

We wondered whether we could also employ CRISPRi to probe gene-regulatory networks in which essential genes play a role. An important pathway in *S. pneumoniae* is development of competence for genetic transformation, which is under the control of a well-studied two-component quorum sensing signaling network (Claverys *et al.*, 2009). Several lines of evidence have shown that the highly conserved ATP-dependent Clp protease, ClpP, in association with an ATPase subunit (either ClpC, ClpE, ClpL or ClpX), is involved in regulation of pneumococcal competence (Charpentier *et al.*, 2000; Chastanet *et al.*, 2001) (Fig. 6A). Identification of the ATPase subunit responsible for ClpP-dependent repression of competence was hampered because of the essentiality, depending on the growth medium and laboratory conditions, of several *clp* mutants including *clpP* and *clpX* (Chastanet *et al.*, 2001). To address this issue, we employed CRISPRi and constructed sgRNAs targeting *clpP*, *clpC*, *clpE*, *clpL* and *clpX*. Competence development was quantified using a *luc* construct, driven by a competence-specific promoter (Slager *et al.*, 2014). As shown in Fig. 6B,

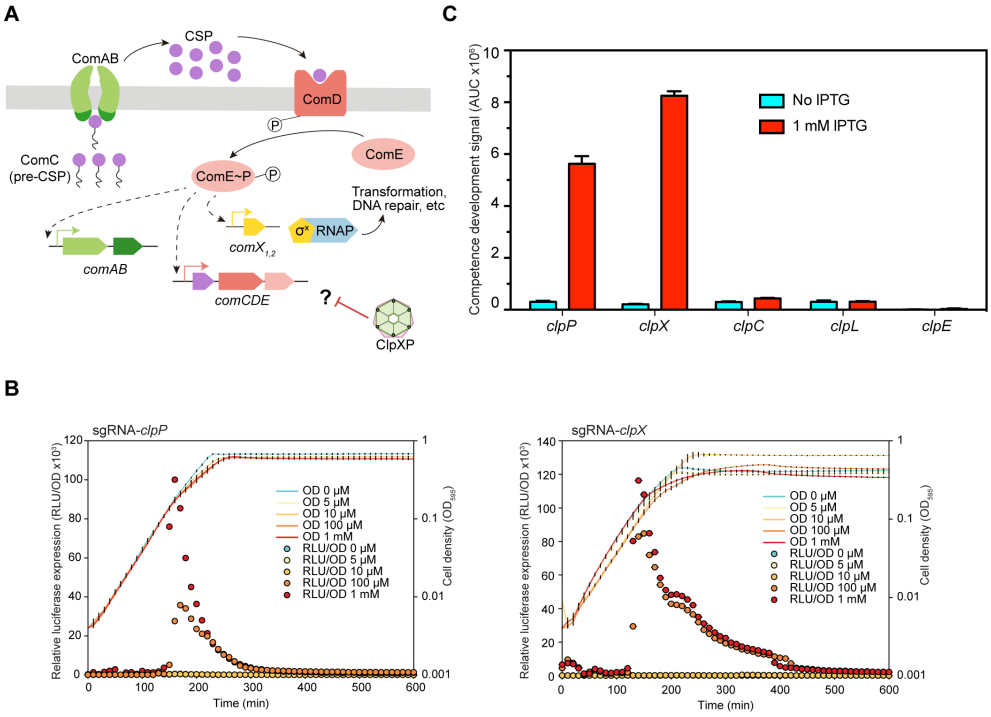

Fig. 6. The ATPase ClpX and the ClpP protease repress competence development.

(**A**) Regulatory network of the competence pathway. Competence is induced when the *comC*-encoded competence-stimulating peptide (CSP), is recognized, cleaved and exported by the membrane transporter (ComAB). Accumulation of CSP then stimulates its receptor (membrane-bound histidine-kinase ComD), which subsequently activates ComE by phosphorylation, which in turn activates the expression of the so-called early competence genes. One of them, *comX*, codes for a sigma factor, which is responsible for the activation of over 100 competence genes, including those required for transformation and DNA repair. Here, we show that the ATPase subunit ClpX, works together with the protease ClpP, repressing competence, probably by negatively controlling the basal protein level of the competence regulatory proteins but the exact mechanism is unknown (question mark). (**B**) Repression of *clpP* or *clpX* by CRISPRi triggers competence development. Activation of competence system is reported by the *ssbB_luc* transcriptional fusion. Detection of competence development was performed in C+Y medium at a pH in which natural competence of the wild type strain is uninduced. IPTG was added to the medium at the beginning at different final concentrations (0, 5 µM, 10 µM, 100 µM, 1 mM). Cell density (OD_{595}) and luciferase activity of the bacterial cultures were measured every 10 minutes. The value represents averages of three replicates with SEM. (**C**) Influence of repression of *clpP, clpX, clpC, clpL*, and *clpE* on competence development. AUC (Area Under the Curve) of the relative luciferase expression curve in panel (**B**) (1 mM IPTG and no IPTG) and Fig. EV5 was calculated and used to represent the competence development signal. The value represents averages of three replicates with SEM.

when expression of ClpP or ClpX was repressed by addition of IPTG, competence development was enhanced, while depleting any of the other ATPase subunits (ClpC, ClpE and ClpL) had no effect on competence (Fig. 6C and Fig. EV5). This shows that ClpX is the main ATPase subunit responsible for ClpP-dependent repression of competence.

Discussion

Here, we developed an IPTG-inducible CRISPRi system to study essential genes in *S. pneumoniae* (Fig. 1). In addition, we adopted a simple and efficient one-step sgRNA engineering strategy using infusion cloning. This approach resulted in approximately 89 % positive sgRNA clones after a single round of transformation, thus enabling high-throughput cloning of sgRNAs.

Growth analysis of the CRISPRi strains targeting the 348 potentially essential genes showed that individual repression of 73 % of the targeted genes led to growth phenotypes, using a stringent cut-off for phenotype detection (Figs 2B-C and Fig. EV2). There could be several reasons why CRISPRi knockdown of the remaining 94 genes did not cause a detectable growth phenotype. Tn-seq sometimes incorrectly assigns an essential function to non-essential genes (van Opijnen *et al.*, 2009; van Opijnen & Camilli, 2013). Also, Tn-seq relies on a round of growth on blood agar plates while our CRISPRi phenotypes were only assayed in liquid C+Y medium. Additionally, we used stringent cut-offs for phenotype definition, which will miss genes with mild growth or lysis phenotypes. Certain genes might also not be repressed well enough by CRISPRi to show a phenotype (in case of stable proteins that only require a few molecules for growth). This can be for instance caused when the sgRNA targets a PAM site far away from the transcription start site, when there is poor access of the sgRNA-dCas9 complex to the target DNA or when there are polar effects within the operon alleviating the essentiality. We can also not exclude a suppressor mutation arising in some of the 'No phenotype' CRISPRi strains, as most CRISPRi knockdowns with growth phenotypes eventually grew out to the same final OD and contain a loss-of-function mutation in the coding sequence of *dcas9* (Fig. EV4).

Based on analysis of the CRISPRi knockdowns, several previously 'hypothetical' genes could be functionally characterized and annotated. For instance, combined with BlastP analysis and determination of *oriC-ter* ratios, we could annotate the pneumococcal primosomal machinery, including DnaA, DnaB, DnaC, DnaD, DnaG and DnaI (Table 1, Appendix Figs S2 and S12). Note that *spd_2030* (*dnaC*) was mis-annotated as *dnaB* in several databases, such as in NCBI (ProteinID: ABJ54728), KEGG (Entry: SPD_2030), Uniprot (Entry: A0A0H2ZNF7), which may be due to the different naming of primosomal proteins in *E. coli* and *B. subtilis* (Briggs *et al.*, 2012; Smits *et al.*, 2011). By characterizing CRISPRi-based knockdowns with cell morphology defects, we identified 4 essential cell wall biosynthesis genes (*murT, gatD, tarP* and *tarQ*), which are promising candidates for future development of novel antimicrobials.

This work and other studies highlight that high-throughput phenotyping by CRISPRi is a powerful approach for hypothesis-forming and functional characterization of essential genes (Peters *et al.*, 2016). We also show that CRISPRi can be used to unravel gene-regulatory networks in which essential genes play a part (Fig. 6). While we shed light on the function of just several previously uncharacterized essential genes, the here-described library contains richer information that needs to be further explored. In addition, CRISPRi screens can be used for mechanism of action (MOA) studies with new bioactive compounds. Indeed, CRISPRi was recently successfully employed to show that *B. subtilis* UppS is the molecular target of compound MAC-0170636 (Peters *et al.*, 2016). We anticipate that the here-described pneumococcal CRISPRi library can function as a novel drug target discovery platform, can be applied to explore host-microbe interactions and will provide a useful tool to increase our knowledge concerning pneumococcal cell biology.

Materials and Methods

Strains, growth conditions and transformation

Oligonucleotides are shown in Dataset EV4 and strains in Appendix Table 1. *S. pneumoniae* D39 and its derivatives were cultivated in C+Y medium, pH = 6.8 (Slager *et al.*, 2014) or Columbia agar with 2.5 % sheep blood at 37ºC. Transformation of *S. pneumoniae* was performed as previously described (Martin *et al.*, 2000), and CSP-1 was used to induce competence. Transformants were selected on Columbia agar supplemented with 2.5 % sheep blood at appropriate concentrations of antibiotics (100 µg/ml spectinomycin, 250 µg/ml kanamycin, 1 µg/ml tetracycline, 40 µg/ml gentamycin, 0.05 µg/ml erythromycin). For construction of depletion strains with the Zn^{2+}-inducible promoter, 0.1 mM $ZnCl_2$/ 0.01 mM $MnCl_2$ was added to induce the ectopic copy of the target gene (mentioned as 0.1 mM Zn^{2+} for convenience). Working stock of the cells, called "T2 cells", were prepared by growing the cells in C+Y medium to OD_{600} = 0.4, and then resuspending the cells with equal volume of fresh medium with 17 % glycerol.

E. coli MC1061 was used for subcloning of plasmids and competent cells were prepared by $CaCl_2$ treatment. The *E. coli* transformants were selected on LB agar with appropriate concentrations of antibiotics (100 µg/ml spectinomycin, 100 µg/ml ampicillin, 50 µg/ml kanamycin).

Construction of an IPTG-inducible CRISPRi system in S. pneumoniae

Streptococcus pyogenes dcas9 (*dcas9sp*) was obtained from Addgene (Addgene #44249, (Qi *et al.*, 2013), and subcloned into plasmid pJWV102 (Veening laboratory collection) with the IPTG-inducible promoter P_{lac} (Sorg, 2016) replacing P_{Zn}, resulting in plasmid pJWV102-P_{lac}-*dcas9sp*. pJWV102-P_{lac}-*dcas9sp* was integrated into the *bgaA* locus in *S. pneumoniae* D39 by transformation. To control P_{lac} expression, a codon-optimized *E. coli lacI* gene driven by the constitutive promoter *PF6* was inserted at the *prsA* locus in *S. pneumoniae* D39 (Sorg, 2016), leading to the construction of strain DCI23. DCI23 was used as the host strain for the insertion of gene-specific sgRNAs, and enables the CRISPRi system. The DNA fragment encoding the single-guide RNA targeting luciferase (sgRNA*luc*) was ordered as a synthetic DNA gBlocks (Integrated DNA Technologies) containing the constitutive *P3* promoter (Sorg *et al.*, 2015).The sgRNA*luc* sequence is transcribed directly after the +1 of the promoter and contains 19 nucleotides in the base-pairing region, which binds to the non-template (NT) strand of the coding sequence of luciferase, followed by an optimized single-guide RNA (Chen *et al.*, 2013) (Fig. EV1A). Then, the sgRNA*luc* with *P3* promoter was cloned into pPEP1 (Sorg *et al.*, 2015) with removing the chloramphenicol resistance marker (pPEPX) leading to the production of plasmid pPEPX-*P3*-sgRNA*luc*, which

integrates into the region between *amiF* and *treR* of *S. pneumoniae* D39. The pPEPX-*P3*-sgRNA*luc* was used as the template for generation of other sgRNAs by infusion cloning or by the inverse PCR method. The *lacI* gene with gentamycin resistance marker and flanked *prsA* regions was subcloned into pPEPY (Veening laboratory collection), resulting in plasmid pPEPY-*PF6-lacI*. This plasmid can be used to amplify *lacI* and integrate it at the *prsA* locus while selecting for gentamycin resistance. The entire pneumococcal CRISPRi system, consisting of plasmids pJWV102-P_{lac}-dcas9*sp*, pPEPY-*PF6-lacI* and pPEPX-*P3*-sgRNA*luc*, is available from Addgene (ID 85588, 85589 and 85590, respectively).

Selection of essential genes

To identify each gene's contribution to fitness for basal level growth, we performed Tn-seq in *S. pneumoniae* D39 essentially as described before (Burghout *et al.*, 2013; Zomer *et al.*, 2012), but with growing cells in C+Y medium at 37ºC. Possibly essential genes were identified using ESSENTIALS (Zomer *et al.*, 2012). Based on that, we included all the identified essential genes, and added extra essential genes identified with similar method in serotype 4 strain TIGR4 by other Tn-seq studies (van Opijnen *et al.*, 2009; van Opijnen & Camilli, 2012). Please note that in the Tn-seq study of 2012, fitness of each gene under 17 in vitro and 2 in vivo conditions was determined and genes were grouped into different classes (van Opijnen & Camilli, 2012). Finally, 391 genes were selected (Dataset EV1).

Oligonucleotides for the CRISPRi library

The 20 nt guide sequences of the sgRNAs targeting different genes were selected with CRISPR Primer Designer (Yan *et al.*, 2015). Briefly, we searched within the coding sequence of each essential gene for a 14-nt specificity region consisting of the 12-nt 'seed' region of the sgRNA and GG of the 3-nt PAM (GGN). sgRNAs with more than one binding site within the pneumococcal genome, as determined by a BLAST search, were discarded. Next, we took a total length of 21-nt (including the +1 of the *P3* promoter and 20-nt of perfect match to the target) and the full-length sgRNA's secondary structure was predicted using ViennaRNA (Lorenz *et al.*, 2011), and the sgRNA sequence was accepted if the dCas9 handle structure was folded correctly (Larson *et al.*, 2013). We chose the guide sequences as close as possible to the 5' end of the coding sequence of the targeted gene (Qi *et al.*, 2013). The sequences of the sgRNAs (20 nt) are listed in Dataset EV3.

Cloning of sgRNA

We used infusion cloning instead of inverse PCR recommended by Larson *et al.* (Larson *et al.*, 2013) because significantly higher cloning efficiencies were obtained with infusion cloning. Two primers, sgRNA_inF_plasmid_linearize_R and sgRNA_

inF_plasmid_linearize_F, were designed for linearization of plasmid pPEPX-*P3*-sgRNA*luc*. These two primers bind directly upstream and downstream of the 19 bp guide sequence for *luc*. To fuse the 20-nt new guide sequence into the linearized vector, two 50-nt complementary primers were designed for each target gene. Each primer contains 15-nt at one end, overlapping with the sequence on the 5′ end of the linearized vector, followed by the 20-nt specific guide sequence for each target gene; and 15-nt overlapping with the sequence on the 3′ end of the linearized vector (Fig. EV2A). The two 50-nt complementary primers were annealed in TEN buffer (10 mM Tris, 1 mM EDTA, 100 mM NaCl, pH = 8) by heating at 95ºC for 5 min and cooling down to room temperature. The annealed product was fused with the linearized vector using the Quick-Fusion Cloning kit (BiMake, Cat. B22612) according to the manufacturer with the exception of using only ½ of the recommended volume per reaction. Each reaction was directly used to transform competent *S. pneumoniae* D39 strain DCI23.

Luciferase assay

S. pneumoniae strains XL28 and XL29 were grown to OD_{600} = 0.4 in 5-ml tubes at 37ºC, and then diluted 1:100 in fresh C+Y medium with or without 1 mM IPTG. Then, in triplicates, 250 µl diluted bacterial culture was mixed with 50 µl of 6× luciferin solution in C+Y medium (2.7 mg/ml, D-Luciferin sodium salt, SYNCHEM OHG) in 96-well plates (Polystyrol, white, flat, and clear bottom; Corning). Optical density at 595 nm (OD_{595}) and luminescence signal were measured every 10 minutes for 10 hours using a Tecan Infinite F200 Pro microtiter plate reader.

Growth assays

For growth curves of strains of the CRISPRi library, T2 cells were thawed and diluted 1:1000 into fresh C+Y medium with or without 1 mM IPTG. Then 300 µl of bacterial culture was added into each well of 96-well plates. OD_{595} was measured every 10 minutes for 18 hours with a Tecan Infinite F200 Pro microtiter plate reader. Specially, for the data shown in Fig. 3, Appendix Fig. S10 and S11, T2 cells were diluted 1:100 in C+Y medium. For growth assays of the depletion strains with the Zn^{2+} inducible promoter, T2 cells were thawed and diluted 1:100 into fresh C+Y medium with or without 0.1 mM Zn^{2+}.

Detection of teichoic acids

Sample preparation. T2 cells of *S. pneumoniae* strains were inoculated into fresh C+Y medium with 0.1 mM Zn^{2+} by 1:50 dilution, and then grown to OD_{600} = 0.15 at 37ºC. Cells were collected at 8000 rcf for 3 min, and resuspended with an equal volume of fresh C+Y medium without Zn^{2+}. Bacterial cultures were diluted 1:10 into C+Y with or without 0.1 mM Zn^{2+} or 1 mM IPTG (for CRISPRi strains), and then incubated at 37ºC.

When OD_{600} reached 0.3, cells were centrifuged at 8000 rcf for 3 min. The pellets were washed once with cold TE buffer (10 mM Tris-Cl, pH 7.5; 1 mM EDTA, pH 8.0), and resuspended with 150 µl of TE buffer. Cells were lysed by sonication.

Detection of teichoic acid with phosphoryl choline antibody MAb TEPC-15.

Protein concentration of the whole cell lysate was determined with the DC protein assay kit (Biorad Cat. 500-0111). Whole cell lysates were mixed with equal volumes of 2× SDS protein loading buffer (100 mM Tris-HCl, pH = 6.8; 4 % SDS; 0.2 % bromphenolblue; 20 % glycerol; 10 mM DTT), and boiled at 95ºC for 5 min. 2 µg of protein were loaded, followed by SDS gel electrophoresis on a 12 % polyacrylamide gel with cathode buffer (0.1 M Tris, 0.1 M Tricine, 0.1 % SDS) on top of the wells and anode buffer (0.2 M Tris/Cl, pH = 9.9) in the bottom. After electrophoresis, samples in the gel were transferred onto a polyvinylidene difluoride (PVDF) membrane as described (Minnen *et al.*, 2011). Teichoic acid was detected with anti-PC specific monoclonal antibody TEPC-15 (M1421, Sigma) by 1:1000 dilution as first antibody, and then with anti-mouse IgG HRP antibody (GE Healthcare UK Limited) with 1:5000 dilution as second antibody. The blots were developed with ECL prime western blotting detection reagent (GE Healthcare UK Limited) and the images were obtained with a Biorad imaging system.

Microscopy

To detect the morphological changes after knockdown of the target genes, strains in the CRISPRi library were induced with IPTG and depletion strains were incubated in C+Y medium without Zn^{2+}, stained with DAPI (DNA dye) and nile red (membrane dye), and then studied by fluorescence microscopy. Specifically, 10 µl of thawed T2 cells was added into 1 ml of fresh C+Y medium, with or without 1 mM IPTG, in a 1.5-ml Eppendorf tube, followed by 2.5 hours of incubation at 37ºC. After that, 1 µl of 1 mg/ml nile red was added into the tube and cells were stained for 4 min at room temperature. Then 1 µl of 1 mg/ml DAPI was added and the mix was incubated for one more minute. Cells were spun down at 8000 rcf for 2 min, and then the pellets were suspended with 30 µl of fresh C+Y medium. 0.5 µl of cell suspension was spotted onto a PBS agarose pad on microscope slides. DAPI, nile red and phase contrast images were acquired with a Deltavision Elite (GE Healthcare, USA). Microscopy images were analyzed with ImageJ.

For fluorescence microscopy of strains containing zinc-inducible GFP fusions, strains were grown in C+Y medium to OD_{600} = 0.1, followed by 10-times dilution in fresh C+Y medium with 0.1 mM Zn^{2+}. After 1 hour of incubation, cells were spun down, washed with PBS and resuspended in 50 µl PBS. 0.5 µl of cell suspension was spotted onto a PBS agarose pad on microscope slides. Visualization of GFP was

performed as described previously (Kjos *et al.*, 2015).

For electron microscopy, T2 cells of *S. pneumoniae* strains were inoculated into C+Y medium with 0.1 mM Zn^{2+} and incubated at 37ºC. When OD_{600} = reached 0.15, the bacterial culture was centrifuged at 8000 rcf for 2 min. The pellets were resuspended into C+Y without Zn^{2+} such that OD_{600} was 0.015, and then cells were incubated again at 37ºC. Bacterial cultures were put on ice to stop growth when OD_{600} reached 0.35. Cells were collected by centrifugation and washed once with distilled water. A small pellet of cells was cryo-fixed in liquid ethane using the sandwich plunge freezing method (Baba, 2008) and freeze-substituted in 1 % osmium tetroxide, 0.5 % uranyl acetate and 5 % distilled water in acetone using the fast low-temperature dehydration and fixation method (McDonald & Webb, 2011). Cells were infiltrated overnight with Epon 812 (Serva, 21045) and polymerized at 60°C for 48 h. 90 nm thick sections were cut with a Reichert ultramicrotome and imaged with a Philips CM12 transmission electron microscope running at 90kV.

Competence assays

The previously described *ssbB_luc* competence reporter system, amplified from strain MK134 (Slager *et al.*, 2014), was transformed into the CRISPRi strains (sgRNA*clpP*, sgRNA*clpX*, sgRNA*clpL*, sgRNA*clpE*, sgRNA*clpC*). Luminescence assays for detection of activation of competence system were performed as previously described (Slager *et al.*., 2014). IPTG was added into C+Y medium (at a non-permissive pH for competence development) at the beginning of cultivation to different final concentrations.

Data availability

Raw Tn-seq data are available at the SRA with accession number SRR5298192; The RNA-Seq data are available at the GEO database with accession number GSE89763.

Supplementary data

Appendix, Expanded View Figures and Dataset EV1-4 are available at MSB online (https://doi.org/10.15252/msb.20167449)

Acknowledgements

We thank A. Zomer, P. Burghout and P. Hermans (Radboud University, Nijmegen) for help with acquiring and analyzing the Tn-seq data. We thank K. Kuipers and M. I. de Jonge for providing the TEPC-15 antibodies and for the TA Western-blotting protocol. V. Benes and B. Haase (GeneCore, EMBL, Heidelberg) are thanked for sequencing support. XL is supported by China Scholarship Council (No. 201506210151).

ADP was supported by a “Marie Curie IF” grant (call H2020-MSCA-IF-2014, number 657546). KK is supported by a NWO VENI fellowship (563.14.003). MK is supported by a grant from the research council of Norway (250976/F20). Work in the Veening lab is supported by the EMBO Young Investigator Program, a VIDI fellowship (864.12.001) from the Netherlands Organization for Scientific Research, Earth and Life Sciences (NWO-ALW), and ERC Starting Grant 337399-PneumoCell.

References

Aprianto R, Slager J, Holsappel S, Veening JW (2016) Time-resolved dual RNA-seq reveals extensive rewiring of lung epithelial and pneumococcal transcriptomes during early infection. Genome biology 17: 198

Avery OT, Macleod CM, McCarty M (1944) Studies on the Chemical Nature of the Substance Inducing Transformation of Pneumococcal Types : Induction of Transformation by a Desoxyribonucleic Acid Fraction Isolated from Pneumococcus Type Iii. The Journal of experimental medicine 79: 137-158

Baba M (2008) Electron microscopy in yeast. Methods in enzymology 451: 133-149

Bartual SG, Straume D, Stamsas GA, Munoz IG, Alfonso C, Martinez-Ripoll M, Havarstein LS, Hermoso JA (2014) Structural basis of PcsB-mediated cell separation in *Streptococcus pneumoniae*. Nature communications 5: 3842

Bikard D, Hatoum-Aslan A, Mucida D, Marraffini LA (2012) CRISPR Interference Can Prevent Natural Transformation and Virulence Acquisition during In Vivo Bacterial Infection. Cell Host Microbe 12: 177-186

Bikard D, Jiang W, Samai P, Hochschild A, Zhang F, Marraffini LA (2013) Programmable repression and activation of bacterial gene expression using an engineered CRISPR-Cas system. Nucleic acids research 41: 7429-7437

Briggs GS, Smits WK, Soultanas P (2012) Chromosomal replication initiation machinery of low-G+C-content Firmicutes. Journal of bacteriology 194: 5162-5170

Brown S, Santa Maria JP, Jr., Walker S (2013) Wall teichoic acids of gram-positive bacteria. Annual review of microbiology 67: 313-336

Burghout P, Zomer A, van der Gaast-de Jongh CE, Janssen-Megens EM, Francoijs KJ, Stunnenberg HG, Hermans PW (2013) *Streptococcus pneumoniae* folate biosynthesis responds to environmental CO2 levels. Journal of bacteriology 195: 1573-1582

Charpentier E, Novak R, Tuomanen E (2000) Regulation of growth inhibition at high temperature, autolysis, transformation and adherence in *Streptococcus pneumoniae* by ClpC. Molecular microbiology 37: 717-726

Chastanet A, Prudhomme M, Claverys JP, Msadek T (2001) Regulation of *Streptococcus pneumoniae* clp genes and their role in competence development and stress survival. Journal of bacteriology 183: 7295-7307

Chen B, Gilbert LA, Cimini BA, Schnitzbauer J, Zhang W, Li GW, Park J, Blackburn EH, Weissman JS, Qi LS, Huang B (2013) Dynamic imaging of genomic loci in living human cells by an optimized CRISPR/Cas system. Cell 155: 1479-1491

Chewapreecha C, Harris SR, Croucher NJ, Turner C, Marttinen P, Cheng L, Pessia A, Aanensen DM, Mather AE, Page AJ, Salter SJ, Harris D, Nosten F, Goldblatt D, Corander J, Parkhill J, Turner P, Bentley SD (2014) Dense genomic sampling identifies highways of pneumococcal recombination. Nature genetics 46: 305-309

Chung KM, Hsu HH, Govindan S, Chang BY (2004) Transcription regulation of ezrA and its effect on cell division of Bacillus subtilis. Journal of bacteriology 186: 5926-5932

Claverys JP, Martin B, Polard P (2009) The genetic transformation machinery: composition, localization, and mechanism. FEMS microbiology reviews 33: 643-656

Damjanovic M, Kharat AS, Eberhardt A, Tomasz A, Vollmer W (2007) The essential tacF gene is responsible for the choline-dependent growth phenotype of *Streptococcus pneumoniae*. Journal of bacteriology 189: 7105-7111

de Jong A, van der Meulen S, Kuipers OP, Kok J (2015) T-REx: Transcriptome analysis webserver for RNA-seq Expression data. BMC genomics 16: 663

Denapaite D, Bruckner R, Hakenbeck R, Vollmer W (2012) Biosynthesis of teichoic acids in *Streptococcus pneumoniae* and closely related species: lessons from genomes. Microbial drug resistance 18: 344-358

Figueiredo TA, Sobral RG, Ludovice AM, Almeida JM, Bui NK, Vollmer W, de Lencastre H, Tomasz A (2012) Identification of genetic determinants and enzymes involved with the amidation of glutamic acid residues in the peptidoglycan of Staphylococcus aureus. PLoS pathogens 8: e1002508

Fischer W, Behr T, Hartmann R, Peter-Katalinić J, Egge H (1993) Teichoic acid and lipoteichoic acid of *Streptococcus pneumoniae* possess identical chain structures. European Journal of Biochemistry 215: 851-857

Gisch N, Kohler T, Ulmer AJ, Muthing J, Pribyl T, Fischer K, Lindner B, Hammerschmidt S, Zahringer U (2013) Structural reevaluation of *Streptococcus pneumoniae* Lipoteichoic acid and new insights into its immunostimulatory potency. The Journal of biological chemistry 288: 15654-15667

Goranov AI, Breier AM, Merrikh H, Grossman AD (2009) YabA of Bacillus subtilis controls DnaA-mediated replication initiation but not the transcriptional response to replication stress. Molecular microbiology 74: 454-466

Hammerschmidt S, Wolff S, Hocke A, Rosseau S, Muller E, Rohde M (2005) Illustration of pneumococcal polysaccharide capsule during adherence and invasion of epithelial cells. Infect Immun 73: 4653-4667

Henriques AO, Glaser P, Piggot PJ, Moran CP, Jr. (1998) Control of cell shape and elongation by the rodA gene in Bacillus subtilis. Molecular microbiology 28: 235-247

Ikeda M, Sato T, Wachi M, Jung HK, Ishino F, Kobayashi Y, Matsuhashi M (1989) Structural similarity among *Escherichia coli* FtsW and RodA proteins and Bacillus subtilis SpoVE protein, which function in cell division, cell elongation, and spore formation, respectively. Journal of bacteriology 171: 6375-6378

Irwin CR, Farmer A, Willer DO, Evans DH (2012) In-fusion(R) cloning with vaccinia virus DNA polymerase. Methods Mol Biol 890: 23-35

Jerga A, Rock CO (2009) Acyl-Acyl carrier protein regulates transcription of fatty acid biosynthetic genes via the FabT repressor in *Streptococcus pneumoniae*. The Journal of biological chemistry 284: 15364-15368

Johnston C, Martin B, Fichant G, Polard P, Claverys JP (2014) Bacterial transformation: distribution, shared mechanisms and divergent control. Nature reviews Microbiology 12: 181-196

Kawai Y, Ogasawara N (2006) Bacillus subtilis EzrA and FtsL synergistically regulate FtsZ ring dynamics during cell division. Microbiology 152: 1129-1141

Kharat AS, Denapaite D, Gehre F, Bruckner R, Vollmer W, Hakenbeck R, Tomasz A (2008) Different pathways of choline metabolism in two choline-independent strains of *Streptococcus pneumoniae* and their impact on virulence. Journal of bacteriology 190: 5907-5914

Khattar MM, Begg KJ, Donachie WD (1994) Identification of FtsW and characterization of a new ftsW division mutant of *Escherichia coli*. Journal of bacteriology 176: 7140-7147

Kim L, McGee L, Tomczyk S, Beall B (2016) Biological and Epidemiological Features of Antibiotic-Resistant *Streptococcus pneumoniae* in Pre- and Post-Conjugate Vaccine Eras: a United States Perspective. Clinical microbiology reviews 29: 525-552

Kjos M, Aprianto R, Fernandes VE, Andrew PW, van Strijp JA, Nijland R, Veening JW (2015) Bright fluorescent *Streptococcus pneumoniae* for live-cell imaging of host-pathogen interactions. Journal of bacteriology 197: 807-818

Kocaoglu O, Tsui HC, Winkler ME, Carlson EE (2015) Profiling of beta-lactam selectivity for penicillin-binding proteins in *Streptococcus pneumoniae* D39. Antimicrob Agents Chemother 59: 3548-3555

Kuipers K, Gallay C, Martinek V, Rohde M, Martinkova M, van der Beek SL, Jong WS, Venselaar H, Zomer A, Bootsma H, Veening JW, de Jonge MI (2016) Highly conserved nucleotide phosphatase essential for membrane lipid homeostasis in *Streptococcus pneumoniae*. Molecular microbiology 101: 12-26

Larson MH, Gilbert LA, Wang X, Lim WA, Weissman JS, Qi LS (2013) CRISPR interference (CRISPRi) for sequence-specific control of gene expression. Nature protocols 8: 2180-2196

Li Y, Weinberger DM, Thompson CM, Trzcinski K, Lipsitch M (2013) Surface charge of *Streptococcus pneumoniae* predicts serotype distribution. Infect Immun 81: 4519-4524

Lorenz R, Bernhart SH, Honer Zu Siederdissen C, Tafer H, Flamm C, Stadler PF, Hofacker IL (2011) ViennaRNA Package 2.0. Algorithms for molecular biology : AMB 6: 26

Lu YJ, Rock CO (2006) Transcriptional regulation of fatty acid biosynthesis in *Streptococcus pneumoniae*. Molecular microbiology 59: 551-566

Maggi S, Massidda O, Luzi G, Fadda D, Paolozzi L, Ghelardini P (2008) Division protein interaction web: identification of a phylogenetically conserved common interactome between *Streptococcus pneumoniae* and *Escherichia coli*. Microbiology 154: 3042-3052

Martin B, Prudhomme M, Alloing G, Granadel C, Claverys JP (2000) Cross-regulation of competence pheromone production and export in the early control of transformation in *Streptococcus pneumoniae*. Molecular microbiology 38: 867-878

Massidda O, Novakova L, Vollmer W (2013) From models to pathogens: how much have we learned about *Streptococcus pneumoniae* cell division? Environ Microbiol 15: 3133-3157

McClure R, Balasubramanian D, Sun Y, Bobrovskyy M, Sumby P, Genco CA, Vanderpool CK, Tjaden B (2013) Computational analysis of bacterial RNA-Seq data. Nucleic acids research 41: e140

McDonald KL, Webb RI (2011) Freeze substitution in 3 hours or less. Journal of microscopy 243: 227-233

Meeske AJ, Riley EP, Robins WP, Uehara T, Mekalanos JJ, Kahne D, Walker S, Kruse AC, Bernhardt TG, Rudner DZ (2016) SEDS proteins are a widespread family of bacterial cell wall polymerases. Nature 537: 634-638

Minnen A, Attaiech L, Thon M, Gruber S, Veening JW (2011) SMC is recruited to oriC by ParB and promotes chromosome segregation in *Streptococcus pneumoniae*. Molecular microbiology 81: 676-688

Mobegi FM, van Hijum SA, Burghout P, Bootsma HJ, de Vries SP, van der Gaast-de Jongh CE, Simonetti E, Langereis JD, Hermans PW, de Jonge MI, Zomer A (2014) From microbial gene essentiality to novel antimicrobial drug targets. BMC genomics 15: 958

Mohammadi T, van Dam V, Sijbrandi R, Vernet T, Zapun A, Bouhss A, Diepeveen-de Bruin M, Nguyen-Disteche M, de Kruijff B, Breukink E (2011) Identification of FtsW as a transporter of lipid-linked cell wall precursors across the membrane. Embo Journal 30: 1425-1432

Morgan C, Rosenkranz HS, Carr HS, Rose HM (1967) Electron microscopy of chloramphenicol-treated *Escherichia coli*. Journal of bacteriology 93: 1987-2002

Morlot C, Noirclerc-Savoye M, Zapun A, Dideberg O, Vernet T (2004) The D,D-carboxypeptidase PBP3 organizes the division process of *Streptococcus pneumoniae*. Molecular microbiology 51: 1641-1648

Munch D, Roemer T, Lee SH, Engeser M, Sahl HG, Schneider T (2012) Identification and in vitro analysis of the GatD/MurT enzyme-complex catalyzing lipid II amidation in Staphylococcus aureus. PLoS pathogens 8: e1002509

Ng WL, Robertson GT, Kazmierczak KM, Zhao J, Gilmour R, Winkler ME (2003) Constitutive expression of PcsB suppresses the requirement for the essential VicR (YycF) response regulator in *Streptococcus pneumoniae* R6. Molecular microbiology 50: 1647-1663

Noirclerc-Savoye M, Le Gouellec A, Morlot C, Dideberg O, Vernet T, Zapun A (2005) In vitro reconstitution of a trimeric complex of DivIB, DivIC and FtsL, and their transient co-localization at the division site in *Streptococcus pneumoniae*. Molecular microbiology 55: 413-424

Noirclerc-Savoye M, Morlot C, Gerard P, Vernet T, Zapun A (2003) Expression and purification of FtsW and RodA from *Streptococcus pneumoniae*, two membrane proteins involved in cell division and cell growth, respectively. Protein expression and purification 30: 18-25

Noirot-Gros MF, Dervyn E, Wu LJ, Mervelet P, Errington J, Ehrlich SD, Noirot P (2002) An expanded view of bacterial DNA replication. Proceedings of the National Academy of Sciences of the United States of America 99: 8342-8347

Ochman H, Gerber AS, Hartl DL (1988) Genetic applications of an inverse polymerase chain reaction. Genetics 120: 621-623

Peters JM, Colavin A, Shi H, Czarny TL, Larson MH, Wong S, Hawkins JS, Lu CH, Koo BM, Marta E, Shiver AL, Whitehead EH, Weissman JS, Brown ED, Qi LS, Huang KC, Gross CA (2016) A Comprehensive, CRISPR-based Functional Analysis of Essential Genes in Bacteria. Cell 165: 1493-1506

Pinho MG, Kjos M, Veening JW (2013) How to get (a)round: mechanisms controlling growth and division of coccoid bacteria. Nature reviews Microbiology 11: 601-614

Prina E, Ranzani OT, Torres A (2015) Community-acquired pneumonia. Lancet 386: 1097-1108

Prudhomme M, Berge M, Martin B, Polard P (2016) Pneumococcal Competence Coordination Relies on a Cell-Contact Sensing Mechanism. PLoS genetics 12: e1006113

Qi LS, Larson MH, Gilbert LA, Doudna JA, Weissman JS, Arkin AP, Lim WA (2013) Repurposing CRISPR as an RNA-Guided Platform for Sequence-Specific Control of Gene Expression. Cell 152: 1173-1183

Rajagopal M, Walker S (2016) Envelope Structures of Gram-Positive Bacteria. Current topics in microbiology and immunology DOI 10.1007/82_2015_5021.

Reinscheid DJ, Gottschalk B, Schubert A, Eikmanns BJ, Chhatwal GS (2001) Identification and molecular analysis of PcsB, a protein required for cell wall separation of group B streptococcus. Journal of bacteriology 183: 1175-1183

Roggiani M, Goulian M (2015) Chromosome-Membrane Interactions in Bacteria. Annual review of genetics 49: 115-129

Sham LT, Barendt SM, Kopecky KE, Winkler ME (2011) Essential PcsB putative peptidoglycan hydrolase interacts with the essential FtsXSpn cell division protein in *Streptococcus pneumoniae* D39. Proceedings of the National Academy of Sciences of the United States of America 108: E1061-1069

Sham LT, Tsui HC, Land AD, Barendt SM, Winkler ME (2012) Recent advances in pneumococcal peptidoglycan biosynthesis suggest new vaccine and antimicrobial targets. Current opinion in microbiology 15: 194-203

Slager J, Kjos M, Attaiech L, Veening JW (2014) Antibiotic-induced replication stress triggers bacterial competence by increasing gene dosage near the origin. Cell 157: 395-406

Smits WK, Merrikh H, Bonilla CY, Grossman AD (2011) Primosomal proteins DnaD and DnaB are recruited to chromosomal regions bound by DnaA in Bacillus subtilis. Journal of bacteriology 193: 640-648

Song JH, Ko KS, Lee JY, Baek JY, Oh WS, Yoon HS, Jeong JY, Chun J (2005) Identification of essential genes in *Streptococcus pneumoniae* by allelic replacement mutagenesis. Molecules and cells 19: 365-374

Sorg RA (2016) Engineering Approaches to Investigate Pneumococcal Gene Expression Regulation and Antibiotic Resistance Development. PhD thesis, ISBN 978-90-367-9258-5.

Sorg RA, Kuipers OP, Veening JW (2015) Gene Expression Platform for Synthetic Biology in the Human Pathogen *Streptococcus pneumoniae*. ACS synthetic biology 4: 228-239

Sorg RA, Veening JW (2015) Microscale insights into pneumococcal antibiotic mutant selection windows. Nature communications 6: 8773

Thanassi JA, Hartman-Neumann SL, Dougherty TJ, Dougherty BA, Pucci MJ (2002) Identification of 113 conserved essential genes using a high-throughput gene disruption system in *Streptococcus pneumoniae*. Nucleic acids research 30: 3152-3162

van Opijnen T, Bodi KL, Camilli A (2009) Tn-seq: high-throughput parallel sequencing for fitness and genetic interaction studies in microorganisms. Nat Methods 6: 767-772

van Opijnen T, Camilli A (2012) A fine scale phenotype-genotype virulence map of a bacterial pathogen. Genome research 22: 2541-2551

van Opijnen T, Camilli A (2013) Transposon insertion sequencing: a new tool for systems-level analysis of microorganisms. Nature reviews Microbiology 11: 435-442

Verhagen LM, de Jonge MI, Burghout P, Schraa K, Spagnuolo L, Mennens S, Eleveld MJ, van der Gaast-de Jongh CE, Zomer A, Hermans PW, Bootsma HJ (2014) Genome-wide identification of genes essential for the survival of *Streptococcus pneumoniae* in human saliva. PloS one 9: e89541

Vollmer W, Tomasz A (2001) Identification of the teichoic acid phosphorylcholine esterase in *Streptococcus pneumoniae*. Molecular microbiology 39: 1610-1622

Wu KF, Huang J, Zhang YQ, Xu WC, Xu HM, Wang LB, Cao J, Zhang XM, Yin YB (2014) A Novel Protein, RafX, Is Important for Common Cell Wall Polysaccharide Biosynthesis in *Streptococcus pneumoniae*: Implications for Bacterial Virulence. Journal of bacteriology 196: 3324-3334

Yan M, Zhou SR, Xue HW (2015) CRISPR Primer Designer: Design primers for knockout and chromosome imaging CRISPR-Cas system. Journal of integrative plant biology 57: 613-617

Zapun A, Philippe J, Abrahams KA, Signor L, Roper DI, Breukink E, Vernet T (2013) In vitro reconstitution of peptidoglycan assembly from the Gram-positive pathogen *Streptococcus pneumoniae*. ACS chemical biology 8: 2688-2696

Zhao H, Sun Y, Peters JM, Gross CA, Garner EC, Helmann JD (2016) Depletion of Undecaprenyl Pyrophosphate Phosphatases Disrupts Cell Envelope Biogenesis in Bacillus subtilis. Journal of bacteriology 198: 2925-2935

Zomer A, Burghout P, Bootsma HJ, Hermans PW, van Hijum SA (2012) ESSENTIALS: software for rapid analysis of high throughput transposon insertion sequencing data. PloS one 7: e43012

Zusman DR, Carbonell A, Haga JY (1973) Nucleoid condensation and cell division in *Escherichia coli* MX74T2 ts52 after inhibition of protein synthesis. Journal of bacteriology 115: 1167-1178

3

SPATIO-TEMPORAL CONTROL OF DNA REPLICATION BY THE PNEUMOCOCCAL CELL CYCLE REGULATOR CCRZ

Clement Gallay*, Stefano Sanselicio*, Mary E. Anderson, Young Min Soh, Xue Liu, Gro A. Stamsås, Simone Pelliciari, Renske van Raaphorst, Morten Kjos, Heath Murray, Stephan Gruber, Alan D. Grossman, Jan-Willem Veening

Preprinted on bioRxiv DOI 10.1101/775536 .

* Joint first authors.

C.G. designed research, performed experiments, analyzed data and wrote the chapter.

Summary

Most bacteria replicate and segregate their DNA concomitantly while growing, before cell division takes place. How bacteria synchronize these different cell cycle events to ensure faithful chromosome inheritance is poorly understood. Here, we identified a conserved and essential protein in pneumococci and related Firmicutes named CcrZ (for Cell Cycle Regulator protein interacting with FtsZ) that couples cell division with DNA replication by controlling the activity of the master initiator of DNA replication, DnaA. The absence of CcrZ causes mis-timed and reduced initiation of DNA replication, which subsequently results in aberrant cell division. We show that CcrZ from *Streptococcus pneumoniae* directly interacts with the cytoskeleton protein FtsZ to place it in the middle of the newborn cell where the DnaA-bound origin is positioned. Together, this work uncovers a new mechanism for the control of the bacterial cell cycle in which CcrZ controls DnaA activity to ensure that the chromosome is replicated at the right time during the cell cycle.

Introduction

Most organisms have mechanisms ensuring that their genome is replicated and segregated prior to cell division. In many bacterial species, DNA replication and cell division occur concomitantly (Boye and Nordström, 2003; Harashima *et al.*, 2013; Reyes-Lamothe and Sherratt, 2019). Different models emerged from the mid-1900's to explain how bacterial cells handle DNA replication together with cell division in *Escherichia coli* or *Bacillus subtilis* (Cooper and Helmstetter, 1968; Donachie, 1968; Kjeldgaard *et al.*, 1958; Schaechter *et al.*, 1958). The current cell-size control model suggests that cells initiate DNA replication independently from their original size, and grow to a constant size independently from their size at birth (adder model) Campos *et al.*, 2014; Si *et al.*, 2019; Taheri-Araghi *et al.*, 2015; Wallden *et al.*, 2016; Wold *et al.*, 1994). How cells sense changes in cell size and convert it to trigger replication initiation is not known, but these models imply the existence of regulatory controls (Hajduk *et al.*, 2016; Kleckner *et al.*, 2014, 2018; Reyes-Lamothe and Sherratt, 2019). However, no such cell cycle regulator has been reported yet for bacteria. Specific regulatory models have been proposed for *E. coli* (Espéli *et al.*, 2012; Huls *et al.*, 2018; Zheng *et al.*, 2016), but these are not applicable to most other organisms, and especially Gram-positive bacteria, that do not contain the proteins proposed to be the regulators. Furthermore, most of the mechanisms known to regulate the initiation of replication and the activity of the replication initiator DnaA in *E. coli* do not exist in other bacteria (Flåtten *et al.*, 2015; Katayama, 2017; Katayama *et al.*, 2017; Løbner-Olesen *et al.*, 1989; Pierucci *et al.*, 1989). This pinpoints a divergence between regulatory systems within bacteria. In line with this notion, changes in DNA replication initiation were shown to alter cell size in *E. coli* and *B. subtilis* but the converse was not true for *B. subtilis* (Hill *et al.*, 2012; Murray and Koh, 2014). Taken together, current data indicates that bacteria evolved different mechanisms to coordinate their cell cycle events.

Although *E. coli* and *B. subtilis* use different systems for regulating their cell cycle, the way they localize their division site is conserved, as both organisms use a variant of the Min system to prevent polymerization of the tubulin-like protein FtsZ away from mid-cell (Bisicchia *et al.*, 2013; Marston *et al.*, 1998). Both species also have a nucleoid occlusion system (Noc) inhibiting Z-ring formation over the chromosome to prevent "cutting" of the chromosome during cell division (Wu and Errington, 2012). Together, the Min and Noc systems ensure that cell division and septation occur when both sister chromatids have been fully replicated and segregated. These systems are however not conserved within all bacteria as the Gram-positive opportunistic human pathogen *S. pneumoniae* lacks homologs of the Min and Noc systems (Pinho *et al.*, 2013).

In contrast to *E. coli* and *B. subtilis*, the pneumococcal Z-ring forms readily over the nucleoid (Land *et al.*, 2013; Pinho *et al.*, 2013). Recently, a pneumococcal specific protein called RocS was identified that might fulfil a similar function as the Noc system by connecting chromosome segregation with capsule production (Mercy *et al.*, 2019). Another *S. pneumoniae* specific protein, called MapZ was shown to guide Z-ring formation, analogous to the Min system in other bacteria (Fleurie *et al.*, 2014; Holečková *et al.*, 2014). During cell growth, nascent MapZ rings are pushed apart by septal peptidoglycan synthesis, allowing for FtsZ polymers to continuously assemble at the newly formed septum (Perez *et al.*, 2019). Importantly, the position of the origin of replication (*oriC*) was shown to be crucial for division site selection in *S. pneumoniae* and the origins mark the positions of future division sites (van Raaphorst *et al.*, 2017). In *S. pneumoniae*, cell division and DNA replication are thus intimately connected. Critically however, it remains unknown how the cell senses when a new round of replication should be initiated.

We hypothesized that an unknown factor could be responsible for coordination of cell division and DNA replication in the pneumococcus. Using high throughput gene silencing with CRISPRi of all essential genes of *S. pneumoniae* (Liu *et al.*, 2017), we examined proteins leading to DNA content defects upon depletion. Here, we describe the identification of CcrZ, a conserved protein that activates DnaA to trigger initiation of DNA replication. Pneumococcal CcrZ localizes at the division site in a FtsZ-dependent manner and its inactivation leads to division defects. Together, our findings show that CcrZ acts as a novel spatio-temporal link between cell division and DNA replication in *S. pneumoniae*.

Results

CcrZ is a conserved bacterial cell cycle protein

We previously generated a knock-down library using CRISPRi (clustered regularly interspaced short palindromic repeats interference) targeting 348 conditionally essential genes of the serotype 2 strain *S. pneumoniae* D39V that were identified by Tn-Seq (transposon-insertion sequencing) (Liu *et al.*, 2017). Here, we investigated the function of *spv_0476*, encoding a protein of unknown function that is conserved in most Firmicutes (>30% identity) (Supplementary Fig. 1a). Silencing of *spv_0476* by CRISPRi led to a drastic reduction of the growth rate as well as appearance of anucleate cells as visualized by DAPI staining (Fig. 1a-b). We renamed SPV_0476 to CcrZ (for Cell Cycle Regulator protein interacting with FtsZ) for reasons explained below. *ccrZ* is in an operon with *trmB*, which encodes a tRNA methyltransferase and this operon structure is conserved across Firmicutes (Supplementary Fig. 1a).

To exclude the possibility that the observed phenotypes of *ccrZ* silencing were caused by polar effects on *trmB* expression, we constructed a deletion of *trmB*. This deletion did not lead to any growth defect (Supplementary Fig. 1b left panel). While Tn-seq indicated that *ccrZ* is essential (Liu *et al.*, 2017), we were able to generate a Δ*ccrZ* deletion mutant, although cells grew very slow.

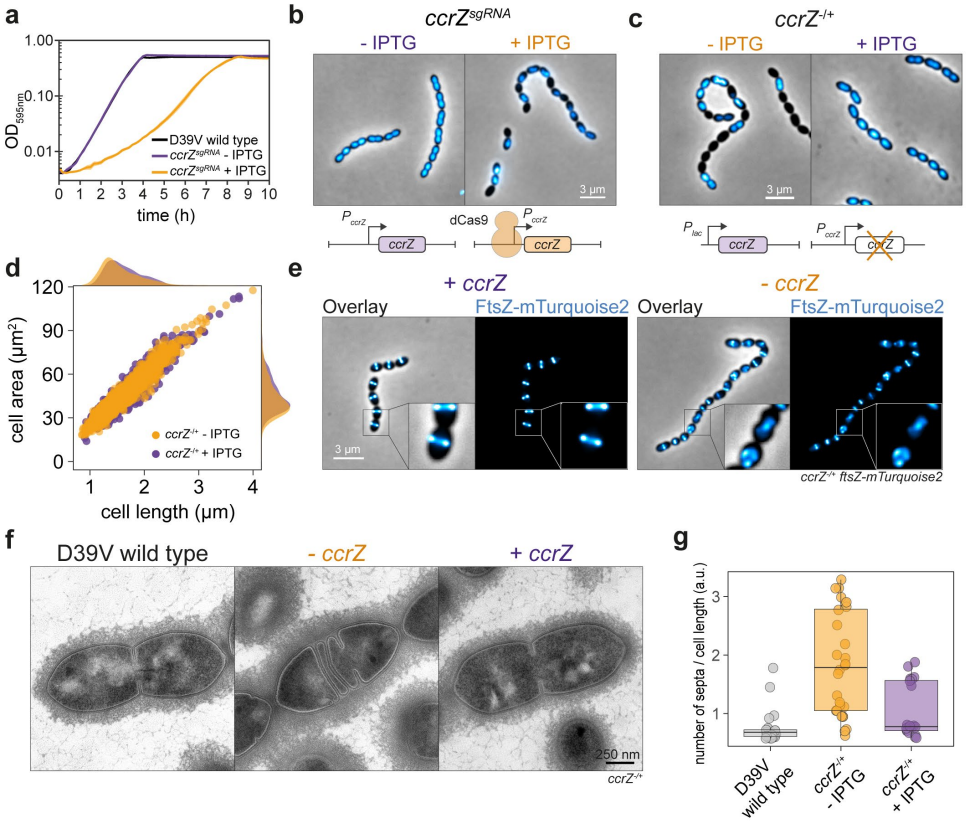

Figure 1. Depletion of CcrZ leads to anucleate cells and division defects

(**a**) growth curve of cells with *ccrZ* targeted by CRISPRi (*ccrZ*^{sgRNA} + IPTG) indicates a clear growth defect when *ccrZ* is silenced. (**b**) *ccrZ* silencing leads to appearance of anucleate cells, as visualized by DAPI staining. (**c**) *ccrZ* depletion by ectopic expression via the IPTG-inducible P_{lac} promoter also leads to cells lacking a nucleoid, as observed by DAPI staining. (**d**) distribution of cell area of *ccrZ*-depleted cells, *ccrZ* depletion leads to a slight decrease in cell length and cell area (P value = 2.2 x 10^{-16}, Wilcoxon rank sum test). (**e**) when a deletion of *ccrZ* is complemented (left panel), FtsZ-mTurquoise2 shows a clear mid-cell localization, while it appears as a blurry signal in several cells upon *ccrZ* depletion (right panel). (**f**) transmission electron microscopy (TEM) indicates that cells depleted for *ccrZ* form multiple, often incomplete, septa. (**g**) distribution of number of septa per cell length as determined by TEM for 22 wild type cells, 28 CcrZ-depleted cells and 17 *ccrZ*-complemented cells (P value = 1 x 10^{-6} for wild type vs CcrZ-depleted cells and P value = 0.0013 for *ccrZ*-complemented vs CcrZ-depleted cells, Wilcoxon rank sum test with Bonferroni adjustment).

We therefore constructed a depletion of CcrZ by ectopically expressing CcrZ under control of either an IPTG- or a Zn^{2+}- inducible promoter (P_{lac} and P_{Zn} respectively) and deleted *ccrZ* from its native location (*ccrZ*$^{-/+}$ and P_{Zn}-*ccrZ*$^{-/+}$ respectively). Depletion of CcrZ led to a significant growth delay at 37°C and 30°C, confirming the CRISPRi observations (Supplementary Fig. 1b). Immunoblotting using a specific antibody raised against purified CcrZ confirmed CcrZ depletion (Supplementary Fig. 1c). In line with the CRISPRi observations, DNA staining of cells depleted for CcrZ showed that 20% of cells lacked a nucleoid (Fig. 1c, 442 cells counted). To test whether the *ccrZ*-deletion phenotype was conserved in other Gram-positive bacteria, we silenced *ccrZ* (*SAOUHSC_01866*, here $ccrZ_{Sa}$) in *Staphylococcus aureus* SH1000 using CRISPRi and deleted the *Bacillus subtilis* 168 *ccrZ* homolog (*ytmP*, here $ccrZ_{Bs}$). Upon $CcrZ_{Sa}$ silencing in *S. aureus*, we observed a high proportion of anucleate cells, as well as a delay in growth. In contrast, no obvious phenotypical changes were observed for *B. subtilis* (Supplementary Fig. 1d). Interestingly, the *S. pneumoniae ccrZ* deletion could not be complemented by expression of *ccrZ* from either *B. subtilis* or *S. aureus* as only very small colonies were present on agar plate. In contrast, depletion of *S. aureus* CcrZ was rescued by expression of CcrZ from *B. subtilis* (Supplementary Fig. 1d).

In addition to an increase of the number of anucleate cells, CcrZ depletion in *S. pneumoniae* also led to slight morphological defects and modest changes in cell size when analyzed by phase contrast microscopy (Fig. 1d). Polysaccharide capsule production has previously been linked to the pneumococcal cell cycle (Nourikyan *et al.*, 2015), but capsule production was not impacted as the amount of capsule was similar between a CcrZ mutant and wild type (Supplementary Fig. 1e). To visualize division sites in live cells, we constructed a translational fusion of mTurquoise2 to the tubulin-like protein FtsZ (as the only copy of FtsZ, expressed from its native genetic location), which assembles into distinct rings at new division sites where it recruits the machinery required to form septa (Du and Lutkenhaus, 2017). As shown in Figure 1e, Z-rings were clearly mis-localized upon CcrZ depletion, with the presence of several aberrant Z-rings in a fraction of the cells (Fig. 1e). To obtain more insights into the morphological defects caused by CcrZ depletion and verify that the increased number of septa are not due to the fluorescent protein fused to FtsZ, we employed transmission electron microscopy (TEM) in untagged cells. While not evident by phase contrast microscopy, when *ccrZ* was depleted we observed frequent aberrant septum formation using TEM, in line with the FtsZ localization data, and many cells harbored two (18 %) to four (4 %) septa while typically only one septum is observed in wild type cells (Fig. 1f-g).

S. pneumoniae CcrZ is part of the divisome

As CcrZ seems to be involved in both chromosome biology and cell division, we examined its subcellular localization. Strikingly, immunofluorescence on fixed cells using a CcrZ-specific antibody demonstrated a clear mid-cell localization (Supplementary Fig. 2a). To assess the localization of CcrZ in live cells, we created several functional fusions of a green fluorescent protein to the N-terminus of CcrZ (*gfp-ccrZ*) or a red fluorescent protein to the C-terminus (*ccrZ-mKate2*) and inserted either construct at the native *ccrZ* locus (Supplementary Fig. 1c). Visualization of fluorescently tagged CcrZ by epifluorescence microscopy in live bacteria showed that CcrZ localizes at mid-cell (Fig. 2a). This localization was also conserved in both the TIGR4 and unencapsulated R6 strains (Supplementary Fig. 2b).

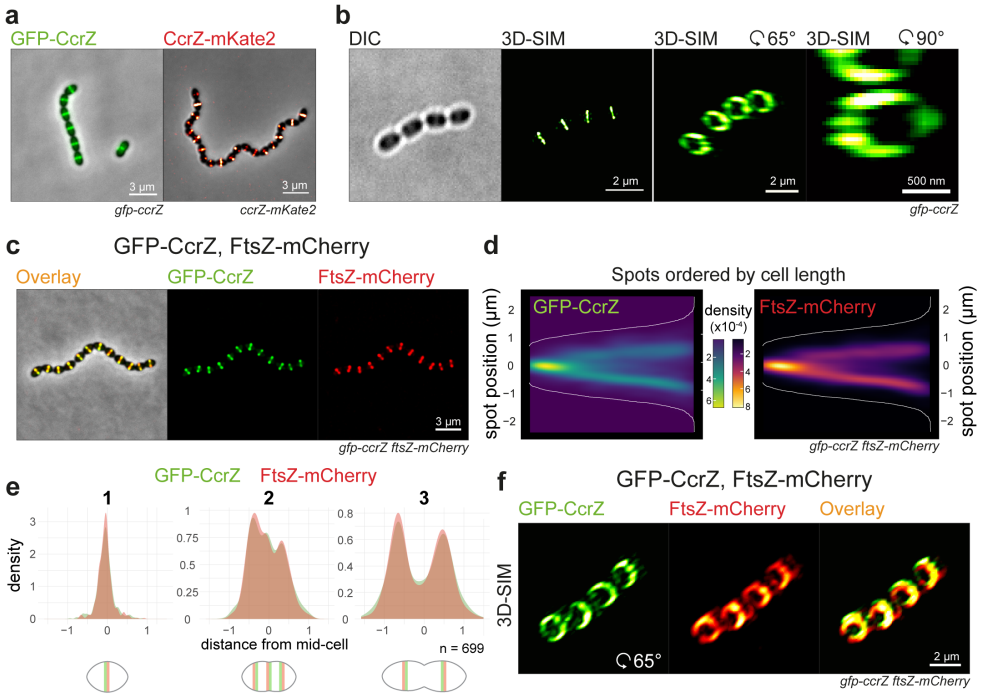

Figure 2. CcrZ co-localizes with FtsZ at new division sites

(**a**) CcrZ localizes at mid-cell in live wild type *S. pneumoniae* cells as observed by epifluorescence microscopy of GFP-CcrZ and CcrZ-mKate2. (**b**) 3D-SIM of GFP-CcrZ and reconstructed volume projection (right) indicate that CcrZ forms a patchy ring at mid-cell. (**c**) GFP-CcrZ and FtsZ-mCherry co-localize in wild type cells. (**d**) localization signal of GFP-CcrZ and FtsZ-mCherry in 699 cells of a double labelled *gfp-ccrZ ftsZ-mCherry* strain, ordered by cell length and represented by a heatmap. (**e**) GFP-CcrZ and FtsZ-mCherry co-localize during the entire cell cycle, as visualized when signal localization over cell length is grouped in three quantiles. (**f**) 3D-SIM co-localization of GFP-CcrZ and FtsZ-mCherry shows a clear co-localizing ring with identical patchy pattern.

Interestingly, $CcrZ_{Sa}$ and $CcrZ_{Bs}$ did not localize as clear rings at mid-cell in *S. aureus* and *B. subtilis* (Supplementary Fig. 2b), indicating that the activity and/or localization of CcrZ in these organisms is regulated differently. In order to get higher spatial resolution of *S. pneumoniae* CcrZ, 240 images (16 stacks) on live cells were acquired using 3D-structured illumination microscopy (3D-SIM) and reconstructed to generate a super resolution image and a 3D fluorescence image of GFP-CcrZ. As shown in Fig. 2b and Supplementary Video 1, CcrZ forms a patchy ring at mid-cell. Furthermore, time-lapse microscopy showed that CcrZ disassembles from the old septum to assemble at the newly formed division site (Supplementary Video 2). To test whether the mid-cell localization of *S. pneumoniae* CcrZ coincides with FtsZ, we constructed a CcrZ / FtsZ double-labelled strain (*gfp-ccrZ ftsZ-mCherry*). As shown in Fig. 2c, CcrZ co-localized with FtsZ and analysis of still images from exponentially growing cells corroborated this observation (Fig. 2c-e, Supplementary Video 3). 3D-SIM also indicated an overlap of GFP-CcrZ and FtsZ-mCherry as well as a similar circular co-localizing pattern at mid-cell (Fig. 2f, Supplementary Fig. 2c and Supplementary Video 4).

Prediction of CcrZ's topology using TMHMM (Krogh *et al.*, 2001) did not indicate the presence of a transmembrane domain; CcrZ's septal localization might then rely on another partner. To identify possible partners, we purified GFP-CcrZ expressed from *S. pneumoniae* and untagged cytosolic sfGFP as a control using anti-GFP nanobodies (GFP-Trap) without cross-linking, and directly analyzed the purified fraction by liquid chromatography-tandem mass spectrometry (LC-MS/MS). Interestingly, we found an enrichment (> 5-fold change) for several proteins from the divisome (FtsZ, PBP2X, EzrA and FtsH) (Supplementary Table 1). To determine which of the candidates might interact directly with CcrZ, we used the NanoBit complementation reporter assay (Bodle *et al.*, 2017; Oliveira Paiva *et al.*, 2019), which uses an enhanced luciferase separated into two different fragments (large bit (LgBit) and small bit (SmBit), respectively). Fusion of two different interacting proteins to each fragment can restore the activity of the luciferase and, in presence of a furimazine-based substrate, produce light. Accordingly, we fused the C-terminal extremity of CcrZ to LgBit (*ccrZ-LgBit*) and putative partners to SmBit and integrated the different constructs at their respective loci under native control. We also fused SmBit to other proteins known to localize at the septum (Cps2E, FtsA, FtsW and ZapA), or to the highly abundant histone-like protein HlpA localizing at the nucleoid and used a strain expressing both HlpA-LgBit and HlpA-SmBit as a positive control of interaction. After addition of the substrate, we could detect a strong and reproducible signal when FtsZ was fused to SmBit and CcrZ to LgBit, as well as a weaker signal for FtsA, EzrA and ZapA, and no detectable signal for any of the other proteins (Fig. 3a). This result indicates that FtsZ and CcrZ in *S. pneumoniae* are in very close proximity in space. Interestingly, using

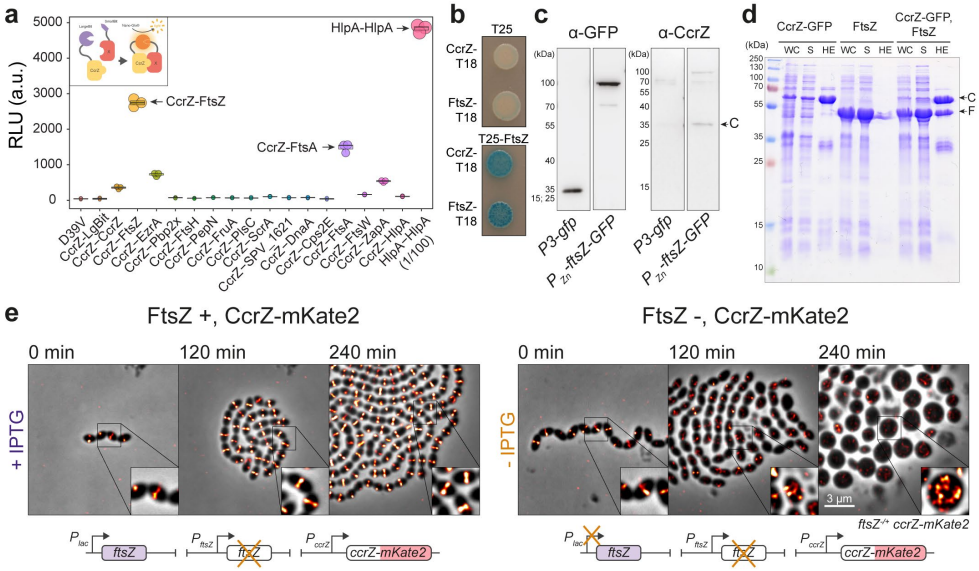

Figure 3. CcrZ directly interacts with FtsZ

(**a**) split-luciferase assay using several combinations with CcrZ-LgBit reveals that CcrZ and FtsZ are in very close proximity, as indicated by a high luminescence signal. FtsA, EzrA and ZapA, all three interacting directly with FtsZ, also gave a slight signal. *hlpA-LgBit hlpA-SmBit* (HlpA-HlpA), here diluted 100 times, is used as positive control. Each dot represents the average of 15 measurements of a technical replicate, with the size of the dot representing the SEM. (**b**) FtsZ-CcrZ interaction confirmation by bacterial two-hybrid. T25 is the empty vector pST25 and T25-FtsZ corresponds to vector pST25-FtsZ used in combination with pUT18-CcrZ (CcrZ-T18) and pUT18-FtsZ (FtsZ-T18). (**c**) affinity purification of FtsZ-GFP from *S. pneumoniae* cells (2nd lane) also pulls down untagged CcrZ (4th lane). Purification of GFP alone (first lane) did not pull CcrZ down (3rd lane). (**d**) FtsZ from *S. pneumoniae* expressed in *E. coli* co-purifies with $CcrZ_{Sp}$-GFP by affinity purification. WC: whole cell extract, S: supernatant, HE: heat eluted products, C: CcrZ, F: FtsZ. (**e**) epifluorescence time-lapse microscopy of CcrZ-mKate2 at 37°C in presence (left panel) or absence (right panel) of FtsZ. When FtsZ amounts are reduced, cells increase their size and CcrZ is de-localized from mid-cell.

a strain expressing both CcrZ-LgBit and CcrZ-SmBit, a weak signal was observed indicating that CcrZ might also self-interact (Fig. 3a).

To confirm the observed interaction with FtsZ, we used a bacterial two-hybrid assay in *E. coli* (Karimova *et al.*, 1998). Again, we observed a robust interaction between CcrZ and FtsZ, while T25-FtsZ did not interact with the empty vector alone, strongly suggesting that CcrZ directly binds to FtsZ (Fig. 3b). Co-immunoprecipitation of FtsZ-GFP from *S. pneumoniae* cells confirmed the *in vivo* interaction with CcrZ (Fig. 3c). Affinity purification of $CcrZ_{Sp}$-GFP when over-expressing $FtsZ_{Sp}$ in *E. coli* also confirmed this interaction as we were able to co-purify FtsZ in large amounts (Fig. 3d). To test whether the localization of CcrZ depends on FtsZ, we constructed a strain expressing CcrZ-mKate2 as well as a second copy of FtsZ under the control of an IPTG-inducible promoter and deleted the native *ftsZ* gene (*ftsZ*$^{-/+}$). As expected, FtsZ depletion led to

aberrant cell morphology and, consistent with a FtsZ-CcrZ interaction, CcrZ-mKate2 was rapidly mis-localized and the signal was spread throughout the cytoplasm (Fig. 3e, Supplementary Video 5). In total, we conclude that CcrZ localizes to new division sites via a direct interaction with FtsZ.

CcrZ controls DNA replication

As shown in Fig. 1c, when cells are depleted for CcrZ, a large proportion of cells become anucleate. To investigate the consequences of lack of CcrZ on chromosome segregation in live cells, we introduced a translational fluorescent fusion of HlpA (Kjos *et al.*, 2015) and deleted *ccrZ*. Localization of HlpA-mKate2 in this slow growing Δ*ccrZ* mutant showed similar results to DAPI stained cells depleted for CcrZ and we observed that 19 % of cells lacked a nucleoid signal (Supplementary Fig. 4a, 4855 cells counted). Time-lapse imaging indicated that cells with defective DNA content had either no DNA at all or chromosomes "guillotined" during septum closure suggesting reduced nucleoid occlusion control in Δ*ccrZ* (Fig. 4a, Supplementary Video 6). We also co-localized FtsZ-CFP with HlpA-mKate2 while depleting CcrZ for a short period of time (2h). Interestingly, we observed many cells with a chromosome localized at only one half of the cell, at one side of the Z-ring (Fig. 4b). The absence of DNA in the other half of the cell could be explained by defective DNA segregation, by impaired replication or by DNA degradation.

When attempting to make clean *ccrZ* deletions, in addition to small colonies typical of slow growing mutants, there were also spontaneous large, wild type-sized colonies. Growth analysis of cells from three of these large colonies (*ccrZ*$^{supp1\text{-}3}$) showed that cells behaved like wild type and DAPI staining revealed a restoration of wild type DNA content (Fig. 4c-d). To verify whether these wild type-like phenotypes were caused by suppressor mutations, the genomes of these fast-growing strains were sequenced. All three strains still contained the *ccrZ* deletion and, in addition, contained a single nucleotide polymorphism elsewhere in the genome (Fig. 4e). Two missense mutations were found in *dnaA* (DnaA-Q247H and DnaA-S292G) and one nonsense mutation in *yabA* (YabA-E93*). Since DnaA promotes initiation of DNA replication and YabA hampers it by preventing interaction of DnaA with DnaN (Felicori *et al.*, 2016), we wondered whether the frequency of DNA replication initiation was changed in a *ccrZ* mutant.

To test this hypothesis, we quantified the copy number ratio between chromosomal origin and terminus regions (*oriC/ter* ratios) using real-time quantitative PCR. In a wild type situation, during exponential growth, the *oriC/ter* ratio varies between 1.4 – 1.8, as most cells have started a round of DNA replication (note that in contrast to *E. coli* and *B. subtilis*, multifork replication does not occur in *S. pneumoniae*) (Slager *et al.*, 2014). Remarkably, depletion of CcrZ resulted in a significantly decreased DNA

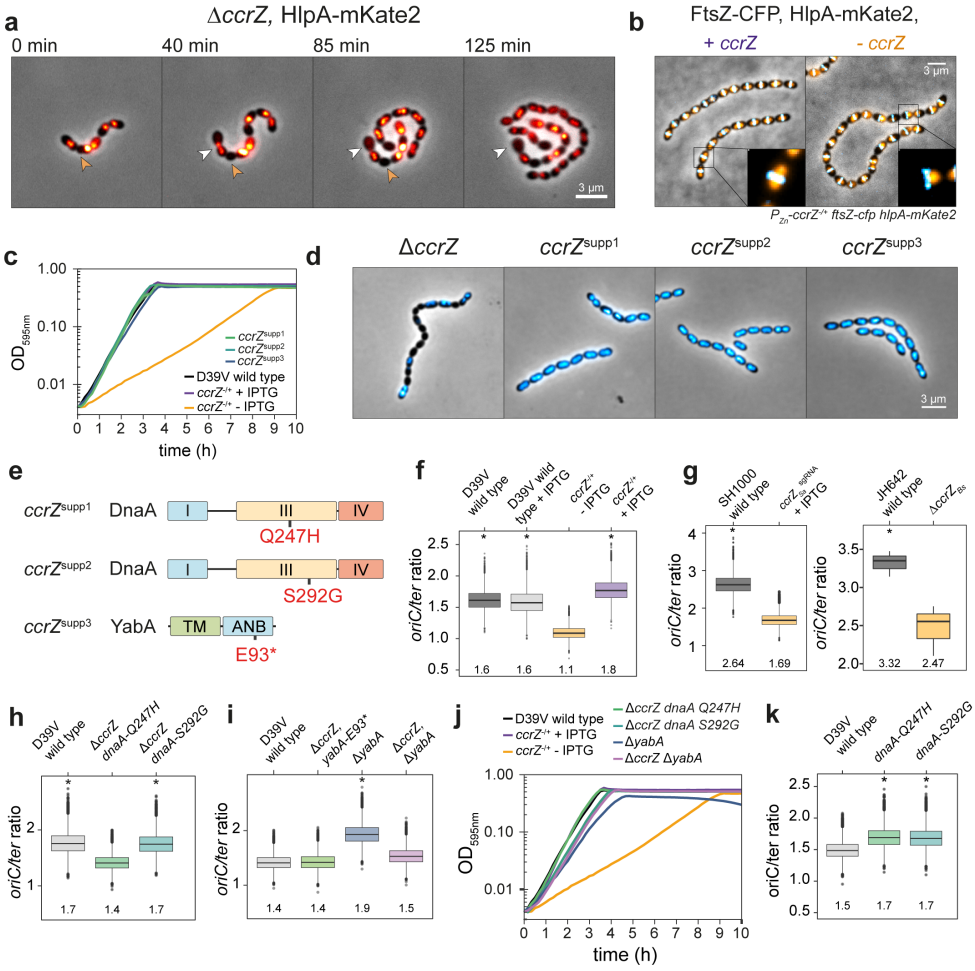

Figure 4. CcrZ-depleted cells under-replicate

(**a**) time-lapse microscopy of HlpA-mKate2 at 30°C in a Δ*ccrZ* mutant shows several cells with defective DNA content. Orange arrows indicate a cell with no nucleoid after cell division; white arrows indicate a cell with "guillotined" DNA. (**b**) co-localization of FtsZ-CFP and HlpA-mKate2 when depleting *ccrZ* indicates that several cells have a nucleoid located only on one side of the Z-ring. (**c**) three isolated *ccrZ* mutants (ccrZ$^{supp1-3}$) restore wild type growth to Δ*ccrZ*. (**d**) DAPI staining of the three selected *ccrZ* suppressors mutants shows a restoration of DNA content. (**e**) schematic representation of the localization of suppressor mutations in the domain III of DnaA and in the DnaA/DnaN binding motif (ANB) of YabA. TM: tetramerization domain. (**f**) *oriC/ter* ratios as determined by RT qPCR for D39V wild type and CcrZ-depleted cells. Average values are indicated under the boxes. CcrZ depletion leads to a clear reduction in *oriC/ter* ratio. (**g**) *oriC/ter* ratios for *S. aureus* upon $ccrZ_{Sa}$ depletion (left) and for *B. subtilis* with $ccrZ_{Bs}$ deletion (right). (**h**) *oriC/ter* ratios of strains with *dnaA* mutations re-inserted into a Δ*ccrZ* background show that these mutations restore replication initiation rates. (**i**) *yabA* deletion leads to an increase in *oriC/ter* ratios, while suppressor mutation *ccrZ*^{supp3} (Δ*ccrZ*, *yabA-E93**) as well as co-deletion of *yabA* together with *ccrZ* (Δ*yabA* Δ*ccrZ*) restored a wild type ratio. (**j**) while *yabA* deletion alters the growth rate, a Δ*yabA* Δ*ccrZ* double mutant grows like wild type. *dnaA Q247H* and *dnaA S292G* mutation also restore a wild type rate in a Δ*ccrZ* mutant. (**k**) *dnaA* mutation in a wildtype background increases the *oriC/ter* ratios. See Methods for statistical tests.

replication initiation rate with an *oriC/ter* ratio of 1.1 vs 1.8 for complemented cells (P value < 0.05) (Fig. 4f). Interestingly, the same observation was made for both *B. subtilis* and *S. aureus*, where deletion or depletion of CcrZ caused a clear reduction in *oriC/ter* ratios (Fig. 4g). As the identified *ccrZ*-bypass mutations were found in DNA replication initiation regulators, we tested whether they would restore the *oriC/ter* ratio in a fresh *ccrZ* deletion background in *S. pneumoniae*. Indeed, the *oriC/ter* ratios for Δ*ccrZ dnaA-S292G,* Δ*ccrZ dnaA-Q247H* and for *yabA-E93** (*ccrZ*^{supp3}) were like wild type (Fig. 4h-i).

The point mutation found in *yabA* causes premature translation termination at the C-terminus of YabA. When *yabA* alone was replaced by an antibiotic resistance cassette, we observed an increase of replication initiation as well as a reduced growth rate; but when *ccrZ* was co-deleted, wild type like growth and a wild type *oriC/ter* ratio was restored (Fig. 4i-j). DnaA suppressor mutations were located in the AAA+ ATPase domain of DnaA and it was previously reported that specific mutations in this domain could increase the initiation rate in *B. subtilis* (Scholefield *et al.*, 2012). To determine if those mutations alone were able to induce over-initiation, we inserted each *dnaA* mutation into a wild type background strain. Marker frequency analysis detected an increase in the *oriC/ter* ratio for both *dnaA* alleles (Fig. 4k). We conclude that mutations that increase the rate of initiation of DNA replication can rescue the Δ*ccrZ* phenotype.

CcrZ is a conserved regulator of DnaA

The results so far suggest that the division defects observed in the absence of CcrZ are due to perturbed Z-ring formation caused by under-replication of the chromosome. To examine whether disruption of DNA replication in general could lead to division defects similar to those of a *ccrZ* mutant, we took advantage of a thermosensitive *dnaA* mutant (*dnaA*^{TS}) in which DNA replication initiation is drastically reduced when cells are grown at the non-permissive temperature (40°C) (Mercy *et al.*, 2019). As expected, when shifted to the non-permissive temperature, many cells were anucleate (Supplementary Fig. 5a). Strikingly, localization of FtsZ-mTurquoise2 in the *dnaA*^{TS} strain at 40°C phenocopied the Δ*ccrZ* mutant, and FtsZ was frequently mis-localized (Fig. 5a). Furthermore, examination by TEM at 40°C showed many cells with aberrant septa like CcrZ-depleted cells (Fig. 5b). As DnaA inactivation leads to strikingly similar phenotypes, these data are consistent with the idea that CcrZ exerts a control on DNA replication initiation.

To test whether CcrZ controls DNA replication via regulating DnaA activity, we made use of the fact that a *B. subtilis* Δ*ccrZ*$_{Bs}$ mutant also under-initiates (Fig. 4g) and a strain was constructed in which DNA replication was driven in a RepN-dependent manner (from a plasmid origin of replication *oriN*) rather than from DnaA-dependent

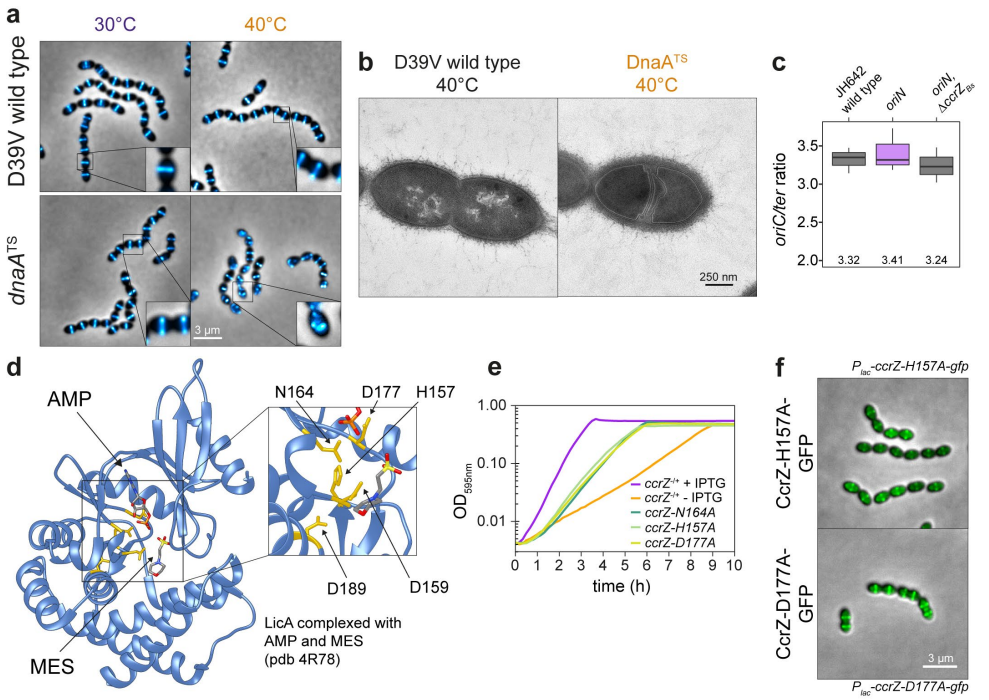

Figure 5. CcrZ activates DnaA-dependent replication initiation

(**a**) localization of FtsZ-mTurquoise2 in a thermo-sensitive DnaA strain (*dnaA*^{TS}) at permissive (30°C) and non-permissive (40°C) temperatures shows that *dnaA* inactivation leads to a similar phenotype as *ccrZ* inactivation. (**b**) TEM of *dnaA*^{TS} at non-permissive temperature (40°C) indicates the presence of multiple septa, similarly to a Δ*ccrZ* mutant. (**c**) when replication is driven in a RepN-dependent manner in *B. subtilis* (*oriN*), no decrease in *ori/ter* ratio can be observed in absence of *ccrZ*$_{Bs}$ (*oriN*, Δ*ccrZ*$_{Bs}$). (**d**) LicA choline kinase structure complexed with AMP and MES (2-(N-morpholino)ethanesulfonic acid). The 5 residues indicated in yellow are conserved between CcrZ and LicA (and highly conserved within Firmicutes). (**e**) mutation of three of these five conserved residues in the putative ATP binding pocket leads to growth defects. (**f**) localization of GFP-CcrZ H157A and GFP-D177A is not impaired.

initiation (from *oriC*). This showed no significant *ori-ter* ratio differences when *ccrZ* was deleted (Fig. 5c), suggesting that CcrZ is an activator of DnaA-dependent initiation of replication in *B. subtilis*. We therefore tested whether CcrZ interacts directly with DnaA to trigger DNA replication and employed bacterial two-hybrid assays and the Split-luc system using pneumococcal CcrZ and DnaA (Fig. 3a and Supplementary Fig. 5b). However, none of these assays revealed a direct protein-protein interaction. It is still possible that CcrZ interacts directly with DnaA, but that we cannot detect it with these assays. Alternatively, another factor might be required for CcrZ's function or CcrZ indirectly affects the activity of DnaA in replication initiation.

CcrZ's conserved residues are essential for its function

S. pneumoniae CcrZ is 264 amino acids long and is predicted to have a single APH (aminoglycoside phosphotransferase enzyme family) domain. Sequence alignment using Psi-BLAST showed homology with phosphotransferase enzyme family proteins, while pairwise comparisons of profile-hidden Markov models (HMMs) using HHpred (Soding *et al.*, 2005) identified homologies with ethanolamine- and choline kinases. Despite various attempts, we have not been able to establish any biochemical activity or nucleotide binding for recombinant purified CcrZ and were unable to produce protein crystals, probably because of its rapid precipitation in solution. Nevertheless, as CcrZ is highly conserved in Firmicutes, we aligned CcrZ protein sequence with 1000 protein sequences from UniRef50 and identified three residues conserved in more than 95% of the proteins (D159, N164 and D177) and two other residues (H157 and D189) in more than 80% (Supplementary Fig. 5c). To determine the position of these residues, the *S. pneumoniae* CcrZ protein sequence was mapped onto the crystal structure of the best hit from the HMM alignment, the choline kinase LicA, in complex with adenosine monophosphate (AMP) (pdb 4R78). Interestingly, these five conserved residues appear to be in spatial proximity to AMP and thus to a putative nucleotide-binding pocket (Fig. 5d). Mutational analysis of these residues showed that at least H157, N164 and D177 are essential for CcrZ's function in *S. pneumoniae* (Fig. 5e), while mutating CcrZ-D159 or CcrZ-D189 did not lead to any growth defect. All three mutants were properly produced (Supplementary Fig. 1c) and CcrZ-H157A and CcrZ-D177A could still localize at the septum (Fig. 5f). Therefore, these three residues are crucial for the function of CcrZ. CcrZ-N164 and CcrZ-D177 residues correspond to LicA-N181 and LicA-D194, respectively, and both residues were shown to interact with the α-phosphate moiety of AMP (Wang *et al.*, 2015). It is therefore very likely that CcrZ-N164 and CcrZ-D177 also contribute to binding of a as of yet unknown nucleotide.

A model for CcrZ-controlled DNA replication in S. pneumoniae

We showed above that CcrZ is fundamental for DnaA-dependent DNA replication initiation in *B. subtilis* and that *S. pneumoniae* CcrZ localizes at mid-cell for most of the cell cycle. In *S. pneumoniae*, once DNA replication initiates at mid-cell, the origins localize at both future division sites, while the replication machinery stays near the Z-ring until completion of replication and closure of the septum (van Raaphorst *et al.*, 2017). We therefore hypothesized that CcrZ is brought to mid-cell by FtsZ to promote initiation of DNA replication. To map the hierarchy of events that take place during the pneumococcal cell cycle, we constructed a triple-labeled strain (strain *ccrZ-mKate2 dnaN-sfTQ*^{OX} *parB*$_p$*-mYFP*) in which CcrZ is fused to a red fluorescent protein, DNA replication is visualized by a DnaN fusion to a cyan fluorescent

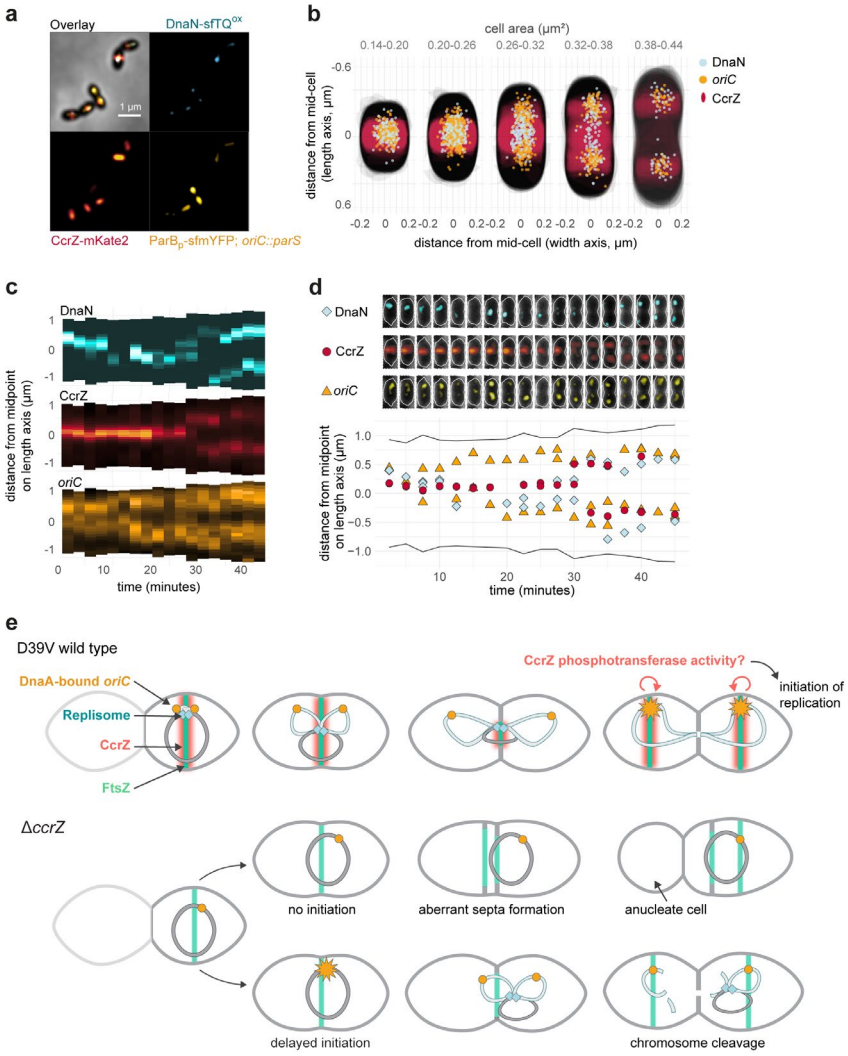

Figure 6. Spatio-temporal localization of CcrZ via FtsZ ensures proper timing of DNA replication in *S. pneumoniae*

(**a**), microscopy of the origin of replication (yellow), replication fork (cyan) and CcrZ (red) in live *S. pneumoniae* wild type background cells. (**b**), DnaN, *oriC* and CcrZ localizations grouped by cell area (µm²) in five equally sized groups. Analyzed from snapshots of exponentially growing cells. (**c**), single-cell kymographs of DnaN, CcrZ and *oriC* localizations in a 2:30 minute interval time-lapse movie. (**d**), tracked DnaN, *oriC* and CcrZ over time in a single cell. Top: overlay of fluorescence, cell outline and phase-contrast of the cell displayed in panel c and bottom: fluorescence localization on the length axis of the same single cell over time. (**e**), model for spatio-temporal control of replication by CcrZ. In *S. pneumoniae*, CcrZ is brought to the middle of the cell where the DnaA-bound origin of replication is already positioned. CcrZ then stimulates DnaA to trigger DNA replication by an as of yet unknown activity, possibly involving a phosphor-transfer event. While the precise regulation and localization of CcrZ seems diverse between different organisms, CcrZ's activity to stimulate DNA replication is conserved, at least in *S. pneumoniae, S. aureus* and *B. subtilis*.

protein, and the origin of replication is marked with a yellow fluorescent reporter (see Methods). Imaging of this strain by short time-lapse fluorescence microscopy (< 1 min) revealed that once CcrZ is assembled at mid-cell, DNA replication initiates and the newly replicated origins of replication are segregating as cells elongate (Fig. 6a-d, Supplementary Video 7). The replication machinery remains near the old division site together with CcrZ, only to move to the new cell division sites once DNA replication is complete. This data supports a model in which FtsZ brings CcrZ to *oriC* to stimulate DnaA to fire a new round of replication ensuring that DNA replication only commences after the origins are well segregated and positioned at the new mid-cell position. Indeed, DnaA co-localizes with CcrZ in new-born cells (Supplementary Fig. 6). In the absence of CcrZ, initiation of DNA replication is mis-timed and occurs too late relative to cellular growth and Z-ring formation, frequently leading to futile division events and anucleate cells (Fig. 6e).

Discussion

Notions of cell cycle events synchronization in bacteria emerged in the mid-1900s and a tremendous amount of work has since been done aiming at explaining how DNA replication, cell growth and cell division are intertwined. Two robust models emerged (adder and sizer) based on observations that cell size and DNA replication events were connected. However, these models were established mainly for rod-shaped bacteria that are capable of multi-fork replication. *S. pneumoniae* differs from these model organisms as it has an ovoid-like shape, lacks the canonical Min and Noc systems and does not perform multi-fork replication. The principal contribution of this work is the identification and initial functional characterization of a new mechanism for cell cycle regulation in *S. pneumoniae* via the CcrZ protein. We show that CcrZ's septal localization occurs via a direct interaction with FtsZ. Our data is consistent with a model in which, once positioned at mid-cell where the DnaA-bound origin of replication is located, CcrZ stimulates DnaA, by an as of yet unknown mechanism, to initiate DNA replication (Fig. 6). Importantly, CcrZ's function of controlling DnaA seems conserved in *S. aureus* and *B. subtilis*, and likely in many other Gram-positive bacteria (Supplementary Fig. 1a).

Besides the production of anucleate cells and cells with cleaved chromosomes, *ccrZ* mutants contain multiple aberrant division septa (Fig. 6e). Notably, this is phenocopied by a temperature sensitive DnaA allele. This indicates that chromosome replication itself, and correct localization of the chromosome has an important role in nucleoid occlusion: when initiation is too late and the new daughter chromosomes are not fully segregated, division can take place over the DNA resulting in dissected chromosomes. In this respect, it is interesting to note that the *S. aureus* Noc system

also controls DNA replication, as Δ*noc* cells over-initiate DNA replication (Pang *et al.*, 2017). In support of our findings, a lethal Δ*noc* Δ*comEB* double mutant could be rescued by a suppressor mutation in $ccrZ_{Sa}$ (Pang *et al.*, 2017), further indicating that $CcrZ_{Sa}$ is also involved in the control of DNA replication in *S. aureus*.

This work uncovers a novel mechanism in which a single protein links cell division with DNA replication control. In this model, Z-ring formation is used as a timer for the initiation of DNA replication. When cell division terminates, leading to the formation of another Z-ring at the new division site, CcrZ is brought along and can activate a new round of DNA replication. This simple system ensures that DNA replication only commences a single time per cell cycle in newborn cells. It will be interesting to see how CcrZ controls the cell cycle in other bacteria, what the involved biochemical activities are and whether CcrZ will prove as a new target for innovative antibiotics.

Methods

Bacterial strains and culture conditions.

All strains, plasmids and primers used are listed in Supplementary Table 1 and Supplementary Table 2.

All pneumococcal strains in this study are derivate of *S. pneumoniae* D39V (Slager *et al.*, 2018), unless specified otherwise, and are listed in Supplementary Table 1. Strains were grown in liquid semi-defined C+Y medium (Domenech *et al.*, 2018) at 37˚C from a starting optical density (OD_{600nm}) of 0.01 until the appropriate OD. Induction of the zinc-inducible promoter (P_{Zn}) was carried out by supplementing the medium with 0.1 mM $ZnCl_2$ and 0.01 mM $MnCl_2$ (Sigma-Aldrich) and the IPTG-inducible promoter (P_{lac}) was activated with 1 mM IPTG (β-D-1-thiogalactopyranoside, Sigma-Aldrich). For all related experiments, depletion strains where first grown without inducer until OD_{600nm} = 0.3 and then diluted 100 times in fresh medium and grown until the desired OD. Transformation of *S. pneumoniae* was performed as described before (Domenech *et al.*, 2018) with cells taken at exponential growth phase (OD_{600nm} = 0.1). When necessary, the medium was supplemented with the following antibiotics: chloramphenicol (0.45 μg.mL^{-1}), erythromycin (0.2 μg.mL^{-1}), kanamycin (250 μg.mL^{-1}), spectinomycin (200 μg.mL^{-1}) and tetracycline (0.5 μg.mL^{-1}).

S. aureus strains are listed in Supplementary Table 1. Cells were grown in brain heart infusion (BHI) medium (Oxoid) with shaking at 37°C. When appropriate, 5 μg.mL^{-1} erythromycin and / or 10 μg.mL^{-1} chloramphenicol was added to the growth medium. All *S. aureus* plasmids were initially made in *E. coli* strain IM08B (Monk *et al.*, 2015). *E. coli* IM08B was grown in LB medium at 37°C with shaking; 100 μg.mL^{-1} ampicillin was added when appropriate. Plasmids were then transformed into *S. aureus* by

electroporation, as described previously (Löfblom *et al.*, 2007).

B. subtilis strains are listed in Supplementary Table 1. Cells were grown with shaking at 37°C in Luria-Bertani (LB) medium or S7 defined minimal medium with MOPS (3-(N-morpholino) propanesulfonic acid) buffer at a concentration of 50 mM rather than 100 mM supplemented with 1 % glucose, 0.1 % glutamate, trace metals, 40 µg.mL^{-1} phenylalanine, and 40 µg.mL^{-1} tryptophan (Jaacks *et al.*, 1989). Standard concentrations of antibiotics were used when appropriate. *B. subtilis* strains were derived from 1A700 or JH642 (*pheA1 trpC2*) (Perego *et al.*, 1988).

Strain construction

Construction of strains is described in the Supplementary Methods.

Microtiter plate-based growth assay

For *S. pneumoniae* growth assays, cells were first grown in C+Y medium pH = 7.4 until mid-exponential growth phase (OD_{595nm} = 0.3) with no inducer at 37°C, after which they were diluted 100 times in fresh C+Y medium supplemented with IPTG or $ZnCl_2$ when appropriate. Cellular growth was then monitored every 10 min at either 37°C or 30°C in a microtiter plate reader (TECAN Infinite F200 Pro). Each growth assay was performed in triplicate. The lowest OD_{595nm} of each growth curve was normalized to 0.004 (detection limit of the reader and initial OD_{595nm} of the inoculum) and the average of the triplicate values were plotted, with the SEM (Standard Error of the Mean) represented by an area around the curve.

For assessment of *S. aureus* growth, CRISPRi knockdown strains were grown overnight in BHI medium. Cultures were then diluted 100-fold and grown until OD_{600nm} = 0.4. The cultures were then re-diluted 200-fold in medium with or without inducer 500 µM IPTG. Growth analysis was performed on a Synergy H1 Hybrid (BioTek) microtiter plate reader at 37°C with measurement of OD_{600nm} every 10 min. Average of the triplicate values were plotted, with the SEM (Standard Error of the Mean) represented by an area around the curve.

Phase contrast and fluorescence microscopy

S. pneumoniae cells were grown in C+Y medium pH = 7.4 at 37°C to an OD_{595nm} = 0.1 without any inducer and diluted 100 times in fresh C+Y medium supplemented when appropriate with IPTG (for activation of dCas9, complementation of CcrZ and FtsZ, or expression of fluorescent fusions) or $ZnCl_2$ (for CcrZ complementation or expression of fluorescent fusions). At OD_{595nm} = 0.1, 1 mL of culture was harvested by centrifugation 1 min at 9,000 x g. For DAPI staining, 1 µg.mL^{-1} DAPI (Sigma-Aldrich) was added to the cells and incubated for 5 min at room temperature prior to centrifugation. For imaging of bulk exponentially growing cultures, cells were washed twice with 1 mL

ice-cold PBS and re-suspended into 50 µL ice-cold PBS; for time-lapse microscopy, cells were washed and re-suspended into 1 mL of fresh pre-warmed C+Y medium. 1 µL of cells were then spotted onto PBS- or C+Y-polyacrylamide (10 %) pads. For time-lapse microscopy, pads were incubated twice for 30 min in fresh C+Y medium at 37˚C prior to spotting. Pads were then placed inside a gene frame (Thermo Fisher Scientific) and sealed with a cover glass as described before (de Jong *et al.*, 2011). Microscopy acquisition was performed either using a Leica DMi8 microscope with a sCMOS DFC9000 (Leica) camera and a SOLA light engine (Lumencor), or using a DV Elite microscope (GE Healthcare) with a sCMOS (PCO-edge) camera and a DV Trulight solid state illumination module (GE Healthcare), and a 100x/1.40 oil-immersion objective. Phase contrast images were acquired using transmission light (100 ms exposure). Still fluorescence images were usually acquired with 700 ms exposure, and time-lapses with 200-300 ms exposure. Leica DMi8 filters set used are as followed: DAPI (Leica 11533333, Ex: 395/25 nm, BS: LP 425 nm, Em: BP 460/50 nm), CFP (Ex: 430/24 nm Chroma ET430/24x, BS: LP 455 Leica 11536022, Em: 470/24 nm Chroma ET470/24m), GFP (Ex: 470/40 nm Chroma ET470/40x, BS: LP 498 Leica 11536022, Em: 520/40 nm Chroma ET520/40m), YFP (Ex: 500/20 nm Chroma ET500/20x, BS: LP 520 Leica 11536022, Em: 535/30 nm Chroma ET535/30m) and mCherry (Chroma 49017, Ex: 560/40 nm, BS: LP 590 nm, Em: LP 590 nm). DeltaVision microscope used a DV Quad-mCherry filter set: GFP (Ex: 475/28 nm, BS: 525/80 nm, Em: 523/36 nm) and mCherry (Ex: 575/25 nm, BS: 605/50, Em: 632/60 nm). Images were processed using either LAS X (Leica) or SoftWoRx (GE Healthcare). For *S. aureus* microscopy, cells were induced as described above, grown until OD_{600nm} = 0.2 and analyzed on a Zeiss AxioObserver with an ORCA-Flash4.0 V2 Digital CMOS camera (Hamamatsu Photonics) through a 100x PC objective. HPX 120 Illuminator (Zeiss) was used as a light source for fluorescence microscopy. Images were processed using ZEN (Zeiss). Signals was deconvolved, when appropriate, using Huygens (SVI) software.

Transmission Electron Microscopy (TEM)

Strains were grown in C+Y medium at either 37°C, or at 30°C for *dnaA*^{TS}, until an OD_{595nm} = 0.3, with or without addition of $ZnCl_2$ (for *ccrZ* complementation or depletion, respectively) and diluted 100 times into 10 mL of fresh C+Y medium. Cells were then grown either at 37°C or at 40°C, for *dnaA* depletion in the *dnaA*^{TS} strain, until OD_{595nm} = 0.15. 5 mL of each sample was then fixed with 2.5 % glutaraldehyde solution (EMS) in phosphate buffer (PB 0.1 M pH = 7.4) (Sigma Aldrich) for 1h at room temperature, followed by 16 h incubation at 4°C. Cells were then post-fixed by a fresh mixture of osmium tetroxide 1 % (EMS) with 1.5 % potassium ferrocyanide (Sigma Aldrich) in PB buffer for 2 h at room temperature. Samples were then washed three times with distilled water and spun down in low melting agarose 2 % (Sigma Aldrich) and solidified in ice. Solid samples were then cut in 1 mm^3 cubes and dehydrated in

acetone solution (Sigma Aldrich) at graded concentrations (30 % for 40 min; 50 % for 40 min; 70 % for 40 min and 100 % for 3 x 1 h). This step was followed by infiltration in Epon (Sigma Aldrich) at graded concentrations (Epon 1/3 acetone for 2 h; Epon 3/1 acetone for 2 h, Epon 1/1 for 4 h and Epon 1/1 for 12 h) and finally polymerized for 48 h at 60°C.Ultra-thin sections of 50 nm were then cut on a Leica Ultracut (Leica Mikrosysteme GmbH) and placed on a copper slot grid 2 x 1 mm (EMS) coated with a polystyrene film (Sigma Aldrich). Sections were subsequently post-stained with 4 % uranyl acetate (Sigma Aldrich) for 10 min, rinsed several times with water, then with Reynolds lead citrate (Sigma Aldrich) for 10 min and rinsed several times with distilled water. Micrographs were taken using a transmission electron microscope Philips CM100 (Thermo Fisher Scientific) equipped with a TVIPS TemCam-F416 digital camera (TVIPS) and using an acceleration voltage of 80 kV. Number of septa and cell length were manually measured on TEM images of cells in the correct focal plane: 22 wild type cells, 28 CcrZ-depleted cells and 17 CcrZ-complemented cells.

3D Structured Illumination Microscopy (3D-SIM)

Samples for 3D-SIM were prepared as described previously by spotting 1 µL onto PBS-10 % acrylamide pads. Acquisition was performed on a DeltaVision OMX SR microscope (GE Healthcare) equipped with a 60x/1.42 NA objective (Olympus) and 488 nm and 568 nm excitation lasers. 16 Z-sections of 0.125 µm each were acquired in Structure Illumination mode with 20 ms exposure and 20 % laser power. The 240 images obtained were reconstructed with a Wiener constant of 0.01, and the volume reconstructed using SoftWoRx.

Image analysis and cells segmentation

All microscopy images were processed using Fiji (fiji.sc). Cell segmentation based on phase contrast images was performed either on Oufti (Paintdakhi *et al.*, 2016) or Morphometrics (Ursell *et al.*, 2017) and fluorescent signals where analyzed using Oufti (for CcrZ and FtsZ), MicrobeJ (Ducret *et al.*, 2016) (for CcrZ) or iSBatch (Caldas *et al.*, 2015) (for DnaN and *oriC*). Fluorescence heat-maps were generated using BactMAP (Raaphorst *et al.*, 2019).

Small-scale expression and GFP resin pull-down of FtsZ and CcrZ-GFP

For affinity purification of $CcrZ_{Sp}$-GFP while expressing $FtsZ_{Sp}$, $ccrZ_{Sp}$ was amplified from D39V genomic DNA with primers 213/214 and the resulting fragment was assembled using Golden Gate allelic replacement strategy (BsaI) with plasmid pET-Gate2 ccdB (pSG436), pSG366, pSG367 and pSG2562, resulting in plasmid pSG2950. *ftsZ* was amplified by PCR 215/216 on D39V genomic DNA and cloned into plasmid pJet1.2, resulting in plasmid pSG4227. The later was then assembled with pSG1694 using Golden Gate assembly, leading to plasmid pSG4268. BL21 DE3 Gold competent

cells were co-transformed with plasmids containing one of each *S. pneumoniae* FtsZ and CcrZ-GFP. Expression was ZYM-5052 autoinduction media (Studier, 2005). Cells were sonicated in buffer containing 50 mM Tris pH 7.5, 150 mM potassium acetate, 5 % glycerol, and 5 mM β-mercaptoethanol (lysis buffer). Supernatant was then mixed with GFP resin which was produced by crosslinking nanobody (Kubala *et al.*, 2010) to NHS-Activated Sepharose 4 Fast Flow beads (GE Healthcare) according to the manufacturer's instructions. After 1 hour of batch binding, resin was washed 10 column volume (CV) with lysis buffer. Beads were then re-suspended in 50 µL of lysis buffer mixed with SDS-PAGE loading dye containing 5 % w/v β-mercaptoethanol and heat treated at 95 ^{0}C for 15 minutes. Supernatant was collected and labelled heat elution (HE) samples. Whole cell lysate (WC), supernatant after sonication (S), and HE were loaded on 15 % SDS-PAGE gels and visualized by Coomassie staining.

Large-scale purification of CcrZ-CPD for antibody production

In order to express a fusion of *S. pneumoniae* CcrZ with a C-terminal cysteine protease domain (CPD), *ccrZ* was amplified by PCR from D39V genomic DNA with primers 213/214 and assembled using Golden Gate allelic replacement strategy (BsaI) with plasmid pET-Gate2 ccdB (pSG436), pSG366, pSG367 and pSG2559. The resulting pSG2949 plasmid was then transformed into BL21 DE3 Gold cells using ZYM-5052 auto-induction media (Studier, 2005). Cells were sonicated in buffer containing 300 mM NaCl, 50 mM Tris pH 7.5, 5 mM β-mercaptoethanol, and protease inhibitor cocktail (PIC). Supernatant was loaded onto a gravity flow column containing HisPur™ Cobalt Resin (Thermo Scientific). Column was washed 5 CV with buffer containing 100 mM NaCl, 20 mM Tris pH 7.5, 5 mM β-mercaptoethanol. Because CcrZ had affinity to the resin even without the CPD, instead of on column tag cleavage, elution was collected with buffer containing 150 mM Imidazole, 100 mM NaCl, 20 mM Tris pH 7.5, 5 mM β-mercaptoethanol, and tag cleavage was performed for 1 hour at 4 ^{0}C by adding 1 mM inositol hexakisphosphate. The sample was further purified using a HitrapQ column and Superdex 200 16/600 pg column (GE). The final storage buffer contained 100 mM NaCl, 20 mM Tris pH 7.5, 1 mM DTT. For antibody production, sample was loaded onto a 15 % SDS PAGE gel. Edge wells were cut out and stained with Coomassie to determine position of CcrZ on the gel. Gel portions containing CcrZ was sent for antibody production by Eurogentec.

Western blot analysis

Cells were grown in C+Y medium until OD_{595nm} = 0.2 and harvested by centrifugation at 8000 x g for 2 min at room temperature from 1 mL of culture. Cells were re-suspended into 150 µL of Nuclei lysis buffer (Promega) containing 0.05 % SDS, 0.025% deoxycholate and 1 % Protease Inhibitor Cocktail (Sigma Aldrich), and incubated at 37°C for 20 min and at 80°C for 5 min in order to lyse them. One

volume of 4X SDS sample buffer (50 mM Tris-HCl pH = 6.8, 2 % SDS, 10 % glycerol, 1 % β-mercaptoethanol, 12.5 mM EDTA and 0.02 % Bromophenol blue) was then added to three volumes of cell lysate sample and heated at 95°C for 10 min. Protein samples were separated by SDS–PAGE (4-20%) and blotted onto polyvinylidene fluoride membranes (Merck Millipore). Membranes were blocked for 1 h with Tris-buffered saline (TBS) containing 0.1 % Tween 20 (Sigma Aldrich) and 5 % dry milk and further incubated for 1 h with primary antibodies diluted in TBS, 0.1 % Tween 20, 5 % dry milk. Polyclonal CcrZ-antiserum concentration used was 1:5000 and commercial monoclonal GFP-IgG (Thermo Fisher Scientific) were used at 1:5000. Membranes were washed four times for 5 min in TBS, 0.1 % Tween 20 and incubated for 1 h with the secondary IgG (HRP-conjugated donkey anti-rabbit antibodies, Promega) diluted 1:20,000 in TBS, 0.1 % Tween 20 and 5 % dry milk. Membranes were then washed four times for 5 min in TBS, 0.1 % Tween 20 and revealed with Immobilon Western HRP substrate (Merck Millipore).

ccrZ-GFP purification with anti-GFP nanobodies

gfp-ccrZ and *P3-gfp* (negative control) strains were grown in C+Y medium at 37°C until OD_{595nm} = 0.2 and cells were harvested by centrifugation 15 min at 3000 x g at 4°C. Cells were then incubated in sucrose buffer (0.1 M Tris-HCl pH = 7.5, 2 mM $MgCl_2$, 1 M sucrose, 1 % Protease Inhibitor Cocktail (Sigma Aldrich), 200 $\mu g.mL^{-1}$ RNase A and 10 $\mu g.mL^{-1}$ DNase (Sigma Aldrich)) for 30 min at 30°C, then incubated in hypotonic buffer (0.1 M Tris-HCl pH = 7.5, 1 mM EDTA, 1 % Triton, 1 % Protease Inhibitor Cocktail, 200 $\mu g.mL^{-1}$ RNase A and 10 $\mu g.mL^{-1}$ DNase) for 15 min at room temperature and cell debris were eliminated by centrifugation 30 min at 15,000 x g at 4°C. Cell lysate was then incubated with equilibrated GFP-Trap resin (Chromotek) at 4°C for 2 h. After several washes with wash buffer (10 mM Tris-HCl pH = 7.5, 150 mM NaCl, 0.5 mM EDTA, 1 % Protease Inhibitor Cocktail), beads were resuspended in 20 µL 8 M Urea, 50 mM triethylammonium bicarbonate (TEAB), pH = 8.0 and reduced with 5 mM DTT for 30 min at 37°C. Cysteines were alkylated by adding 20 mM iodoacetamide and incubated for 30 min at room temperature in the dark. Samples were diluted 1:1 with TEAB buffer and digested by adding 0.1 µg of modified Trypsin (Promega) and incubated overnight at 37°C, followed by a second digestion for 2 h with the same amount of enzyme. The supernatant was collected, diluted 2 times with 0.1 % formic acid and desalted on strong cation exchange micro-tips (StageTips, Thermo Fisher scientific) as described (Kulak *et al.*, 2014). Peptides were eluted with 1.0 M ammonium acetate (100 µL). Dried samples were resuspended in 25 µL 0.1 % formic acid, 2 % acetonitrile prior being subjected to nano LC-MS/MS.

LC-MS/MS analysis

Tryptic peptide mixtures (5 µL) were injected on a Dionex RSLC 3000 nanoHPLC system (Dionex, Sunnyvale, CA, USA) interfaced via a nanospray source to a high resolution QExactive Plus mass spectrometer (Thermo Fisher Scientific). Peptides were separated on an Easy Spray C18 PepMap nanocolumn (25 or 50 cm x 75 µm ID, 2 µm, 100 Å, Dionex) using a 35 min gradient from 4 to 76 % acetonitrile in 0.1 % formic acid for peptide separation (total time: 65 min). Full MS survey scans were performed at 70,000 resolution. In data-dependent acquisition controlled by Xcalibur software (Thermo Fisher), the 10 most intense multiply charged precursor ions detected in the full MS survey scan were selected for higher energy collision-induced dissociation (HCD, normalized collision energy NCE = 27 %) and analysis in the orbitrap at 17,500 resolution. The window for precursor isolation was of 1.6 m/z units around the precursor and selected fragments were excluded for 60 sec from further analysis.

MS data were analyzed using Mascot 2.5 (Matrix Science, London, UK) set up to search the UniProt (www.uniprot.org) protein sequence database restricted to *S. pneumoniae* D39 / NCTC 7466 taxonomy (339 SWISSPROT sequences + 1586 TrEMBL sequences). Trypsin (cleavage at K,R) was used as the enzyme definition, allowing 2 missed cleavages. Mascot was searched with a parent ion tolerance of 10 ppm and a fragment ion mass tolerance of 0.02 Da (QExactive Plus). Iodoacetamide derivative of cysteine was specified in Mascot as a fixed modification. N-terminal acetylation of protein, oxidation of methionine and phosphorylation of Ser, Thr, Tyr and His were specified as variable modifications. Scaffold software (version 4.4, Proteome Software Inc., Portland, OR) was used to validate MS/MS based peptide and protein identifications, and to perform datas*et al*ignment. Peptide identifications were accepted if they could be established at greater than 90.0 % probability as specified by the Peptide Proph*et al*gorithm (Andrew Keller *et al.*, 2002) with Scaffold delta-mass correction. Protein identifications were accepted if they could be established at greater than 95.0 % probability and contained at least 2 identified peptides. Protein probabilities were assigned by the Protein Proph*et al*gorithm (Alexey I. Nesvizhskii *et al.*, 2003). Proteins that contained similar peptides and could not be differentiated based on MS/MS analysis alone were grouped to satisfy the principles of parsimony. Proteins sharing significant peptide evidence were grouped into clusters.

Split luciferase assay

S. pneumoniae cells were grown in C+Y medium at 37°C until OD_{595nm} = 0.2 and washed once with fresh C+Y medium. 1 % NanoGlo Live Cell substrate (Promega) was then added and luminescence was measured 20 times at 37°C every 30 sec in plate reader (TECAN Infinite F200 Pro). Measurements were performed in triplicate

and the average values were plotted, with the SEM (Standard Error of the Mean) represented by the dot size.

Bacterial two-hybrid

The bacterial two-hybrid assay was based on the method from Karimova *et al.* (Karimova *et al.*, 1998) with the following modifications. *dnaA*, *ccrZ* and *ftsZ* genes from *S. pneumoniae* D39V were cloned both into the low copy-number vector pUT18 and into the high copy-number vector pST25 (Ouellette *et al.*, 2014) using the enzymes BamHI and KpnI. *Escherichia* coli strain HM1784 (BTH101 Δ*rnh*::*kan*) was transformed using each combination of plasmids. Chemically competent cells were incubated on ice for 60 min, heat shocking at 42°C for 90 sec and then inoculated at 37°C in 3 mL of LB media supplemented with ampicillin (100 µg/mL) and spectinomycin (50 µg/mL) with mild agitation for 16 hours. The $A_{600\ nm}$ was adjusted to 0.5, cultures were diluted 1:1000 and a 5 µL aliquot was spotted on a nutrient agar plate containing antibiotics (as above) containing 0.006 % X-gal. Plates were incubated at 30°C for 48 hours and the images were captured using a digital camera.

Co-immunoprecipitation of CcrZ and FtsZ-GFP with anti-GFP nanobodies

S. pneumoniae cells were grown in C+Y medium at 37°C until OD_{595nm} = 0.2 and harvested by centrifugation 15 min at 3,000 x g at 4°C. Cells were lysed using GFP-Trap_A Lysis buffer (Chromotek), 0.25 % Deoxycolate, 1 % Protease Inhibitor Cocktail incubated at room temperature for 10 min followed by incubation at 4°C for 20 min. Cell lysate was incubated with equilibrated GFP-Trap resin (Chromotek) at 4°C for 2 h. The resin was then washed 3 times in GFP-Trap_A Wash buffer (Chromotek) and GFP-proteins were eluted using SDS sample buffer at 95°C for 10 min and analyzed by immunoblotting.

Genome resequencing of ccrZ suppressors by NGS

Strains $ccrZ^{supp1}$, $ccrZ^{supp2}$ and $ccrZ^{supp3}$ were grown in C+Y medium at 37°C until OD_{595nm} = 0.3 and cells were harvested by centrifugation 1 min at 10,000 x g. Pellet was then re-suspended into Nuclei lysis buffer (Promega) containing 0.05 % SDS, 0.025% deoxycholate and 200 $\mu g.mL^{-1}$ RNase A at 37°C for 20 min, in order to lyse the cells and Protein Precipitation Solution (Promega) was added. DNA was then precipitated using isopropanol. The extracted genomes were then analyzed by Illumina sequencing by GATC Biotech (Eurofins Genomics). Mutations were mapped onto D39V genome using breseq pipeline (Deatherage and Barrick, 2014). Genomes sequences are available at SRA (accession number PRJNA564501).

oriC/ter ratios determination by RT-qPCR

Determination of *S. pneumoniae oriC/ter* ratios was performed as followed. Cells were pre-grown until OD_{600nm} = 0.4 in C+Y medium at 37°C, with or without inducer (Zn^{2+} or IPTG) for complementation and depletion conditions, respectively. Cells were then diluted 100 times in fresh C+Y medium supplemented when appropriate with inducer and harvested for genomic DNA isolation when they reached OD_{600nm} = 0.1 (exponential phase). For normalization (*oriC/ter* ratio of 1), *dnaA* thermosensitive strain was grown for 2h at non-permissive temperature (40°C) in C+Y medium and harvested for chromosomal DNA isolation. As a negative (overinitiating) control, wild type *S. pneumoniae* was incubated 2h with 0.15 µg.mL^{-1} HPUra (DNA replication inhibitor) at 37°C prior to harvesting. Primers pairs OT1/OT2 and OT3/OT4 were used to amplify the *oriC* and *ter* regions respectively. Amplification by Real-Time qPCR was performed using SYBR Select Master Mix (Applied Biosystems) on a StepOne Plus Real-Time PCR System (Applied Biosystems), in triplicate. For *S. aureus oriC/ter* ratio determination, overnight cultures were diluted 100-fold and grown until OD_{600nm} = 0,4. These cultures were then re-diluted 200-fold in medium with 500 µM IPTG and grown until OD_{600nm} = 0.2. As reference samples with assumed *oriC/ter* ratio of 1, wild type *S. aureus* SH1000 cells at OD_{600nm} = 0.15 were supplemented with 50 µg.mL^{-1} rifampicin (inhibiting replication initiation) and incubated for 2 hours for replication run-out. Cells were then harvested and lysed enzymatically by addition of 0.2 mg.mL^{-1} lysostaphin and 10 mg.mL^{-1} lysozyme, and genomic DNA was isolated using the Wizard Genomic DNA Purification Kit (Promega). qPCR reactions of 10 µL were set up with 5 µL PowerUpTM SYBR™ Green Master Mix (Applied Biosystems), 500 nM of each primer OT5/OT and OT7/OT8 and 20 ng of DNA. In both cases, amplification efficiencies of the primers and *oriC/ter* ratios were determined as described previously (Slager *et al.*, 2014). Data were plotted as whiskers plot were whiskers represent the 10th and 90th percentile of data from Monte Carlo simulations, * P value < 0.05, significantly up. For *B. subtilis oriC/ter* ratios determination, cultures were grown to mid-exponential phase in LB medium and diluted back to OD_{600nm} = 0.05 and grown to mid-exponential phase (OD_{600nm} = 0.2 - 0.4) at 37°C. Cells were harvested in ice-cold methanol (1:1 ratio) and pelleted. Genomic DNA was isolated using Qiagen DNeasy kit with 40 µg.mL^{-1} lysozyme. The copy number of the origin (*oriC*) and terminus (*ter*) were quantified by qPCR to generate the *oriC/ter* ratio. qPCR was done using SSoAdvanced SYBR master mix and CFX96 Touch Real-Time PCR system (Bio-Rad). Primers used to quantify the origin region were OT9/OT10. Primers used to quantify the terminus region were OT11/OT12. Origin-to-terminus ratios were determined by dividing the number of copies (as indicated by the Cp values measured through qPCRs) of the origin by the number of copies quantified at the terminus. Ratios were normalized to the origin-to-terminus ratio of a temperature

sensitive mutant, *dnaB134* (KPL69), that was grown to have synchronized replication initiation, resulting in 1:1 ratio of the *oriC/ter*. Data were plotted as whiskers plot. *P value < 0.05 (t-test), significantly up.

Quantifications and statistical analysis

Data analysis was performed using R and Prism (Graphpad). When comparing wild type phenotypes with *ccrZ* depletion/complementation, a Wilcoxon rank sum test with Bonferroni adjustment was used as we did not assume a normal distribution, since some mutant cells can behave like wild type because of the variable time of depletion or possible leakiness of P_{lac} or P_{Zn}.

Data shown are represented as mean of at least three replicates ± SEM if data came from one experiment with replicated measurement, and ± SD if data came from separate experiments.

Acknowledgements

We appreciate the assistance from the Electron Microscopy Facility (EMF) and the Protein Analysis Facility (PAF) at the University of Lausanne (UNIL) and thank them for their support. We thank Wiep Klaas Smits (LUMC) for the Split-luc sequences and Tanneke den Blaauwen (UVA) for the mTQ^{ox} sequence prior to publication, Arnau Domenech (UNIL) for construction of strain *hlpA-LgBit hlpA-SmBit* and Zhian Salehian (NMBU) for help with cloning. Work in the Kjos lab is supported by a FRIMEDBIO grant (project number 250976) and a JPIAMR grant (project number 296906) from the Research Council of Norway. Work in the Murray lab was supported by a Wellcome Trust Senior Research Fellowship (204985/Z/16/Z) and a grant from the Biotechnology and Biological Sciences Research Council (BB/P018432/1). Work in the Grossman lab was supported, in part, by the National Institute of General Medical Sciences of the National Institutes of Health under award number R37 GM041934 and R35 GM122538. Work in the Veening lab is supported by the Swiss National Science Foundation (SNSF) (project grant 31003A_172861), a JPIAMR grant (40AR40_185533) from SNSF, a Novartis Foundation grant (#17B064) and ERC consolidator grant 771534-PneumoCaTChER.

References

Alexey I. Nesvizhskii, *,†, Andrew Keller, *,†, Eugene Kolker, ‡ and, and Aebersold, R. (2003). A Statistical Model for Identifying Proteins by Tandem Mass Spectrometry.

Andrew Keller, *,†, Alexey I. Nesvizhskii, *,†, Eugene Kolker, and, and Aebersold, R. (2002). Empirical Statistical Model To Estimate the Accuracy of Peptide Identifications Made by MS/MS and Database Search.

Bisicchia, P., Arumugam, S., Schwille, P., and Sherratt, D. (2013). MinC, MinD, and MinE drive counter-oscillation of early-cell-division proteins prior to Escherichia coli septum formation. MBio *4*, e00856-13.

Bodle, C.R., Hayes, M.P., O'Brien, J.B., and Roman, D.L. (2017). Development of a bimolecular luminescence complementation assay for RGS: G protein interactions in cells. Anal. Biochem. *522*, 10–17.

Boye, E., and Nordström, K. (2003). Coupling the cell cycle to cell growth. EMBO Rep. *4*, 757–760.

Caldas, V.E.A., Punter, C.M., Ghodke, H., Robinson, A., and van Oijen, A.M. (2015). iSBatch: a batch-processing platform for data analysis and exploration of live-cell single-molecule microscopy images and other hierarchical datasets. Mol. Biosyst. *11*, 2699–2708.

Campos, M., Surovtsev, I.V., Kato, S., Paintdakhi, A., Beltran, B., Ebmeier, S.E., and Jacobs-Wagner, C. (2014). A Constant Size Extension Drives Bacterial Cell Size Homeostasis. Cell *159*, 1433–1446.

Cooper, S., and Helmstetter, C.E. (1968). Chromosome replication and the division cycle of Escherichia coli Br. J. Mol. Biol. *31*, 519–540.

Deatherage, D.E., and Barrick, J.E. (2014). Identification of mutations in laboratory-evolved microbes from next-generation sequencing data using breseq. Methods Mol. Biol. *1151*, 165–188.

Domenech, A., Slager, J., and Veening, J.-W. (2018). Antibiotic-Induced Cell Chaining Triggers Pneumococcal Competence by Reshaping Quorum Sensing to Autocrine-Like Signaling. Cell Rep. *25*, 2390-2400.e3.

Donachie, W.D. (1968). Relationship between cell size and time of initiation of DNA replication. Nature *219*, 1077–1079.

Du, S., and Lutkenhaus, J. (2017). Assembly and activation of the *Escherichia coli* divisome. Mol. Microbiol. *105*, 177–187.

Ducret, A., Quardokus, E.M., and Brun, Y. V (2016). MicrobeJ, a tool for high throughput bacterial cell detection and quantitative analysis. Nat. Microbiol. *1*, 16077.

Espéli, O., Borne, R., Dupaigne, P., Thiel, A., Gigant, E., Mercier, R., and Boccard, F. (2012). A MatP-divisome interaction coordinates chromosome segregation with cell division in E. coli. EMBO J. *31*, 3198–3211.

Felicori, L., Jameson, K.H., Roblin, P., Fogg, M.J., Garcia-Garcia, T., Ventroux, M., Cherrier, M. V., Bazin, A., Noirot, P., Wilkinson, A.J., *et al.* (2016). Tetramerization and interdomain flexibility of the replication initiation controller YabA enables simultaneous binding to multiple partners. Nucleic Acids Res. *44*, 449–463.

Flåtten, I., Fossum-Raunehaug, S., Taipale, R., Martinsen, S., and Skarstad, K. (2015). The DnaA Protein Is Not the Limiting Factor for Initiation of Replication in Escherichia coli. PLOS Genet. *11*, e1005276.

Fleurie, A., Lesterlin, C., Manuse, S., Zhao, C., Cluzel, C., Lavergne, J.-P., Franz-Wachtel, M., Macek, B., Combet, C., Kuru, E., *et al.* (2014). MapZ marks the division sites and positions FtsZ rings in Streptococcus pneumoniae. Nature *516*, 259–262.

Hajduk, I. V., Rodrigues, C.D.A., and Harry, E.J. (2016). Connecting the dots of the bacterial cell cycle: Coordinating chromosome replication and segregation with cell division. Semin. Cell Dev. Biol. *53*, 2–9.

Harashima, H., Dissmeyer, N., and Schnittger, A. (2013). Cell cycle control across the eukaryotic kingdom. Trends Cell Biol. *23*, 345–356.

Hill, N.S., Kadoya, R., Chattoraj, D.K., and Levin, P.A. (2012). Cell Size and the Initiation of DNA Replication in Bacteria. PLoS Genet. *8*, e1002549.

Holečková, N., Doubravová, L., Massidda, O., Molle, V., Buriánková, K., Benada, O., Kofroňová, O., Ulrych, A., and Branny, P. (2014). LocZ is a new cell division protein involved in proper septum placement in Streptococcus pneumoniae. MBio *6*, e01700-14.

Huls, P.G., Vischer, N.O.E., and Woldringh, C.L. (2018). Different Amounts of DNA in Newborn Cells of Escherichia coli Preclude a Role for the Chromosome in Size Control According to the "Adder" Model. Front. Microbiol. *9*, 664.

Jaacks, K.J., Healy, J., Losick, R., and Grossman, A.D. (1989). Identification and characterization of genes controlled by the sporulation-regulatory gene spo0H in Bacillus subtilis. J. Bacteriol. *171*, 4121–4129.

de Jong, I.G., Beilharz, K., Kuipers, O.P., and Veening, J.-W. (2011). Live Cell Imaging of Bacillus subtilis and Streptococcus pneumoniae using Automated Time-lapse Microscopy. J. Vis. Exp.

Karimova, G., Pidoux, J., Ullmann, A., and Ladant, D. (1998). A bacterial two-hybrid system based on a reconstituted signal transduction pathway. Proc. Natl. Acad. Sci. U. S. A. *95*, 5752–5756.

Katayama, T. (2017). Initiation of DNA Replication at the Chromosomal Origin of E. coli, oriC. (Springer, Singapore), pp. 79–98.

Katayama, T., Kasho, K., and Kawakami, H. (2017). The DnaA Cycle in Escherichia coli: Activation, Function and Inactivation of the Initiator Protein. Front. Microbiol. *8*, 2496.

Kjeldgaard, N.O., MaalOe, O., and Schaechter, M. (1958). The Transition Between Different Physiological States During Balanced Growth of Salmonella typhimurium. J. Gen. Microbiol. *19*, 607–616.

Kjos, M., Aprianto, R., Fernandes, V.E., Andrew, P.W., van Strijp, J.A.G., Nijland, R., and Veening, J.-W. (2015). Bright fluorescent Streptococcus pneumoniae for live-cell imaging of host-pathogen interactions. J. Bacteriol. *197*, 807–818.

Kleckner, N., Fisher, J.K., Stouf, M., White, M.A., Bates, D., and Witz, G. (2014). The bacterial nucleoid: nature, dynamics and sister segregation. Curr. Opin. Microbiol. *22*, 127–137.

Kleckner, N.E., Chatzi, K., White, M.A., Fisher, J.K., and Stouf, M. (2018). Coordination of Growth, Chromosome Replication/Segregation, and Cell Division in E. coli. Front. Microbiol. *9*, 1469.

Krogh, A., Larsson, B., von Heijne, G., and Sonnhammer, E.L.. (2001). Predicting transmembrane protein topology with a hidden markov model: application to complete genomes. J. Mol. Biol. *305*, 567–580.

Kubala, M.H., Kovtun, O., Alexandrov, K., and Collins, B.M. (2010). Structural and thermodynamic analysis of the GFP:GFP-nanobody complex. Protein Sci. *19*, 2389–2401.

Kulak, N.A., Pichler, G., Paron, I., Nagaraj, N., and Mann, M. (2014). Minimal, encapsulated proteomic-sample processing applied to copy-number estimation in eukaryotic cells. Nat. Methods *11*, 319–324.

Land, A.D., Tsui, H.-C.T., Kocaoglu, O., Vella, S.A., Shaw, S.L., Keen, S.K., Sham, L.-T., Carlson, E.E., and Winkler, M.E. (2013). Requirement of essential Pbp2x and GpsB for septal ring closure in Streptococcus pneumoniae D39. Mol. Microbiol. *90*, 939–955.

Liu, X., Gallay, C., Kjos, M., Domenech, A., Slager, J., van Kessel, S.P., Knoops, K., Sorg, R.A., Zhang, J.-R., and Veening, J.-W. (2017). High-throughput CRISPRi phenotyping identifies new essential genes inStreptococcus pneumoniae. Mol. Syst. Biol. *13*, 931.

Løbner-Olesen, A., Skarstad, K., Hansen, F.G., von Meyenburg, K., and Boye, E. (1989). The DnaA protein determines the initiation mass of Escherichia coli K-12. Cell *57*, 881–889.

Löfblom, J., Kronqvist, N., Uhlén, M., Ståhl, S., and Wernérus, H. (2007). Optimization of electroporation-mediated transformation: Staphylococcus carnosus as model organism. J. Appl. Microbiol. *102*, 736–747.

Marston, A.L., Thomaides, H.B., Edwards, D.H., Sharpe, M.E., and Errington, J. (1998). Polar localization of the MinD protein of Bacillus subtilis and its role in selection of the mid-cell division site. Genes Dev. *12*, 3419–3430.

Mercy, C., Ducret, A., Slager, J., Lavergne, J.-P., Freton, C., Nagarajan, S.N., Garcia, P.S., Noirot-Gros, M.-F., Dubarry, N., Nourikyan, J., *et al.* (2019). RocS drives chromosome segregation and nucleoid protection in Streptococcus pneumoniae. Nat. Microbiol. 1.

Monk, I.R., Tree, J.J., Howden, B.P., Stinear, T.P., and Foster, T.J. (2015). Complete Bypass of Restriction Systems for Major Staphylococcus aureus Lineages. MBio *6*, e00308-15.

Murray, H., and Koh, A. (2014). Multiple Regulatory Systems Coordinate DNA Replicaton with Cell Growth in Bacillus subtilis. PLoS Genet. *10*, e1004731.

Nourikyan, J., Kjos, M., Mercy, C., Cluzel, C., Morlot, C., Noirot-Gros, M.-F., Guiral, S., Lavergne, J.-P., Veening, J.-W., and Grangeasse, C. (2015). Autophosphorylation of the Bacterial Tyrosine-Kinase CpsD Connects Capsule Synthesis with the Cell Cycle in Streptococcus pneumoniae. PLOS Genet. *11*, e1005518.

Oliveira Paiva, A.M., Friggen, A.H., Qin, L., Douwes, R., Dame, R.T., and Smits, W.K. (2019). The Bacterial Chromatin Protein HupA Can Remodel DNA and Associates with the Nucleoid in Clostridium difficile. J. Mol. Biol. *431*, 653–672.

Ouellette, S.P., Rueden, K.J., Gauliard, E., Persons, L., de Boer, P.A., and Ladant, D. (2014). Analysis of MreB interactors in Chlamydia reveals a RodZ homolog but fails to detect an interaction with MraY. Front. Microbiol. *5*, 279.

Paintdakhi, A., Parry, B., Campos, M., Irnov, I., Elf, J., Surovtsev, I., and Jacobs-Wagner, C. (2016). Oufti: an integrated software package for high-accuracy, high-throughput quantitative microscopy analysis. Mol. Microbiol. *99*, 767–777.

Pang, T., Wang, X., Lim, H.C., Bernhardt, T.G., and Rudner, D.Z. (2017). The nucleoid occlusion factor Noc controls DNA replication initiation in Staphylococcus aureus. PLoS Genet. *13*, e1006908.

Perego, M., Spiegelman, G.B., and Hoch, J.A. (1988). Structure of the gene for the transition state regulator, abrB: regulator synthesis is controlled by the spo0A sporulation gene in Bacillus subtilis. Mol. Microbiol. *2*, 689–699.

Perez, A.J., Cesbron, Y., Shaw, S.L., Villicana, J.B., Tsui, H.-C.T., Boersma, M.J., Ye, Z.A., Tovpeko, Y., Dekker, C., Holden, S., *et al.* (2019). Movement dynamics of divisome proteins and PBP2x:FtsW in cells of Streptococcus pneumoniae. Proc. Natl. Acad. Sci. *116*, 3211–3220.

Pierucci, O., Rickert, M., and Helmstetter, C.E. (1989). DnaA protein overproduction abolishes cell cycle specificity of DNA replication from oriC in Escherichia coli. J. Bacteriol. *171*, 3760–3766.

Pinho, M.G., Kjos, M., and Veening, J.-W. (2013). How to get (a)round: mechanisms controlling growth and division of coccoid bacteria. Nat. Rev. Microbiol. *11*, 601–614.

Raaphorst, R. van, Kjos, M., and Veening, J.-W. (2019). BactMAP: an R package for integrating, analyzing and visualizing bacterial microscopy data. BioRxiv 728782.

van Raaphorst, R., Kjos, M., and Veening, J.-W. (2017). Chromosome segregation drives division site selection inStreptococcus pneumoniae. Proc. Natl. Acad. Sci. U. S. A. *114*, E5959–E5968.

Reyes-Lamothe, R., and Sherratt, D.J. (2019). The bacterial cell cycle, chromosome inheritance and cell growth. Nat. Rev. Microbiol. 1.

Schaechter, M., MaalOe, O., and Kjeldgaard, N.O. (1958). Dependency on Medium and Temperature of Cell Size and Chemical Composition during Balanced Growth of Salmonella typhimurium. J. Gen. Microbiol. *19*, 592–606.

Scholefield, G., Errington, J., and Murray, H. (2012). Soj/ParA stalls DNA replication by inhibiting helix formation of the initiator protein DnaA. EMBO J. *31*, 1542–1555.

Si, F., Le Treut, G., Sauls, J.T., Vadia, S., Levin, P.A., and Jun, S. (2019). Mechanistic Origin of Cell-Size Control and Homeostasis in Bacteria. Curr. Biol. *29*, 1760-1770.e7.

Slager, J., Kjos, M., Attaiech, L., and Veening, J.-W. (2014). Antibiotic-Induced Replication Stress Triggers Bacterial Competence by Increasing Gene Dosage near the Origin. Cell *157*, 395–406.

Slager, J., Aprianto, R., and Veening, J.-W. (2018). Deep genome annotation of the opportunistic human pathogen Streptococcus pneumoniae D39. Nucleic Acids Res. *46*, 9971–9989.

Soding, J., Biegert, A., and Lupas, A.N. (2005). The HHpred interactive server for protein homology detection and structure prediction. Nucleic Acids Res. *33*, W244–W248.

Studier, F.W. (2005). Protein production by auto-induction in high density shaking cultures. Protein Expr. Purif. *41*, 207–234.

Taheri-Araghi, S., Bradde, S., Sauls, J.T., Hill, N.S., Levin, P.A., Paulsson, J., Vergassola, M., and Jun, S. (2015). Cell-size control and homeostasis in bacteria. Curr. Biol. *25*, 385–391.

Ursell, T., Lee, T.K., Shiomi, D., Shi, H., Tropini, C., Monds, R.D., Colavin, A., Billings, G., Bhaya-Grossman, I., Broxton, M., *et al.* (2017). Rapid, precise quantification of bacterial cellular dimensions across a genomic-scale knockout library. BMC Biol. *15*, 17.

Wallden, M., Fange, D., Lundius, E.G., Baltekin, Ö., and Elf, J. (2016). The Synchronization of Replication and Division Cycles in Individual E. coli Cells. Cell *166*, 729–739.

Wang, L., Jiang, Y.-L., Zhang, J.-R., Zhou, C.-Z., and Chen, Y. (2015). Structural and Enzymatic Characterization of the Choline Kinase LicA from Streptococcus pneumoniae. PLoS One *10*, e0120467.

Wold, S., Skarstad, K., Steen, H.B., Stokke, T., and Boye, E. (1994). The initiation mass for DNA replication in Escherichia coli K-12 is dependent on growth rate. EMBO J. *13*, 2097–2102.

Wu, L.J., and Errington, J. (2012). Nucleoid occlusion and bacterial cell division. Nat. Rev. Microbiol. *10*, 8–12.

Zheng, H., Ho, P.-Y., Jiang, M., Tang, B., Liu, W., Li, D., Yu, X., Kleckner, N.E., Amir, A., and Liu, C. (2016). Interrogating the Escherichia coli cell cycle by cell dimension perturbations. Proc. Natl. Acad. Sci. U. S. A. *113*, 15000–15005.

Supplementary Information

Supplementary videos are available online at https://www.biorxiv.org/content/10.1101/775536v1.supplementary-material

Supplementary Video 1. 3D-SIM of GFP-CcrZ in wild type cells. Volume projection of 240 reconstructed 3D-SIM images shows CcrZ forming patchy rings.

Supplementary Video 2. Time lapse microscopy of GFP-CcrZ in live cells. Localization overtime of GFP-CcrZ at 30°C every 10 min shows that CcrZ localizes exclusively at the division site.

Supplementary Video 3. Time lapse analysis of GFP-CcrZ and FtsZ-mCherry in live cells. Localization of GFP-CcrZ and FtsZ-mCherry at 30°C every 10 min shows that CcrZ and FtsZ co-localize overtime.

Supplementary Video 4. 3D-SIM of GFP-CcrZ and FtsZ-mCherry in wild type cells. Volume projection of 240 reconstructed 3D-SIM images shows that FtsZ and CcrZ form a similar ring and co-localize.

Supplementary Video 5. Time lapse microscopy of CcrZ-mKate2 in FtsZ depleted cells. Depletion of FtsZ overtime shows a rapid spread of CcrZ-mKate2 signal in the cytoplasm.

Supplementary Video 6. Time lapse analysis of HlpA-mKate2 in Δ*ccrZ* cells. Localization overtime of HlpA-mKate2 in *ccrZ*-deleted cells shows absence of nucleus and "guillotined" chromosome in several cells.

Supplementary Video 7. Time lapse analysis of CcrZ-mKate2, DnaN-sfTQ^{ox} and ParB$_p$-sfmYFP in live cells. Localization every minute of CcrZ-mKate2, DnaN-sfTQ^{OX} and ParB$_p$-sfmYFP shows that the origin of replication is first brought to the future division site, while the replication machinery localizes at mid-cell with CcrZ, until CcrZ re-localizes to the new division site to start a new round of replication.

Supplementary Table 1: Ratio of spectral counts between GFP-CcrZ and GFP from LC-MS/MS

Identified Proteins	Fold change (GFP-CcrZ / GFP)
SPV_0476 (CcrZ)	27
ScrA	12
PepN	8.5
Pbp2X	8.3
FruA	7.4
EzrA	7.4
SPV_1621	6.8
FtsZ	6.6
PlsC	6
FtsH	5.1
DnaA	2.8

Supplementary figure 1. *ccrZ* deletion phenotype is conserved in *S. aureus*

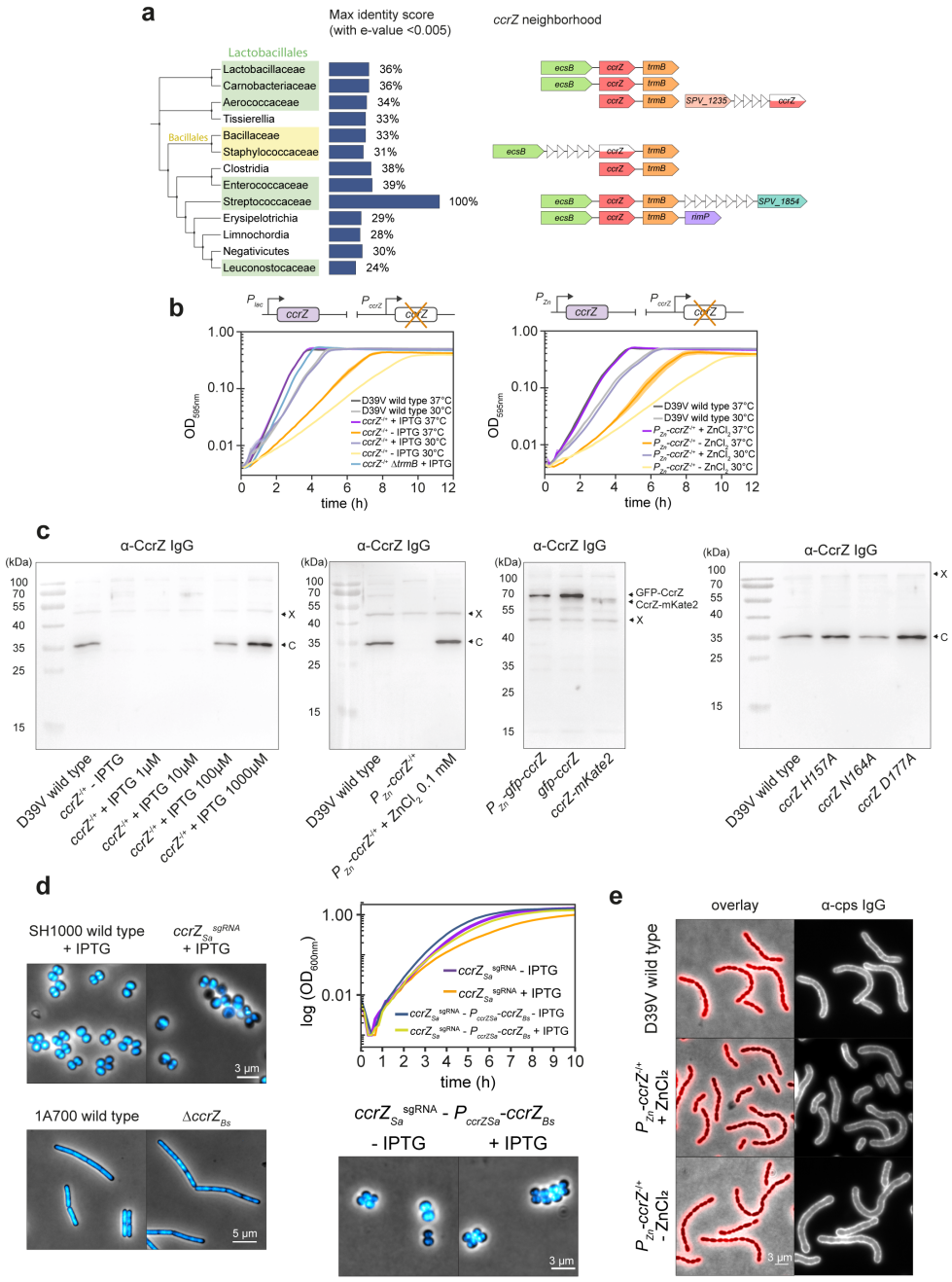

(**a**) left: CcrZ conservation in firmicutes. Percentages indicate the highest percent identity, for each class, obtained using PSI-BLAST with NIH sequences. Right: genes co-occurrence in several genomes (data obtained from https://string-db.org; see Methods). Horizontal section indicate complexity in neighborhood score assignment; white triangles indicate missing annotation. (**b**) growth curves at 37°C and 30°C of *ccrZ* depletion mutants using P_{lac} (left) or P_{Zn} (right). (**c**) western blot from different pneumococcal strains. C: native CcrZ size; X: unknown protein recognized by α-CcrZ IgG. (**d**) microscopy of DAPI-stained *S. aureus* upon *ccrZ* silencing shows anucleate cells, while *B. subtilis* Δ*ccrZ* mutant did not present nucleoid defects. Right-top: growth defect upon *S. aureus ccrZ* silencing ($ccrZ_{Sa}^{sgRNA}$ + IPTG) is rescued by expression of $ccrZ_{Bs}$ ($ccrZ_{Sa}^{sgRNA}$-P_{ccrZSa}-$ccrZ_{Bs}$ + IPTG). Associated microscopy of DAPI-stained cells (bottom-right) also confirmed the complementation of $ccrZ_{Sa}$ by $ccrZ_{Bs}$. (**e**) immunostaining of the polysaccharide capsule of *S. pneumoniae* wild type and upon CcrZ depletion.

Supplementary figure 2. Septal localization of CcrZ in *S. pneumoniae*.

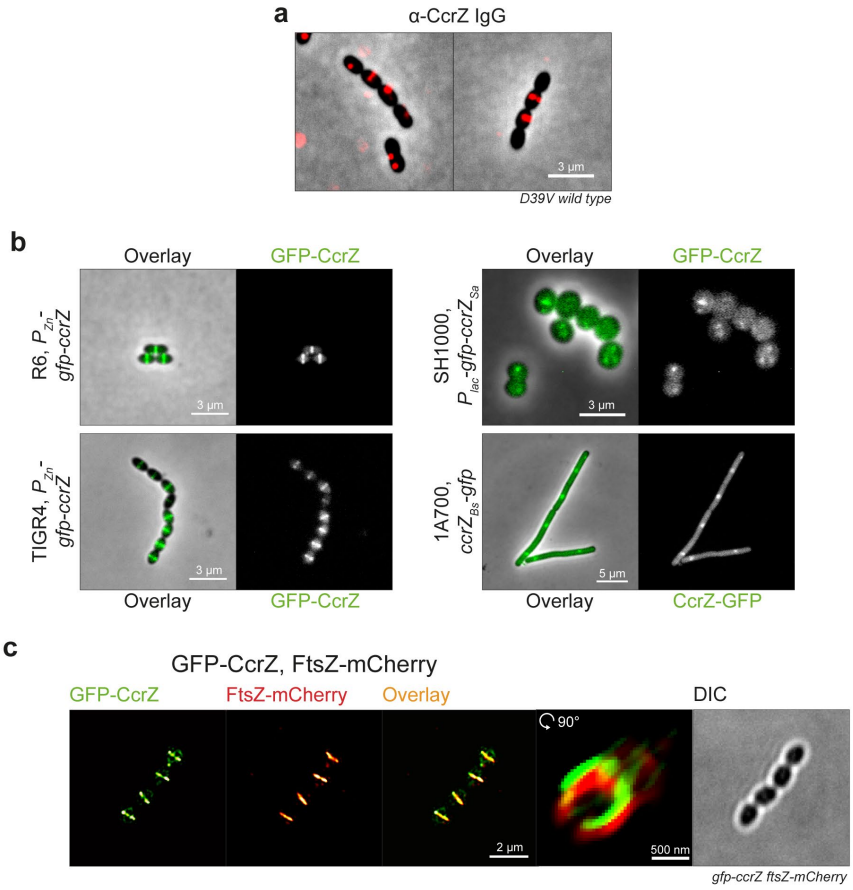

(**a**) immunostaining of CcrZ in wild type *S. pneumoniae* shows a septal localization. (**b**) localization of CcrZ in other pneumococcal strains (un-encapsulated R6 strain and capsular serotype 4 TIGR4) and in *S. aureus* SH1000, as well as in *B. subtilis* 1A700. (**c**) 3D-SIM of GFP-CcrZ and FtsZ-mCherry and reconstructed volume projection of both.

Supplementary figure 3. Deletion of *ccrZ* leads to anucleate cells

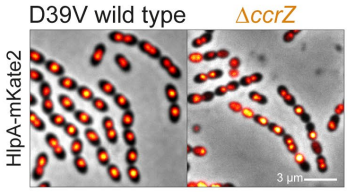

Localization of the nucleoid associated protein HlpA (HlpA-mKate2) in a *ccrZ* mutant shows anucleate cells.

Supplementary figure 4. CcrZ activity is crucial for proper replication initiation as a *dnaA*^{TS} mutant phenocopied a *ccrZ* deletion

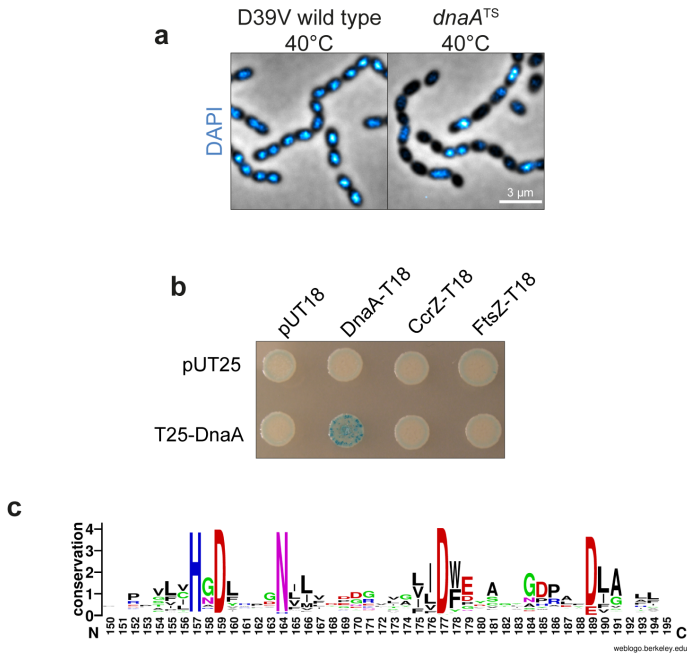

(**a**) microscopy of DAPI-stained DnaA thermosensitive strain at non-permissive temperature (40°C) indicates several anucleate cells, compared to a wild type grown in identical conditions. (**b**) no interaction was detected between DnaA and CcrZ using bacterial-2-hybrid, while a positive DnaA-DnaA self-interaction is visible. (**c**) five (H157, D159, N164, D177 and D189) most conserved residues between 1000 different CcrZ sequences from different bacterial species; sequences obtained from UniRef50 database.

Supplementary figure 5. Transient co-localization of CcrZ and DnaA

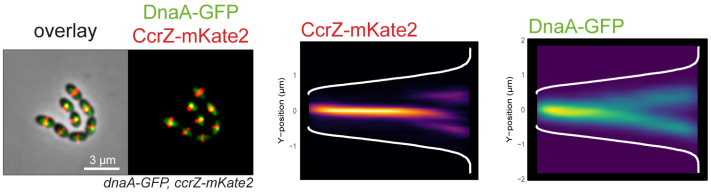

Co-localization of CcrZ-mKate2 with DnaA-GFP (left) and corresponding heatmap of signal distribution over cell length (right) show that DnaA and CcrZ co-localize at the beginning of the cell cycle.

Supplementary Methods

Strains constructions

All strains and plasmids used for constructions are listed in Supplementary Table 1 and all primers are listed in Supplementary Table 2.

All *S. pneumoniae* strains were constructed by integrating into the chromosome by double homologous recombination either circular plasmids or linear DNA fragments possessing two ~1 kb region homology assembled using standard restriction-ligation, PCR assembly, Gibson assembly or Golden Gate assembly. In all cases parental strains were transformed directly with the assembled products. Constructs were confirmed by PCR and the resulting fragment sequenced.

P_{Zn}-*ccrZ*$^{+/+}$ and *ccrZ*$^{+/+}$. For insertion of a second copy of *spv_0476* (*ccrZ*) under control of either P_{Zn} or *Plac*, *spv_0476* with its native RBS was amplified by PCR from D39V genome with primers 1/2 or 1/9 respectively and cloned into pMK11 vector (van Raaphorst *et al*., 2017) between EcoRI-SpeI restriction sites allowing for the genetic fusion P_{Zn}-*spv_0476* to be inserted in place of *bgaA* (coding for β-galactosidase) locus, or cloned into pPEPY (Keller *et al*., 2019) between EcoRI-BamHI sites to obtain the genetic fusion *Plac-spv_0476* for insertion in place of the *cil* locus (chromosomal integration locus – disrupting the non-coding *spv_2165* gene). pMK11-*spv_0476* was then transformed into D39V wild type and pPEPY-*spv_0476* into D39V *lacI* (Liu *et al*., 2017) as this strains expresses constitutively the repressor LacI.

P_{Zn}-*ccrZ*$^{-/+}$ and *ccrZ*$^{-/+}$. For deletions of *spv_0476,* both flanking regions of the gene were amplified by PCR on D39V genome with primers 3/4 and 5/6 and assembled using Gibson assembly (Gibson *et al*., 2009) to an erythromycin resistant marker amplified from a strain *ftsZ-mKate2*-ery (van Raaphorst *et al*., 2017) with primers 7/8. The final product was transformed into P_{Zn}-*ccrZ*$^{+/+}$ strain in presence of $ZnCl_2$ in order to express the extra copy of *ccrZ*. The resulting *ccrZ*::*ery* product together with the flanking regions was amplified from the P_{Zn}-*ccrZ*$^{-/+}$ genome with primers 10/11 and transformed into *ccrZ*$^{+/+}$ in presence of IPTG.

ftsZ-spc and *ftsZ-mTurquoise2*. The spectinomycin resistance marker s*pc* was amplified by PCR from was plasmid pPEP23 (Sorg *et al*., 2015) with primers 16/17, *ftsZ* and flanking regions were amplified on D39V genome with primers 12/13 and 14/15. All three fragments were assembled using Golden Gate assembly with BsmBI (Engler *et al*., 2008) and the resulting product transformed into D39V wild type. *mTurquoise2* was amplified from vector mTurquoise2-pBAD (addgene) with primers 19/20, *ftsZ-linker* was amplified from *ftsZ-mKate2* strain (van Raaphorst *et al*., 2017) with primers 12/18 and downstream flanking region of *ftsZ* with *spc* amplified on *ftsZ-spc* genome with primers 15/21. All three fragments were assembled using Golgen Gate assembly

(BsmBI) and transformed into D39V wild type in order to replace the native *ftsZ* with *ftsZ-mTurquoise2-ery* fusion.

ccrZ$^{-/+}$ *ftsZ-mTurquoise2* and *dnaA*^{TS} *mTurquoise2*. *ftsZ-mTurquoise2* genetic fusion and flanking regions were amplified by PCR with primers 12/15 from *ftsZ-mTurquoise2* strain and inserted either into *ccrZ*$^{-/+}$ strain in presence of IPTG to keep high levels of CcrZ (*ccrZ*$^{-/+}$ *ftsZ-mTurquoise2*) or into the thermosensitive *dnaA* mutant *dnaA*^{TS} (Mercy *et al*., 2019) (*dnaA*^{TS} *mTurquoise2*).

ccrZ$^{-/+}$ Δ*trmB*. For co-deletion of *ccrZ* and *trmB* (same operon and overlapping), upstream region of *ccrZ* was amplified by PCR on D39V genome with primers 22/23, erythromycin resistance marker was amplified with primers 24/25 on *ccrZ*$^{-/+}$ genome and downstream region of *trmB* was amplified on D39V genome with primers 26/27. All three fragments were assembled using Golden Gate (BsaI) and inserted into strain *ccrZ*$^{-/+}$ in presence of IPTG.

P_{Zn}-*ccrZ-gfp*, P_{Zn}-*ftsZ-gfp*, P_{Zn}-*gfp-ccrZ*, R6 P_{Zn}-*gfp-ccrZ* and TIGR4 P_{Zn}-*gfp-ccrZ*. For translational fusion of monomeric superfolder green fluorescent protein (msfGFP) at the C-terminal extremities of CcrZ and FtsZ, *ccrZ* and *ftsZ* together with their respective RBS were amplified by PCR on D39V genome with primers 28/29 and 30/31, respectively, and cloned into plasmid pMK17 (van Raaphorst *et al*., 2017) between restriction sites NotI-SpeI, allowing for insertion of fusion *ccrZ-gfp* or *ftsZ-gfp* under control of P_{Zn} at the *bgaA* locus. The final product was then transformed into D39V wild type, R6 (Hoskins *et al*., 2001) and TIGR4 (Tettelin *et al*., 2001). For translational fusion of msfGFP at the N-terminal extremity of CcrZ (as *ccrZ* 3′ region overlaps with *trmB* 5′ region), *ccrZ* excluding the START codon and including STOP codon was first amplified by PCR from D39V genome with primers 32/33 and cloned into pCG6 (Liu *et al*., 2017) between restriction sites SpeI-NotI, allowing for genetic fusion of *msfgfp* to the 5′ of *ccrZ* under control of P_{Zn}. pCG6 derivates from pMK17 and can therefore integrates into the *bgaA* locus. D39V wild type was then transformed with the final product.

gfp-ccrZ and *gfp-ccrZ ftsZ-mCherry*. *gfp-ccrZ* fragment was amplified by PCR from P_{Zn}-*gfp-ccrZ* strain with primers 37/38, upstream flanking region was amplified with primers 34/35 from D39V genome and a kanamycin marker was amplified with primers 36/39 from pPEP2K1 (Sorg *et al*., 2016). All three fragments where assembled by Gibson assembly and transformed into D39V wild type resulting in strain *gfp-ccrZ*, with *gfp-ccrZ* fusion in place of native *ccrZ* and under control of the native P_{ccrZ} promoter. For co-localization of CcrZ with FtsZ, *ftsZ-mCherry* was amplified by PCR with primers 12/15 from *ftsZ-mCherry* strain (van Raaphorst *et al*., 2017) and transformed into *gfp-ccrZ* strain.

ftsZ$^{+/+}$ and *ftsZ*$^{-/+}$. For insertion of an inducible ectopic version of *ftsZ*, *ftsZ* gene was amplified from D39V genome by PCR with primers 40/41 and cloned into vector pPEPY between EcoRI and BamHI restriction sites. D39V *lacI* was then transformed with the ligated product, leading to insertion of P_{lac}-*ftsZ* in the *cil* locus. Spectinomycin marker together with *ftsZ* downstream region were amplified with primers 15/42 from strain *ftsZ-spc* and the region upstream of *ftsZ* START codon was amplified by PCR from D39V genome with primers 43/44. Both fragments were assembled using Golden Gate assembly (BsmBI) and the strain *ftsZ*$^{+/+}$ was transformed with the resulting product in presence of IPTG, to keep a high level of FtsZ, leading to the depletion strain *ftsZ*$^{-/+}$.

ccrZ-mKate2 and *ftsZ*$^{-/+}$ *ccrZ-mKate2*. For genetic fusion of *ccrZ* with the fluorescent protein mKate2, *ccrZ* upstream and downstream regions where amplified by PCR with primers 45/46 and 49/50, respectively, from D39V genome and *mKate2-ery* (with linker) was amplified with primers 47/48 from *ftsZ-mKate2* strain. All three fragments were assembled by Golden Gate assembly (BsmBI) and the product transformed into D39V wild type. *ccrZ-mKate2* was then amplified by PCR from the previously created strain with primers 50/51 and the product transformed into *ftsZ*$^{-/+}$ strain in presence of IPTG to keep a high level of FtsZ.

ccrZ-LgBit. In order to fuse *ccrZ* to *LgBit* sequence in place of the native *ccrZ*, upstream region of *ccrZ* was amplified by PCR with primers 52/53 and the downstream region together with erythromycin marker was amplified with primers 54/55 on strain *ccrZ-mKate2*. A gBlocks fragment (Integrated DNA Technologies) containing the *LgBit* sequence flanked with two BsaI sites was synthesised. Both PCR fragments and gBlocks were assembled using Golden Gate assembly (BsaI) and inserted into D39V wild type by transformation.

ftsZ-SmBit and *ccrZ-LgBit ftsZ-SmBit*. For fusion of *ftsZ* with *SmBit* sequence, *SmBit* sequence was synthesized as a gBlocks fragment (Integrated DNA Technologies) and amplified by PCR with primers 56/57. *ftsZ* with its upstream region sequence were amplified with primers 58/59 on D39V genome and the downstream region with spectinomycin marker were amplified with primers 60/61 on strain *ftsZ-spc*. All three fragments were then assembled with Golden Gate assembly (BsmBI) and transformed into D39V wild type and *ccrZ-LgBit* strains.

ccrZ-SmBit and *ccrZ-LgBit ccrZ-SmBit*. For *ccrZ-SmBit* construction, *ccrZ* upstream and downstream regions were amplified by PCR with primers 62/63 and 66/67, respectively, on D39V gDNA and SmBit was amplified with primers 64/65 from strain *ftsZ-SmBit*. All three fragments were assembled with Golden Gate assembly (BsmBI) and the product was transformed into strain D39V wild type. *ccrZ-SmBit* was then amplified by PCR with primers 70/67 from the resulting strain and *ccrZ-*

LgBit, with upstream region was amplified with primers 68/69 from strain *ccrZ-LgBit*. The two fragments obtained were assembled by Golden Gate assembly (BsmBI) and transformed into D39V wild type.

ccrZ-LgBit cps2E-SmBit, ccrZ-LgBit hlpA-SmBit, ccrZ-LgBit dnaA-SmBit, ccrZ-LgBit ezrA-SmBit, ccrZ-LgBit ftsA-SmBit, ccrZ-LgBit ftsH-SmBit, ccrZ-LgBit ftsW-SmBit, ccrZ-LgBit pepN-SmBit, ccrZ-LgBit pbp2x-SmBit, ccrZ-LgBit zapA-SmBit, ccrZ-LgBit fruA-SmBit, ccrZ-LgBit plsC-SmBit, ccrZ-LgBit scrA-SmBit and *ccrZ-LgBit spv_1621-SmBit*. All fourteen double LgBit-SmBit labeled strains were constructed as followed. *SmBit* fragment was amplified by PCR from *ftsZ-SmBit* genome with primers 71/72 when using BsmbI and 73/74 when using BsaI (for *dnaA-SmBit and ezrA-SmBit*). *cps2E, hlpA, dnaA, ezrA, ftsA, ftsH, ftsW, pepN, pbp2x, zapA, fruA, plsC, scrA* and *spv_1621* upstream (of Start codon) regions were amplified from D39V genome with primers 75/76, 79/80, 83/84, 87/88, 91/92, 95/96, 99/100, 103/104, 107/108, 111/112, 115/116, 119/120, 123/124 and 127/128, respectively, and downstream regions were amplified from D39V genome with primers 77/78, 81/82, 85/86, 89/90, 93/94, 97/98, 101/102, 105/106, 109/110, 113/114, 117/118, 121/122, 125/126 and 129/130, respectively. Each downstream and upstream fragment was assembled to *SmBit* fragment using Golden Gate assembly (BsmBI for all except *dnaA* and *ezrA* using BsaI) and transformed into strain *ccrZ-LgBit*.

hlpA-LgBit and *hlpA-LgBit hlpA-SmBit*. For construction of the final strain *hlpA-LgBit hlpA-SmBit* used as positive control for SplitLuc assay as HlpA proteins interact together (O'Neil *et al*., 2016), a first strain *hlpA-LgBit* was made as followed. *Prs1* upstream region was amplified by PCR with primers 131/132 on strain VL2429 (Veening lab collection) and fragment *LgBit* fuse to chloramphenicol resistant marker, together with *prs1* downstream region was amplified with primers 135/136 from strain VL2429. *hlpA* was amplified with primers 133/134 from D39V genome. All three fragments were assembled by overlapping PCR using primers 131/136 and transformed into D39V wild type. *hlpA-SmBit* was amplified from strain *ccrZ-LgBit hlpA-SmBit* with primers 79/82 and transformed into the previously created strain *hlpA-LgBit*, leading to strain *hlpA-LgBit hlpA-SmBit*.

hlpA-mKate2 Δ*ccrZ*. *ccrZ* ::*ery* fragment was amplified by PCR with primers 10/11 on strain *ccrZ*$^{-/+}$ and transformed into *hlpA-mKate2* strain (van Raaphorst *et al*., 2017).

P_{Zn}-*ccrZ*$^{+/+}$ *ftsZ-cfp*, P_{Zn}-*ccrZ*$^{+/+}$ *ftsZ-cfp hlpA-mKate2* and P_{Zn}-*ccrZ*$^{-/+}$ *ftsZ-cfp hlpA-mKate2*. *ftsZ-cfp* was amplified from *ftsZ-cfp* strain (van Raaphorst *et al*., 2017) by PCR with primers 12/15 and transformed into strain P_{Zn}-*ccrZ*$^{+/+}$ leading to strain P_{Zn}-*ccrZ*$^{+/+}$ *ftsZ-cfp*. *hlpA-mKate2* was amplified by PCR from strain *hlpA-mKate2* (van Raaphorst *et al*., 2017) with primers 137/138 and the resulting fragment was used for transformation of strain P_{Zn}-*ccrZ*$^{+/+}$ *ftsZ-cfp*. The newly created strain P_{Zn}-*ccrZ*$^{+/+}$ *ftsZ-*

cfp hlpA-mKate2 was then transformed in presence of IPTG with *ccrZ*::*ery* fragment amplified by PCR with primers 10/11 on strain *ccrZ*$^{-/+}$, resulting in strain P_{Zn}-*ccrZ*$^{-/+}$ *ftsZ-cfp hlpA-mKate2*.

ccrZ^{supp1}, *ccrZ*^{supp2} and *ccrZ*^{supp3}. The deletion fragment *ccrZ*::*ery* was amplified by PCR with primers 10/11 on strain *ccrZ*$^{-/+}$ and inserted in place of *ccrZ* in strain D39V wild type. Among the 10,000 colonies appearing on erythromycin-agar plates, 200 colonies were as large as wild type colony, while nearly 9,800 were very small colonies. 3 large colonies were cultivated, and their growth was assessed by plate-reader assay, before to be stored at -80°C. Mutation determination is described in *Genome resequencing of ccrZ suppressors by NGS* section. *ccrZ*^{supp1} has a 741G>T substitution leading to DnaA-Q247H and an additional insertion 13_14insA into *licD2*; *ccrZ*^{supp2} has a 874G>T substitution leading to DnaA-S292G; and *ccrZ*^{supp3} had a 277G>T substitution leading to YabA E93* (insertion of STOP codon).

Δ*ccrZ dnaA-Q247H* and Δ*ccrZ dnaA-S292G*. For re-insertion of the two *dnaA* point mutations in wild type background, fragments corresponding to *dnaA-Q247H* and *dnaA-S292G* with flanking region (marker-less) were first constructed by PCR assembly. The fragment corresponding to *dnaA-Q247H*_up was amplified on D39V genome with primers 143/140 and *dnaA-Q247H*_down was amplified with primers 139/144; a final PCR with primers 143/144 using both fragments as template led to the final *dnaA-Q247H* product. *dnaA-S292G* fragment was constructed in the same way using primers 143/142 and 141/144. Either assemblies were then inserted into D39V wild type, together with the deletion fragment *ccrZ*::*ery* (amplified by PCR with primers 10/11 on strain *ccrZ*$^{-/+}$), allowing for selection. In both cases, small colonies with few large colonies (2%) were present and only the large colonies were selected for confirmation by PCR and sequencing.

kan-ccrZ, dnaA-Q247H and *dnaA-S292G*. In order to re-insert *ccrZ* into strain Δ*ccrZ dnaA-Q247H* and Δ*ccrZ dnaA-S292G*, a strain *kan-ccrZ* was constructed as intermediate. The upstream region of *ccrZ*, together with *kan* (kanamycin resistant marker), was amplified by PCR on strain *gfp-ccrZ* with primers 45/145 and *ccrZ* gene was amplified with primers 146/11 on D39V genome. Both fragments were then assembled using Golden Gate assembly (BsmBI) and inserted into D39V wild type. *kan-ccrZ* fragment was amplified by PCR from the resulting strain *kan-ccrZ* with primers 22/55. Strains Δ*dnaA Q247H* and Δ*dnaA S292G* were then transformed with the obtained DNA fragments and selected for kanamycin resistance, allowing for replacement of *ccrZ*::*ery* with *kan-ccrZ*.

Δ*yabA* and Δ*yabA* Δ*ccrZ*. For *yabA* deletion, sequences upstream and downstream of *yabA* were amplified on D39V genome by PCR with primers 147/148 and 151/152, and spectinomycin resistance marker was amplified on pPEP23 with primers 149/1509.

All fragments were then assembled using Golden Gate assembly (BsmBI) and inserted into D39V wild type. Δ*yabA* strain was then transformed with a fragment *ccrZ*::*ery* amplified by PCR with primers 10/11 on strain *ccrZ*$^{-/+}$ resulting in strain Δ*yabA* Δ*ccrZ*.

ccrZ-N164A, *ccrZ-H157A* and *ccrZ-D177A*. Insertion of *ccrZ* point mutations into P_{Zn}-*ccrZ*$^{+/+}$ strain was performed as followed. For *ccrZ-N164A*, *kan-ccrZ_up* was amplified on *kan-ccrZ* genome with primers 45/154 and *ccrZ_down* was amplified with primers 153/11 on D39V genome. Both fragments were assembled by PCR assembly using primers 45/11. *ccrZ-H157A* and *ccrZ-D177A* were constructed in a similar manner, with primers 45/156, 155/11, 45/158 and 157/11 respectively. All three assembled products were then inserted into strain P_{Zn}-*ccrZ*$^{+/+}$ in presence of $ZnCl_2$ in order to keep high CcrZ levels.

P_{lac}-*ccrZ-gfp*, P_{lac}-*ccrZ-H157A-gfp*, P_{lac}-*ccrZ-N164A-gfp* and P_{lac}-*ccrZ-D177A-gfp*. For insertion of *ccrZ* fused to *gfp* under control of P_{lac} promoter, *ccrZ-gfp* was amplified from P_{Zn}-*ccrZ-gfp* strain genome with primers 161/162 and plasmid pPEPZ (Keller *et al*., 2019) was amplified by PCR with primers 159/160. Assembly of both fragments using Golden Gate (BsmBI) and insertion into D39V *lacI* strain allowed insertion of P_{lac}-*ccrZ-GFP* into the *zip* locus (pPEPZ integration platform - causing disruption of the non-coding gene *spv_2417*). To mutate *ccrZ-gfp*, PCR assembly was used for the three mutants. For P_{lac}-*ccrZ-H157A-gfp*, upstream of the *zip* locus together with P_{lac}-*ccrZ_up* were amplified by PCR with primers 163/156 and *ccrZ-gfp_down* with downstream region of *zip* locus was amplified with primers 155/164, from P_{lac}-*ccrZ-gfp* genome. Both fragments were assembled by PCR assembly using primers 163/164. P_{lac}-*ccrZ-N164A-gfp* and P_{lac}-*ccrZ-D177A-gfp* fragments were constructed in a similar manner, using primers 163/154, 153/164, 163/158 and 157/164 respectively. All three products were then inserted into strain D39V *lacI*.

comCDE-parS$_p$*ccrZ-mKate2*,*parB*$_p$*-YFP**comCDE-parS*$_p$*ccrZ-mKate2* and *dnaN-mTQ*^{ox} *parB*$_p$*-YFP comCDE-parS*$_p$ *ccrZ-mKate2*. In order to visualize the replication machinery together with the origin of replication and CcrZ, a first strain was made, expressing CcrZ-mKate2 and containing $parS_p$ sites from *Lactococcus lactis* (able to bind $parB_p$ proteins from *L. lactis*) in the genome close to the origin of replication *oriC*. *comCDE-parS*$_p$ was amplified by PCR from strain D39V, *comCDE-parS*$_p$ *bgaA*::*parB*$_p$*-sfmGFP* (van Raaphorst *et al*., 2017) using primers 165/166 and the resulting fragment was transformed into strain *ccrZ-mKate2*. Plasmid pMK19-02 (carrying *bgaA*::P_{Zn}-*parB*$_p$*-msfYFP*, Veening Lab collection) was transformed into the resulting strain *comCDE-parS*$_p$ *ccrZ-mKate2*. To prevent any alteration in replication process, the genetic fusion of *dnaN* with *sfmTurquoise2*^{ox} was introduced as a second copy downstream of the original *dnaN* gene. *dnaN* and upstream region were amplified by PCR with primers 167/168 from D39V genome, the second *dnaN* copy was amplified with

primers 169/170 from D39V genome, *sfmTurquoise2^{ox}* with linker were amplified with primers 173/174 from strain D39V, *CEP::P3-spv_1159-sfmTurquoise2^{ox}-opt* (Veening lab collection), chloramphenicol resistance marker (*cam*) was amplified with primers 175/176 from *hlpA-mKate2* strain and downstream of *dnaN* was amplified with primers 171/172 from D39V genome. All five fragments were assembled using Golden Gate assembly (BsaI for the three first fragments and BsaI / SapI for the two others) and transformed into strain *parB$_p$-YFP comCDE-parS$_p$ ccrZ-mKate2*.

ccrZ-mKate2 P$_{Zn}$-dnaA-GFP. *dnaA* was amplified from D39V genome by PCR with primers 177/178 and the resulting fragment was digested with NotI-SpeI restriction enzymes and ligated into plasmid pMK17, allowing genetic fusion with *msfgfp* under control of Zn^{2+}-inducible promoter. The resulting product was transformed into strain *ccrZ-mKate2*.

ccrZ$_{Sa}^{sgRNA}$ and *ccrZ$_{Sa}^{sgRNA}$ P$_{ccrZSa}$-ccrZ$_{Bs}$*. Inverse PCR was used to construct sgRNA-plasmid, as described previously (Liu *et al*., 2017; Stamsås *et al*., 2018); in which the phosphorylated primer 179 was combined with gene specific forward primers containing the 20 bp targeting region as overhangs. Primer 180 was used as specific primer to construct the plasmid pCG248-sgRNA(*ccrZ$_{Sa}$*). The sgRNA was designed to target the 5′ end *ccrZ$_{Sa}$*. For construction of the complementation plasmid pCG248-sgRNA(*ccrZ$_{Sa}$*)-*P$_{ccrZ}$-ccrZ$_{Bs}$*, *B. subtilis ccrZ*-homolog, *ytmP* (*ccrZ$_{Bs}$*), was fused to the *ccrZ$_{Sa}$* promoter and integrated into plasmid pCG248-sgRNA(*ccrZ$_{Sa}$*). *ccrZ$_{Bs}$* was amplified from plasmid pSG3174 (pUC19-*ccrZ$_{Bs}$*, see below) using primers 183/184. *ccrZ$_{Sa}$* -promoter (*P$_{ccrZSa}$*) was amplified from *S. aureus* SH1000 genome using primers 181/182. Both fragments were fused in a second PCR step, using primers 181/184. The resulting fragment was digested with restriction enzymes BamHI and KpnI and ligated into plasmid pCG248-sgRNA(*ccrZ$_{Sa}$*).

P$_{lac}$-gfp-ccrZ$_{Sa}$. For expression of CcrZ-GFP under control of an IPTG-inducible promoter in *S. aureus* SH1000, *ccrZ$_{Sa}$* gene was amplified from genomic DNA of *S. aureus* SH1000 using primers 185/186. The fragment was digested with NcoI and BamHI and ligated into the corresponding sites of plasmid pLOW-*parB-msfgfp*. The resulting plasmid expressing the translational fusion CcrZ$_{Sa}$-msfGFP fusion under control of an IPTG-inducible promoter was then transformed into SH1000 strain.

All *B. subtilis* strains were constructed by integrating into the chromosome by double homologous recombination using either genomic DNA or linear DNA fragments possessing two ~1 kb region homology. Assembled products were introduced into parent strains using natural transformation. Constructs were confirmed by PCR and the resulting fragment sequenced.

1A700 Δ*ccrZ$_{Bs}$*. In frame deletion of *ccrZ* homolog in *B. subtilis*, *ytmP* (*ccrZ$_{Bs}$*),

was performed using Golden Gate allelic replacement strategy as described before (Diebold-Durand *et al*., 2019). Upstream homology region of $ccrZ_{Bs}$ was amplified by PCR with primers 187/188 and ligated into plasmid pUC19 (leading to pSG3174), 5′ region and 3′ region (including downstream homology of $ccrZ_{Bs}$) were amplified with primers pairs 189/190 and 191/192 and ligated into plasmid pUC19 (leading to pSG3178 and pSG3177, respectively). The three resulting plasmids and plasmid pSG0682 (Diebold-Durand *et al*., 2019) (carrying an erythromycin resistance cassette) where assembled together with Golden Gate backbone plasmid pSG1525 (Diebold-Durand *et al*., 2019) and transformed into 1A700 wild type.

$ccrZ_{Bs}$-*gfp*. For translational fusion of $ccrZ_{Bs}$ with msfGFP, $ccrZ_{Bs}$ (*ytmP*) was amplified by PCR with primers 193/194 and ligated into plasmid pUC19 (leading to pSG3175), *msfgfp* was amplified with primers 195/196 and ligated into plasmid pUC19 (giving pSG3179) and homology region downstream of $ccrZ_{Bs}$ was amplified with primers pair 189/190 and ligated into pUC19 (leading to pSG3176). The three plasmids obtained and plasmid pSG0682 were assembled using Golden Gate and transformed into 1A700 wild type strain.

Δ$ccrZ_{Bs}$. Deletion of $ccrZ_{Bs}$ was constructed by replacing the open reading frame with a chloramphenicol resistance cassette (cam) by using linear Gibson assembly fragments containing ~1KB of flanking homology for $ccrZ_{Bs}$. Upstream of *ytmP* ($ccrZ_{Bs}$) was amplified using primers 197/198; the chloramphenicol resistance cassette was amplified from pGEM::*cat* (Youngman *et al*., 1989) using primers 199/200; downstream of $ccrZ_{Bs}$ was amplified using primers 201/202.

oriN and *oriN* Δ$ccrZ_{Bs}$. Strain *oriN* was constructed by introducing the heterologous origin and initiator (*oriN/repN*) (Hassan *et al*., 1997) in place of *oriC* and introducing a constitutive promoter to drive expression of *dnaN*. The constitutive promoter used was Ppen (Yansura and Henner, 1984) with the following sequence replacing the -10 to -35 box (5′- GTTGCATTTATTCTTAGATAGTGTAATACT-3′). The various fragments were amplified by PCR and assembled using Gibson assembly. The fragments were amplified using the following primers and templates: upstream *dnaA* was amplified using primer 203/204, kanamycin cassette was amplified from pGK67 (Lemon *et al*., 2001) using primers 205/206, *oriN*/*repN* was amplified from pDL110 (Hassan *et al*., 1997) using primers 207/208, Ppen2027 was amplified from CAL2072 using 209/210 and *dnaN* was amplified with primers 211/212. The assembled fragments were then transformed into strain JH642 (*oriN*) or Δ$ccrZ_{Bs}$ (*oriN* Δ$ccrZ_{Bs}$).

Capsule immunofluorescence

For fluorescence analysis of *S. pneumoniae* polysaccharide capsule, cells were grown in C+Y medium at 37°C until OD_{595nm} = 0.1 and 1:1000 diluted serum anti-serotype 4 from rabbit (Neufeld antisera, Statens Serum Institut) was added for 5 min at 4°C. Cells were washed three times with fresh C+Y medium and 1 $mg.mL^{-1}$ of secondary antibody anti-rabbit coupled to Alexa Fluor 555 (Invitrogen) was added for 5 min at 4°C. Cells were then spotted onto a PBS-agarose slide. Acquisition of the fluorescent signal was performed on DV Elite microscope with mCherry filter set (Ex: 575/25 nm, BS: 605/50, Em: 632/60 nm).

Conservation and gene neighborhood

CcrZ protein sequence was aligned against all non-redundant protein sequences from NIH (ncbi.nlm.nih.gov) using PSI-BLAST for different firmicutes families. Sequences with highest identity were then aligned using Clustal Omega (ebi.ac.uk/Tools/msa/clustalo) and a phylogenetic three was generated by iTOL (Interactive Tree Of Life; itol.embl.de). Gene neighborhood data were obtained from the STRING database (Szklarczyk *et al*., 2019). For residues conservation data, 1000 sequences of *ccrZ* homologs where retrieved with PSI-BLAST (ebi.ac.uk) from the UniRef50 database. Conservation visualization was obtained using WebLogo 3 (weblogo.threeplusone.com). Sequences were then aligned using Clustal Omega and CcrZ sequence with conservation scores was mapped using UCSF Chimera (cgl.ucsf.edu/chimera) onto the crystal structure of *S. pneumoniae* LicA (PDB 4R78), the closest homolog protein using HMM-HMM comparison with HHpred (Zimmermann *et al*., 2018).

Supplementary Table 2: List of all bacterial strains and plasmids used in this study

***S. pneumoniae* strains**	**Relevant genotype**	**Reference**
D39V wild type	*S. pneumoniae* serotype 2	Avery *et al.*, 1944
R6 wild type	*S. pneumoniae* D39 derivative	gift from C. Grangeasse laboratory, Lyon France
TIGR4 wild type	*S. pneumoniae* serotype 4	Tettelin *et al.*, 2001
ccrZ^{sgRNA}	D39V, *prs1*::*lacI*, *bgaA*::P_{lac}-*dCas, CEP*::*P3-ccrZ-sgRNA*; Gen^R, Tet^R, Spc^R	Liu *et al.*, 2017
P_{Zn}-*ccrZ*$^{+/+}$	D39V, *bgaA*::P_{Zn}-*spv_0476*; Tet^R	This study
P_{Zn}-*ccrZ*$^{-/+}$	D39V, *bgaA*::P_{Zn}-*spv_0476*, Δ*spd_0476*; Tet^R, Ery^R	This study
D39V *lacI*	D39V, *prs1*::*lacI*; Gen^R	Liu *et al.*, 2017
ccrZ$^{+/+}$	D39V, *prs1*::*lacI*, *cil*::P_{lac}-*spv_0476*; Gen^R, Kan^R	This study
ccrZ$^{-/+}$	D39V, *prs1*::*lacI*, *cil*::P_{lac}-*spv_0476*, Δ*spd_0476*; Gen^R, Kan^R, Ery^R	This study
ftsZ-spc	D39V, *ftsZ-spc*; Spc^R	This study
ftsZ-mTurquoise2	D39V, *ftsZ*::*ftsZ-mTurquoise2*; Spc^R	This study
ccrZ$^{-/+}$ *ftsZ-mTurquoise2*	D39V, *prs1*::*lacI*, *cil*::P_{lac}-*spv_0476*, Δ*spd_0476*, *ftsZ*::*ftsZ-mTurquoise2*; Gen^R, Kan^R, Ery^R, Spc^R	This study
dnaA^{TS}	D39V, *dnaA*::*dnaA-M398T*	Mercy *et al.*, 2019
dnaA^{TS} *ftsZ-mTurquoise2*	D39V, *dnaA* thermosensitive; *ftsZ*::*ftsZ-mTurquoise2; Spc*^{R}	This study
ccrZ$^{-/+}$ Δ*trmB*	D39V, *prs1*::*lacI*, *cil*::P_{lac}-*spv_0476*, *spv_0476-trmB*::*ery*; Gen^R, Kan^R, Ery^R	This study
P_{Zn}-*ccrZ-gfp*	D39V, *bgaA*::P_{Zn}-*spv_0476-msfgfp*; Tet^R	This study
P_{Zn}-*gfp-ccrZ*	D39V, *bgaA*::P_{Zn}-*msfgfp-spv_0476*; Tet^R	This study
P_{Zn}-*ftsZ-gfp*	D39V, *bgaA*::P_{Zn}-*ftsZ-msfgfp*; Tet^R	This study
R6 P_{Zn}-*gfp-ccrZ*	R6, *bgaA*::P_{Zn}-*msfGFP-spv_0476;* Tet^R	This study
TIGR4 P_{Zn}-*gfp-ccrZ*	TIGR4, *bgaA*::P_{Zn}-*msfGFP-spv_0476;* Tet^R	This study
gfp-ccrZ	D39V, *spv_0476*::*msfgfp-spv_0476*; Kan^R	This study
ftsZ-mCherry	D39V, *ftsZ*::*ftsZ-mCherry*; Kan^R	van Raaphorst *et al.*, 2017
gfp-ccrZ ftsZ-mCherry	D39V, *spv_0476*::*msfgfp-spv_0476*, *ftsZ*::*ftsZ-mCherry*; Kan^R, Ery^R	This study
ftsZ$^{+/+}$	D39V, *prs1*::*lacI*, *cil*::P_{lac}-*ftsZ*; Gen^R, Kan^R	This study
ftsZ$^{-/+}$	D39V, *prs1*::*lacI*, *cil*::P_{lac}-*ftsZ*, Δ*ftsZ*; Gen^R, Kan^R, Spc^R	This study
ftsZ-mKate2	D39V, *ftsZ*::*ftsZ-mKate2*; Ery^R	van Raaphorst *et al.*, 2017
ccrZ-mKate2	D39V, *spv_0476*::*spv_0476-mKate2*; Ery^R	This study

***S. pneumoniae* strains**	**Relevant genotype**	**Reference**
ftsZ$^{-/+}$ *ccrZ-mKate2*	D39V, *prs1*::*lacI*, *cil*::P_{lac}-*ftsZ*, Δ*ftsZ*, *spv_0476*::*spv_0476-mKate2*; Gen^R, Spc^R, Kan^R, Ery^R	This study
ccrZ-LgBit	D39V, *spv_0476*::*spv_0476-LgBit*; Ery^R	This study
ftsZ-SmBit	D39V, *ftsZ*::*ftsZ-SmBit*; Spc^R	This study
ccrZ-LgBit ftsZ-SmBit	D39V, *spv_0476*::*spv_0476-LgBit*, *ftsZ*::*ftsZ-SmBit*; Ery^R, Spc^R	This study
ccrZ-LgBit ccrZ-SmBit	D39V, *spv_0476*::*spv_0476-LgBit-spv_0476-SmBit*; Ery^R, Spc^R	This study
ccrZ-LgBit cps2E-SmBit	D39V, *spv_0476*::*spv_0476-LgBit*, *cps2E*::*cps2E-SmBit*; Ery^R, Spc^R	This study
ccrZ-LgBit hlpA-SmBit	D39V, *spv_0476*::*spv_0476-LgBit*, *hlpA*::*hlpA-SmBit*; Ery^R, Spc^R	This study
ccrZ-LgBit dnaA-SmBit	D39V, *spv_0476*::*spv_0476-LgBit*, *dnaA*::*dnaA-SmBit*; Ery^R, Spc^R	This study
ccrZ-LgBit ezrA-SmBit	D39V, *spv_0476*::*spv_0476-LgBit*, *ezrA*::*ezrA-SmBit*; Ery^R, Spc^R	This study
ccrZ-LgBit ftsA-SmBit	D39V, *spv_0476*::*spv_0476-LgBit*, *ftsA*::*ftsA-SmBit*; Ery^R, Spc^R	This study
ccrZ-LgBit ftsH-SmBit	D39V, *spv_0476*::*spv_0476-LgBit*, *ftsH*::*ftsH-SmBit*; Ery^R, Spc^R	This study
ccrZ-LgBit ftsW-SmBit	D39V, *spv_0476*::*spv_0476-LgBit*, *ftsW*::*ftsW-SmBit*; Ery^R, Spc^R	This study
ccrZ-LgBit pepN-SmBit	D39V, *spv_0476*::*spv_0476-LgBit*, *pepN*::*pepN-SmBit*; Ery^R, Spc^R	This study
ccrZ-LgBit pbp2x-SmBit	D39V, *spv_0476*::*spv_0476-LgBit*, *pbp2x*::*pbp2x-SmBit*; Ery^R, Spc^R	This study
ccrZ-LgBit zapA-SmBit	D39V, *spv_0476*::*spv_0476-LgBit*, *zapA*::*zapA-SmBit*; Ery^R, Spc^R	This study
ccrZ-LgBit fruA-SmBit	D39V, *spv_0476*::*spv_0476-LgBit*, *fruA*::*fruA-SmBit*; Ery^R, Spc^R	This study
ccrZ-LgBit plsC-SmBit	D39V, *spv_0476*::*spv_0476-LgBit*, *plsC*::*plsC-SmBit*; Ery^R, Spc^R	This study
ccrZ-LgBit scrA-SmBit	D39V, *spv_0476*::*spv_0476-LgBit*, *scrA*::*scrA-SmBit*; Ery^R, Spc^R	This study
ccrZ-LgBit spv_1621-SmBit	D39V, *spv_0476*::*spv_0476-LgBit*, *spv_*1621::*spv_*1621-*SmBit*; Ery^R, Spc^R	This study
comCDE-LgBit	D39V, *prs1*::P_{comC}-*comC-comD-comE-LgBit*; Cam^R	Veening Lab collection
hlpA-LgBit	D39V, *prs1*::P_{hlpA}-*hlpA-LgBit*; Cam^R	This study
hlpA-LgBit hlpA-SmBit	D39V, *prs1*::P_{hlpA}-*hlpA-LgBit*, *hlpA*::*hlpA-SmBit;* Cam^R, Spc^R	This study
P3-gfp	D39V, *cep*::*P3-sfgfp*; Spc^R	Sorg *et al*., 2015
hlpA-mKate2	D39V, *hlpA*::*hlpA-hlpA-mKate2*; Cam^R	Kjos *et al*., 2015

***S. pneumoniae* strains**	**Relevant genotype**	**Reference**
hlpA-mKate2 ΔccrZ	D39V, *hlpA*::*hlpA-hlpA-mKate2*; Δ*spd_0476*; Cam^R, Ery^R	van Raaphorst *et al.*, 2017
ftsZ-cfp	D39V, *ftsZ*::*ftsZ-cfp*; Kan^R	van Raaphorst *et al.*, 2017
P_{Zn}*-ccrZ*$^{+/+}$ *ftsZ-cfp*	D39V, *bgaA*::P_{Zn}*-spv_0476*, *ftsZ*::*ftsZ-cfp*; Tet^R, Kan^R	This study
P_{Zn}*-ccrZ*$^{+/+}$ *ftsZ-cfp hlpA-mKate2*	D39V, *bgaA*::P_{Zn}*-spv_0476*, *ftsZ*::*ftsZ-cfp, hlpA*::*hlpA-hlpA-mKate2*; Tet^R, Kan^R, Cam^R	This study
P_{Zn}*-ccrZ*$^{-/+}$ *ftsZ-cfp hlpA-mKate2*	D39V, *bgaA*::P_{Zn}*-spv_0476*, *ftsZ*::*ftsZ-cfp, hlpA*::*hlpA-hlpA-mKate2*, Δ*spd_0476*; Tet^R, Kan^R, Cam^R, Ery^R	This study
ccrZ^{supp1}	D39V, Δ*spd_0476*, *dnaA*::*dnaA-Q247H,* 13_14insA *licD2*; Ery^R	This study
ccrZ^{supp2}	D39V, Δ*spd_0476*, *dnaA*::*dnaA-S292G*; Ery^R	This study
ccrZ^{supp3}	D39V, Δ*spd_0476*, *yabA*::*yabA-E93**; Ery^R	This study
ΔccrZ dnaA-Q247H	D39V, Δ*spd_0476*, *dnaA*::*dnaA-Q247H*; Ery^R	This study
ΔccrZ dnaA-S292G	D39V, Δ*spd_0476*, *dnaA*::*dnaA-S292G*; Ery^R	This study
kan-ccrZ	D39V, *spv_0476*::*kan-spv_0476*; Kan^R	This study
dnaA-Q247H	D39V, *spv_0476*::*kan-spv_0476*, *dnaA*::*dnaA-Q247H*; Kan^R	This study
dnaA-S292G	D39V, *spv_0476*::*kan-spv_0476*, *dnaA*::*dnaA-S292G*; Kan^R	This study
ΔyabA	D39V, Δ*yabA*; Spc^R	This study
ΔyabA ΔccrZ	D39V, Δ*yabA*, Δ*spd_0476*; Spc^R, Ery^R	This study
ccrZ-N164A	D39V, *bgaA*::P_{Zn}*-spv_0476*, *spv_0476*::*kan-spv_0476-N164A*; Tet^R, Kan^R	This study
ccrZ-H157A	D39V, *bgaA*::P_{Zn}*-spv_0476*, *spv_0476*::*kan-spv_0476-H157A*; Tet^R, Kan^R	This study
ccrZ-D177A	D39V, *bgaA*::P_{Zn}*-spv_0476*, *spv_0476*::*kan-spv_0476-D177A*; Tet^R, Kan^R	This study
P_{lac}*-ccrZ-gfp*	D39V, *prs1*::*lacI*, *zip*::P_{lac}*-spv_0476-msfgfp*; Gen^R, Spc^R	This study
P_{lac}*-ccrZ-H157A-gfp*	D39V, *prs1*::*lacI*, *zip*:: P_{lac}*-spv_0476-H157A-msfgfp*; Gen^R, Spc^R	This study
P_{lac}*-ccrZ-N164A-gfp*	D39V, *prs1*::*lacI*, *zip*:: P_{lac}*-spv_0476-N164A-msfgfp*; Gen^R, Spc^R	This study
P_{lac}*-ccrZ-D177A-gfp*	D39V, *prs1*::*lacI*, *zip*:: P_{lac}*-spv_0476-D177A-msfgfp*; Gen^R, Spc^R	This study
comCDE-parS_p *ccrZ-mKate2*	D39V, *spv_0476*::*spv_0476-mKate2, comCDE*::*comCDE-par*S_p; Ery^R	This study
parB_p*-YFP comCDE-par*S_p *ccrZ-mKate2*	D39V, *spv_0476*::*spv_0476-mKate2, comCDE*::*comCDE-par*S_p*, bgaA*::P_{Zn}*-parB*^{p}*-msfYFP*; Ery^R, Tet^R	This study

***S. pneumoniae* strains**	**Relevant genotype**	**Reference**
dnaN-mTQ^{ox} parB$_p$-YFP comCDE-parS$_p$ ccrZ-mKate2	D39V, *spv_0476::spv_0476-mKate2, comCDE::comCDE-parS$_p$, bgaA::P$_{Zn}$-parB^p-msfYFP,* ; Ery^R, Tet^R, Cam^R	This study
comCDE-parS$_p$ parB$_p$-GFP	D39V, *comCDE-parS$_p$ bgaA::parB$_p$-sfmGFP*; Kan^R	van Raaphorst *et al.*, 2017
spv_1159-mTurquoise2^{ox}	D39V, *CEP::P3-spv_1159-sfmTurquoise2^{ox}-opt;* Spc^R	Veening Lab collection
ccrZ-mKate2 P$_{Zn}$-dnaA-GFP	D39V, *ccrZ::ccrZ-mKate2, bgaA::P$_{Zn}$-dnaA-msf-GFP;* Ery^R, Tet^R	This study
***S. aureus* strains**	**Relevant genotype**	**Reference**
SH1000	*S. aureus* SH1000	Horsburgh *et al.*, 2002
SH1000 *dcas9*	SH1000, *pLOW-dcas9;* Ery^R	Stamsås *et al.*, 2018
ccrZ$_{Sa}^{sgRNA}$	SH1000, *pLOW-dcas9*, *pCG248-sgRNA(ccrZ$_{Sa}$);* Ery^R, Cam^R	This study
ccrZ$_{Sa}^{sgRNA}$ P$_{ccrZSa}$-ccrZ$_{Bs}$	SH1000, *pLOW-dcas9*, *pCG248-sgRNA(ccrZ$_{Sa}$)-P$_{ccrZSa}$-ccrZ$_{Bs}$;* Ery^R, Cam^R	This study
P$_{lac}$-gfp-ccrZ$_{Sa}$	SH1000, *pLOW-m(sf)gfp-ccrZ$_{Sa}$;* Ery^R	This study
***B. subtilis* strains**	**Relevant genotype**	**Reference**
1A700	*B. subtilis* 1A700	Gruber lab collection
1A700 Δ*ccrZ$_{Bs}$*	1A700, Δ*ytmP*; Ery^R	This study
ccrZ$_{Bs}$-gfp	1A700, *ytmP-msfgfp*; Ery^R	This study
JH642	*B. subtilis* JH642	Perego *et al.*, 1988
JH642 Δ*ccrZ$_{Bs}$*	JH642, Δ*ytmP*; Cam^R	This study
oriN	JH642, *oriC::oriN-repN, Ppen-dnaN*; Kan^R	This study
oriN, ΔccrZ$_{Bs}$	JH642, *oriC::oriN-repN, Ppen-dnaN, ΔytmP*; Cam^R; Can^R	This study
dnaB134	*dnaB* temperature sensitive mutant	Grossman lab collection

Plasmids		**Reference**
pPEPY	Vector with *Plac,* allowing integration into *S. pneumoniae* CIL locus (*spv_2166-spv_2165*); Kan^R	Keller *et al.*, 2019
pPEPZ	Vector with *Plac,* allowing integration into *S. pneumoniae* ZIP locus (spv_2416-*spv_2419*); Spc^R	Keller *et al.*, 2019
pCG6	pMK17 derivative, encoding *ccrZ* fused to 3'of *msfyfp;* Tet^R	Liu *et al.*, 2017
pMK11	Vector with P$_{Zn}$ (P$_{czcD}$) allowing integration into *S. pneumoniae bgaA* locus; Tet^R	van Raaphorst *et al.*, 2017
pMK17	pMK11 derivative, encoding *msfgfp;* Tet^R	van Raaphorst *et al.*, 2017

Plasmids		Reference
pMK19-02	pMK17 derivative, encoding *parB* fused to *msfyfp;* Tet^R	Veening Lab collection
pLOW-dcas9	*dcas9* downstream of P_{lac} promoter; Amp^R, Ery^R	Stamsås *et al*., 2018
pCG248-sgRNA(ccrZ$_{Sa}$)	For constitutive expression of sgRNA(*ccrZ$_{Sa}$*); Amp^R, Cam^R	This study
pCG248-sgRNA(ccrZ$_{Sa}$)-P$_{ccrZSa}$-ccrZ$_{Bs}$	For constitutive expression of sgRNA(*ccrZ$_{Sa}$*), *ccrZ$_{Bs}$* (*ytmP*) expressed from P_{ccrZSa}; Amp^R, Cam^R	This study
pLOW-*msggfp-parB*	*msfgfp-parB* fusion downstream of P_{lac} promoter; Amp^R, Ery^R	Kjos Lab collection
pGK67	pGEM derivative, carrying a kanamycin resistance cassette; Cam^R	Lemon *et al*., 2001
pDL110	pJH101 derivative, carrying *oriN-repN* from pBPA23; Amp^R	Hassan *et al*., 1997
pUT18	Encoding CyaA T18 domain under control of P_{lac}; Amp^R	Ouellette *et al*., 2014
pST25	Encoding CyaA T25 domain under control of P_{lac}; Spc^R	Ouellette *et al*., 2014
pUC19	pUC18 derivative, inverted MCS, Amp^R	Addgene
pJET1.2	pJET1.2	Invitrogen
pSG1525	pET-Gate2 derivative with MazEF toxin-antitoxin system for Golden gate assembly selection; Kan^R	Diebold-Durand *et al*., 2019
pSG0682	pJET1.2 derivative with erythromycin (*ermB*) cassette; Ery^R	Diebold-Durand *et al*., 2019
pSG3174	pUC19 derivative, carrying *ccrZ$_{Bs}$* (*ytmP*); Amp^R	This study
pSG3177	pUC19 derivative, carrying sequence of upstream region of *ccrZ$_{Bs}$* (*ytmP*); Amp^R	This study
pSG3178	pUC19 derivative, carrying sequence of downstream region of *ccrZ$_{Bs}$* (*ytmP*); Amp^R	This study
pSG3175	pUC19 derivative, carrying *ccrZ$_{Bs}$* (*ytmP*) with no STOP codon for fusion with *msfgfp*; Amp^R	This study
pSG3176	pUC19 derivative, carrying sequence of downstream region of *ccrZ$_{Bs}$* (*ytmP*); Amp^R	This study
pSG3179	pUC19 derivative, carrying *msfgfp*; Amp^R	This study
pSG2949	pET-Gate2 derivative, encoding *ccrZ* with C-terminal cysteine protease domain (CPD) with a 10his tag ; Kan^R	This study
pSG2950	pET-Gate2 derivative, encoding *ccrZ* fused to *sfgfp* with a 10his tag ; Kan^R	This study
pSG4227	pJET1.2 derivative, carrying *ftsZ* from *S. pneumoniae*; Amp^R	This study
pSG1694	pET-Gold1 derivative encoding a *ccdB* cassette, used for Golden gate assembly ; Amp^R	Gruber Lab collection

Plasmids		**Reference**
pSG4268	pETGold1 derivative encoding *ftsZ* from *S. pneumoniae ;* Kan^R	This study
pSG436	pET-Gate2 derivative encoding *ccdB* cassette ; Kan^R	Gruber Lab collection
pSG366	pJET1.2 derivative carrying short sequence2 for Golden gate assembly ; Amp^R	Gruber Lab collection
pSG367	pJET1.2 derivative carrying short sequence3 for Golden gate assembly ; Amp^R	Gruber Lab collection
pSG2559	pET-Gold1 derivative carrying C-terminal cysteine protease domain (CPD) with a 10his tag; Amp^R	Gruber Lab collection
pSG2562	pET-Gold1 derivative carrying *sfGFP* with a 10his ; Amp^R	Gruber Lab collection
***E. coli* strains**		
HM1784	BTH101 derivative, F^-, *cya-99*, *araD139*, *galE15*, *galK16*, *rpsL1*, *hsdR2*, *mcrA1*, *mcrB1,* Δ*rnh*::*kan*; Str^R	Ouellette *et al*., 2014
IM08B	K12 DH10B derivative, *mcrA,* Δ(*mrr-hsdRMS-mcrBC*), φ80*lacZ*Δ*M15,* Δ*lacX74, recA1, araD139,* Δ(*ara-leu*)7697, *galU, galK, rpsL, endA1, nupG,* Δ*dcm*, Ω*Phelp-hsdMS* (CC8-2), Ω*PN25-hsdS* (CC8-1); Str^R	Monk *et al*., 2015
BL21 DE3 Gold	B F^-, *ompT, hsdS*(r_B^- m_B^-), *dcm*$^+$, *gal*λ(DE3), *endA,* Hte; Tet^R	Agilent Technologies

Abbreviations: Tet^R: tetracycline resistance; Kan^R: kanamycin resistance; Cam^R: chloramphenicol resistance; Ery^R: erythromycin resistance; Spc^R: spectinomycin resistance; Gen^R: gentamycin resistance; Amp^R: ampicillin resistance; SmBit: Small Bit; LgBit: Large Bit

Supplementary Table 3: Oligonucleotides used in this study

name	forward / reverse	sequence (5' > 3')
1	F	CGATGGAATTCGAAACTTTATACGGAGGAAAGAAATG
2	R	GCGCACTAGTTCATCTTCTCTTTCCATACTTGTCT
3	F	CACTTATTTTTCCTAGATTCCA
4	R	TGTTCATATGAAAATTCCTCCGGGCGCGACTTCTTTCCTC-CGTATAAAGTTTCCT
5	F	AGTTATCTATTATTTAACGGGAGGAAATAAGACAAGTAT-GGAAAGAGAAGATGAG
6	R	CATATATTCCATAGTCAACTC
7	F	GTCGCGCCCGGAGGAATTTTCATATG
8	R	TTATTTCCTCCCGTTAAATAATAGA
9	R	GCGCGGATCCTCATCTTCTCTTTCCATACTTGTCT
10	F	CATTTCTTCGCTGTTTCTTC
11	R	GGAAATATTGTTCTGGGAAG
12	F	CGGATTTCCAACAAGCTTCA
13	R	GGAACGTCGTCTCCGTTTTAACGATTTTTGAAAAATG-GAGG
14	F	GGAACGTCGTCTCGTAGTTTTCAAAAATCGTTAAGTA-AATGAATG
15	R	CCAAATAGTCCAAACAACGAC
16	F	GGAACGTCGTCTCGAAACGAGGTGAAATCATGAGC
17	R	GGAACGTCGTCTCGACTAATTGAGAGAAGTTTC-TATAGAATTTT
18	R	GGATTCCCGTCTCCACTCCTTTAGCTGCAGCTTC
19	F	GGATTCCCGTCTCCGAGTGAGCAAGGGCGAGGAG
20	R	GGATTCCCGTCTCCGTTTTACTTGTACAGCTCGTCC
21	F	GGATTCCCGTCTCGAAACGAGGTGAAATCATGAGC
22	F	CAGCCATAGAGGAGATCATCATGTA
23	R	TGCGCTAGGTCTCCTTTCTTTCCTCCGTATAAAGTTTC
24	F	TGCGCTAGGTCTCGGAAATGAACAAAAATATAAAATAT-TCTCAAAACT
25	R	TGCGCTAGGTCTCGTCTTATTTCCTCCCGTTAAATA-ATAGAT
26	F	TGCGCTAGGTCTCGAAGAGATAGCCTAAAATTAGGCTG
27	R	GGCTGCTACACGACCAAACTCAG
28	F	GCATGCGGCCGCAAACTTTATACGGAGGAAAGAAATG
29	R	CGCCACTAGTTCTTCTCTTTCCATACTTGTCTCGG
30	F	GCATGCGGCCGCATAAAGAGGAAAAATAAATTATGAC
31	R	GCGCACTAGTACGATTTTTGAAAAATGGAGGTGTA
32	F	GCGCACTAGTGATTTGGGTGATAATGAGC
33	R	GCATGCGGCCGCTCATCATCTTCTCTTTCCATACTTGT
34	F	GTACTGCCTGCGTGGTTATC
35	R	ACGGATCCCCAGCTTGCGCGTCCTCTTCT-CAAAGAAAAGCCTCTGGATTG
36	R	CTATTCGTCAACCACTCTAACCCGAAGATATAAAACAT-CAGAGTATGGAC
37	F	TCTGATGTTTTATATCTTCGGGTTAGAGTGGTT-GACGAATAGGCCAAAAACTAGTAGAATAGTAAG-GAAACTTTATACGGAGGAAAGAAATGAAACATCT-TAGCTCAAAAGGAGAAGAGC
38	R	TCATCTTCTCTTTCCATACTTGTCTC
39	F	GAGGACGCGCAAGCTGGGGATCCGT
40	F	CGATGGAATTCAATAAAGAGGAAAAATAAATTATG
41	R	GCGCGGATCCTTAACGATTTTTGAAAAATGGAGGTG
42	F	TGTCCTCCGTCTCCTAACGAGGTGAAATCATGAGC
43	R	GGAAATTACGGATCAAGATG
44	R	TGTCCTCCGTCTCCGTTAATTTATTTTTCCTCTTTATTCGT-CA
45	F	GCTATGTGGTCGGATTTTGGTT
46	R	CAGGACACGTCTCGATCTTCTCTTTCCATACTTGTCT
47	F	CAGGACACGTCTCGAGATCCGGATCTGGTGGAGAA
48	R	CAGGACACGTCTCGACTTATTTCCTCCCGTTAAATA-ATAGAT
49	F	CAGGACACGTCTCCAAGTATGGAAAGAGAAGATGA-GAGT
50	R	CCAAACGGCTATCAAATACTTCA
51	F	GCTATGTGGTCGGATTTTGGTT
52	F	CTTTGAGAATCGGGTTAGAG
53	R	GCTGTCAGGTCTCGCCTCTTCTCTTTCCATACTTGTCT
54	F	GCTGTCAGGTCTCCTAACCCGGAGGAATTTTCA
55	R	GGCCATGGATCTGAAAAGTTC
56	F	GGAAGGTCGTCTCCTCGTACAACAGATTCAGTCGTTT
57	R	TGCCGATCGTCTCCTACATCGCTG
58	F	GATCGGAAGCATGTTTGACG
59	R	GGAAGGTCGTCTCCACGAACAATCGATTCACGGCG
60	F	TGCCGATCGTCTCGTGTAGATGTTCTAGTCGTCGTGAATC
61	R	CCAGCTAAAACATGACAAGC
62	F	GACAATTCTTGGTTAGGGCT
63	R	TGAGGGTCGTCTCCCTCTTCTCTTTCCATACTTGTCT
64	F	TGAGGGTCGTCTCCAGAGGCGGCTCATCAGGCGGCG
65	R	TGAGGGTCGTCTCCACCTAATTGAGAGAAGTTTCTATAG
66	F	TGAGGGTCGTCTCCAGGTATGGAAAGAGAAGATGA-GAGT
67	R	ATTCGGACGGTTTTCTTACGCG
68	F	GATACCCAAGCCAATCCAGAGGC
69	R	TGAGGGTCGTCTCGGTTATTTCCTCCCGTTAAATAATAGAT
70	F	TGAGGGTCGTCTCCTAACTTTATACGGAGGAAAGAAAT-GG

name	forward / reverse	sequence (5' > 3')
71	F	CCCGTATCGTCTCTGGCGGCTCATCAGGCGGCGGC
72	R	CCCGTATCGTCTCCCTAATTGAGAGAAGTTTCTATAG
73	F	CCCGTATGGTCTCTGGCGGCTCATCAGGCGGCGGC
74	R	CCCGTATGGTCTCCCTAATTGAGAGAAGTTTCTATAG
75	F	CTACTTAGTGCTGTGAGAGAAGC
76	R	CCCGTATCGTCTCCCGCCCTTCGCTCCATCTCTCA
77	F	CCCGTATCGTCTCGTTAGTTTACTTTTGTTTTAGACTACTAG
78	R	GCTTCTGCAATTCGTTGGCTAG
79	F	AGCATAAATAGCAGCACCTA
80	R	CCCGTATCGTCTCCCGCCTTTAACAGCGTCTTTAAGAGCTTTACC
81	F	CCCGTATCGTCTCGTTAGTCAGTCTTTAAAAAGCCTATTGTATC
82	R	GCGATGGTTTCAATATCCAAGTG
83	F	GGCTGTATCAGCCGCTTTAGCTGTC
84	R	CCCGTATGGTCTCCCGCCTTTGATTTTCTTTTTGATTGATTCA
85	F	CCCGTATGGTCTCGTTAGTTTGTGGATAACTTTTAGTTTTTTATC
86	R	CACCAGTAACCTGATCAGTATCGA
87	F	GGCCTTAAGTCATATTGTGGATCGT
88	R	CCCGTATGGTCTCCCGCCAAAACGAATCGTTTCACGTGTTTTC
89	F	CCCGTATGGTCTCGTTAGTAAAAGAAAAAGATTTTATTGTGTGAG
90	R	TGCCTCTGCAGCCTTCAAATGGCGG
91	F	GATGCAGCAGCAACTGCTATC
92	R	CCCGTATCGTCTCCCGCCTTCGTCAAACATGCTTCCGATC
93	F	CCCGTATCGTCTCGTTAGAGAGGAAAAATAAATTATGAC
94	R	CTCACGGTAGTTAGTAGCAGATCTA
95	F	GAGGTAATGACGAACGTGAACAAAC
96	R	CCCGTATCGTCTCCCGCCTTTTTCGTCATTCATTTTTGACTTTAC
97	F	CCCGTATCGTCTCGTTAGCCCTGAGAGAGGCTGGAGCCTC
98	R	TTAGGCACGCCGCCAGCGTTCGTCC
99	F	GCGCCTTGCAGTTGGTTCGAAACC
100	R	CCCGTATCGTCTCCCGCCCTTCAACAGAAGGTTCATTGGTTG
101	F	CCCGTATCGTCTCGTTAGGATAAAGAAAGGATAGTTTATGTCTC
102	R	GAATATCAAACAAGGCACGACGG
103	F	CACTGAAAATACTGCCCACTATATT
104	R	CCCGTATCGTCTCCCGCCTGCATTTCCGTATTGAAGAACAACTGC
105	F	CCCGTATCGTCTCGTTAGATAAGCCTAAAATAAAAAGAAAACTCAGC
106	R	CGATAGATTTCTTCCTGCCCATAGC
107	F	GAAGGATTGACTGGTGGCAGAATG
108	R	CCCGTATCGTCTCCCGCCGTCTCCTAAAGTTAATGTAATTTTT
109	F	CCCGTATCGTCTCGTTAGTATGTTTATTTCCATCAGTGCTG
110	R	CATCAGCTTCGCCTTATCTACAACC
111	F	GAGATCACGCGCAATGACAGAAGAA
112	R	CCCGTATCGTCTCCCGCCTAAGGAATCCTCAATCTTGCTCTGT
113	F	CCCGTATCGTCTCGTTAGCAGAGCAAGATTGAGGATTCCTTATG
114	R	CGACGGATTCGCGCCAATTCTTCAC
115	F	GATGAGTGGTGTATCTCAAATG
116	R	CCCGTATCGTCTCCCGCCTGCTTGTGGTTTGCGTAGGTAACCA
117	F	CCCGTATCGTCTCGTTAGAAAAATAGAAAAATGAAAAGATTGG
118	R	CAAAGCTAGCAAAGGTTGCTTCTAA
119	F	GGTCATGAGATTGAGCTTGTCC
120	R	CCCGTATCGTCTCCCGCCTGCAAGTTCTTCTCTTTTCTTATCT
121	F	CCCGTATCGTCTCGTTAGAAGAAATGAACCTTGGCCAAACAGC
122	R	TTCCTACGTTCGACATTACCCACTA
123	F	CATGTCTATCCTTGGACTCTTTGTC
124	R	CCCGTATCGTCTCCCGCCGATTTTCACTTCGATCACAGCATCCC
125	F	CCCGTATCGTCTCGTTAGTCAATCCTCTCTAATGTGAAAACG
126	R	GTCGCTACCGTCCGTAATCACTTAA
127	F	GACCTGCCATGAGTTTGTTGAAACT
128	R	CCCGTATCGTCTCCCGCCAAGAGTATAGGCCATGGCCCCTGC
129	F	CCCGTATCGTCTCGTTAGAAATCTCTTTAAACCATGTCAGC
130	R	GCGGCTGTCGCAGAGTTGAGACAAA
131	F	ATGTCTTTTTCTGATTTAAAGCTGTTTGCCC
132	R	CTATTTCTTCCAATTTTATTTATTTTGAAGGCGAATGCTCTATCCAGC
133	F	GCTGGATAGAGCATTCGCCTTCAAAATAAATAAAATTGGAAGAAATAG
134	R	GCCGCCGCCGCCTGATGAGCCGCCTTTAACAGCGTCTTTAAGAGCTTTAC
135	F	GTAAAGCTCTTAAAGACGCTGTTAAAGGCGGCTCATCAGGCGGCGGCGGC
136	R	CTTGTCCCCACTGACAATGGTAATATC
137	F	GATTGTAACCGATTCATCTG

name	forward / reverse	sequence (5' > 3')
138	R	GGAATGCTTGGTCAAATCTA
139	F	CAAGCAAAAACATATTGTCCTAACG
140	R	CGTTAGGACAATATGTTTTTGCTTG
141	F	GCCATTTTACAACGTAAAACGGAAC
142	R	GTTCCGTTTTACGTTGTAAAATGGC
143	F	TCTTCTTTTATCCCCAACCTG
144	R	GAGTCTGTGAAATCTGTGGA
145	R	ACCCTGACGTCTCGTTTCTTTCCTCCGTATAAAGTTTC
146	F	ACCCTGACGTCTCCGAAATGGATTTGGGTGATAATGAGC
147	F	GCTACTTCTCTATATTGCCAGTC
148	R	CACGAACCGTCTCGCATAAAACAGC-CCTTTCCTTTCTTTATCATTC
149	F	CACGAACCGTCTCGTATGAGCAATTTGATTAACG-GAAAAATAC
150	R	CACGAACCGTCTCGGCCTAATTGAGAGAAGTTTC-TATAGAATTTTTC
151	F	CACGAACCGTCTCCAGGCATGCAGAT-TCAAAAAAGTTTTAAGG
152	R	CCCTTTCTTTCATCTTCTTCCC
153	F	GTACGACATAGTGCTTGGATTGAGAC
154	R	GTCTCAATCCAAGCACTATGTCGTAC
155	F	GCGACCATTGTCGCTGGAGATGTACG
156	R	CGTACATCTCCAGCGACAATGGTCGC
157	F	GATTTATTTAGTAGCTTGGGATTCGG
158	R	CCGAATCCCAAGCTACTAAATAAATC
159	R	GCGTCACGTCTCAGCATTATTTTTCCTCCTTATTTAT
160	F	GCGTCACGTCTCACGGATCCCTCCAGTAACTCGAGAA
161	F	GCGTCACGTCTCAATGCAAACTTTATACGGAG-GAAAGAAATGG
162	R	GCGTCACGTCTCATCCGGCTTACTTATAAAGCTCATCCAT-GCC
163	F	GCCAATAAATTGCTTCCTTGTTTTG
164	R	AATAATTCTTTCTTTGACACCGTATATG
165	F	GATGTTATTGAACATCAAGTGAGACTAGAG
166	R	AATCGCCATCTTCCAATCCC
167	F	AATTGCGGCCGCAGGAGGTTATCATGTCAATTTAT-CAAGAATTTG
168	R	AGTGGGTCTCCCTTTCACTTAATTTGTACGAACTGG
169	F	AGTGGGTCTCGAAAGGAGAATCCATGATTCATTTTT
170	R	AGTGGGTCTCGATCCATTTGTACGAACTGGTGTAATG
171	F	GGTTGCTCTTCGGAAAGAGGTTGAGCCTGGCTC
172	R	CAAAGGCGTCTTCACGTCCTTG
173	F	TCACGGTCTCGGGATCCGGATCTGGTGGA
174	R	TCACGGTCTCGTAGCTTATTATTATTTGTATAGTTCGTC-CATGC
175	F	TCACGGTCTCCGCTAGTAGGAGGCATATCAAATGA
176	R	TGAGGCTCTTCGTTCTGCCGCTTATAAAAGCCAG
177	F	GCATGCGGCCGCAATAGTAAAGGAGGAGAAAGGATTG
178	R	CGCCACTAGTTTTGATTTTCTTTTTGATTGATTCA
179	R	TATAGTTATTATACCAGGGGGACAGTGC
180	F	GCTGATAATGCCGCAATAAAGTTTAAGAGCTATGCTG-GAAACAG
181	F	TCGAGGATCCTAGAGTTTATCGCCTACAGAG
182	R	GTAATTGTCCCAACCAGTTCAT CTCGTCCACCT-CACTTTCAA
183	F	TTGAAAGTGAGGTGGACGAG ATGAACTGGTTGGGA-CAATTAC
184	R	ACTGGGTACCTTAATCAACAATTCGTTTCATGAGGA
185	F	GATCCCATGGAGCAGTTTTATCAATTAGG
186	R	TCCGGGGATCCAAATAAACATGTTACTATTCATAACT
187	F	GTTACAGAATTCGGTCTCGCGAGTAGCACCGATTGTTC-CGGAACC
188	R	GTTACATCTAGAGGTCTCGTATTTCAAGCAAAACTCTTA-AGATCTGATGC
189	F	GTTACAGAATTCGGTCTCGAGGTCATATCCTCATGAAAC-GAATTGTTG
190	R	GTTACATCTAGAGGTCTCTATGGCAATATCTGC-GTTTTCAGCC
191	R	GTTACAGAATTCGGTCTCGCCTGTAATCAGGAATAC-GAATCCATTTGC
192	R	GTTACATCTAGAGGTCTCGACCTAGTAATTGTCCCAAC-CAGTTCAT
193	F	GTTACAGAATTCGGTCTCGTCTACGAAGTTTGTGC-TATAGCGCTAAAATTTAAAG
194	R	GTTACATCTAGAGGTCTCGCTCCATCAACAATTC-GTTTCATGAGG
195	F	GTTACAGAATTCGGTCTCAGGAGCAGGCGGTAGCGG-CAGCGGTGGCTCA
196	R	GTTACATCTAGAGGTCTCTCAGGTCATTTG-TATAGTTCATCCATGC
197	F	CAAATCGAGACTGACGTATGTCAG
198	R	TCAGGAATACGAATCCATTTGCTC
199	F	GGGTAGAGCAAATGGATTCGTATTCCTGAGGCTTAAC-TATGCGGCATCAG
200	R	GCTGGATAGACTAGAAACGATTAGCCCGG-TATTTTCTCCTTACGCATCTG
201	F	GGCTAATCGTTTCTAGTCTATCCAG
202	R	CAAGCTGTGATGCATGGAATTG
203	F	TACGCCAACCATACTTAATAGCA
204	R	CGCAACTGTCCATACTCTGATGTCTATTATGGTTG-CAAGAAATAAAAG
205	F	CTTTTATTTCTTGCAACCATAATAGACATCAGAGTATGG-ACAGTTGCG

name	forward / reverse	sequence (5' > 3')
206	R	GGAAAAGATTTTAGGAGGAAGCTGAACCATTTGAGGTGATAGGTAAG
207	F	GTTGAACTAATGGGTGCAGCTTCCTCCTAAAATCTTTTCCCAT
208	R	CGTTTTTTCGGAAAGAAGAATATGTAGAAGAAGTTATTGATG
209	F	CTTCTACATATTCTTCTTTCCGAAAAAACGGTTGCATTTA
210	R	TCCTCCTAACGGATAATGTATGCAGCCGACTCAAACATCAAATC
211	F	GCTGCATACATTATCCGTTAGGAGGATAAAAATGAAATTCACGAT TCAAAAAGATCGTC
212	R	CTGTATCAATTGAAATCGGATTTGC
213	F	CTCGAGGGTCTCACGAGAATAATTTTGTTTAACTTTAAGAAGGAGATATACATATGGATTTGGGTGATAATGAGCTAACACTG
214	R	GCTGCAGGTCTCAGCCAGCTCTTCTCTTTCCATACTTGTCTCGGAAATG
215	F	GCAGCCCGTCTCATATGATGACATTTTCATTTGATACAGCTGCTGC
216	R	CGTCTCACAGGTTAACGATTTTTGAAAAATGGAGGTGTATCC
OT1	F	ACGGTCTATCCCAGCTGTTG
OT2	R	ATAGGCGCGTGCTTCTTCTA
OT3	F	GAAAAGTACCATCCCCAGCA
OT4	R	AGCCTTGGTGCCTATCATTG
OT5	F	TGCATATCCGCGTCAAATAG
OT6	R	GCATGAATGACGGTCGTATG
OT7	F	CGCGTGTAGGTATTGCGTTA
OT8	R	CTTCGCGCACTTGAATAACA
OT9	F	TTGCCGCAGATTGAAGAG
OT10	R	AGGTGGACACTGCAAATAC
OT11	F	CGCGCTGACTCTGATATTATG
OT12	R	CAAAGAGGAGCTGCTGTAAC

Supplementary Information References

Avery, O. T., Macleod, C. M. & McCarty, M. Studies on the chemical nature of the substance inducing transformation of pneumococcal types : induction of transformation by a desoxyribonucleic acid fraction isolated from pneumococcus type III. J. Exp. Med. 79, 137–58 (1944).

Diebold-Durand, M.-L., Bürmann, F., and Gruber, S. (2019). High-Throughput Allelic Replacement Screening in Bacillus subtilis. (Humana, New York, NY), pp. 49–61.

Engler, C., Kandzia, R., and Marillonnet, S. (2008). A one pot, one step, precision cloning method with high throughput capability. PLoS One 3, e3647.

Gibson, D.G., Young, L., Chuang, R.-Y., Venter, J.C., Hutchison, C.A., and Smith, H.O. (2009). Enzymatic assembly of DNA molecules up to several hundred kilobases. Nat. Methods 6, 343–345.

Hassan, A.K., Moriya, S., Ogura, M., Tanaka, T., Kawamura, F., and Ogasawara, N. (1997). Suppression of initiation defects of chromosome replication in Bacillus subtilis dnaA and oriC-deleted mutants by integration of a plasmid replicon into the chromosomes. J. Bacteriol. 179, 2494–2502.

Horsburgh, M. J. *et al.* sigmaB modulates virulence determinant expression and stress resistance: characterization of a functional rsbU strain derived from Staphylococcus aureus 8325-4. J. Bacteriol. 184, 5457–67 (2002).

Hoskins, J., Alborn, W.E., Arnold, J., Blaszczak, L.C., Burgett, S., DeHoff, B.S., Estrem, S.T., Fritz, L., Fu, D.J., Fuller, W., *et al.* (2001). Genome of the bacterium Streptococcus pneumoniae strain R6. J. Bacteriol. 183, 5709–5717.

Keller, L.E., Rueff, A.-S., Kurushima, J., Veening, J.-W., Keller, L.E., Rueff, A.-S., Kurushima, J., and Veening, J.-W. (2019). Three New Integration Vectors and Fluorescent Proteins for Use in the Opportunistic Human Pathogen Streptococcus pneumoniae. Genes (Basel). 10, 394.

Kjos, M. *et al.* Bright fluorescent Streptococcus pneumoniae for live-cell imaging of host-pathogen interactions. J. Bacteriol. 197, 807–18 (2015).

Lemon, K.P., Kurtser, I., and Grossman, A.D. (2001). Effects of replication termination mutants on chromosome partitioning in Bacillus subtilis. Proc. Natl. Acad. Sci. U. S. A. 98, 212–217.

Liu, X., Gallay, C., Kjos, M., Domenech, A., Slager, J., van Kessel, S.P., Knoops, K., Sorg, R.A., Zhang, J.-R., and Veening, J.-W. (2017). High-throughput CRISPRi phenotyping identifies new essential genes inStreptococcus pneumoniae. Mol. Syst. Biol. 13, 931.

Monk, I. R., Tree, J. J., Howden, B. P., Stinear, T. P. & Foster, T. J. Complete Bypass of Restriction Systems for Major Staphylococcus aureus Lineages. MBio 6, e00308-15 (2015).

Mercy, C., Ducret, A., Slager, J., Lavergne, J.-P., Freton, C., Nagarajan, S.N., Garcia, P.S., Noirot-Gros, M.-F., Dubarry, N., Nourikyan, J., *et al*. (2019). RocS drives chromosome segregation and nucleoid protection in Streptococcus pneumoniae. Nat. Microbiol. 1.

O'Neil, P., Lovell, S., Mehzabeen, N., Battaile, K., and Biswas, I. (2016). Crystal structure of histone-like protein from Streptococcus mutans refined to 1.9 Å resolution. Acta Crystallogr. Sect. F, Struct. Biol. Commun. 72, 257–262.

Ouellette, S. P. *et al*. Analysis of MreB interactors in Chlamydia reveals a RodZ homolog but fails to detect an interaction with MraY. Front. Microbiol. 5, 279 (2014).

Perego, M., Spiegelman, G. B. & Hoch, J. A. Structure of the gene for the transition state regulator, abrB: regulator synthesis is controlled by the spo0A sporulation gene in Bacillus subtilis. Mol. Microbiol. 2, 689–699 (1988).

van Raaphorst, R., Kjos, M., and Veening, J.-W. (2017). Chromosome segregation drives division site selection in Streptococcus pneumoniae. Proc. Natl. Acad. Sci. U. S. A. 114, E5959–E5968.

Sorg, R.A., Kuipers, O.P., and Veening, J.-W. (2015). Gene Expression Platform for Synthetic Biology in the Human Pathogen Streptococcus pneumoniae. ACS Synth. Biol. 4, 228–239.

Sorg, R.A., Lin, L., van Doorn, G.S., Sorg, M., Olson, J., Nizet, V., and Veening, J.-W. (2016). Collective Resistance in Microbial Communities by Intracellular Antibiotic Deactivation. PLOS Biol. 14, e2000631.

Stamsås, G.A., Myrbråten, I.S., Straume, D., Salehian, Z., Veening, J.-W., Håvarstein, L.S., and Kjos, M. (2018). CozEa and CozEb play overlapping and essential roles in controlling cell division in Staphylococcus aureus. Mol. Microbiol. 109, 615–632.

Szklarczyk, D., Gable, A.L., Lyon, D., Junge, A., Wyder, S., Huerta-Cepas, J., Simonovic, M., Doncheva, N.T., Morris, J.H., Bork, P., *et al.* (2019). STRING v11: protein-protein association networks with increased coverage, supporting functional discovery in genome-wide experimental datasets. Nucleic Acids Res. 47, D607–D613.

Tettelin, H., Nelson, K.E., Paulsen, I.T., Eisen, J.A., Read, T.D., Peterson, S., Heidelberg, J., DeBoy, R.T., Haft, D.H., Dodson, R.J., *et al*. (2001). Complete genome sequence of a virulent isolate of Streptococcus pneumoniae. Science 293, 498–506.

Yansura, D.G., and Henner, D.J. (1984). Use of the Escherichia coli lac repressor and operator to control gene expression in Bacillus subtilis. Proc. Natl. Acad. Sci. U. S. A. 81, 439–443.

Youngman, P., Poth, H., Green, B., York, K., Olmedo, G., Olmeda, G., and Wager-Smith, K. (1989). Methods for genetic manipulation, cloning and functional analysis of sporulation genes in Bacillus subtilis.

Zimmermann, L., Stephens, A., Nam, S.-Z., Rau, D., Kübler, J., Lozajic, M., Gabler, F., Söding, J., Lupas, A.N., and Alva, V. (2018). A Completely Reimplemented MPI Bioinformatics Toolkit with a New HHpred Server at its Core. J. Mol. Biol. 430, 2237–2243.

4

HIGHLY CONSERVED NUCLEOTIDE PHOSPHATASE ESSENTIAL FOR MEMBRANE LIPID HOMEOSTASIS IN *STREPTOCOCCUS PNEUMONIAE*

Kirsten Kuipers*, Clement Gallay*, Václav Martínek, Manfred Rohde, Markéta Martínková, Samantha L. van der Beek, Wouter S.P. Jong, Hanka Venselaar, Aldert Zomer, Hester Bootsma, Jan-Willem Veening#, Marien I. de Jonge#

Published in Molecular Microbiology (2016) 101(1), 12-26. DOI 10.1111/mmi.13312.

* Joint first authors; # shared supervision; this chapter was also part of the PhD thesis of Kirsten Kuipers.

C.G. aided in research design and strain construction, performed fluorescence microscopy and growth analysis, analyzed data and co-wrote the paper.

Summary

Proteins belonging to the DHH family, a member of the phosphoesterase superfamily, are produced by most bacterial species. While some of these proteins are well studied in *Bacillus subtilis* and *Escherichia coli*, their functions in *Streptococcus pneumoniae* remain unclear. Recently, the highly conserved DHH subfamily 1 protein PapP (SP1298) has been reported to play an important role in virulence. Here, we provide a plausible explanation for the attenuated virulence of the *papP* mutant. Recombinant PapP specifically hydrolyzed nucleotides 3′-phosphoadenosine-5′-phosphate (pAp) and 5′-phosphoadenylyl-(3′–>5′)-adenosine (pApA). Deletion of *papP*, potentially leading to pAp/pApA accumulation, resulted in morphological defects and mis-localization of several cell division proteins. Incubation with both polar solvent and detergent led to robust killing of the *papP* mutant, indicating that membrane integrity is strongly affected. This is in line with previous studies showing that pAp inhibits the ACP synthase, an essential enzyme involved in lipid precursor production. Remarkably, partial inactivation of the lipid biosynthesis pathway, by inhibition of FabF or depletion of FabH, phenocopied the *papP* mutant. We conclude that pAp and pApA phosphatase activity of PapP is required for maintenance of membrane lipid homeostasis providing an explanation how inactivation of this protein may attenuate pneumococcal virulence.

Introduction

Streptococcus pneumoniae is a Gram-positive α-hemolytic bacterium and one of the leading causes of infection-related mortality worldwide (Walker *et al*., 2013). This human-specific pathogen mainly resides on the mucosal surface of the upper respiratory tract generally resulting in asymptomatic carriage (O'Brien *et al*., 2009, Kadioglu *et al*., 2008). However, *S. pneumoniae* may transit to other tissues causing a broad range of diseases varying from non-invasive infections such as otitis media and sinusitis, to more severe invasive disease, including pneumonia, meningitis and sepsis (O'Brien *et al*., 2009, Drijkoningen & Rohde, 2014).

Recently, the protein SP1298 of *S. pneumoniae* TIGR4 (here renamed to PapP for phosphoadenosine-5′-phosphate and 5′-phosphoadenylyl-(3′−>5′)-adenosine phosphatase, see results) was discovered using GAF and Tn-Seq and appears to be a highly conserved protein across the different pneumococcal serotypes (Bijlsma *et al*., 2007, van Opijnen & Camilli, 2012). Inactivation of this gene strongly reduced virulence at different stages of pneumococcal disease, as studied in murine models of colonization, otitis media, pneumonia, and bacteremia (Cron *et al*., 2011, Bai *et al*., 2013), suggesting a critical role for PapP in pneumococcal virulence.

PapP is annotated as DHH subfamily 1 protein as it contains the two domains DHH and DHH1. The DHH subfamily 1 is part of the superfamily of phosphoesterases (Aravind & Koonin, 1998). Within the phosphoesterases two subfamilies exist: the subfamily 2 found in eukaryotes, and the subfamily 1 found in archaea and bacteria. Although these proteins appear to be expressed by most bacteria, little is known about the function of DHH subfamily 1 proteins in *S. pneumoniae*.

PapP shares sequence homology with YtqI of *B. subtilis*, which has both oligonuclease and pAp-phosphatase activity (Mechold *et al*., 2007). Of note, most sequence homology is shared with SMU.1297, a *Streptococcus mutants* protein that was reported as pAp phosphatase *in vitro*, but which lacks an oligonuclease activity and is required for superoxide stress tolerance (Zhang & Biswas, 2009). Recently, the PapP ortholog in strain D39 (SPD_1153) sharing 98% amino acid identity was annotated as Pde2 (PDE: phosphodiesterase) (Bai *et al*., 2013). They showed that PapP synergizes with SP2205 (or Pde1) in a two-step in vitro process, converting c-di-AMP and pApA into AMP. Based on enzymatic assays, they hypothesized a role for PapP in cell wall maintenance and signaling (Bai *et al*., 2013), while the conversion of pAp, as previously found for other homologous proteins, was not described. Therefore, the function of this nucleotide phosphatase remains largely enigmatic, although most studies suggest that PapP homologs convert pAp, a byproduct of the panthotenate and CoA synthesis, into AMP (Zhang & Biswas, 2009, Mechold *et al*., 2007, McAllister *et al*., 2000). More specifically, pAp is released upon generation

of the acyl carrier protein (ACP), an essential precursor for the initiation of *de novo* fatty acid synthesis. Furthermore, it has been shown that ACP synthase activity can be inhibited by increased pAp concentrations (McAllister *et al*., 2000).

In this study we demonstrate that PapP is a nucleotide phosphatase converting pAp and pApA into AMP *in vitro*. Deletion of *papP* directly influenced the cell morphology and the localization dynamics of several key cell division proteins in a temperature dependent manner. Furthermore, we discovered that the membrane integrity of the *papP* mutant was disrupted and that partial inactivation of the lipid biosynthesis process resulted in a similar Δ*papP* phenotype, thus providing a molecular explanation for reduced *S. pneumoniae* virulence.

Results

Protein conservation and structure prediction

Protein sequence homology analyses revealed that PapP of *S. pneumoniae* TIGR4 (serotype 4) is a highly conserved phosphatase in Gram-positive bacteria, mycoplasmas and phytoplasmas. Of the 127 most conserved homologous proteins, two are well described in literature that are both 3′-phosphoadenosine-5′-phosphate (pAp) phosphatases: NrnA, also known as YtqI (*Bacillus spp.*), and SMU.1297 (*Streptococcus mutans*) (Supporting Information Table S1). The latter is 68% identical to PapP (Mechold *et al*., 2007, Zhang & Biswas, 2009).

Homology-based structural modeling predicts PapP to be a homodimer (Fig. 1A-C). The catalytic site is formed by Asp26, Asp28, Asp82, His105 and Asp155, containing a manganese (Mn^{2+}) ion as co-factor (Fig. 1C). No transmembrane or membrane interacting domains were identified, which suggests that PapP is a cytoplasmic protein (Fig. 1A-C). To confirm this localization, we fused a monomeric superfolder green fluorescent protein (GFP) to the C-terminal extremity of PapP. This genetic fusion was integrated at the non-essential *bgaA* locus, under the control of a zinc-inducible promoter (*papP-gfp*). As expected, the fluorescent signal was detected throughout the cell (Supplementary Fig. 1), confirming the cytoplasmic localization of PapP.

PapP converts both nucleotide substrates pAp and pApA into AMP

To confirm that PapP is a pAp phosphatase, the protein was purified, reconstituted with Mn^{2+}, incubated with its substrate and subjected to HPLC analysis to measure hydrolysis. Purified PapP was able to convert pAp to AMP and phosphate with a K_m value of 580 ± 70 µM and a K_m/K_{cat} of 19 ± 3 $s^{-1}.M^{-1}$ (Fig. 1D). The enzymatic activity increased by adding manganese, but only slightly by magnesium ions (Supplementary Fig. 2), confirming that Mn^{2+} is indeed the co-factor as predicted by protein homology

modeling (Fig. 1A-C). Highly efficient hydrolysis of 5′-phosphoadenylyl-(3′−>5′)-adenosine (pApA) by PapP was also detected a K_m value of 67 ± 20 µM and a K_m/K_{cat} of 2100 ± 500 $s^{-1}.M^{-1}$ (Fig. 1D). A similar K_m value (23.96 ± 7.78 µM) was reported for the PapP ortholog from *S. pneumoniae* D39 named SPD_1153 or Pde2 (Bai *et al.*, 2013). No hydrolysis of ADP, ATP, c-di-AMP and c-di-GMP was found in the presence of PapP (Supplementary Fig. 3). This underlines the enzyme specificity for hydrolysis of 3'-phosphate group of linear adenine-containing nucleotides, but also indicates that it is more flexible regarding the size of the substrate, as the two substrates differ significantly in their length. In conclusion, these data confirm the 3′-phosphatase activity of PapP toward pAp and pApA substrates.

S. pneumoniae deficient for papP shows aberrant morphologies

It was established that deletion of *papP* leads to reduction of pneumococcal virulence at many stages of disease (Cron *et al.*, 2011). In order to understand the underlying mechanisms of virulence attenuation when the pAp phosphatase is absent, we investigated the cell morphology of a *S. pneumoniae* TIGR4 strain deficient for *papP* (Δ*papP*). Morphology analysis by phase contrast microscopy and membrane staining with Nile red revealed that the *papP* mutant only forms diplococci at early exponential growth phase, while the wild type forms long chains (Fig. 2A). This is in line with the study of the PapP ortholog in *S. pneumoniae* D39 (serotype 2) where deletion of *pde2* led to significantly shorter chains (Bai *et al.*, 2013). Another striking observation was that the cell-poles of the *papP* mutant were pointier compared to the wild type cells when measuring the pole-angles of the cells (Supplementary Fig. 4). Furthermore, cells of the *papP* mutant were significantly longer and had a wider cell diameter (Fig. 2B). To characterize the cell morphology in higher resolution we performed scanning electron microscopy (SEM). The micrographs confirmed that the *papP* deficient strain displayed a substantial shorter chain length consisting of only few cocci with sharp cell-poles (Fig. 2C). Protrusions on the cell surface appeared in all *S. pneumoniae* strains and could likely be capsule artifacts induced by the method (Qin *et al.*, 2013). Complementation of *papP* deletion by an ectopic version of *papP* (Δ*papP**) reversed the diplococcus phenotype, as this strain only forms long chains and possesses a wild type cell pole angularity (Fig. 2A and Supplementary Fig. 3). SEM pictures of this strain also confirmed that reversion of *papP* mutation restored the wild-type phenotype (Fig. 2C). These observations suggest that *papP* deficiency affects the chain formation of *S. pneumoniae*. In addition to morphology defects, analysis of the growth rate in liquid culture at 37°C revealed that the *papP* mutant demonstrates a reduced growth rate with a doubling time of 46 min (95% confidence interval 44.1 to 49.1 min) versus 34 min (95% confidence interval 35.5 to 37.4 min) for the wild type (Fig. 2D). Taken together, these results indicate that absence of PapP directly influences the cell morphology and growth of *S. pneumoniae*.

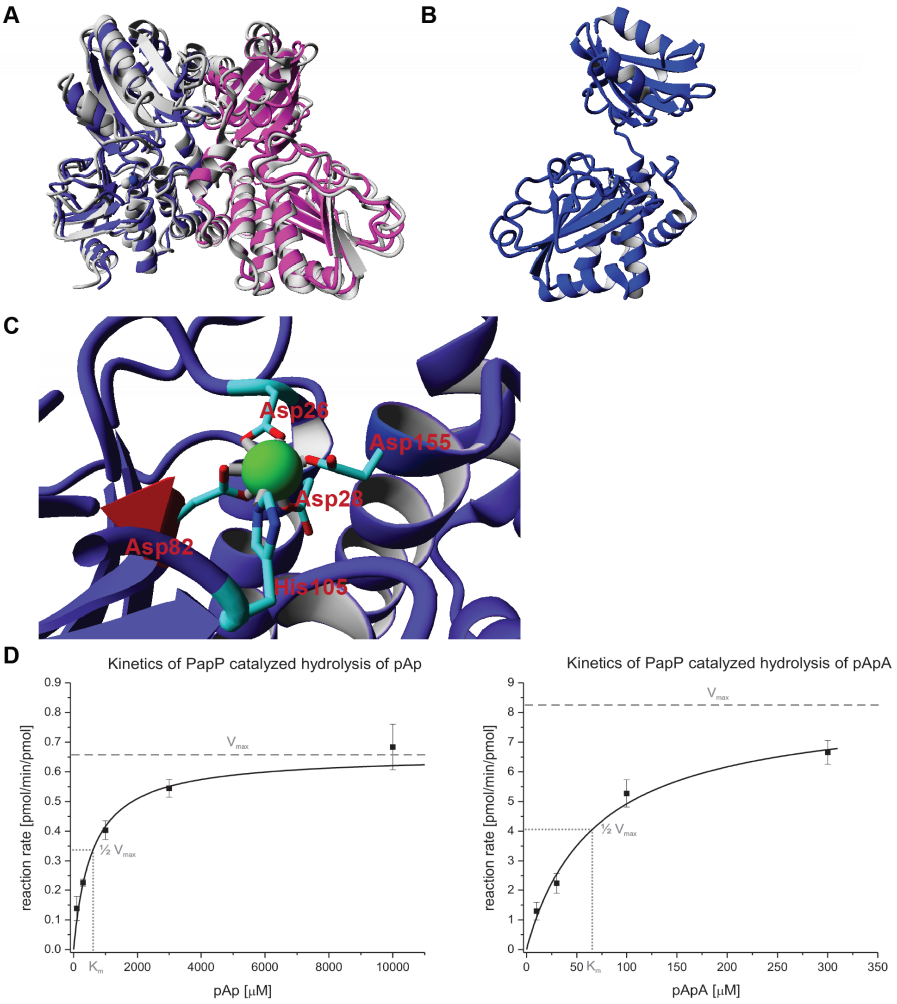

Figure 1. PapP structure and enzymatic activity.

The predicted structure of PapP is based on the crystal structure of SH1221 from *S. haemolyticus* (43% shared identity). (**A**) PapP is predicted to form a homodimer. The PapP model was structurally aligned with the SH1221 template (gray). PapP monomers are indicated in blue and pink. (**B**) Monomeric structure of PapP. (**C**) The catalytic site is predicted to contain a Mn^{2+} ion (green sphere) bound by Asp26, Asp28, Asp82, His105 and Asp155. (**D**) Steady-state kinetic analysis of PapP catalyzed hydrolysis of pAp (left) and pApA (right) with the corresponding K_m and V_{max} values. The reaction rates were determined from the AMP product formation and the kinetic parameters were obtained from non-linear Michaelis–Menten fits. AMP concentrations were analyzed using HPLC. All data are the mean ± SD (n = 3).

The polysaccharide capsule is unaffected in the absence of PapP

It is known that the polysaccharide capsule plays a crucial role in virulence of *S. pneumoniae*. Indeed, the non-encapsulated *S. pneumoniae* R6 strain (derivate from D39 strain) is non-virulent. Interestingly, strain R6 only forms diplococci instead of chains (Berg *et al*., 2013). Taking this into account, the phenotype observed in absence of PapP may be caused by perturbations in capsule production. To test this, we performed immunofluorescence microscopy using a serotype 4 specific capsule antibody. Interestingly, the signal illustrative for capsule presence appeared similar among wild type, mutant, and complemented strain (Fig. 3A). This suggests that despite the morphological differences, the *papP* mutant displayed a normal polysaccharide capsule. To confirm that loss of PapP has no effect on capsule production, bacterial lysates were assayed for the amount of capsule. A non-encapsulated mutant of TIGR4, TIGR4Δ*cps*, was included as negative control (Fig. 3B). Strikingly, all three TIGR4 strains, wild-type, mutant and complemented strain, showed similar capsule polysaccharide levels (Fig. 3B). These data clearly indicate that the polysaccharide capsule remained intact in *S. pneumoniae* deficient for PapP. Hence, capsule alterations do not explain the atypical morphology of the mutant.

Effects of papP inactivation on the cell wall

To explore whether cell wall homeostasis may be influenced by inactivation of *papP*, qualitative and quantitative analyses were performed to probe the phosphorylcholine moieties of the pneumococcal teichoic acids. No differences were found in phosphorylcholine production between wild type, mutant, and complemented strain, as measured in a quantitative ELISA (Fig. 4A). The phosphorylcholine migration pattern as determined by Western blotting appeared identical between the three variants (Fig. 4B). These data indirectly indicate that lipoteichoic acid (LTA) and wall techoic acid (WTA) are unaffected in the *papP* mutant. Additionally, no significant differences in amount of lipoproteins were measured in Δ*papP*, Δ*papP**, and wild type (Supplementary Fig. 5).

Furthermore, the effect of absence of *papP* on peptidoglycan was studied in a lysozyme killing assay. Notably, the *papP* mutant was significantly more sensitive to lysozyme, exemplified by a 2-fold reduced survival, as compared to wild type and the complemented mutant strain (Fig. 4C). Of note, survival of the Δ*papP* strain (mean survival of 32.3%) was over 15-fold higher than a Δ*sp1479* strain (mean survival of 1.8%), which lacks peptidoglycan *N*-acetylglucosamine deacetylase A (PgdA), an enzyme directly involved in peptidoglycan cross-linking (Fig. 4C) (Davis *et al*., 2008). The reduced sensitivity to lysozyme as compared to the Δ*sp1479* mutant implies that this may not be caused by a direct effect on peptidoglycan.

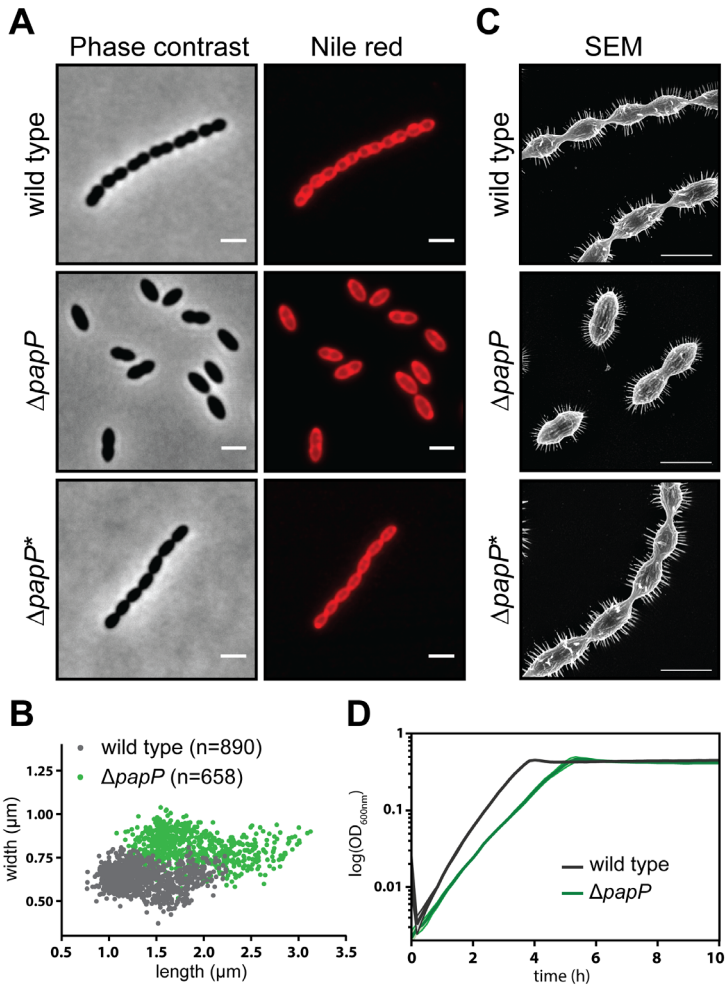

Figure 2. Morphological and growth defects of the *papP* mutant.

(**A**) Phase contrast microscopy (left panel) and Nile red staining (right panel) of TIGR4 wild type, Δ*papP* and Δ*papP**. Scale bar, 3 µm. (**B**) Cell width (p-value < 0.0001) and cell length (p-value < 0.0001) distribution of TIGR4 wild type (dark gray) and Δ*papP* (green). (**C**) Scanning electron micrographs (SEM) of TIGR4 wild type, Δ*papP* and Δ*papP**. Scale bar, 1,5 µm. (**D**) Growth curve of TIGR4 wild type (dark gray) and Δ*papP* (green) at 37°C in liquid C+Y medium. SEM for TIGR4 wild type and Δ*papP* are shown in clear grey and clear green, respectively.

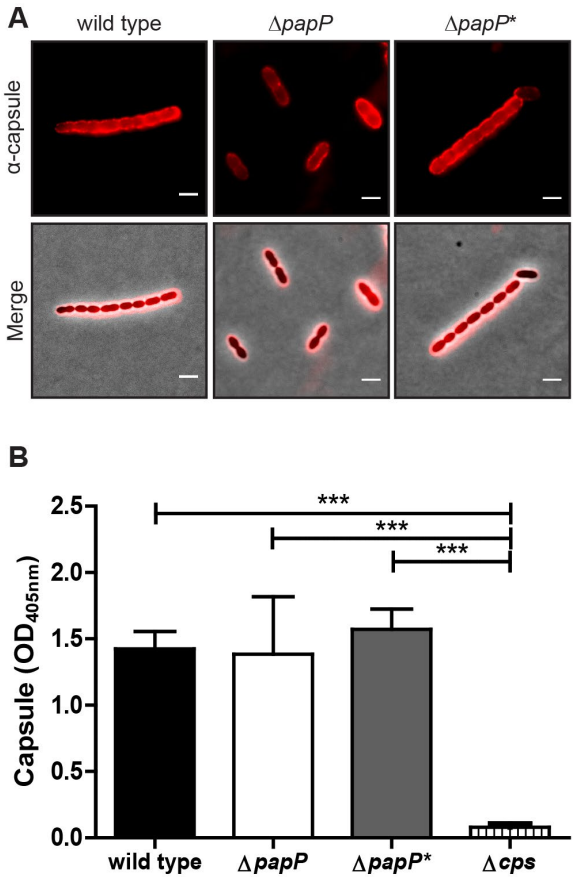

Figure 3. Intact polysaccharide capsule in *papP*-deficient *S. pneumoniae*.

(**A**) Immunofluorescence staining (α-capsule) of the polysaccharide capsule of TIGR4 wild type, Δ*papP* and Δ*papP** using anti-serotype 4 antibodies. Scale bar, 3 μm. (**B**). All strains were screened for capsule expression in an ELISA-based assay, with an acapsular derivative (Δ*cps*) as negative control. Data are normalized from three independent experiments performed in duplicate. Results are illustrated at average ± SEM and compared by one-way ANOVA and Tukey's multiple comparison test. Significance is illustrated with ***, P< 0.001; **, P<0.01; *, P<0.05.

Loss of papP perturbs cell division protein dynamics

The cell division machinery of *S. pneumoniae* involves many important proteins that fine-tune the cell shape (Massidda *et al.*, 2013, Pinho *et al.*, 2013). Deregulation of these proteins could therefore result in cell morphology defects. In order to determine whether the morphological changes of the Δ*papP* mutant could be attributed to a deregulation of the division process, we inserted an ectopic copy of a N-terminal GFP fusion of the early cell division protein FtsA under control of a zinc-inducible promoter in both wild type and Δ*papP* strains, resulting in strains CG16 and CG18,

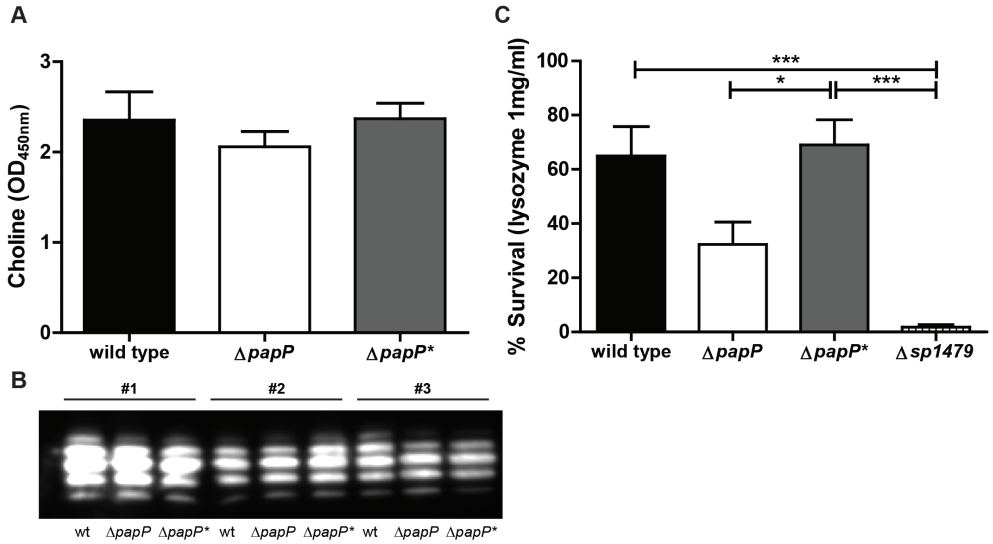

Figure 4. The effect of PapP absence on cell wall components.

(**A**) Cell-wall anchored choline levels of wild type, mutant (Δ*papP*) and complemented mutant strains (Δ*papP**) as measured by an ELISA-based assay. A higher OD_{450nm} indicates a higher choline content. (**B**) Analysis of phosphorylcholine in the cell wall by Western blotting. The phosphorylcholine migration pattern analyzed by SDS-PAGE and Western blotting in wild type (wt), *papP* mutant (Δ*papP*) and complemented (Δ*papP**) strains. The results represent phosphorylcholine migration patterns from three independent experiments (#1, #2, #3). (**C**) Survival of pneumococcal strains in a lysozyme killing assay, with negative control Δ*sp1479*. Choline expression levels show normalized data from three independent experiments performed in duplicate. Lysozyme data are combined from four independent assays. Results are provided as average ± SEM and compared by one-way ANOVA and Tukey's multiple comparison test. Significance is illustrated with ***, P< 0.001; **, P<0.01; *, P<0.05.

respectively. As expected, in the wild type cells, FtsA is recruited early at the new septum and thus localizes exclusively at mid-cell at early exponential growth phase (Fig. 5A). However, the signal in the *papP* mutant appears to be at mid-cell but also at the old division site (Fig. 5A). To exclude that addition of Zn^{2+} induced synthetic effects, we constructed a strain expressing a functional fusion of the early cell division protein FtsZ with the red fluorescent protein mKate2 (strains CG14 and CG22). This construct was inserted at the TIGR4 *ftsZ* locus, under the native promoter in order to keep the original FtsZ expression level. Fluorescence microscopy confirmed the localization of FtsZ at mid-cell in both wild type and Δ*papP* (Fig. 5B). To better understand the localization dynamics of FtsZ, we performed time-lapse fluorescence microscopy at 37°C. Interestingly, while FtsZ was instantly disassembled from the old septum and re-assembled at the new septum in the wild type strain (Fig. 5C, Supplementary Movies 1 and 2), it slowly moved from the old septum to the new septum in the Δ*papP* mutant (Fig. 5C, Supplementary Movies 1 and 2). Similar results

were obtained for GFP-FtsA (Supplementary Movie 3). To further characterize the dynamics of these two cell division proteins, the distance between FtsA or FtsZ and the closest pole of the cell was measured. When plotted with the cell length, two different clusters are clearly visible for the wild type, indicating that FtsA and FtsZ are either at the old or the new division site, or at both positions (Fig. 5D and E). However, the two distinct clusters disappeared for the mutant strain, giving way to a heterogeneous distribution (Fig. 5D and E). This indicates that FtsA and FtsZ are not only present at both the old and new septum, but also in between these two positions at one moment of the cell cycle (Fig. 5F). Taken together, these results show that inactivation of *papP* results in mis-localization of FtsA and FtsZ.

Localization of cell division proteins is temperature dependent in the ΔpapP strain

To characterize the FtsZ dynamics of the *papP* mutant in more detail, we used time-lapse fluorescence microscopy to follow the cells on a semi-solid matrix at 30°C, a temperature known to slow down the cell cycle compared to the previous experiments performed at 37°C. Surprisingly, whereas FtsZ is well localized at mid-cell in the wild type, it appears to be completely mis-localized in the Δ*papP* mutant after a few division cycles, followed by a quick death of the cells (Fig. 6A and Supplementary Movie 4). Identical results were obtained with GFP-FtsA (Supplementary Movie 5). Fluorescence microscopy of cells grown at 30°C until early exponential growth phase in liquid medium confirmed the previous observations since many cells displayed abnormal morphologies and FtsZ was frequently mis-localized (Fig. 6B). This excludes an indirect effect of the fluorescence time-lapse microscopy technique for FtsZ mis-localization. Growth in liquid C+Y medium at 30°C also indicated a temperature sensitivity of the Δ*papP* strain since it entered in stationary phase at lower cell density (Fig. 6C). These data suggest that the *papP* mutant is cold sensitive, especially when also harboring a FtsZ-RFP fusion. To further characterize the temperature sensitivity, the mutant strain was grown at even lower temperatures (25°C) and FtsZ localization was monitored. Despite a very slow growth at this temperature, FtsZ is still well localized in the wild type strain (Fig. 6D). Surprisingly, the mutant strain shows many elongated cells displaying a helical pattern of FtsZ (Fig. 6D). Thus, our data indicate that absence of the pAp phosphatase (PapP) leads to mis-localization of cell division proteins in a temperature-dependent manner.

Lack of PapP diminishes cell membrane integrity

Many cell division proteins are directly or indirectly anchored to the cell membrane. For instance, FtsA is a membrane-associated protein that anchors FtsZ (Pichoff & Lutkenhaus, 2005). A change in membrane properties can thus impact their localization. To assess whether membrane integrity may be reduced upon *papP* deletion, pneumococcal strains were screened for survival in both organic solvent

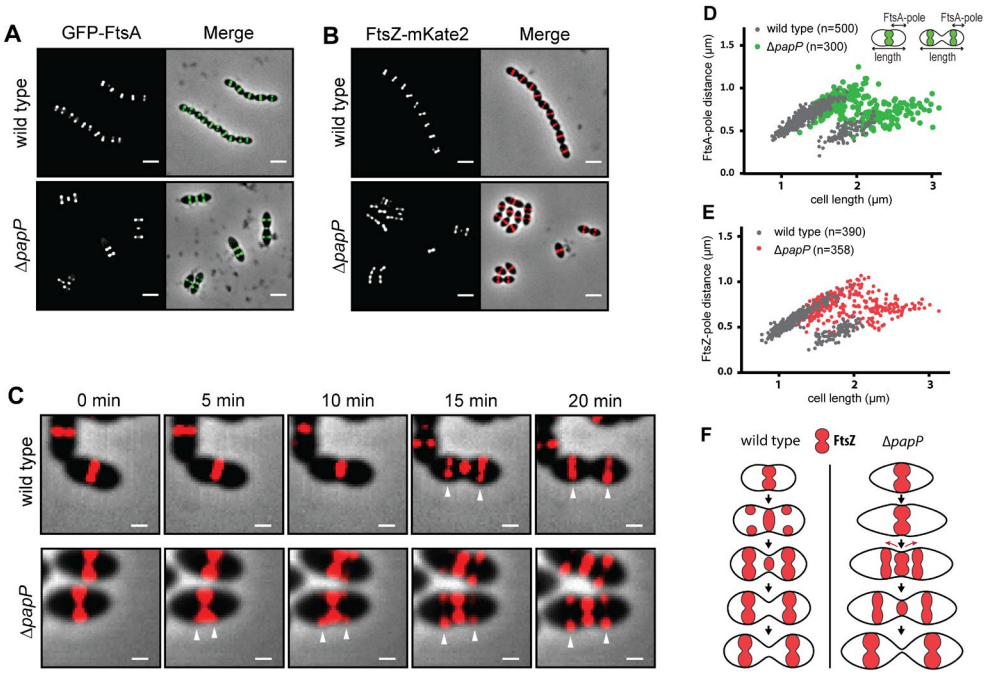

Figure 5. FtsA and FtsZ dynamics are impaired in Δ*papP*.

(**A**) Localization of GFP-FtsA in live TIGR4 wild type and Δ*papP*. The GFP fluorescent signal (left panel) is overlaid with the phase contrast image (right panel). Scale bar, 3 µm. (**B**) Localization of FtsZ-mKate2 in live TIGR4 wild type and Δ*papP*. The mKate2 signal (left panel) is overlaid with the phase contrast image (right panel). Scale bar, 3 µm. (**C**). Fluorescence time-lapse microscopy of FtsZ-mKate in TIGR4 wild type and Δ*papP* at 37°C. The fluorescent signal is overlaid with the phase contrast. The white arrows indicate the localization of the newly formed Z-ring. Scale bar, 0.5 µm. (**D**) Distance between GFP-FtsA and the closest pole of TIGR4 wild type and Δ*papP* depending on cell size. (**E**) Distance between FtsZ-mKate2 and the closest pole of TIGR4 wild type and Δ*papP* depending on cell size. (**F**) Model of TIGR4 wild type and Δ*papP* cell division. Compared to the wild type situation where FtsZ (red) seems to be directly reassembled at the new division site, it seems to slowly slide from the old to the new septum in the *papP* mutant (green arrows) over the cell cycle. Cells of the *papP* mutant also appear bigger and pointier.

and detergent killing assays. As hypothesized, the *papP* mutant appeared highly susceptible for ethanol (Fig. 7A) and Triton X-100 in comparison with the wild type strain and the complemented mutant (Fig. 7B). Survival in absence of *papP* was reduced approximately 5- and 4-fold in ethanol (13%) and Triton X-100 (20%) killing assays, respectively. These data clearly indicate an increased sensitivity of *S. pneumoniae* deficient for *papP* to both organic and solvent compounds that is likely caused by an unstable and more accessible membrane. This is supported by the increased sensitivity of the *papP* mutant against selected antibiotics (Supporting Information Table S4).

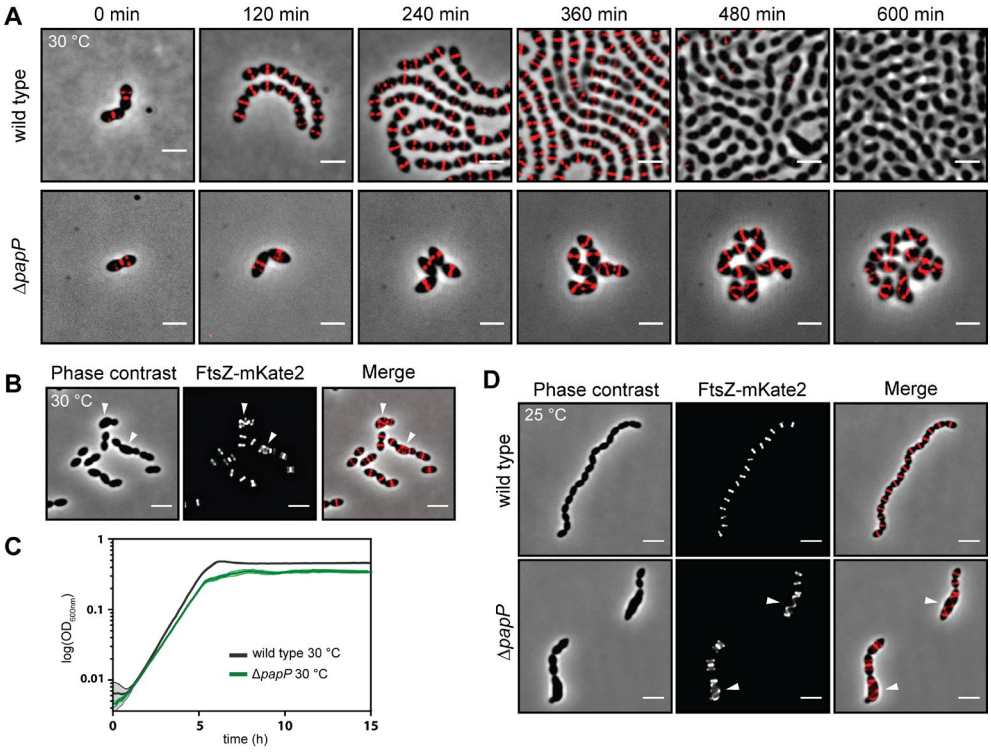

Figure 6. FtsZ localization is temperature dependent in Δ*papP*.

(**A**) Time lapse fluorescence microscopy of FtsZ-mKate2 in TIGR4 wild type and Δ*papP* at 30°C. The fluorescent signal is overlaid with the phase contrast. Scale bar, 3 µm. (**B**) Localization of FtsZ-mKate2 in live TIGR4 wild type and Δ*papP* grown at 30°C. Overlay between the phase contrast images (left panel) and the mKate2 signal (middle panel) is shown (right panel). The white arrows indicate the aberrant localization of FtsZ. Scale bar, 3 µm. (**C**) Growth curve of TIGR4 wild type (dark gray) and Δ*papP* (green) at 30°C. SEM for TIGR4 wild type and Δ*papP* are shown in clear grey and clear green, respectively. (**D**) Localization of FtsZ-mKate2 in live TIGR4 wild type and Δ*papP* grown at 25°C. Overlay between the phase contrast images (left panel) and the mKate2 signal (middle panel) is shown (right panel). The white arrows indicate the helical pattern of FtsZ. Scale bar, 3 µm.

FabF or FabH inactivation phenocopy papP deletion

In order to investigate whether the phenotype of the *papP* mutant is the result of fatty acid biosynthesis perturbation, we sought to partially inactivate this process. Bacterial type II fatty-acid synthasis (FASII) inhibition seems a good strategy as these enzymes are involved in essential steps of the fatty acid biosynthesis (Parsons & Rock, 2013). For instance, the proteins FabH and FabF are respectively responsible for the initiation and elongation of the fatty acid chains. However, due to their essentiality, their inactivation by deleting the corresponding genes is not possible. On the other hand, it has been reported that FabF can by inactivated by a bacteriostatic drug, platensimycin (Wang *et al.*, 2006). To examine the effect of fatty acid synthesis

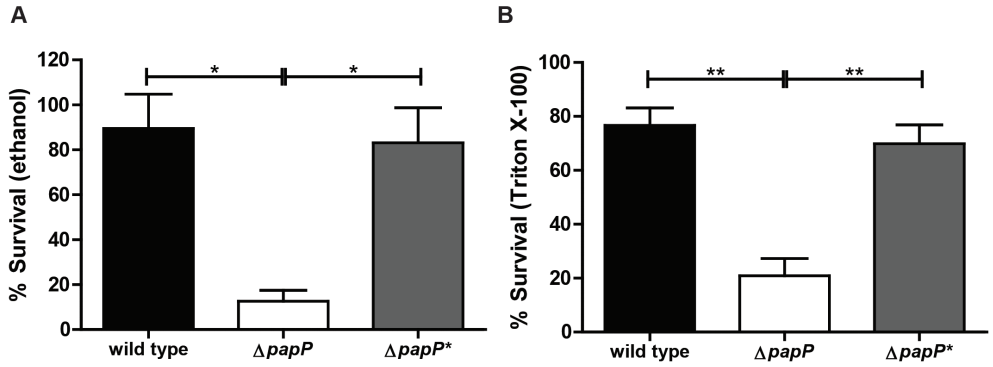

Figure 7. Loss of PapP increases susceptibility to organic solvent and detergent.

Survival of pneumococcal strains, wild type, mutant (Δ*papP*), and complemented mutant strain (Δ*papP**), in an (**A**) organic solvent ethanol and (**B**) detergent Triton X-100 killing assay. Ethanol and Triton X-100 killing show normalized data from three independent experiments performed in duplicate. Results are provided as average ± SEM and compared by one-way ANOVA and Tukey's multiple comparison test. Significance is illustrated with ***, P< 0.001; **, P<0.01; *, P<0.05.

inhibition by platensimycin on pneumococcal morphology, the wild type strain was grown in the presence of 0.75 μg.mL^{-1} platensimycin to early exponential growth phase and cell morphology was assessed by phase contrast microscopy. A concentration was used at which the maximum optical density of *S. pneumoniae* was reduced by two-fold (MC50) (Supplementary Fig. 6) (Prudhomme *et al*., 2006). Strikingly, platensimycin treatment resulted in the formation of only diplococci (Fig. 8A) and chains of cells were no longer observed. This shows that partial inactivation of the fatty acid biosynthesis by inactivation of FabF is able to phenocopy the *papP* mutant in this regard.

Next, we assessed the effect of FabH depletion on *S. pneumoniae* morphology by constructing a strain expressing an ectopic version of *fabH* under a zinc-inducible promoter and made a deletion of the native *fabH* gene in presence of Zn^{2+} (Δ*fabH**). Phase contrast microscopy revealed a wild type phenotype when grown in the presence of 0.1 mM Zn^{2+} (Fig. 8B). Zinc absence is sufficient for minor expression of FabH, which is likely due to the leakage of the zinc-inducible promoter (Sorg *et al*., 2015), Strikingly, when grown without zinc, chain formation was absent and cells display a diplococcus phenotype (Fig. 8B). Apparently, reducing available FabH also phenocopies inactivation of *papP*. Taken together, these results strongly indicate that PapP deficiency affects the fatty acid biosynthesis resulting in the observed morphological defects.

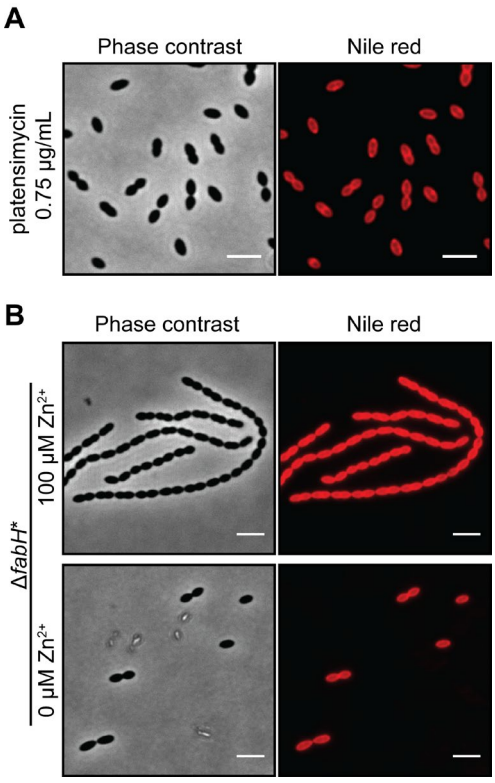

Figure 8. Partial inactivation of lipid synthesis phenocopies Δ*papP* morphology

(**A**) Phase contrast microscopy (left panel) and Nile red staining (right panel) of TIGR4 wild type grown in presence of 0.75 µg/mL platensimycin. Scale bar, 3 µm. (**B**) Phase contrast microscopy (left panels) and Nile red staining (right panels) of Δ*fabH** grown in presence of 100 µM Zn^{2+} (upper panels) or without (lower panels). Scale bar, 3 µm.

Discussion

The *papP* deletion mutant showed in a previous study decreased virulence in all stages of pneumococcal disease, which strongly indicates a critical role for *papP* in *S. pneumoniae* pathogenesis (Cron *et al.*, 2011). Remarkably, *S. pneumoniae* deficient for *papP* showed an abnormal morphology and was substantially weaker in various killing assays compared to wild type strains and the complemented mutant. Altogether, our data indicate that loss of *papP* results in a cell integrity defect, rather than loss of a specific virulence factor as suggested previously (Cron *et al.*, 2011, Bai *et al.*, 2013).

In this study we show that PapP is a phosphatase able to convert two adenine-nucleotide substrates, 3′-phosphoadenosine-5′-phosphate (pAp) and 5′-phosphoadenylyl-(3′−>5′)-adenosine (pApA). Hydrolysis of pApA by

S. pneumoniae D39 PapP ortholog (Pde2) was recently described and hypothesized to be implicated in c-di-AMP signaling and cell wall homeostasis, as pApA is a product of in vitro degradation of c-di-AMP (Corrigan *et al*., 2011, Bai *et al*., 2013). However, it is unknown in which quantities and during which other metabolic processes pApA is produced in *S. pneumoniae*. More importantly, its biological role remains largely unknown. A possibility is that pApA is a metabolite generated during other *S. pneumoniae* metabolic processes, including lipid metabolism, which may be undetectable due to a fast degradation into end products like AMP. This theory is supported by our observation that PapP breakdown of pApA is remarkably rapid (Fig. 1D).

In addition to pAp as substrate, Uemera and colleagues reported that Nrn degrades short RNAs, *e.g.* nanoRNAs. This dual preference for nanoRNA and pAp conversion has also been described for other DHH subfamily 1 proteins, including RecJ, Orn, and YtqI (Mechold *et al*., 2007, Wakamatsu *et al*., 2011, Mechold *et al*., 2006), suggesting a similar activity for PapP. Whether nanoRNA degradation contributes to the phenotype of *S. pneumoniae* deficient for PapP remains speculative. Namely, Mechold and colleagues reported that RNase activity is redundant (Mechold *et al*., 2007), indicating that absence of a single RNase would not affect RNA metabolism. In addition, RNase activity has not been described for *S. mutans* protein SMU.1297, which shares 68% homology with PapP (Zhang & Biswas, 2009).

It is remarkable that PapP is highly conserved in Gram-positive bacteria, mycoplasmas and phytoplasmas, all containing a single membrane. In this regard, it is tempting to speculate that these single membrane-containing bacteria are more vulnerable for distortion of the lipid membrane homeostasis. Our findings demonstrate that loss of a single protein results in a weakened membrane integrity of *S. pneumoniae* (Figs. 7A and B), which makes PapP an attractive target for therapeutic interventions for Gram-positive infections.

Perturbing the membrane altered the localization dynamics of key cell division proteins FtsA and FtsZ (Figs.5-6). A recent body of work has shown that cell division in *S. pneumoniae* is orchestrated by a complicated phosphorylation cascade via the eukaryotic-type serine-threonine kinase StkP (Manuse *et al*., 2015). It would be interesting to see what the effects of membrane perturbations, such as those caused by *papA* deletion, are on the signaling at the level of StkP and downstream proteins.

In conclusion, we hypothesize that in *S. pneumoniae* lacking the pAp phosphatase PapP, pAp and pApA levels will increase thereby inhibiting AcpS (McAllister *et al*., 2000). Subsequently, decreased enzyme activity may lead to reduced precursor formation, which is required to start fatty acid synthesis, thereby hampering *de novo* lipid production (McAllister *et al*., 2000). The resulting reduction in membrane integrity

provides a plausible explanation for altered cell morphology and susceptibility and thereby reduced virulence of *papP* deficient *S. pneumoniae* (Cron *et al*., 2011). Investigating newly discovered conserved pneumococcal proteins will improve our understanding of pneumococcal physiology and pathogenesis. Gaining insight into *S. pneumoniae* membrane homeostasis and virulence may reveal potential targets that will aid the development of future therapeutics and vaccines to treat and prevent pneumococcal disease.

Methods

Pneumococcal strains, growth conditions and transformation

Pneumococcal strains were routinely grown at 37°C on Blood Agar (BA) or in liquid cultures of Todd Hewitt broth with 5 g/L yeast extract (THY). For microscopy analyses, strains were grown in C+Y medium at 37°C, 30°C or 25°C. For transformation, *S. pneumoniae* was grown in THY or C+Y medium pH = 6.8 until $O.D_{600nm}$ = 0.1; then 0.2 µg/mL of synthetic CSP-2 (Competence-Stimulating Peptide 2) was added and the cells were incubated at 37°C for 12 min. After DNA addition, cells were incubated at 30°C for 20 min, then diluted 10 times in THY or C+Y medium, followed by incubation for 1.5 h at 37°C. Transformants were selected on Blood agar or Columbia agar supplemented with 3% (v/v) sheep blood and the appropriate antibiotic. For induction of the P_{Zn} promoter, 100 µM $ZnCl_2$ was added to liquid medium or agar plates. When required, the growth medium was supplemented with 150 µg/ml spectinomycin (Sp), 500 µg/ml kanamycin (Kan), 0.5 µg/mL tetracycline (Tc) or 0.25 µg/mL erythromycin (Ery). Strains and plasmids construction are detailed in SI Methods. Strains are listed in Table 1, plasmids and primers are listed in tables S2-S3 respectively.

Table 1. *Streptococcus pneumoniae* strains used in this study

Strain	Relevant characteristics	Reference
TIGR4	Serotype 4 strain, TIGR4 wild type	(Tettelin *et al*., 2001)
papP-gfp	TIGR4, *bgaA*::P_{Zn}-*papP-gfp* (Tc^r)	This study
CG14	TIGR4, *ftsZ*::*ftsZ-mKate2* (Ery^r)	This study
CG16	TIGR4, *bgaA*::P_{Zn}-*gfp-ftsA* (Tc^r)	This study
Δ*papP*	TIGR4, *papP*::*spc* (Sp^r)	(Cron *et al*., 2011)
Δ*cps*	TIGR4, Deletion of the capsule operon	(Cron *et al*., 2009)

Δ*sp1479*	TIGR4, *sp1479*::*spc* (Sp^r)	This study
CG22	TIGR4, *papP*::*spc*, *ftsZ*::*ftsZ-mKate2* (Sp^r, Ery^r)	This study
CG18	TIGR4, *papP*::*spc*, *bgaA*::P_{Zn}-*gfp-ftsA* (Sp^r, Tc^r)	This study
Δ*papP**	TIGR4, *papP*::*spc*, IS1167::pCEP-*papP* (Sp^r Kan^r)	This study
Δ*fabH**	TIGR4, *fabH*::*ery*, bgaA::P_{Zn}-*fabH* (Ery^r, Tc^r)	This study

Sp^r: Spectinomycin resistant; Kan^r: Kanamycin resistant; Tc^r: tetracycline resistant; Ery^r: erythromycin resistant

Bioinformatic protein conservation analyses and homology modeling

To study the conservation of SP1298 (PapP), the amino acid sequence was aligned with BLAST against the Concise Microbial Protein database with one orthologous sequence per species to avoid overrepresentation. 514 proteins (e-value <0.001) were selected and aligned using ClustalOmega (Sievers *et al*., 2011). PapP was located in a specific clade containing 127 proteins. Proteins in this clade were subsequently coupled to species and function using the batch retrieval option in the Protein Information Resource (PIR) (Wu *et al*., 2003) (Supporting Information Table S1).

A homology model for SP1298 was built using the experimentally solved 3D-structure of SH1221 protein from *Staphylococcus haemolyticus* as a template (PDB file 3DEV). These proteins share 43% sequence identity. A fast model algorithm with standard parameter settings in the YASARA & WHAT IF Twinset was used for model building and analysis (Krieger *et al*., 2002, Vriend, 1990).

Protein expression and purification

The expression and purification of PapP was performed as follows. BL21-pLC1298 (Cron *et al*., 2011) was grown at 37˚C in LB medium supplemented with 0.2% glucose and 100 µg/ml ampicillin. When the culture reached an OD_{660nm} of 1.0, the incubation temperature was shifted to 18˚C and growth was continued for 2h. The culture was then diluted into fresh medium with 0.2% glucose and 100 µg/ml ampicillin to an OD_{660nm} of 0.5. A concentration of 100 µM isopropyl-β-D-thiogalactopyranoside (IPTG) was added to induce the overexpression of PapP and the culture was grown overnight at 18˚C to prevent the formation of inclusion bodies.

The cells were harvested by centrifugation, re-suspended in ice-cold PBS containing 300 mM NaCl, 5 mM Imidazole and Complete protease inhibitor cocktail (Roche), and lysed by two passages through a One Shot cell disrupter (Constant systems). Cell debris and membrane material was removed by low-speed centrifugation at 8,000 x g for 20 min at 4˚C and subsequent ultracentrifigation of the low-speed supernatant at 208,500 x g for 90 min at 4˚C. The supernatant was loaded onto a 1 ml HiTrap TALON crude column (GE Healthcare) and PapP was eluted with a

linear gradient of 5 - 500 nM Imidazole in PBS containing 300 nM NaCl at 125 mM Imidazole concentration. The elution peak was collected and dialyzed at 4˚C against PBS containing 10% glycerol (w/v) using 12,000 – 14,000 MWCO SpectraPor4 dialysis membranes (Spectrumlabs). The protein was analyzed for purity with SDS-PAGE and Coomassie G250 staining and stored at -80˚C in glycerol-containing dialysis buffer to preserve the enzymatic activity.

Protein reconstitution with manganese

The concentration of purified PapP was determined spectroscopically at 280 nm using extinction coefficient 35870 $M^{-1}.cm^{-1}$. The molar extinction coefficient was predicted by ProtParam tool (Gasteiger E., 2015). The Mn^{2+} concentration in PapP sample was determined using AA-spectrometer AAS3 (Carl Zeiss, Germany).

To ensure full saturation of the enzyme with Mn^{2+}, PapP was incubated with 1:2 molar excess of $MnCl_2$ for 20 min at room temperature. Unbound manganese ions were removed using gel filtration on Sephadex G-50 (2.5 cm, 5 ml column) in 50 mM phosphate buffer pH 7.4 in presence of 5% glycerol.

Enzymatic activity assays

Kinetic experiments with reconstituted enzyme were conducted in 80 mM phosphate buffer (pH 7.4) containing 1 µM $MnCl_2$ using 0.002 and 0.1 µM enzyme for 0-10000 µM 3′-phosphoadenosine-5′-phosphate (pAp, Santa Cruz Biotechnology, USA) and 0-300 µM 5′-phosphoadenylyl-(3′ –> 5′)-adenosine (pApA, Biolog, USA), respectively. The reaction was stopped after 3, 6, and 9 min incubation at 25°C by immediate injection to the HPLC system. The reaction rate was determined as an increase of AMP product; different reaction stoichiometries for pApA and pAp hydrolysis were considered. The kinetic data were analyzed using non-linear Hill's fit (considering Hill's coefficient = 1) implemented in program Origin version 7.5 (OriginLab).

The AMP concentrations in incubation mixture were determined by ion-pair reversed-phase chromatography using method inspired by Nakajima *et al*. (Nakajima *et al*., 2010). Fifteen µl aliquots of the incubation mixtures were injected into a monolithic C18 column (Chromolith RP-18e, 10 x 4.6 mm; Merck) and analyzed using Agilent 1200 HPLC System with detection at 260 nm. Mobile phase A contained 70 mM potassium phosphate buffer pH 6.0, with 4 mM Tetrabutylammonium hydrogensulphate (TBAS, Sigma-Aldrich, USA), as an ion-pair reagent; mobile phase B was methanol. The gradient was delivered at a flow rate of 2 ml/min according to the following program: 100% buffer A for 0.06 min; 0–50% linear gradient of B for 1.0 min; 50% B for 0.25 min; and 100% buffer A for 0.4 min. AMP (Sigma-Aldrich, USA), pAp and pApA standards were used for external calibration. Also ADP, ATP (Sigma-Aldrich, USA) and c-diAMP and c-diGMP (Biolog, USA) were analyzed as

potential enzyme substrates using the same method.

Scanning electron microscopy

Bacteria were grown to early exponential growth phase (OD_{600nm} = 0.1) in C+Y medium and fixed with 2% formaldehyde. Scanning electron microscopy analyses were performed as described previously (Hammerschmidt *et al.*, 2005). Briefly, for scanning electron microscopy (SEM) samples were dehydrated with a graded series of acetone on ice for 15 min for each step. Samples were subjected to critical-point drying with liquid CO_2 (CPD030; Balzers, Liechtenstein). The dried samples were covered with an approximately 10-nm-thick gold film by sputter coating (SCD040; Balzers Union, Liechtenstein) before examination with a field emission scanning electron microscope (Zeiss DSM 982 Gemini) using an Everhart Thornley SE detector and an in-lens detector at a 50:50 ratio at an acceleration voltage of 5 kV.

Phase contrast and epifluorescence microscopy

S. pneumoniae was grown in C+Y medium to early exponential growth phase (OD_{600nm} = 0.1), washed once in PBS and spotted onto a PBS-agarose slide. Microscopy pictures were acquired using a DV Elite microscope (Applied Precision) with either a sCMOS (PCO) or a CoolSNAP HQ^2 (Photometrics) camera, using Solid State Illumination (Applied Precision), with a 100x oil-immersion objective. Phase contrast images were acquired with 200 ms exposure time. To visualize the GFP fluorescence, a GFP filter (excitation 461/489 nm; emission 501/559 nm) was used. The mKate2 fluorescence was monitored using a mCherry filter (excitation 562/588 nm; emission 602/648 nm). The exposure time used for both GFP and mKate2 fluorescence was 600 ms. Pictures were acquired and deconvolved using Softworx (Applied Precision) and analyzed using Fiji (http://fiji.sc).

Membrane staining fluorescence microscopy

In order to visualize the membrane of *S. pneumoniae* with Nile red, the cells were grown in C+Y medium to early exponential growth phase (OD_{600nm} = 0.1) and incubated with 5 µg/mL Nile red for 5 min. The cells were washed once in PBS and spotted onto a PBS-agarose slide. Fluorescence acquisition of Nile red was performed as described above using a TRITC filter (excitation 528/556 nm; emission 571/616 nm) with an exposure time of 300 ms. Pictures were acquired with Softworx and analyzed using Fiji.

Time-lapse fluorescence microscopy

S. pneumoniae was grown in C+Y medium to late log phase (OD_{600nm} = 0.3) and diluted 100 times in fresh C+Y medium supplemented (when appropriate) with 0.1 mM $ZnCl_2$ and incubated for 45 min. Cells were washed once in fresh C+Y

medium and spotted onto a polyacrylamide (10%) slide incubated with C+Y medium, if required complemented with $ZnCl_2$. Acrylamide pieces were placed inside a Gene Frame (Thermo Fisher Scientific) and sealed with the cover glass essentially as described (de Jong *et al*., 2011). Acquisition of fluorescence was performed on a DV Elite microscope with a sCMOS camera at 37°C or 30°C. The filters used to visualize the GFP or mKate2 fluorescence are the same as described above. Exposure time used was 500 ms with 32% excitation light. Movies were acquired and deconvolved using Softworx and analyzed using Fiji.

Immunofluorescence microscopy

For fluorescence analysis of the polysaccharide capsule of *S. pneumoniae*, the strains were grown in C+Y medium at 37°C to exponential growth phase (OD_{600nm} = 0.1), then 1:1000 diluted serum anti-serotype 4 from rabbit (Neufeld antisera, Statens Serum Institut) was added for 5 min at 4°C. Afterward, the cells were washed 3 times in pre-warmed C+Y medium and 1 µg/mL of secondary antibody anti-rabbit coupled to Alexa Fluor 555 (Invitrogen) was added for 5 min at 4°C. The cells were then washed once again in pre-warmed C+Y medium and once with PBS before being spotted onto a PBS-agarose slide. Acquisition of the fluorescent signal was performed on Nikon Ti-E microscope (Nikon) equipped with a CoolSNAP HQ^2 camera, an Intensilight light source, with a 100x oil-immersion objective. To visualize the Alexa Fluor 555 fluorescence, a TRITC filter (excitation 528/556 nm; emission 571/616 nm) was used with an exposure time of 800 ms. Pictures were analyzed afterwards with Fiji.

Capsule quantification

Equal mid-log phase bacterial amounts were re-suspended in deionized water and chloroform and shaken for 5 min using TissueLyser LT (Qiagen). Subsequent centrifugation at 13,000 x g for 10 min resulted in layer separation of which the aqueous layer contained polysaccharides. These samples were subjected to plates coated with anti-serotype 4 (Statens Serum institute, Neufeld Antisera), followed by incubation with mouse anti-prevnar sera and subsequent alkaline-phosphatase-conjugated anti-mouse IgG (Sigma Aldrich). After each step the plates were washed with Phosphate Buffered Saline supplemented with 0.1% Tween-20 (PBST). Substrate solution (p-nitrophenyl phosphate in 10 mM diethanolamine and 0.5 mM magnesium chloride buffer pH 9.5) was added and absorbance was measured at 405 nm.

Quantitative analyses of cell wall phosphorylcholine

Equal amounts of mid-log phase grown pneumococci were resuspended in PBS and lysed in 0.5 gram acid-washed glass beads (150-212 µm) for 5 min at max speed using a TissueLyser LT (Qiagen). Maxisorp high binding affinity plates (Nunc) were coated

with bacterial lysates in carbonate coating buffer (0.1 M carbonate/bicarbonate pH 9.6) at 4°C overnight. For choline detection, plates were incubated with mouse monoclonal TEPC-15 (Sigma) and secondary HRP-conjugated Rabbit anti-mouse antibody (DAKO). Signal was developed using 3,3′,5,5′-Tetramethylbenzidine (TMB) phospho-citrate buffer and the reaction was stopped using 1.8 M sulfuric acid. Absorbance was measured at 450 nm. Detection of the choline migration pattern using Western Blot is described in the Supporting Information Materials and Methods.

Lysozyme, ethanol, and Triton X-100 killing assays

Mid-log phase bacterial pellets were re-suspended in 1 mg/mL lysozyme (Merck), 25% ethanol (Merck), or 0.025% Triton X-100 (Sigma). Incubation with lysozyme was performed at 37˚C for 30 min and incubation with ethanol or Triton X-100 was done at room temperature for 10 min. At indicated time points (0, 10 or 30 min), samples were 10-fold serially diluted in PBS and spotted onto BA plates that were incubated at 37˚C overnight. The following day, single colonies were counted and percentage survival was calculated.

Growth curve assay

In order to follow the growth of *S. pneumoniae*, the strains were grown in C+Y medium at 37°C to early exponential growth phase (OD_{600nm} = 0.1), then diluted to an $O.D_{600nm}$ = 0.001. The growth was monitored in a microtiter plate reader (TECAN Infinite F200 Pro) by measuring the OD_{600nm} every 10 min either at 37°C or 30°C. Each growth curve assay was performed in triplicate.

Statistical tests

All statistical analyses were performed using GraphPad Prism version 5.0 (Graphpad Software). Quantification of capsule and cell wall phosphorylcholine, and the killing assays were repeated in at least three independent experiments all performed in duplicate. Data were normalized to wild type assayed in the control condition (PBS), and illustrated as mean ± standard error of the mean (SEM). Groups were compared with one-way analysis of variance (ANOVA) and Tukey's multiple comparison post-test. A P-value of ≤ 0.05 was considered statistically significant.

Acknowledgments

K.K. and M.d.J. were supported by Agentschap NL [PneumoVac, nr. OM111009]. Work in the Veening lab is supported by the EMBO Young Investigator Program, a VIDI fellowship (864.12.001) from the Netherlands Organisation for Scientific Research, Earth and Life Sciences (NWO-ALW) and ERC starting grant 337399-PneumoCell. The authors thank Dr. Jakub Hraníček from the Charles University in Prague, for

assistance with determination of Mn^{2+} concentration in the PapP sample using AAS analysis, Prof. Sven Hammerschmidt and Dr. Franziska Voß for providing the α-enolase α-MetQ, α-PpmA, α-PsaA, and α-SlrA antibodies, and Dr. Jeroen Langereis for his helpful input.

References

Aravind, L. & E.V. Koonin, (1998) A novel family of predicted phosphoesterases includes Drosophila prune protein and bacterial RecJ exonuclease. Trends Biochem Sci 23: 17-19.

Bai, Y., J. Yang, L.E. Eisele, A.J. Underwood, B.J. Koestler, C.M. Waters, D.W. Metzger & G. Bai, (2013) Two DHH subfamily 1 proteins in Streptococcus pneumoniae possess cyclic di-AMP phosphodiesterase activity and affect bacterial growth and virulence. J Bacteriol 195: 5123-5132.

Berg, K.H., G.A. Stamsas, D. Straume & L.S. Havarstein, (2013) Effects of low PBP2b levels on cell morphology and peptidoglycan composition in Streptococcus pneumoniae R6. J Bacteriol 195: 4342-4354.

Bijlsma, J.J., P. Burghout, T.G. Kloosterman, H.J. Bootsma, A. de Jong, P.W. Hermans & O.P. Kuipers, (2007) Development of genomic array footprinting for identification of conditionally essential genes in Streptococcus pneumoniae. Appl Environ Microbiol 73: 1514-1524.

Corrigan, R.M., J.C. Abbott, H. Burhenne, V. Kaever & A. Grundling, (2011) c-di-AMP is a new second messenger in Staphylococcus aureus with a role in controlling cell size and envelope stress. PLoS Pathog 7: e1002217.

Cron, L.E., H.J. Bootsma, N. Noske, P. Burghout, S. Hammerschmidt & P.W. Hermans, (2009) Surface-associated lipoprotein PpmA of Streptococcus pneumoniae is involved in colonization in a strain-specific manner. Microbiology 155: 2401-2410.

Cron, L.E., K. Stol, P. Burghout, S. van Selm, E.R. Simonetti, H.J. Bootsma & P.W. Hermans, (2011) Two DHH subfamily 1 proteins contribute to pneumococcal virulence and confer protection against pneumococcal disease. Infect Immun 79: 3697-3710.

Davis, K.M., H.T. Akinbi, A.J. Standish & J.N. Weiser, (2008) Resistance to mucosal lysozyme compensates for the fitness deficit of peptidoglycan modifications by Streptococcus pneumoniae. PLoS Pathog 4: e1000241.

de Jong, I.G., K. Beilharz, O.P. Kuipers & J.W. Veening, (2011) Live Cell Imaging of Bacillus subtilis and Streptococcus pneumoniae using Automated Time-lapse Microscopy. J Vis Exp.

Drijkoningen, J.J. & G.G. Rohde, (2014) Pneumococcal infection in adults: burden of disease. Clin Microbiol Infect 20 Suppl 5: 45-51.

Gasteiger E., H.C., Gattiker A., Duvaud S., Wilkins M.R., Appel R.D., Bairoch A, (2015) Protein Identification and Analysis Tools on the ExPASy Server. Humana Press.

Hammerschmidt, S., S. Wolff, A. Hocke, S. Rosseau, E. Muller & M. Rohde, (2005) Illustration of pneumococcal polysaccharide capsule during adherence and invasion of epithelial cells. Infect Immun 73: 4653-4667.

Kadioglu, A., J.N. Weiser, J.C. Paton & P.W. Andrew, (2008) The role of Streptococcus pneumoniae virulence factors in host respiratory colonization and disease. Nat Rev Microbiol 6: 288-301.

Krieger, E., G. Koraimann & G. Vriend, (2002) Increasing the precision of comparative models with YASARA NOVA--a self-parameterizing force field. Proteins 47: 393-402.

Manuse, S., A. Fleurie, L. Zucchini, C. Lesterlin & C. Grangeasse, (2015) Role of eukaryotic-like serine/threonine kinases in bacterial cell division and morphogenesis. FEMS Microbiol Rev.

Massidda, O., L. Novakova & W. Vollmer, (2013) From models to pathogens: how much have we learned about Streptococcus pneumoniae cell division? Environ Microbiol 15: 3133-3157.

McAllister, K.A., R.B. Peery, T.I. Meier, A.S. Fischl & G. Zhao, (2000) Biochemical and molecular analyses of the Streptococcus pneumoniae acyl carrier protein synthase, an enzyme essential for fatty acid biosynthesis. J Biol Chem 275: 30864-30872.

Mechold, U., G. Fang, S. Ngo, V. Ogryzko & A. Danchin, (2007) YtqI from Bacillus subtilis has both oligoribonuclease and pAp-phosphatase activity. Nucleic Acids Res 35: 4552-4561.

Mechold, U., V. Ogryzko, S. Ngo & A. Danchin, (2006) Oligoribonuclease is a common downstream target of lithium-induced pAp accumulation in Escherichia coli and human cells. Nucleic Acids Res 34: 2364-2373.

Nakajima, K., S. Kitazume, T. Angata, R. Fujinawa, K. Ohtsubo, E. Miyoshi & N. Taniguchi, (2010) Simultaneous determination of nucleotide sugars with ion-pair reversed-phase HPLC. Glycobiology 20: 865-871.

O'Brien, K.L., L.J. Wolfson, J.P. Watt, E. Henkle, M. Deloria-Knoll, N. McCall, E. Lee, K. Mulholland, O.S. Levine & T. Cherian, (2009) Burden of disease caused by Streptococcus pneumoniae in children younger than 5 years: global estimates. Lancet 374: 893-902.

Parsons, J.B. & C.O. Rock, (2013) Bacterial lipids: metabolism and membrane homeostasis. Prog Lipid Res 52: 249-276.

Pichoff, S. & J. Lutkenhaus, (2005) Tethering the Z ring to the membrane through a conserved membrane targeting sequence in FtsA. Mol Microbiol 55: 1722-1734.

Pinho, M.G., M. Kjos & J.W. Veening, (2013) How to get (a)round: mechanisms controlling growth and division of coccoid bacteria. Nat Rev Microbiol 11: 601-614.

Prudhomme, M., L. Attaiech, G. Sanchez, B. Martin & J.P. Claverys, (2006) Antibiotic stress induces genetic transformability in the human pathogen Streptococcus pneumoniae. Science (80-) 313: 89-92.

Qin, L., Y. Kida, Y. Imamura, K. Kuwano & H. Watanabe, (2013) Impaired capsular polysaccharide is relevant to enhanced biofilm formation and lower virulence in Streptococcus pneumoniae. Journal of infection and chemotherapy : official journal of the Japan Society of Chemotherapy 19: 261-271.

Sievers, F., A. Wilm, D. Dineen, T.J. Gibson, K. Karplus, W. Li, R. Lopez, H. McWilliam, M. Remmert, J. Soding, J.D. Thompson & D.G. Higgins, (2011) Fast, scalable generation of high-quality protein multiple sequence alignments using Clustal Omega. Mol Syst Biol 7: 539.

Sorg, R.A., O.P. Kuipers & J.W. Veening, (2015) Gene expression platform for synthetic biology in the human pathogen Streptococcus pneumoniae. ACS synthetic biology 4: 228-239.

Tettelin, H., K.E. Nelson, I.T. Paulsen, J.A. Eisen, T.D. Read, S. Peterson, J. Heidelberg, R.T. DeBoy, D.H. Haft, R.J. Dodson, A.S. Durkin, M. Gwinn, J.F. Kolonay, W.C. Nelson, J.D. Peterson, L.A. Umayam, O. White, S.L. Salzberg, M.R. Lewis, D. Radune, E. Holtzapple, H. Khouri, A.M. Wolf, T.R. Utterback, C.L. Hansen, L.A. McDonald, T.V. Feldblyum, S. Angiuoli, T. Dickinson, E.K. Hickey, I.E. Holt, B.J. Loftus, F. Yang, H.O. Smith, J.C. Venter, B.A. Dougherty, D.A. Morrison, S.K. Hollingshead & C.M. Fraser, (2001) Complete genome sequence of a virulent isolate of Streptococcus pneumoniae. Science (80-) 293: 498-506.

van Opijnen, T. & A. Camilli, (2012) A fine scale phenotype-genotype virulence map of a bacterial pathogen. Genome Res 22: 2541-2551.

Vriend, G., (1990) WHAT IF: a molecular modeling and drug design program. J Mol Graph 8: 52-56, 29.

Wakamatsu, T., K. Kim, Y. Uemura, N. Nakagawa, S. Kuramitsu & R. Masui, (2011) Role of RecJ-like protein with 5'-3' exonuclease activity in oligo(deoxy)nucleotide degradation. J Biol Chem 286: 2807-2816.

Walker, C.L., I. Rudan, L. Liu, H. Nair, E. Theodoratou, Z.A. Bhutta, K.L. O'Brien, H. Campbell & R.E. Black, (2013) Global burden of childhood pneumonia and diarrhoea. Lancet 381: 1405-1416.

Wang, J., S.M. Soisson, K. Young, W. Shoop, S. Kodali, A. Galgoci, R. Painter, G. Parthasarathy, Y.S. Tang, R. Cummings, S. Ha, K. Dorso, M. Motyl, H. Jayasuriya, J. Ondeyka, K. Herath, C. Zhang, L. Hernandez, J. Allocco, A. Basilio, J.R. Tormo, O. Genilloud, F. Vicente, F. Pelaez, L. Colwell, S.H. Lee, B. Michael, T. Felcetto, C. Gill, L.L. Silver, J.D. Hermes, K. Bartizal, J. Barrett, D. Schmatz, J.W. Becker, D. Cully & S.B.

Singh, (2006) Platensimycin is a selective FabF inhibitor with potent antibiotic properties. Nat New Biol 441: 358-361.
Wu, C.H., L.S. Yeh, H. Huang, L. Arminski, J. Castro-Alvear, Y. Chen, Z. Hu, P. Kourtesis, R.S. Ledley, B.E. Suzek, C.R. Vinayaka, J. Zhang & W.C. Barker, (2003) The Protein Information Resource. Nucleic Acids Res 31: 345-347.
Zhang, J. & I. Biswas, (2009) 3'-Phosphoadenosine-5'-phosphate phosphatase activity is required for superoxide stress tolerance in Streptococcus mutans. J Bacteriol 191: 4330-4340.

Supplementary Information

Supplementary Movies

Supplementary movies 1 to 5 can be found in the online version of this article at the publisher's website.

Supplementary Table 1. Functional homologs (127) of PapP in other species

Protein ID	Protein Name	Length	Organism Name	GO Slim Func.
A0AJ24_LISW6	DHH family protein	311	Listeria welshimeri serovar 6b (strain ATCC 35897 /DSM 20650 / SLCC5334)	0043167 : ion binding; 0003676 : nucleic acid binding; 0016787 : hydrolase activity
A4W2W3_STRS2	Putative uncharacterized protein	314	Streptococcus suis (strain 98HAH33)	0043167 : ion binding; 0003676 : nucleic acid binding; 0016787 : hydrolase activity
A4VWL0_STRSY	Putative uncharacterized protein	253	Streptococcus suis (strain 05ZYH33)	0043167 : ion binding; 0003676 : nucleic acid binding; 0016787 : hydrolase activity
A4IRR2_GEOTN	Phosphoesterase, DHH family protein	315	Geobacillus thermodenitrificans (strain NG80-2)	0043167 : ion binding; 0003676 : nucleic acid binding; 0016787 : hydrolase activity
A3CNB8_STRSV	Conserved uncharacterized protein	311	Streptococcus sanguinis (strain SK36)	0043167 : ion binding; 0016787 : hydrolase activity
A8YTI6_LACH4	Putative uncharacterized protein	318	Lactobacillus helveticus (strain DPC 4571)	0043167 : ion binding; 0003676 : nucleic acid binding; 0016787 : hydrolase activity
A8FG63_BACP2	Putative uncharacterized protein ytqI	313	Bacillus pumilus (strain SAFR-032)	0043167 : ion binding; 0003676 : nucleic acid binding; 0016787 : hydrolase activity
A8AWI8_STRGC	DHH subfamily 1 protein	314	Streptococcus gordonii (strain Challis / ATCC 35105 /CH1 / DL1 / V288)	0043167 : ion binding; 0016787 : hydrolase activity
A7Z7L3_BACA2	YtqI	313	Bacillus amyloliquefaciens (strain FZB42)	0043167 : ion binding; 0003676 : nucleic acid binding; 0016787 : hydrolase activity
A7GTQ2_BACCN	Phosphoesterase RecJ domain protein	310	Bacillus cereus subsp. cytotoxis (strain NVH 391-98)	0043167 : ion binding; 0003676 : nucleic acid binding; 0016787 : hydrolase activity
A5VIX5_LACRD	Phosphoesterase, RecJ domain protein	319	Lactobacillus reuteri (strain DSM 20016)	0043167 : ion binding; 0003676 : nucleic acid binding; 0016787 : hydrolase activity
A5IYN4_MYCAP	Putative uncharacterized protein	328	Mycoplasma agalactiae (strain PG2)	0043167 : ion binding; 0016787 : hydrolase activity
A5IYN3_MYCAP	Putative uncharacterized protein	322	Mycoplasma agalactiae (strain PG2)	0043167 : ion binding; 0003676 : nucleic acid binding; 0016787 : hydrolase activity
B1YKB7_EXIS2	Phosphoesterase RecJ domain protein	312	Exiguobacterium sibiricum (strain DSM 17290 / JCM 13490 / 255-15)	0043167 : ion binding; 0003676 : nucleic acid binding; 0016787 : hydrolase activity
B1V8W9_PHYAS	Phosphoesterase family protein	326	Phytoplasma australiense	0043167 : ion binding; 0003676 : nucleic acid binding; 0016787 : hydrolase activity
B1V8W7_PHYAS	Exopolyphosphatase-related protein	313	Phytoplasma australiense	0043167 : ion binding; 0016787 : hydrolase activity
B1MZW6_LEUCK	Exopolyphosphatase-related protein	336	Leuconostoc citreum (strain KM20)	0043167 : ion binding; 0003676 : nucleic acid binding; 0016787 : hydrolase activity
B1HX20_LYSSC	Putative uncharacterized protein	327	Lysinibacillus sphaericus (strain C3-41)	0043167 : ion binding; 0003676 : nucleic acid binding; 0016787 : hydrolase activity
A9NE37_ACHLI	DHH domain protein	314	Acholeplasma laidlawii (strain PG-8A)	0043167 : ion binding; 0003676 : nucleic acid binding; 0016787 : hydrolase activity
A9NE36_ACHLI	Putative uncharacterized protein	313	Acholeplasma laidlawii (strain PG-8A)	0043167 : ion binding; 0003676 : nucleic acid binding; 0016787 : hydrolase activity
B2GB23_LACF3	Putative uncharacterized protein	319	Lactobacillus fermentum (strain NBRC 3956 / LMG 18251)	0043167 : ion binding; 0003676 : nucleic acid binding; 0016787 : hydrolase activity
B7HFC1_BACC4	DHH subfamily 1 protein	356	Bacillus cereus (strain B4264)	0043167 : ion binding; 0003676 : nucleic acid binding; 0016787 : hydrolase activity
B7GGS3_ANOFW	Bifunctional oligoRNAse and pAp phosphatase	315	Anoxybacillus flavithermus (strain DSM 21510 / WK1)	0043167 : ion binding; 0003676 : nucleic acid binding; 0016787 : hydrolase activity
B5ZBR4_UREU1	DHH family protein	321	Ureaplasma urealyticum serovar 10 (strain ATCC 33699 / Western)	0043167 : ion binding; 0003676 : nucleic acid binding; 0016787 : hydrolase activity
B4U293_STREM	DHH subfamily 1 protein	310	Streptococcus equi subsp. zooepidemicus (strain MGCS10565)	0043167 : ion binding; 0003676 : nucleic acid binding; 0016787 : hydrolase activity

B3WC65_LACCB	Phosphoesterase, DHH family protein	318	Lactobacillus casei (strain BL23)	0043167 : ion binding; 0003676 : nucleic acid binding; 0016787 : hydrolase activity
B3WBG0_LACCB	Exopolyphosphatase-related protein	310	Lactobacillus casei (strain BL23)	0043167 : ion binding; 0003676 : nucleic acid binding; 0016787 : hydrolase activity
B3R0I6_PHYMT	Exopolyphosphatase-related protein	313	Phytoplasma mali (strain AT)	0043167 : ion binding; 0003676 : nucleic acid binding; 0016787 : hydrolase activity
B3PNF5_MYCA5	DHH family phosphoesterase	325	Mycoplasma arthritidis (strain 158L3-1)	0043167 : ion binding; 0003676 : nucleic acid binding; 0016787 : hydrolase activity
B3PNF4_MYCA5	DHH family phosphoesterase	329	Mycoplasma arthritidis (strain 158L3-1)	0043167 : ion binding; 0003676 : nucleic acid binding; 0016787 : hydrolase activity
C0MHB3_STRS7	Putative uncharacterized protein	310	Streptococcus equi subsp. zooepidemicus (strain H70)	0043167 : ion binding; 0003676 : nucleic acid binding; 0016787 : hydrolase activity
C0MC11_STRE4	Putative uncharacterized protein	310	Streptococcus equi subsp. equi (strain 4047)	0043167 : ion binding; 0003676 : nucleic acid binding; 0016787 : hydrolase activity
B9E7A9_MACCJ	Putative uncharacterized protein	314	Macrococcus caseolyticus (strain JCSC5402)	0043167 : ion binding; 0003676 : nucleic acid binding; 0016787 : hydrolase activity
B9DRQ1_STRU0	Putative uncharacterized protein	311	Streptococcus uberis (strain ATCC BAA-854 / 0140J)	0043167 : ion binding; 0003676 : nucleic acid binding; 0016787 : hydrolase activity
B9DN99_STACT	Putative uncharacterized protein	313	Staphylococcus carnosus (strain TM300)	0043167 : ion binding; 0003676 : nucleic acid binding; 0016787 : hydrolase activity
C6SPZ6_STRMN	Putative uncharacterized protein	310	Streptococcus mutans serotype c (strain NN2025)	0043167 : ion binding; 0003676 : nucleic acid binding; 0016787 : hydrolase activity
C5WFM6_STRDG	Phosphoesterase, DHH family protein	313	Streptococcus dysgalactiae subsp. equisimilis (strain GGS_124)	0043167 : ion binding; 0003676 : nucleic acid binding; 0016787 : hydrolase activity
C5J5G4_MYCCR	Mgp-operon protein 1	326	Mycoplasma conjunctivae (strain ATCC 25834 / HRC/581 / NCTC 10147)	0043167 : ion binding; 0003676 : nucleic acid binding; 0016787 : hydrolase activity
C5J5G3_MYCCR	Mgp-operon protein 1	328	Mycoplasma conjunctivae (strain ATCC 25834 / HRC/581 / NCTC 10147)	0043167 : ion binding; 0003676 : nucleic acid binding; 0016787 : hydrolase activity
C5D669_GEOSW	Phosphoesterase RecJ domain protein	315	Geobacillus sp. (strain WCH70)	0043167 : ion binding; 0003676 : nucleic acid binding; 0016787 : hydrolase activity
C4L485_EXISA	Phosphoesterase RecJ domain protein	322	Exiguobacterium sp. (strain ATCC BAA-1283 / AT1b)	0043167 : ion binding; 0003676 : nucleic acid binding; 0016787 : hydrolase activity
C1KVM2_LISMC	Putative uncharacterized protein	311	Listeria monocytogenes serotype 4b (strain Clip81459)	0043167 : ion binding; 0003676 : nucleic acid binding; 0016787 : hydrolase activity
D2BPL5_LACLK	Phosphoesterase, DHH family	307	Lactococcus lactis subsp. lactis (strain KF147)	0043167 : ion binding; 0016787 : hydrolase activity
D1J8W9_MYCHP	Putative uncharacterized protein	328	Mycoplasma hominis (strain ATCC 23114 / NBRC 14850 / NCTC 10111 / PG21)	0043167 : ion binding; 0003676 : nucleic acid binding; 0016787 : hydrolase activity
D1J8W8_MYCHP	Putative uncharacterized protein	325	Mycoplasma hominis (strain ATCC 23114 / NBRC 14850 / NCTC 10111 / PG21)	0043167 : ion binding; 0016787 : hydrolase activity
C9RTI1_GEOSY	Phosphoesterase RecJ domain protein	315	Geobacillus sp. (strain Y412MC61)	0043167 : ion binding; 0003676 : nucleic acid binding; 0016787 : hydrolase activity
C7TN24_LACRL	Phosphoesterase, DHH family protein	310	Lactobacillus rhamnosus (strain Lc 705)	0043167 : ion binding; 0003676 : nucleic acid binding; 0016787 : hydrolase activity
C7THB2_LACRL	Phosphoesterase, DHH family protein	318	Lactobacillus rhamnosus (strain Lc 705)	0043167 : ion binding; 0003676 : nucleic acid binding; 0016787 : hydrolase activity
C7TAL5_LACRG	Phosphoesterase; (SubName: Full=Phosp- hoes- terase, DHH family protein)	318	Lactobacillus rhamnosus (strain ATCC 53103 / GG)	0043167 : ion binding; 0003676 : nucleic acid binding; 0016787 : hydrolase activity
C7T7Z0_LACRG	Phosphoesterase, DHH family protein; (SubName: Full=Putative phosphoes- terase)	310	Lactobacillus rhamnosus (strain ATCC 53103 / GG)	0043167 : ion binding; 0003676 : nucleic acid binding; 0016787 : hydrolase activity
D5T587_LEUKI	Exopolyphosphatase-related protein (Putative)	330	Leuconostoc kimchii (strain IMSNU 11154 / KCTC 2386 / IH25)	0043167 : ion binding; 0003676 : nucleic acid binding; 0016787 : hydrolase activity
D5H1H4_LACCS	Phosphoesterase, DHH family protein	318	Lactobacillus crispatus (strain ST1)	0043167 : ion binding; 0016787 : hydrolase activity

Supplementary Table 1. Continued

Protein ID	Protein Name	Length	Organism Name	GO Slim Func.
D5E4R6_MYCCM	MgpA-like DHH family phosphoesterase	323	Mycoplasma crocodyli (strain ATCC 51981 / MP145)	0043167 : ion binding; 0003676 : nucleic acid binding; 0016787 : hydrolase activity
D5E4R5_MYCCM	MgpA-like DHH family phosphoesterase	323	Mycoplasma crocodyli (strain ATCC 51981 / MP145)	0043167 : ion binding; 0003676 : nucleic acid binding; 0016787 : hydrolase activity
D5DTV8_BACMQ	Oligoribonuclease (NanoRNAse); (EC=3.1.-.-)	312	Bacillus megaterium (strain ATCC 12872 / QMB1551)	0043167 : ion binding; 0003676 : nucleic acid binding; 0016787 : hydrolase activity
D5DMX4_BACMD	Oligoribonuclease (NanoRNAse); (EC=3.1.-.-)	312	Bacillus megaterium (strain DSM 319)	0043167 : ion binding; 0003676 : nucleic acid binding; 0016787 : hydrolase activity
D3VQT3_MYCA6	Putative uncharacterized protein	328	Mycoplasma agalactiae (strain 5632)	0043167 : ion binding; 0016787 : hydrolase activity
D3VQT2_MYCA6	Putative uncharacterized protein	322	Mycoplasma agalactiae (strain 5632)	0043167 : ion binding; 0003676 : nucleic acid binding; 0016787 : hydrolase activity
D3UNF8_LISSS	Phosphoesterase family protein	311	Listeria seeligeri serovar 1/2b (strain ATCC 35967 / DSM 20751 / CIP 100100 / SLCC 3954)	0043167 : ion binding; 0003676 : nucleic acid binding; 0016787 : hydrolase activity
D3QC64_STALH	Phosphoesterase, DHH family protein	314	Staphylococcus lugdunensis (strain HKU09-01)	0043167 : ion binding; 0003676 : nucleic acid binding; 0016787 : hydrolase activity
D3HCH7_STRG3	Putative uncharacterized protein	314	Streptococcus gallolyticus (strain UCN34)	0043167 : ion binding; 0003676 : nucleic acid binding; 0016787 : hydrolase activity
D3FWZ7_BACPE	Phosphoesterase, DHH	317	Bacillus pseudofirmus (strain OF4)	0043167 : ion binding; 0003676 : nucleic acid binding; 0016787 : hydrolase activity
D2P2K5_LISM1	Putative uncharacterized protein	312	Listeria monocytogenes serotype 1/2a (strain 08-5578)	0043167 : ion binding; 0003676 : nucleic acid binding; 0016787 : hydrolase activity
NRNA_BACSU	Bifunctional oligoribonuclease and PAP phosphatase nrnA	313	Bacillus subtilis	0016787 : hydrolase activity; 0043167 : ion binding; 0003676 : nucleic acid binding
MGP1_MYCPN	Mgp-operon protein 1; (Short=Mgp1; AltName: Full=ORF-1 protein)	324	Mycoplasma pneumoniae (strain ATCC 29342 / M129)	0043167 : ion binding; 0003676 : nucleic acid binding; 0016787 : hydrolase activity
MGP1_MYCGE	Mgp-operon protein 1; (Short=Mgp1; AltName: Full=ORF-1 protein)	318	Mycoplasma genitalium (strain ATCC 33530 / G-37 / NCTC 10195)	0043167 : ion binding; 0003676 : nucleic acid binding; 0016787 : hydrolase activity
Y549_MYCPN	Uncharacterized protein MG371 homolog	325	Mycoplasma pneumoniae (strain ATCC 29342 / M129)	0043167 : ion binding; 0003676 : nucleic acid binding; 0016787 : hydrolase activity
D5TJZ3_BACT1	Phosphoesterase, DHH family protein	310	Bacillus thuringiensis (strain BMB171)	0043167 : ion binding; 0003676 : nucleic acid binding; 0016787 : hydrolase activity
E0TWM6_BACPZ	Oligoribonuclease (NanoRNAse), 3',5'-bisphos-phate nucleotidase	313	Bacillus subtilis subsp. spizizenii (strain ATCC 23059 / NRRL B-14472 / W23)	0043167 : ion binding; 0003676 : nucleic acid binding; 0016787 : hydrolase activity
E0TJW2_MYCHH	MgpA-like DHH family phosphoesterase	321	Mycoplasma hyorhinis (strain HUB-1)	0043167 : ion binding; 0016787 : hydrolase activity
E0TJW1_MYCHH	Putative MgpA-like protein	325	Mycoplasma hyorhinis (strain HUB-1)	0043167 : ion binding; 0003676 : nucleic acid binding; 0016787 : hydrolase activity
D8MEQ1_LEUGT	Phosphoesterase, DHH family	338	Leuconostoc gasicomitatum (strain DSM 15947 / CECT 5767 / JCM 12535 / LMG 18811 / TB1-10)	0043167 : ion binding; 0003676 : nucleic acid binding; 0016787 : hydrolase activity
D8GE84_LACCZ	Exopolyphosphatase-related protein	310	Lactobacillus casei (strain Zhang)	0043167 : ion binding; 0003676 : nucleic acid binding; 0016787 : hydrolase activity
D7D206_GEOSC	3'(2'),5'-bisphosphate nucleotidase; (EC=3.1.3.7)	315	Geobacillus sp. (strain C56-T3)	0016787 : hydrolase activity; 0043167 : ion binding; 0003676 : nucleic acid binding
D6XSR9_BACIE	Phosphoesterase RecJ domain protein	314	Bacillus selenitireducens (strain ATCC 700615 / DSM 15326 / MLS10)	0043167 : ion binding; 0003676 : nucleic acid binding; 0016787 : hydrolase activity
E3IER1_GEOS0	3'(2'),5'-bisphosphate nucleotidase; (EC=3.1.3.7)	315	Geobacillus sp. (strain Y4.1MC1)	0016787 : hydrolase activity; 0043167 : ion binding; 0003676 : nucleic acid binding
Q04EG3_OENOB	Phosphoesterase, DHH family protein	330	Oenococcus oeni (strain BAA-331 / PSU-1)	0043167 : ion binding; 0003676 : nucleic acid binding; 0016787 : hydrolase activity

Q045P8_LACGA	Phosphoesterase, DHH family protein	339	Lactobacillus gasseri (strain ATCC 33323 / DSM 20243)	0043167 : ion binding; 0003676 : nucleic acid binding; 0016787 : hydrolase activity
Q03VU5_LEUMM	Exopolyphosphatase-related protein	326	Leuconostoc mesenteroides subsp. Mesenteroides (strain ATCC 8293 / NCDO 523)	0043167 : ion binding; 0003676 : nucleic acid binding; 0016787 : hydrolase activity
Q03R41_LACBA	Phosphoesterase, DHH family protein	321	Lactobacillus brevis (strain ATCC 367 / JCM 1170)	0043167 : ion binding; 0003676 : nucleic acid binding; 0016787 : hydrolase activity
Q03ER6_PEDPA	Phosphoesterase, DHH family protein	311	Pediococcus pentosaceus (strain ATCC 25745 / 183-1w)	0043167 : ion binding; 0003676 : nucleic acid binding; 0016787 : hydrolase activity
F9UQJ8_LACPL	Phosphoesterase, DHH family	318	Lactobacillus plantarum (strain ATCC BAA-793 / NCIMB 8826 / WCFS1)	0043167 : ion binding; 0003676 : nucleic acid binding; 0016787 : hydrolase activity
F9UND9_LACPL	Phosphoesterase, DHH family	325	Lactobacillus plantarum (strain ATCC BAA-793 / NCIMB 8826 / WCFS1)	0043167 : ion binding; 0003676 : nucleic acid binding; 0016787 : hydrolase activity
Q1G945_LACDA	Phosphoesterase (DHH family)	319	Lactobacillus delbrueckii subsp. bulgaricus (strain ATCC 11842 / DSM 20081)	0043167 : ion binding; 0003676 : nucleic acid binding; 0016787 : hydrolase activity
Y371_MYCGE	Uncharacterized protein MG371	324	Mycoplasma genitalium (strain ATCC 33530 / G-37 / NCTC 10195)	0043167 : ion binding; 0003676 : nucleic acid binding; 0016787 : hydrolase activity
Q2NIG0_AYWBP	Exopolyphosphatase-related protein	316	Aster yellows witches'-broom phytoplasma (strain AYWB)	0043167 : ion binding; 0003676 : nucleic acid binding; 0016787 : hydrolase activity
Q1WT30_LACS1	Phosphoesterase, DHH family protein	324	Lactobacillus salivarius (strain UCC118)	0043167 : ion binding; 0003676 : nucleic acid binding; 0016787 : hydrolase activity
Q1JCP8_STRPB	Phosphoesterase, DHH family protein	277	Streptococcus pyogenes serotype M12 (strain MGAS2096)	0043167 : ion binding; 0003676 : nucleic acid binding; 0016787 : hydrolase activity
Q602E5_MYCH2	Putative uncharacterized protein	327	Mycoplasma hyopneumoniae (strain 232)	0043167 : ion binding; 0003676 : nucleic acid binding; 0016787 : hydrolase activity
Q602E4_MYCH2	Putative uncharacterized protein	326	Mycoplasma hyopneumoniae (strain 232)	0043167 : ion binding; 0003676 : nucleic acid binding; 0016787 : hydrolase activity
Q5WEE8_BACSK	Phosphoesterase	309	Bacillus clausii (strain KSM-K16)	0043167 : ion binding; 0003676 : nucleic acid binding; 0016787 : hydrolase activity
Q5M4W8_STRT2	Putative uncharacterized protein	314	Streptococcus thermophilus (strain ATCC BAA-250 / LMG 18311)	0043167 : ion binding; 0003676 : nucleic acid binding; 0016787 : hydrolase activity
Q4L745_STAHJ	Similar to unknown protein	312	Staphylococcus haemolyticus (strain JCSC1435)	0043167 : ion binding; 0003676 : nucleic acid binding; 0016787 : hydrolase activity
Q4A6C5_MYCS5	Putative MgpA-like protein	318	Mycoplasma synoviae (strain 53)	0043167 : ion binding; 0003676 : nucleic acid binding; 0016787 : hydrolase activity
Q4A673_MYCS5	Putative MgpA-like protein	322	Mycoplasma synoviae (strain 53)	0043167 : ion binding; 0003676 : nucleic acid binding; 0016787 : hydrolase activity
Q4A672_MYCS5	Putative MgpA-like protein	322	Mycoplasma synoviae (strain 53)	0043167 : ion binding; 0003676 : nucleic acid binding; 0016787 : hydrolase activity
Q49YD3_STAS1	Putative uncharacterized protein	311	Staphylococcus saprophyticus subsp. Saprophyticus (strain ATCC 15305 / DSM 20229)	0043167 : ion binding; 0003676 : nucleic acid binding; 0016787 : hydrolase activity
Q38YP2_LACSS	Putative phosphoesterase, DHH family	317	Lactobacillus sakei subsp. sakei (strain 23K)	0043167 : ion binding; 0003676 : nucleic acid binding; 0016787 : hydrolase activity
Q2SSY0_MYCCT	DHH phosphoesterase family protein, putative	316	Mycoplasma capricolum subsp. capricolum (strain California kid / ATCC 27343 / NCTC 10154)	0043167 : ion binding; 0003676 : nucleic acid binding; 0016787 : hydrolase activity
Q6YPH9_ONYPE	Exopolyphosphatase-related protein	322	Onion yellows phytoplasma (strain OY-M)	0043167 : ion binding; 0003676 : nucleic acid binding; 0016787 : hydrolase activity
Q6MU91_MYCMS	DHH family protein (MgpA-like protein)	316	Mycoplasma mycoides subsp. mycoides SC (strain PG1)	0043167 : ion binding; 0003676 : nucleic acid binding; 0016787 : hydrolase activity
Q6KIM3_MYCMO	Mgpa-like protein	329	Mycoplasma mobile (strain ATCC 43663 / 163K / NCTC 11711)	0043167 : ion binding; 0003676 : nucleic acid binding; 0016787 : hydrolase activity
Q6F0X7_MESFL	Exopolyphosphatase-like	314	Mesoplasma florum (strain ATCC 33453 / NBRC 100688 / NCTC 11704 / L1) (Acholeplasma florum)	0043167 : ion binding; 0003676 : nucleic acid binding; 0016787 : hydrolase activity
Q6F0I1_MESFL	Exopolyphosphatase-like	314	Mesoplasma florum (strain ATCC 33453 / NBRC 100688 / NCTC 11704 / L1) (Acholeplasma florum)	0043167 : ion binding; 0003676 : nucleic acid binding; 0016787 : hydrolase activity

Supplementary Table 1. Continued

Protein ID	Protein Name	Length	Organism Name	GO Slim Func.
Q65G74_BACLD	YtqI	314	Bacillus licheniformis (strain DSM 13 / ATCC 14580)	0043167 : ion binding; 0003676 : nucleic acid binding; 0016787 : hydrolase activity
Q8EVH9_MYCPE	Predicted phosphoesterase	323	Mycoplasma penetrans (strain HF-2)	0043167 : ion binding; 0003676 : nucleic acid binding; 0016787 : hydrolase activity
Q8EPC9_OCEIH	Hypothetical conserved protein	315	Oceanobacillus iheyensis (strain DSM 14371 / JCM 11309 / KCTC 3954 / HTE831)	0043167 : ion binding; 0003676 : nucleic acid binding; 0016787 : hydrolase activity
Q8E126_STRA5	DHH family protein	311	Streptococcus agalactiae serotype V	0043167 : ion binding; 0003676 : nucleic acid binding; 0016787 : hydrolase activity
Q8DTN6_STRMU	Putative uncharacterized protein	310	Streptococcus mutans	0043167 : ion binding; 0003676 : nucleic acid binding; 0016787 : hydrolase activity
Q8CS65_STAES	Putative uncharacterized protein	312	Staphylococcus epidermidis (strain ATCC 12228)	0043167 : ion binding; 0003676 : nucleic acid binding; 0016787 : hydrolase activity
Q835K4_ENTFA	DHH family protein	317	Enterococcus faecalis (Streptococcus faecalis)	0043167 : ion binding; 0003676 : nucleic acid binding; 0016787 : hydrolase activity
Q81KY2_BACAN	DHH subfamily 1 protein	310	Bacillus anthracis	0043167 : ion binding; 0003676 : nucleic acid binding; 0016787 : hydrolase activity
Q817E6_BACCR	Phosphoesterase, DHH family protein	310	Bacillus cereus (strain ATCC 14579 / DSM 31)	0043167 : ion binding; 0003676 : nucleic acid binding; 0016787 : hydrolase activity
Q7NC44_MYCGA	Exopolyphosphatase-related protein	322	Mycoplasma gallisepticum (strain R(low / passage 15 / clone 2))	0043167 : ion binding; 0003676 : nucleic acid binding; 0016787 : hydrolase activity
Q7NAY6_MYCGA	Phosphodiesterase	328	Mycoplasma gallisepticum (strain R(low / passage 15 / clone 2))	0043167 : ion binding; 0003676 : nucleic acid binding; 0016787 : hydrolase activity
Q74KV5_LACJO	Putative uncharacterized protein	321	Lactobacillus johnsonii (strain CNCM I-12250 / La1 / NCC 533)	0043167 : ion binding; 0016787 : hydrolase activity
Q6YPI1_ONYPE	Putative uncharacterized protein	312	Onion yellows phytoplasma (strain OY-M)	0043167 : ion binding; 0016787 : hydrolase activity
Q9K834_BACHD	BH3173 protein	314	Bacillus halodurans	0043167 : ion binding; 0003676 : nucleic acid binding; 0016787 : hydrolase activity
Q9CHJ6_LACLA	Putative uncharacterized protein yheB	307	Lactococcus lactis subsp. lactis (strain IL1403) (Streptococcus lactis)	0043167 : ion binding; 0016787 : hydrolase activity
Q9A0L5_STRP1	Phosphoesterase, DHH family protein	313	Streptococcus pyogenes serotype M1	0043167 : ion binding; 0003676 : nucleic acid binding; 0016787 : hydrolase activity
Q98RI7_MYCPU	MGPA-LIKE (Mycoplasma genitalium) PROTEIN	324	Mycoplasma pulmonis (strain UAB CTIP)	0043167 : ion binding; 0003676 : nucleic acid binding; 0016787 : hydrolase activity
Q98PN0_MYCPU	MGPA-LIKE (Mycoplasma genitalium) PROTEIN	324	Mycoplasma pulmonis (strain UAB CTIP)	0043167 : ion binding; 0003676 : nucleic acid binding; 0016787 : hydrolase activity
Q97QC1_STRPN	DHH subfamily 1 protein	311	Streptococcus pneumoniae	0043167 : ion binding; 0003676 : nucleic acid binding; 0016787 : hydrolase activity
Q92BE0_LISIN	Lin1610 protein	311	Listeria innocua	0043167 : ion binding; 0003676 : nucleic acid binding; 0016787 : hydrolase activity
Q8Y6V6_LISMO	Lmo1575 protein	311	Listeria monocytogenes	0043167 : ion binding; 0003676 : nucleic acid binding; 0016787 : hydrolase activity
Q9PQ72_UREPA	Conserved hypothetical	321	Ureaplasma parvum serovar 3 (strain ATCC 700970)	0043167 : ion binding; 0003676 : nucleic acid binding; 0016787 : hydrolase activity

Supplementary Table 2. Plasmids used in this study

Plasmids	Relevant characteristics	Reference
pMK17-gfp-papP	*Amp, tet, bgaA,* P_{Zn}*-papP-gfp*	This study
pJWV25-gfp-ftsA	*Amp, tet, bgaA,* P_{Zn}*-gfp-ftsA*	(Beilharz *et al.*, 2012)
pMK11-fabH	*Amp, tet, bgaA,* P_{Zn}*-fabH*	This study

Supplementary Table 3. Primers used in this study

Name	Sequence
papP-FW-NotI	GCATGCGGCCGCAGAAAGAATTGAGGTTATTTATGGA
papP-RV-XbaI	CGCCTCTAGAGTTTTTAAGCAAGTTTTTTAACTTTTGG
fabH-FW-EcorI	CGATGGAATTCTTTTTGGAGGATTTGAAATAATGGC
fabH-RV-SpeI	GCGCACTAGTCTAAATTGTAAGAATGAGCGTGCC
fabH-up-FW	CTGGATGGTCAGGGTTGTTGGTATT
fabH-up-RV-ery	GTTCATATGAAAATTCCTCCGGGCGTTATTTCAAATCCTC-CAAAAATTGG
fabH-down-RV	TTCTCTGGCTTTCATCATCGGTTTC
fabH-down-FW-ery	TTTAACGGGAGGAAATAAGCTGGTAATCATGTGGTGAACA-CATTGTT
ery-FW-FabH	CCAATTTTTGGAGGATTTGAAATAACGCCCGGAGGAATTTTCATAT-GAAC
ery-RV-FabH	AACAATGTGTTCACCACATGATTACCAGCTTATTTCCTCCCGTTAAA
ftsZ-up-FW	CCTGTTATTGCTCGTATCGCCAAA
ftsZ-down-RV	ATCAAAACCGAACTCACCCTGTTGAT

Supplementary Table 4. Antibiotic susceptibility using Disk Diffusion measured as inhibition zone (mm)

	Wild type	Δ*papP*	Δ*papP**
penicillin	37 mm	48 mm	36 mm
erythromycin	26 mm	34 mm	24 mm
trimethroprim	12 mm	17 mm	10 mm

Supplementary Figure 1. Cytoplasmic localization of PapP fused to the m(sf)GFP in live *S. pneumoniae* using fluorescence microscopy.

The GFP fluorescent signal (left panel) and the phase contrast image (middle panel) are overlaid in the right panel. Scale bar, 2 µm

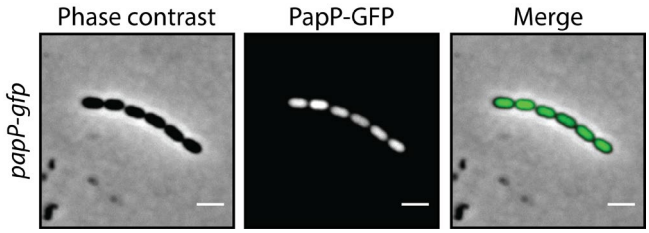

Supplementary Figure 2. The effect of manganese (Mn^{2+}) and magnesium (Mg^{2+}) supplementation on PapP enzymatic activity towards substrate pAp.

0.1 µM PapP was incubated with 6 µM pAp in 30 mM potassium phosphate buffer pH=7. The stimulation effects of bivalent cations were observed as formation of the product (AMP) and decrease of the substrate (pAp) without or in presence of 0.3 µM $MgCl_2$ or $MnCl_2$.

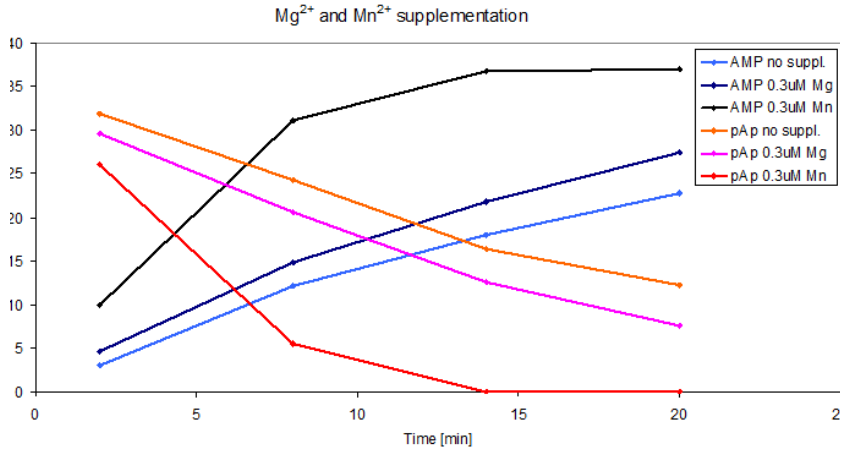

Supplementary Figure 3. Comparison of papP mediated hydrolysis of c-di-AMP and pAp. 100 µM c-di-AMP was incubated at 25°C in presence of 0.1 µM papP.

(**A**). After 10 min an aliquot of incubation mixture was analyzed for parental compound and AMP product using HPLC (blue line). Afterwards, pAp was added into the mixture (100 µM final concentration) and after 10 min incubation another aliquot was analyzed (red line). (**B**) A detailed view of the above shown chromatographic records with zoomed y-axis. No detectable presence of AMP (which should be eluted around 0.57 min) was found in presence of c-di-AMP substrate.

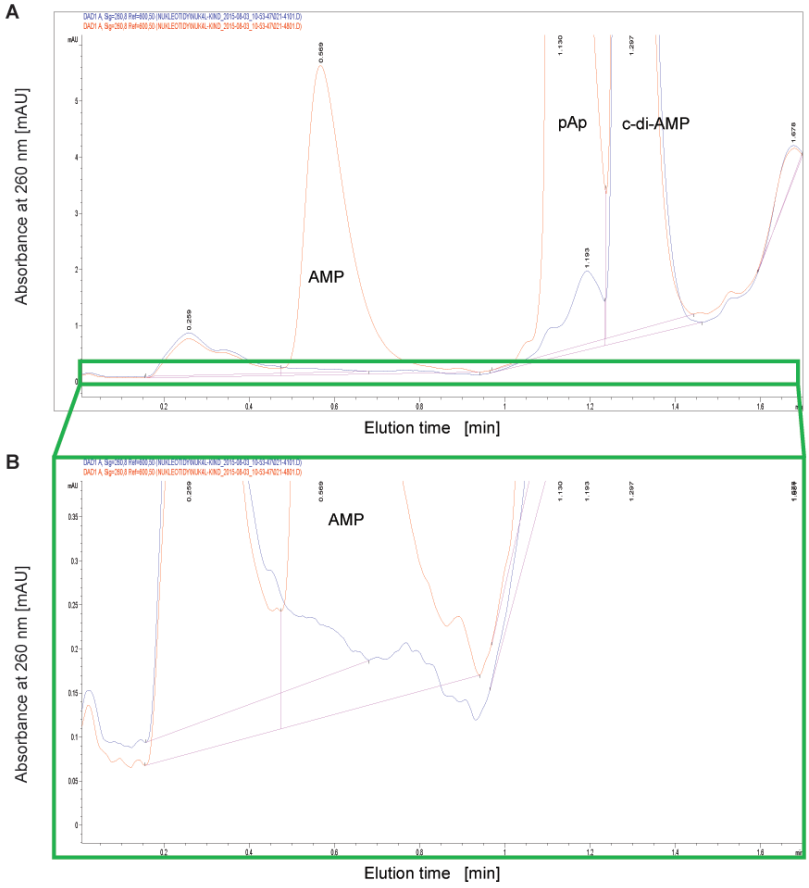

Supplementary Figure 4. Cell-poles pointiness of the *papP* mutant.

Cell-poles angles were manually measured for > 200 cells for the wild type (black), Δ*papP* (white), Δ*papP** (grey) or the wild type subjected to 1 min chain disruption by bead beater (wild type BB). Results are illustrated at average ± SD and compared by one-way ANOVA and Tukey's multiple comparison test. Significance is illustrated with ****, P< 0.0001.

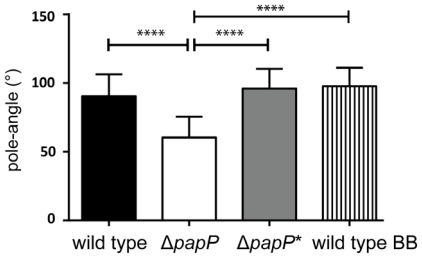

Supplementary Figure 5. The influence of papP deletion on lipoprotein expression.

The presence of (**A**) cytoplasmic protein enolase (control) and lipoproteins (**B**) MetQ, (**C**) PpmA, (**D**) PsaA, and (**E**) SlrA in wild type (wt), PapP mutant (Δ) and complemented (*) strains was analyzed by Western blotting. Results are illustrated from three independent experiments (#1, #2, #3). Graphs illustrate mean values from densitometric analysis of experiments #1, #2, and #3.

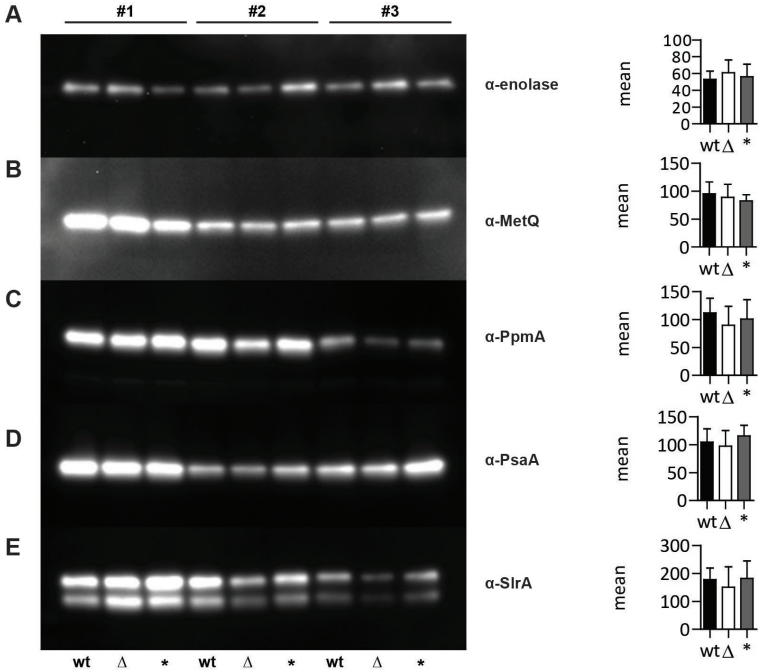

Supplementary Figure 6. Determination of optimal platensimycin concentration.

Growth curve of TIGR4 wild type at 37°C in liquid C+Y medium complemented with different platensimycin concentrations. An optimal concentration was used where the maximum optical density of *S. pneumoniae* was reduced by two-fold.

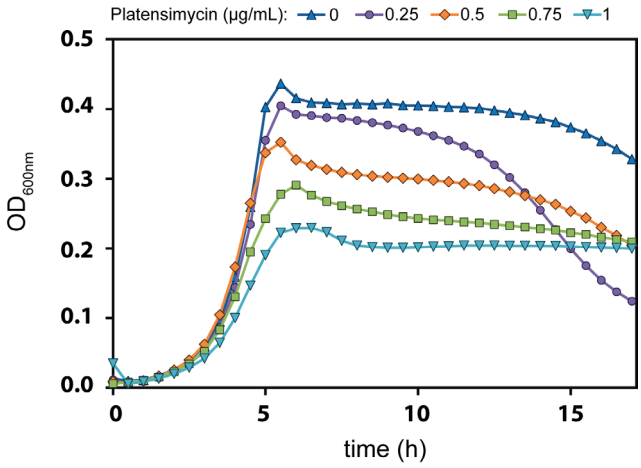

Supplementary Methods

Western blotting to determine phosphorylcholine in the cell wall

Bacterial lysates were obtained as described (see Materials & Methods: 'Quantitative analyses of cell wall phosphorylcholine'). Lysates were diluted in Tricine sample buffer (1M Tris-Cl pH 6.8), loaded on Tris acrylamide gels (29:1 acrylamide/bis, 0.3% SDS in 3M Tris-Cl pH 8.45, 80% glycerol), and ran at 100 V. Samples were transferred to a PVDF membrane using a semi-wet system (Bio-Rad) applied to 230 mA. Subsequently, the membrane was incubated with primary mAb TECP-15 (Sigma) followed by incubation with secondary HRP-conjugated rabbit anti-mouse antibody (DAKO). Signal was developed using ECL prime western blotting detection reagent (Amersham, GE Healthcare) and detected using enhanced chemiluminescence with a FluorChem E apparatus (Westburg).

Strain construction

Plasmids used in this study are listed in table S2, primers are listed in table S3. TIGR4 Δ*papP* and Δ*papP** were constructed as previously described (Cron *et al.*, 2011). Strain *papP-gfp* was constructed by transformation of *S. pneumoniae* TIGR4 wild

type with plasmid pMK17-*papP*. This plasmid was constructed by amplifying *papP* on TIGR4 genomic DNA using oligos papP-FW-NotI and papP-RV-XbaI. The resulting PCR product was digested using NotI and XbaI and ligated in the corresponding sites of plasmid pMK17 (M. Kjos and J.-W. Veening, unpublished data) allowing insertion of a C-terminal fusion of *papP* with the monomeric super-folder GFP into the *bgaA* locus under control of the zinc-inducible promoter P_{czcD} (P_{Zn}). Transformants were selected on Columbia agar supplemented with tetracycline. Both strains CG16 (TIGR4, *bgaA*::P_{Zn}-*gfp-ftsA*) and CG18 (TIGR4, *papP*::*spc*, *bgaA*::P_{Zn}-*gfp-ftsA*) were constructed by transformation of S. pneumoniae TIGR4 wild type and Δ*papP*, respectively, with plasmid pJWV25-*gfp-ftsA* (Beilharz *et al*., 2012) in order to introduce a genetic fusion *gfp-ftsA* into the *bgaA* locus under control of the zinc inducible promoter P_{Zn}. In order to create the strains CG14 (*ftsZ*::*ftsZ-mKate2*) and CG22 (*papP*::*spc*, *ftsZ*::*ftsZ-mKate2*), *S. pneumoniae* TIGR4 wild type and Δ*papP*, were transformed with a DNA fragment *ftsZ-mKate2-ery* constructed as described by Beilharz *et al*. (Beilharz *et al*., 2015) and amplified with oligos ftsZ-up-FW and ftsZ-down-RV. This allows introduction of a genetic fusion *ftsZ-mKate2* in place of the native *ftsZ* gene under control of the native promoter. Transformants were selected on Columbia-agar with erythromycin. Strain Δ*fabH** was constructed in two steps. First, TIGR4 wild type was transformed with plasmid pMK11-*fabH*. This plasmid was obtained by amplifying the gene *fabH* on TIGR4 genomic DNA using oligos fabH-FW-EcorI and fabH-RV-SpeI and by ligating this product into the plasmid pMK11 allowing insertion of an ectopic version of *fabH* under control of the zinc inducible promoter P_{Zn} into the *bgaA* locus. Afterwards, the resulting strain was transformed with a DNA fragment corresponding to the flanking region of *fabH* and an erythromycin marker. This latter construct was obtained by assembling the fragments corresponding to the upstream and the downstream region of *fabH* with the erythromycin marker using Gibson assembly. The upstream part was amplified from chromosomal DNA using primers fabH-up-FW and fabH-up-RV-ery and the downstream part using primers fabH-down-RV and fabH-down-FW-ery. The fragment corresponding to the erythromycin marker was amplified on plasmid pJWV502 (Beilharz *et al.*, 2012) using oligos ery-FW-fabH and ery-RV-fabH. Transformants were selected on Columbia agar supplemented with 0.25 µg/mL erythromycin.

Antibiotic susceptibility assay

Susceptibility to selected antibiotics was tested using the disc diffusion assay. Overnight cultures were suspended in PBS and used for inoculation of BA plates. Discs (SensiDisc, Becton Dickenson) were dispensed onto the plates after which 5 µL of the following antibiotics was applied: penicillin (0.25 µg/µL), erythromycin (3 µg/µL), trimethroprim (2.5 µg/µL), and ciprofloxacin (1 µg/µL) based on EUCAST standards. BA plates were placed at 37°C overnight and the diameter of bacteria-free

zones were measured the next day.

Western blotting for detection of lipoproteins

Bacterial lysates were obtained as described (see Materials & Methods: 'Quantitative analyses of cell wall phosphorylcholine'). Lysates were diluted in sample buffer supplemented with 50 mM β-mercaptoethanol, loaded on pre-cast 4-15% gradient gels (Bio-Rad), and ran at 100 V. Samples were transferred to a PVDF membrane (Thermo Scientific) using a semi-wet blotting system (Bio-Rad) at 230 mA. Subsequently, the membrane was incubated with primary mAb against lipoproteins MetQ, PpmA, PsaA, and SlrA (mouse IgGs), and control protein enolase (Rabbit IgG) followed by incubation with secondary HRP-conjugated antibodies (DAKO). Signal was developed using ECL prime western blotting detection reagent (Amersham, GE Healthcare) and detected using enhanced chemiluminescence with a FluorChem E apparatus (Westburg). Densitometric analyses were performed with ImageJ software (Fiji) (Schneider *et al*., 2012).

Supplementary Information References

Beilharz, K., L. Novakova, D. Fadda, P. Branny, O. Massidda & J.W. Veening, (2012) Control of cell division in *Streptococcus pneumoniae* by the conserved Ser/Thr protein kinase StkP. *Proc Natl Acad Sci USA* 109: E905-913.

Beilharz, K., R. van Raaphorst, M. Kjos & J.W. Veening, (2015) Red Fluorescent Proteins for Gene Expression and Protein Localization Studies in *Streptococcus pneumoniae* and Efficient Transformation with DNA Assembled via the Gibson Assembly Method. *Appl Environ Microbiol* 81: 7244-7252.

Cron, L.E., K. Stol, P. Burghout, S. van Selm, E.R. Simonetti, H.J. Bootsma & P.W. Hermans, (2011) Two DHH subfamily 1 proteins contribute to pneumococcal virulence and confer protection against pneumococcal disease. *Infect Immun* 79: 3697-3710.

Schneider, C.A., W.S. Rasband & K.W. Eliceiri, (2012) NIH Image to ImageJ: 25 years of image analysis. *Nat Methods* 9: 671-675.

5

DISCUSSION

Most of the major discoveries and advances on bacterial research originate from studies of organisms referred to as "model organisms". This terminology seems somewhat discriminatory as several pathways and molecular mechanisms harbored by *Streptococcus pneumoniae* do not fall in any of these traditional "models".

S. pneumoniae, the pathogen to not neglect

S. pneumoniae is a major human pathogen which is often underestimated, as it can become virulent when the host immune system is weakened (*e.g.* during viral infection, as people get older, in case of immunodeficiency, *etc.*). Facing a constant increase of resistance towards antibiotics, more and more governments are making pneumococcal vaccination mandatory, but changes in mentality can take time. For instance, in France, the vaccination against pneumococcus (PCV13) became mandatory only from January 1st, 2018. The increasing awareness of the pathogenicity of *S. pneumoniae* should also incite us to re-estimate where efforts in fundamental research should go.

Although the biology of *S. pneumoniae* is similar to that of most Firmicutes, it has developed its own unique systems. To better understand this major pathogen, it is therefore crucial to unravel these pathways. However, identification of new unknown system can be tedious, largely because of the way proteins are categorized. Most unknown proteins are automatically defined and annotated based on sequence homology with known proteins from other organisms. While a majority of proteins have well conserved functions, others can have diverged during evolution. The overconfidence about what we know regarding biological processes can lead us to omit new essential factors involved either in known pathways or completely new unknown pathways. It is therefore crucial to sometimes take a step back and begin from broad screenings.

From phenotype to function using CRISPRi

Transposon sequencing (Tn-Seq) greatly contributes to the determination of gene and operon essentiality (van Opijnen and Camilli, 2013). However, this approach rapidly shows technical limitations, leading to bottlenecks and variation, which strongly impact the results and can often cause an over-extimation in the number of essential genes. The data generated from Tn-Seq therefore needs to be carefully verified in order to handpick interesting candidates. Tn-Seq often identifies several hundreds of genes as more or less essential and validating their essentiality individually may prove tedious. To counter this technical difficulty, we instead used CRISPR interference where only the sgRNA is variable between mutants and thus requires only one cloning step. We showed in **Chapter 2** that when targeting essential genes, after expressing dCas9 in *S. pneumoniae*, a clear phenotype can be observed after a few hours (depletions

were carried out for 2 h). This allowed us to rapidly and efficiently assess the growth, cell morphology and DNA content of every single mutant constructed. Using this technique we aimed at identifying new candidates involved in different biological pathways, whether their function was already known or not, by phenotyping 348 genes identified as essential by different Tn-Seq studies. This type of screening was already performed in a small subset of *B. subtilis* genes, where 289 known or proposed essential genes were silenced, and the resulting phenotypes categorized based on growth and cell morphology (Peters *et al.*, 2016). However, the authors did not compare the DNA content of the mutants nor observe in detail the cell shape. Here we used DAPI staining to reveal the chromosomal DNA and a membrane dye to visualize the shape of *S. pneumoniae* in detail upon silencing. It is also surprising that among the 4,260 proteins of *B. subtilis* 168 (Kunst *et al.*, 1997), only 289 (6.8 % of the total) were targeted. This would either indicate that *B. subtilis* core processes require fewer protein than in *S. pneumoniae*, or that this study omitted several essential proteins. When performing CRISPRi phenotyping in *S. pneumoniae*, we found that silencing of 73 % of the potentially essential genes identified by Tn-Seq (some of them in operons) led to a growth phenotype (increased lysis or growth delay). 27 % of the genes previously identified as essential by Tn-Seq were in fact not essential in our laboratory conditions. We cannot exclude that these genes could be essential in different growth conditions, or with a longer time of gene silencing. It is important to note that CRISPRi did not exclude (also when using Tn-Seq) that the essentiality arises from down-regulation of the entire operon and not only from a single gene. To exclude that the observed effect came from silencing of downstream genes we also constructed standard gene depletions of the relevant candidates.

When comparing the phenotypes observed upon silencing of known genes from different pathways (DNA replication, peptidoglycan biosynthesis, septum constriction, *etc.*) together with depletion phenotypes of each "essential" gene, we identified several genes that were simply lacking annotations and we therefore re-annotated them, based on sequence homology. We also identified two genes involved in teichoic acid biosynthesis pathway. SPV_1198 showed homology with teichoic acid precursor polymerase (Denapaite *et al.*, 2012), which was consistent with our observations and we therefore renamed it to TarP for teichoic acid ribitol polymerase. We could not, on the other hand, deduce the function of SPV_1197, although our results seem to indicate that it works in concert with TarP, we thus renamed it TarQ. It was proposed that both proteins work by direct interaction (Denapaite *et al.*, 2012), however the exact function remains to be determined, and the existence of this interaction verified.

This screening also allowed us to identify MurT and GatD, both involved in peptidoglycan biosynthesis. MurT and GatD have not been automatically annotated based on sequence homology, but our CRISPRi screening indicated that these two proteins might be involved in cell wall synthesis. We found that MurT and GatD sequences from *S. aureus* were highly similar to those of SPV_1416 and SPV_1417 and we therefore renamed them accordingly. The peptidoglycan composition of *S. aureus* and *S. pneumoniae* is very similar, as they both have a pentapeptide L-Ala-D-Glu-L-Lys-D-Ala-D-Ala linking the disaccharide subunits GlcNAc and MurNAc. It was found that the D-Glu of the pentapeptide is amidated by MurT and GatD in *S. aureus* (Münch *et al*., 2012). The role of this amidation supposedly helps to reduce the susceptibility towards the host immune-system (Gustafson *et al*., 1994). In line with a role in pathogenicity, it appears that GatD and MurT are conserved in several Gram positive pathogens such as *S. pneumoniae* and *Mycobacterium tuberculosis* (but are absent from *B. subtilis*).

Finally, CRISPRi also helped us to refine the role of ClpP and ClpX in natural competence development of *S. pneumoniae*. By repressing the Clp protease ClpP and associated ATPase subunit ClpX we could show that *S. pneumoniae*'s natural competence was activated at an environmental pH that normally prevents activation of competence. It was previously shown that either ClpC, ClpE, ClpL, or ClpX was responsible for competence repression, but the exact subunit was not reported (Charpentier and Tuomanen, 2000; Chastanet *et al*., 2001). The use of CRISPRi allowed us to selectively inactivate each sub-unit, without the need to create sequential mutants (mutant creation relies on a functional competence process to import the exogenous DNA). We concluded that ClpPX complex is the principal repressor of competence development in *S. pneumoniae*. The precise target of this complex still needs to be determined in the future, but this could be facilitated by the use of CRISPRi.

Although each phenotype obtained after our main screening needed to be confirmed by traditional gene-deletion / -depletion, we could very easily and quickly identify interesting targets and candidates for future studies. Unlike Tn-Seq where the gene is permanently inactivated, the use of an inducible promoter in front of *dCas9* during CRISPRi phenotyping can help to isolate and define a function for genes that are normally very essential, or nearly essential, and whose deletion can be tedious (because of slow growth).

Overall, a broad high throughput genetic study such as CRISPRi phenotyping is extremely useful at rapidly categorizing proteins of unknown function based on depletion phenotype. Such a technique could be applied to other bacterial organisms in order to create a phenotypic map of all silenced essential genes. This could maybe

reveal genes that are believed to be part of a specific pathway but that eventually play other roles. This type of phenotyping could be helpful at identifying moonlighting proteins, that share different functions beside their main role. This is for instance the case for glyceraldehyde-3-phosphate dehydrogenase (GAPD) or enolase that, beside their roles in glycolysis, are involved in virulence of *S. pneumoniae* (Henderson and Martin, 2011).

Pneumococcal cell cycle regulation

In **Chapter 3**, we took advantage of the CRISPRi library to look for mutants with DNA content defects that would have severe growth and morphological defects (similar to the inhibition of DnaA). DnaA is the main replication initiation regulator in bacteria but increasing its concentration in *B. subtilis* was not enough to trigger DNA over-replication, which implies that other mechanisms are required to initiate DNA replication in Firmicutes. Looking for cells with DNA content defects when unknown putative proteins are silenced could therefore lead us to new factors crucial for either DNA replication or chromosome segregation. As a result, we focused on CcrZ, as cells lacking CcrZ were mis-shaped but also lacked DNA.

We showed that CcrZ is a septal protein interacting with the divisome via FtsZ and that DNA replication takes place from the time CcrZ is brought to mid cell until completion of DNA replication. Our data shows strong evidence that this regulation is dependent on the main DNA replication initiator DnaA (at least in *B. subtilis*). We thus hypothesized that CcrZ acts directly on DnaA bound to the origin of replication *oriC* to trigger initiation, although we have not yet determined the exact molecular mechanism. Our model fits with the microscopy observation where *oriC* localizes to the future division site (by a mechanism that is still to be discovered), and that replication is initiated once CcrZ is brought to this same location. This system ensures a strong control of DNA replication, timed by cell division. Each time a cell division event happens, DNA replication is triggered by CcrZ and replication occurs until completion. We hypothesize from co-localization data of the terminus with FtsZ (van Raaphorst *et al*., 2017) that FtsZ starts to disassemble from the old septum (*i.e.* the DNA replication site) right after completion of replication of the terminus region. Because of the limitations of optical epifluorescence microscopy, we cannot exactly state whether FtsZ bundles depolymerize after or before this final replication step. If our hypothesis is verified, it might imply the existence of a regulatory system able to "sense" the state of DNA replication and to drive FtsZ re-localization. Such a hypothetical system was described for *E. coli*. In this system, the protein MatP binds and organizes the *ter* region and influences the Z-ring precision through an interaction with the division site via ZapAB (Espéli *et al*., 2012; Wang and Rudner,

2014) and FtsK. In this model, DNA replication procession can control cell division (Kleckner *et al*., 2018). However, no MatP homolog exists in Gram positive bacteria. It therefore does not exclude that other system(s) can ensure that DNA replication is terminated prior to starting cell division.

Upon deletion of *ccrZ*, we observed a clear reduction of DNA replication initiation, but also interestingly, severe perturbations in cell morphology and Z-ring placement (as showed when localizing FtsZ in a CcrZ or DnaA^{TS} mutant). Specifically, we observed cells with several unfinished septa. From these phenotypes it seems that, in *S. pneumoniae*, chromosome integrity is essential for proper division placement. This is in line with the observation that proper segregation of *oriC* is driving division site selection in *S. pneumoniae* (van Raaphorst *et al*., 2017). It was shown that the origin of replication could localize at the new division site slightly prior to MapZ, therefore acting as a beacon for division site formation, but this implies the existence of a mechanism (intrinsic or by unknown factor(s)) actively localizing the origin "near" the division site. However, this mechanism still needs to be discovered.

It cannot be excluded that the septation defects observed in a Δ*ccrZ* mutant arise from deregulation of a completely unknown / cell division unrelated mechanism induced by chromosome damage, leading to repression of several proteins. It is interesting to note that many well studied organisms have a so-called SOS system (*e.g. E. coli* SulA (Schoemaker *et al*., 1984) and *S. aureus* SosA (Bojer *et al*., 2019)) able to pause the cell cycle upon DNA damage in order to leave time for the cell to repair the damaged DNA. *S. pneumoniae* however seems to lack homologs of the SOS regulatory system. In that respect, we indeed often observe that upon defective DNA replication initiation (using a Δ*ccrZ* or DnaA^{TS} mutant in **Chapter 3** or when silencing DNA replication proteins in **Chapter 2**), cells become either more round or slightly elongated, but not enlarged nor showing paused growth. In *S. pneumoniae,* natural competence is most likely contributing to DNA repair, as cells with DNA damage will activate the transcription of competence genes in order to uptake DNA from the environment (Straume *et al*., 2015). It is therefore possible that the morphological defects are due to an unstopped cell cycle upon DNA damage, and not to direct effects of chromosome integrity or CcrZ itself on cell division machinery.

Although the function of CcrZ seems to be conserved in *B. subtilis* and *S. aureus*, it is surprising to find that the septal localization is only found in *S. pneumoniae*. CcrZ from *B. subtilis* appears cytoplasmic / spotty and *S. aureus* CcrZ seems to form a focus on the nucleoid. *ccrZ* deletion in *S. aureus* led to similar defects as in *S. pneumoniae*, as we observed the appearance of several anucleate cells, as well as a delay in growth. Interestingly, it was shown that the nucleoid occlusion protein Noc from *S. aureus* could control DNA replication and that its absence could lead to

replication over-initiation (Pang *et al*., 2017). When using Tn-Seq in a *noc*-deletion background, the authors of this study identified two genes, *rbd* and *comEB,* that become conditionally essential. When constructing double mutants Δ*noc* Δ*rbd* and Δ*noc* Δ*comEB*, they obtained spontaneous suppressor mutations in DnaA but also, not highlighted in their article, in *SAOUHSC_01866* (*ccrZ*$_{Sa}$). As CcrZ$_{Sa}$ and DnaA promote DNA replication initiation, these mutations most likely contribute to lowering initiation, and therefore counteracting the over-initiation defects of a Δ*noc*. Although they do not provide a clear explanation of how DNA replication is controlled by Noc in *S. aureus*, they could not rule out that Noc is able to recognize another molecular target to mediate its effect on replication. It would be interesting to verify whether 1) CcrZ in *S. aureus* co-localizes with the origin of replication or the replication machinery and 2) whether CcrZ directly interacts with Noc to work in pair in controlling replication initiation. This could indicate that CcrZ synchronizes DNA replication with cell division in *S. aureus* not by interaction with FtsZ and the division site, but with Noc. If CcrZ$_{Sa}$ function is dependent on Noc in *S. aureus*, it might explain why the septal localization is not conserved. This scenario cannot apply to *S. pneumoniae* as no existence of a Noc homolog was ever reported. The observation that the chromosome is often cut in a *ccrZ* mutant likely rules out the presence of a nucleoid occlusion system in *S. pneumoniae*. If a similar system was present, we would most likely not be able to observe "guillotined" chromosomes at such a high frequency. The observation that DnaA depletion mimics a CcrZ depletion mutant also excludes the possibility that CcrZ directly controls a hypothetical Noc system or itself acts as a Noc protein, as cells show several cut nuclei, even when CcrZ is present.

Even though DNA replication initiation defects in the absence of CcrZ occurred in *S. pneumoniae, B. subtilis* and *S. aureus*, we did not observe morphological or growth defects for *B. subtilis*. First of all, although we observed a clear reduction of initiation in a *B. subtilis* JH642 Δ*ccrZ* mutant, the *oriC/ter* ratio was still around 2.5 (vs ~1.2 for *ccrZ*$_{Sp}$ mutant), indicating that cells were still able to initiate multifork replication. Other regulatory systems are present in *B. subtilis* and one of them, using the protein Soj (ParA), can decrease DNA replication by directly binding DnaA therefore preventing helix formation at the initiation complex (Murray and Errington, 2008). It would be interesting to see what happens in the case of deletion of *ccrZ*$_{Bs}$ in a Soj over-expression / deletion mutant. The absence of morphological defects in *B. subtilis* is still puzzling. Its cell cycle is very different from that of *S. pneumoniae*, as it uses the Min system, has a Noc system, and Soj. Both *S. aureus* and *S. pneumoniae* lack a Min system and it is possible that CcrZ evolved differently in these organisms. Further work is needed to determine whether CcrZ$_{Bs}$ can, besides its role in controlling replication initiation, influence septum formation in *B. subtilis* (similarly to what was

observed in *S. pneumoniae*) or whether disruption of septum closure could modulate $CcrZ_{Bs}$ activity. It would also be interesting to examine the effect of *ccrZ* deletion in other Firmicutes, particularly in potential pathogens.

CcrZ is annotated as putative phosphotransferase because of the presence of the so called Brenner's motif [(CS)HNDhX_3N] (Brenner, 1987), responsible for phosphotransfer reactions (Aoyama *et al*., 2000). We could not directly assess CcrZ activity when CcrZ was purified using a 6xHis tag most likely because of its rapid precipitation. In our hands, purification of CcrZ fused to GFP was possible but no ATPase activity was observed *in vitro*, nor binding of ATP. Sequence alignments predicts the secondary structure of CcrZ to be very similar to that of the choline kinase LicA, which is known to bind ADP/ATP. We showed that residues that are crucial for the ATP moiety (P-loop) are conserved between CcrZ and LicA, reinforcing a possible GTP/ATPase activity of CcrZ. LicA can bind choline, as it adds a phosphate group onto this substrate, and a specific choline kinase motif [(ILV)X_2ID(FWY)E(YF)X_3NX_3(FYW)DX_6E] seems to be even conserved between CcrZ and LicA, but the residues responsible for formation of the hydrophobic pocket for the choline are not present in CcrZ. It can be that either CcrZ folding replaces those residues by other hydrophobic amino acids, or that the substrate is not Choline. Interestingly, aligning the variable region between LicA and CcrZ does not return any other candidate. One option could be that CcrZ is a totally unique kinase that has not been described before. It would therefore be crucial to continue to optimize the purification method to purify CcrZ. This could help us to resolve its 3D structure in order to acquire additional information on the type of substrate it binds. Since CcrZ binds FtsZ, co-purification of CcrZ together with FtsZ, or purification of a CcrZ-FtsZ fusion, may be an alternative to help the purification process. However, it is important to keep in mind that the GTPase activity of FtsZ could influence the findings. The identification of CcrZ's enzymatic activity and structure is key to develop new drugs able to target CcrZ specifically. This is a potential alternative to the use of broad-spectrum antibiotic treatment, where we could specifically target *S. pneumoniae* or *S. aureus* or, in some cases, most Firmicutes. This kind of strategy has already been utilized by targeting FtsZ, and several inhibitors have already been synthesized, some of them exhibiting a strong activity against *S. aureus* (Tripathy and Sahu, 2019). However, FtsZ is present in nearly all bacteria and using inhibitors active only on a subset of bacteria would likely prove less toxic for the host commensal bacteria.

Lipid composition is crucial for proper cell division

In future studies, other genes identified as essential in the CRISPRi phenotyping of **Chapter 2** could be tested to see whether their silencing attenuates *S. pneumoniae* pathogenicity. For instance, we observed that *spd_1153* silencing using CRISPRi

led to increased lysis of *S. pneumoniae*. This gene was previously identified by conditional lethal screening using genomic array footprinting (GAF ; technique based on transposons insertions) as its disruption led to reduction of pneumococcal virulence (Cron *et al.*, 2011). The authors therefore indicated that PapP (SPD_1153 in D39 and SP1298 in TIGR4 strain) could be an interesting vaccine candidate. It was shown that in D39 PapP is a DHH subfamily 1 phosphatase (one DHH domain associated to DHHA1 domain), able to convert c-di-AMP and 5'-phosphoadenylyl-(3'5')-adenosine (5'-pApA; a degradation product of c-di-AMP) into AMP (Bai *et al.*, 2013; Corrigan and Gründling, 2013). In **Chapter 4**, we provide a mechanistic explanation of how virulence is reduced in strain TIGR4 lacking PapP. We showed that PapP from TIGR4 was not able to hydrolyze c-di-AMP, but was able to convert pApA and pAp (phosphoadenosine-5'-phosphate) into AMP *in vitro*. pAp is a byproduct of Co-enzyme A produced during biosynthesis of vitamin B_5 or Holo-ACP, an acyl carrier for biosynthesis of fatty acids (McAllister *et al.*, 2000). It was shown that increasing amount of pAp could inhibit the acyl carrier protein synthase AcpS (crucial for production of Holo-ACP), therefore decreasing synthesis of fatty acids (Fig. 1). Supporting this model, we found that a PapP-deficient mutant of TIGR4 had an increased sensitivity to polar solvents and detergents, indicating an impaired membrane integrity. This mutant also showed morphological defects, with cells not growing in chains and with "pointy" poles. We found that inhibition of fatty acid biosynthesis using antibiotics (platensimycin), or depletion of an essential gene of the pathway (*fabH*), phenocopied a *papP* mutant, therefore validating that the phenotype observed results from impaired lipid biosynthesis.

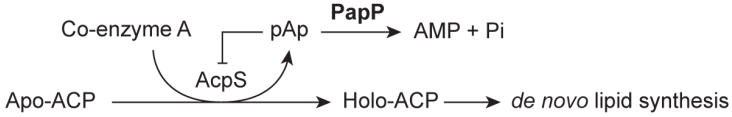

Figure 1. Enzymatic reaction catalyzed by PapP.
pAp: phosphoadenosine-5'-phosphate; Pi: inorganic phosphate; ACP: Acyl Carrier Protein; AcpS: ACP synthase

Interestingly, the localization dynamics of FtsA and FtsZ (tethered to the membrane by FtsA) were clearly affected upon *papP* deletion, as the Z-ring seemed to slowly "slide" from the old to the new septum instead of the typical de-assembling and re-assembling dynamics observed at 37°C. Strikingly, lowering the temperature to 30°C, therefore decreasing membrane fluidity, led to delocalization of the Z-ring and elongated cells with "twisted" FtsZ ring. It is interesting to see that the membrane fluidity, and not only directly the peptidoglycan composition, could influence the divisome dynamics and localization. It was shown that inactivation of GpsB, a paralog

of DivIVA, can also lead to a "twisted towel" phenotype (Fleurie *et al*., 2014). DivIVA is able to interact with the membrane and is thought to localize where the membrane is negatively curved and directly controls cell elongation (Beilharz *et al*., 2012; Hammond *et al*., 2019). Although the exact function of GpsB is not fully understood, it was found to interact with PBPs and act as a negative regulator of DivIVA to prevent cell elongation (Cleverley *et al*., 2019). As a result, in its absence, cells elongate and adopt a "twisted" phenotype, with FtsZ forming a long helical pattern in the cell. Why the decreased membrane fluidity in a sp*1298* mutant also leads to elongated cells should be investigated in the future. It would be also interesting to determine what is responsible for the "pointy ends" phenotype in a SP1298 mutant. In D39 wild type, DivIVA localizes at the poles and at the septum, we therefore looked at its localization in absence of SP1298. A preliminary observation was that DivIVA seemed to accumulate more at the pole than at the septum in Δ*sp1298* than the wild type background at both 37°C and 30°C. This localization should be precisely quantified in the future. Photo-activated localization microscopy (PALM), a type of super resolution microscopy relying on switching of emission signal of photo-activatable fluorescent proteins, could be used to evaluate the number of DivIVA molecules present at the pole at a certain point in the cell cycle in the mutant. As DivIVA can interact with the lipids of the membrane via N-terminal amphipathic helices, the change in lipid composition or in membrane fluidity could directly influence its localization, therefore impacting the cell shape at the poles.

Lipid composition can also directly influence the curvature of the cell, as well as the membrane tension and osmotic pressure (Beltrán-Heredia *et al*., 2017). Interestingly, cell wall synthesis can occur only when the membrane tension is below a threshold, and increased lipid biosynthesis can reduce surface tension (Rojas *et al*., 2017). In case of a decrease in lipid availability, and thus membrane synthesis, peptidoglycan biosynthesis can therefore be affected. The exact molecular mechanisms for coordination of membrane synthesis with cell wall synthesis is unknown, but it was proposed that the flippase of lipid II could have such a role, as it is responsible for flipping cell wall precursors across the plasma membrane (Rojas and Huang, 2018). This system allows cell wall synthesis to be balanced with membrane synthesis, and eventually to be balanced with pressure. Turgor pressure can be very high in bacteria, for example it was shown to be nearly 1.9 MPa (19 atmospheres) in *B. subtilis* (Whatmore and Reed, 1990). In *E. coli*, lipid displacement induced by increased or decreased turgor pressure can be sensed by the mechanosensory protein MscS, which can then adjust the turgor pressure accordingly (Pliotas *et al*., 2015). By extent, if lipid composition is changed, regulation of turgor pressure will also be perturbed. *S. pneumoniae* does not have MscS proteins, but it would be interesting to see whether other mechanosensory systems are present.

S. pneumoniae cell cycle: lessons from phenotype

In *S. pneumoniae*, binary fission happens at mid-cell, together with DNA replication, while both newly replicated chromosomes are pulled / pushed apart symmetrically into each of the future daughter cells. One cell division event is always accompanied by one DNA replication initiation event. If this control fails, cells can end up with several chromosomes, which unbalances the DNA / cell volume ratio, therefore affecting the entire cell cycle, and additionally increasing the amount of overall proteins in the cell. In this thesis, we showed that CcrZ exerts a direct control on DNA replication initiation in *S. pneumoniae* by interacting with the division machinery, therefore ensuring that initiation only happens once at mid-cell and can start again when the second division machinery is assembling. This is the first time that such a system is described. In a Min-free context, *S. pneumoniae* uses unique mechanisms to localize the divisome at mid-cell, although the exact factor still needs to be identified. We showed that lipid integrity is essential for this process, and might be too often omitted in some studies. Thus, we would like to highlight that all factors: teichoic acid, lipid and peptidoglycan biosynthesis should always be taken into consideration when studying new mutants. More than providing answers, this thesis highlights the need for a better understanding of the biology of *S. pneumoniae* and opens the way for the identification of new cell cycle regulation mechanisms that may be conserved across a broad range of different bacteria.

Model organisms are practical to unravel highly conserved pathways, but conclusions drawn from these models should not be systematically used to depict all "bacteria" when used in the literature. *B. subtilis* is not a pathogen, and an essential conserved pathway may play a role in pathogenicity in other species. By taking a step back and analyzing essential genes through a broader approach, we successfully identified a conserved mechanism of synchronization of DNA replication with cell division for at least two major pathogens (*i.e. S. aureus* and *S. pneumoniae*). We also showed that membrane composition can impact virulence of *S. pneumoniae*. Gaining insight into the biology of *S. pneumoniae* will enable us to understand its pathogenicity and may help to identify pathways which are conserved in less well-studied pathogens.

References

Aoyama, C., Yamazaki, N., Terada, H., and Ishidate, K. (2000). Structure and characterization of the genes for murine choline/ethanolamine kinase isozymes alpha and beta. J. Lipid Res. *41*, 452–464.

Bai, Y., Yang, J., Eisele, L.E., Underwood, A.J., Koestler, B.J., Waters, C.M., Metzger, D.W., and Bai, G. (2013). Two DHH subfamily 1 proteins in *Streptococcus pneumoniae* possess cyclic di-AMP phosphodiesterase activity and affect bacterial growth and virulence. J. Bacteriol. *195*, 5123–5132.

Beilharz, K., Novakova, L., Fadda, D., Branny, P., Massidda, O., and Veening, J.-W. (2012). Control of cell division in *Streptococcus pneumoniae* by the conserved Ser/Thr protein kinase StkP. Proc. Natl. Acad. Sci. U. S. A. *109*, E905–E913.

Beltrán-Heredia, E., Almendro-Vedia, V.G., Monroy, F., and Cao, F.J. (2017). Modeling the Mechanics of Cell Division: Influence of Spontaneous Membrane Curvature, Surface Tension, and Osmotic Pressure. Front. Physiol. *8*, 312.

Bojer, M.S., Wacnik, K., Kjelgaard, P., Gallay, C., Bottomley, A.L., Cohn, M.T., Lindahl, G., Frees, D., Veening, J., Foster, S.J., *et al.* (2019). SosA inhibits cell division in *Staphylococcus aureus* in response to DNA damage. Mol. Microbiol. mmi.14350.

BRENNER, S. (1987). Phosphotransferase sequence homology. Nature *329*, 21–21.

Charpentier, E., and Tuomanen, E. (2000). Mechanisms of antibiotic resistance and tolerance in *Streptococcus pneumoniae*. Microbes Infect. *2*, 1855–1864.

Chastanet, A., Prudhomme, M., Claverys, J.P., and Msadek, T. (2001). Regulation of *Streptococcus pneumoniae* clp genes and their role in competence development and stress survival. J. Bacteriol. *183*, 7295–7307.

Cleverley, R.M., Rutter, Z.J., Rismondo, J., Corona, F., Tsui, H.-C.T., Alatawi, F.A., Daniel, R.A., Halbedel, S., Massidda, O., Winkler, M.E., *et al.* (2019). The cell cycle regulator GpsB functions as cytosolic adaptor for multiple cell wall enzymes. Nat. Commun. *10*, 261.

Corrigan, R.M., and Gründling, A. (2013). Cyclic di-AMP: another second messenger enters the fray. Nat. Rev. Microbiol. *11*, 513–524.

Cron, L.E., Stol, K., Burghout, P., van Selm, S., Simonetti, E.R., Bootsma, H.J., and Hermans, P.W.M. (2011). Two DHH Subfamily 1 Proteins Contribute to Pneumococcal Virulence and Confer Protection against Pneumococcal Disease. Infect. Immun. *79*, 3697–3710.

Denapaite, D., Brückner, R., Hakenbeck, R., and Vollmer, W. (2012). Biosynthesis of Teichoic Acids in *Streptococcus pneumoniae* and Closely Related Species: Lessons from Genomes. Microb. Drug Resist. *18*, 344–358.

Espéli, O., Borne, R., Dupaigne, P., Thiel, A., Gigant, E., Mercier, R., and Boccard, F. (2012). A MatP-divisome interaction coordinates chromosome segregation with cell division in *E. coli*. EMBO J. *31*, 3198–3211.

Fleurie, A., Manuse, S., Zhao, C., Campo, N., Cluzel, C., Lavergne, J.-P., Freton, C., Combet, C., Guiral, S., Soufi, B., *et al.* (2014). Interplay of the Serine/Threonine-Kinase StkP and the Paralogs DivIVA and GpsB in Pneumococcal Cell Elongation and Division. PLoS Genet. *10*, e1004275.

Gustafson, J., Strässle, A., Hächler, H., Kayser, F.H., and Berger-Bächi, B. (1994). The femC locus of *Staphylococcus aureus* required for methicillin resistance includes the glutamine synthetase operon. J. Bacteriol. *176*, 1460–1467.

Hammond, L.R., White, M.L., and Eswara, P.J. (2019). ¡vIVA la DivIVA! J. Bacteriol. *201*, e00245-19.

Henderson, B., and Martin, A. (2011). Bacterial Moonlighting Proteins and Bacterial Virulence. 155–213.

Hill, N.S., Kadoya, R., Chattoraj, D.K., and Levin, P.A. (2012). Cell Size and the Initiation of DNA Replication in Bacteria. PLoS Genet. *8*, e1002549.

Kleckner, N.E., Chatzi, K., White, M.A., Fisher, J.K., and Stouf, M. (2018). Coordination of Growth, Chromosome Replication/Segregation, and Cell Division in *E. coli*. Front. Microbiol. *9*, 1469.

Kunst, F., Ogasawara, N., Moszer, I., Albertini, A.M., Alloni, G., Azevedo, V., Bertero, M.G., Bessières, P., Bolotin, A., Borchert, S., et al. (1997). The complete genome sequence of the Gram-positive bacterium *Bacillus subtilis*. Nature *390*, 249–256.

McAllister, K.A., Peery, R.B., Meier, T.I., Fischl, A.S., and Zhao, G. (2000). Biochemical and molecular analyses of the *Streptococcus pneumoniae* acyl carrier protein synthase, an enzyme essential for fatty acid biosynthesis. J. Biol. Chem. *275*, 30864–30872.

Münch, D., Roemer, T., Lee, S.H., Engeser, M., Sahl, H.G., and Schneider, T. (2012). Identification and in vitro Analysis of the GatD/MurT Enzyme-Complex Catalyzing Lipid II Amidation in *Staphylococcus aureus*. PLoS Pathog. *8*, e1002509.

Murray, H., and Errington, J. (2008). Dynamic Control of the DNA Replication Initiation Protein DnaA by Soj/ParA. Cell *135*, 74–84.

van Opijnen, T., and Camilli, A. (2013). Transposon insertion sequencing: a new tool for systems-level analysis of microorganisms. Nat. Rev. Microbiol. *11*, 435–442.

Pang, T., Wang, X., Lim, H.C., Bernhardt, T.G., and Rudner, D.Z. (2017). The nucleoid occlusion factor Noc controls DNA replication initiation in *Staphylococcus aureus*. PLoS Genet. *13*, e1006908.

Peters, J.M., Colavin, A., Shi, H., Czarny, T.L., Larson, M.H., Wong, S., Hawkins, J.S., Lu, C.H.S., Koo, B.-M., Marta, E., *et al*. (2016). A Comprehensive, CRISPR-based Functional Analysis of Essential Genes in Bacteria. Cell *165*, 1493–1506.

Pliotas, C., Dahl, A.C.E., Rasmussen, T., Mahendran, K.R., Smith, T.K., Marius, P., Gault, J., Banda, T., Rasmussen, A., Miller, S., *et al*. (2015). The role of lipids in mechanosensation. Nat. Struct. Mol. Biol. *22*, 991–998.

van Raaphorst, R., Kjos, M., and Veening, J.-W. (2017). Chromosome segregation drives division site selection in*Streptococcus pneumoniae*. Proc. Natl. Acad. Sci. U. S. A. *114*, E5959–E5968.

Rojas, E.R., and Huang, K.C. (2018). Regulation of microbial growth by turgor pressure. Curr. Opin. Microbiol. *42*, 62–70.

Rojas, E.R., Huang, K.C., and Theriot, J.A. (2017). Homeostatic Cell Growth Is Accomplished Mechanically through Membrane Tension Inhibition of Cell-Wall Synthesis. Cell Syst. *5*, 578-590.e6.

Schoemaker, J.M., Gayda, R.C., and Markovitz, A. (1984). Regulation of cell division in *Escherichia coli*: SOS induction and cellular location of the sulA protein, a key to lon-associated filamentation and death. J. Bacteriol. *158*, 551–561.

Slager, J., Aprianto, R., and Veening, J.-W. (2018). Deep genome annotation of the opportunistic human pathogen *Streptococcus pneumoniae* D39. Nucleic Acids Res. 46, 9971–9989.

Straume, D., Stamsås, G.A., and Håvarstein, L.S. (2015). Natural transformation and genome evolution in *Streptococcus pneumoniae*. Infect. Genet. Evol. *33*, 371–380.

Tripathy, S., and Sahu, S.K. (2019). FtsZ inhibitors as a new genera of antibacterial agents. Bioorg. Chem. *91*, 103169.

Wang, X., and Rudner, D.Z. (2014). Spatial organization of bacterial chromosomes. Curr. Opin. Microbiol. *22*, 66–72.

Whatmore, A.M., and Reed, R.H. (1990). Determination of turgor pressure in *Bacillus subtilis*: a possible role for K+ in turgor regulation. J. Gen. Microbiol. *136*, 2521–2526.

SUMMARY

Academic summary

Understanding how bacteria grow and divide is crucial to appreciate the multitude of molecular processes that these organisms regulate around us. Importantly, it is also necessary to gain as much information as possible on pathogenic strains to better fight them. *Streptococcus pneumoniae* is a commensal bacterium that can become a serious pathogen. It is held responsible for millions of deaths yearly as it can easily infect aging adults or immunocompromised people. Since vaccination is only partially effective and since many pneumococcal strains are resistant to several antibiotics, there is an urge to identify novel therapeutic targets. *S. pneumoniae* is a Gram-positive bacterium and is therefore highly related to *Bacillus subtilis*. It has however fundamental differences, that reflects how in fact they are not as related as it is often assumed. Many mechanisms that are known in other organisms are still in the grey zone for the pneumococcus.

Some of the most important questions that remain are how the division machinery finds its exact location at mid-cell in *S. pneumoniae* and how this assembly synchronizes with DNA replication and chromosome segregation. In other well studied model bacteria (*e.g. Escherichia coli* or *B. Subtilis*) the Min system is primarily responsible for localizing the main division protein FtsZ at mid-cell. How cells can sense the division state and trigger DNA replication initiation in these organisms is however unclear and is subject to different assumptions. As the Min system is absent in *S. pneumoniae*, alongside many other "conserved" mechanisms, it seems that it has developed its own specific systems. Identifying these systems and pathways can highlight new unknown proteins that could be used as potential target for drug development. Targeting the core cell cycle proteins can be relevant as these processes are often essential and might be conserved only in a subset of bacteria. Ideal targets would be proteins specific to *S. pneumoniae* and essentials for its growth.

Different methods can be used to identify new essential bacterial genes. The most common of all being Transposon Insertion Sequencing (Tn-Seq). Tn-Seq relies on the insertion of transposable elements everywhere in the genome, in order to create genes or operons disruptions. Quantification of these insertions by next-generation sequencing can inform us whether a gene is dispensable or essential. This method however tends to overestimate essential genes and the experimental validation of the data obtained can be tedious. Tn-Seq insertions in genes strictly essentials can also not be studied further, as the mutants will not be able to grow. Tn-Seq studies performed in *S. pneumoniae* suggest that nearly 350 genes are essential and many of them have unknown functions. In order to have a fast and reliable method to quickly analyze the depletions effect of all the genes predicted to be essential, we developed an inducible system based on

clustered regularly interspaced short palindromic repeats interference (CRISPRi). While transposon insertion disrupts the open reading frame of the gene, leading to either no transcription or aborted translation, CRISPRi relies on an inactive Cas9 targeting the promoter region of the gene of interest, therefore blocking transcription. In **Chapter 2**, we first silenced a set of known genes from essential pathways and further analyzed their growth, morphology and DNA content to create a depletion "phenotypic map". Next, we silenced all genes of unknown function from *S. pneumoniae* that were found essential in Tn-Seq studies and analyzed the depletion phenotypes to compare them to our phenotypic map. This method allowed us to annotate several genes that were ignored or mis-annotated by automatized bioinformatic approaches (*e.g.* MurT and GatD, both involved in peptidoglycan biosynthesis) but also to identify two novel proteins (TarP and TarQ) involved in teichoic acids biosynthesis. The use of CRISPRi also allowed us to study genes that were hard to work on because of their essentiality and demonstrated the involvement of the protease ClpX in competence development.

Among the unknown proteins that we classified as involved in DNA replication or chromosome segregation we also selected the protein CcrZ. In **Chapter 3**, we demonstrated that CcrZ is a novel DNA replication regulator that coordinates cell division with chromosome replication. In bacteria, the main DNA replication initiator DnaA is responsible for recruiting the DNA replication complex at the origin of replication but little is known about its regulation overtime. In *S. pneumoniae*, DnaA-mediated replication initiates at mid-cell and occurs at this location until termination. How cells can sense when to initiate a new round of replication once per cycle is not known. We showed that the putative phosphotransferase CcrZ interacts with the main cell division protein FtsZ to localize at the division site at mid-cell. CcrZ appears to be essential for DnaA-mediated DNA replication initiation as in its absence cells were under-replicating and formed abnormal septa. Altogether, coordination of cell division with DNA replication by CcrZ is an effective system to ensure that replication occurs only at mid-cell and that a new round of DNA replication starts when CcrZ localizes at the new division site. This indicated a strong correlation between cell division and DNA replication in *S. pneumoniae*.

In **Chapter 4**, we showed that lipid composition is crucial for cell morphology and survival of *S. pneumoniae*. It was previously shown that inactivation of the protein PapP strongly reduced pneumococcal pathogenesis. Upon deletion of *papP*, we observed morphological defects and aberrant localization of the cell division proteins FtsZ and FtsA. We determined that PapP is a DHH subfamily 1 phosphatase able to produce AMP from pAp (phosphoadenosine-5'-phosphate), an inhibitor of fatty

acid biosynthesis. In absence of PapP, pAp accumulates and leads to a decrease in fatty acid biosynthesis. This change in lipid composition was directly responsible for change in morphology, indicating a link between cell division and lipid composition of the membrane.

The work presented in this thesis opens the way to identification of new cell cycle regulation mechanisms that might appear to be conserved for a broad range of different bacteria. The data can be relevant for future research on new antibacterial compounds, but also to better understand the biology of other less-studied organisms.

6

Non-technical summary

Bacteria are essential for life on earth. These ~1µm (1/1000 millimeter) organisms contribute to all kind of crucial processes and studying their biology can help us understand better this massive microscopic world. Some pathogenic bacteria can cause infections, and it is therefore necessary to stop their growth in order to prevent their duplication and consequently prevent a stronger invasion. *Streptococcus pneumoniae* is a bacterium usually found in the throat of healthy people, but it can often become a pathogen and lead to serious infections such as pneumonia or meningitis. In case of such infections, antibiotics are usually used as they are very effective. They are often synthetic molecules that generally inactivate crucial essential proteins. However, more and more strains are becoming resistant to several antibiotics. To find new antibiotics targets, it is crucial to understand the biology of *S. pneumoniae*. This bacterium has a rugby-ball shape and it divides at the middle, at the cell "equator", by pinching the cell into two new cells. It is not yet fully known what is responsible for the division machinery to localize at mid-cell. It is also important to keep in mind that while the mother cell is slowly creating two daughter cells, the DNA (forming one chromosome) is also being duplicated at the middle of the cell and each new copy pulled into the two new cells (DNA replication). These processes of cell division and DNA replication are essential, meaning that if any protein of these mechanisms could be inactivated, *S. pneumoniae* would stop duplicating and growing. This type of protein would be an ideal antibacterial drug target.

A large-scale phenotyping to characterize unknown proteins

Proteins are the products of genes (DNA sequences) and their production can be blocked directly at the gene level. One way to identify essential proteins is to randomly inactivate each gene and see whether they are essential (*S. pneumoniae* has ~2.000 genes). The Tn-Seq method (transposon insertion sequencing) can be used to randomly insert one small DNA fragment per cell into all pneumococcal genes to inactivate them. After growing all the bacteria, only the cells with insertions in dispensable genes survive, the genes with no insertion are, by definition, essential. Using DNA sequencing, it is possible to determine which gene was inactivated and therefore identify which genes are essential. Using this technique around 350 genes were found to be essential in the pneumococcus. Validating their essentiality would however take a long time with traditional methods as each gene would need to be removed individually. Instead, we made use of the CRISPRi technique which can inactivate simply and quickly every gene (**Chapter 2**). We inactivated all the genes that we found essential and for which no function was known. We then looked at the growth of each mutant and assessed the cell shape using microscopy. The phenotypes that we obtained (rate of growth, cell shape, *etc*.) were classified

to form a "phenotypical map". When comparing the phenotypes of such mutants with the phenotypes from known genes, we were able to extract the function of some unknown proteins. For instance, we could find the two proteins (MurT and GatD) involved in biosynthesis of the cell wall (which is the main protective barrier of the cell), but also TarP and TarQ, involved in production of teichoic acids, which are essential compounds anchored in the cell wall.

One ring to synchronize the cell cycle

Using this screening, we also identified a protein with unknown function that seemed to be involved in DNA biology and named it CcrZ (**Chapter 3**). In normal situation, *S. pneumoniae* needs to ensure that one cell contains one chromosome. Thus, when it divides into two new cells, it needs to copy its DNA at the right time and only once. How a cell can sense that division will take place and that it needs to activate the duplication of its DNA is not known, as any kind of trigger was never described for other bacteria. For the first time, we described a protein that is directly linking cell division with DNA replication to coordinate duplication of the chromosome in time. We found that CcrZ localizes at the middle of the cell, at the division site. In its absence, we observe that DNA replication was drastically reduced. Thus, CcrZ can activate DNA replication initiation. This rather simple system ensures that when cells start to divide, chromosome replication starts and goes on until a new round of division.

Membrane composition crucial for cell morphology

When one cell divides, it produces more cell envelope at the division site to produce and "grow" two new cells. This cell envelope is composed of two layers: a cell wall on the outside and a lipid membrane underneath. Lipid membrane is a double layer of fatty acids that is not accessible for water. Without cell wall, a cell would lose its shape; without membrane, there would not be life as it is essential for energy production (and countless other properties). A tremendous amount of research was performed to understand how the cell wall composition influences the cell morphology. Therefore, it is crucial to understand what changes in lipids composition of the lipid membrane would do to the cell shape. In **Chapter 4**, we have characterized a protein (PapP) that is critical for proper lipid synthesis. We have shown that when this protein was absent cells were having morphological defects, and the dynamic of the division site was impacted. We concluded that changes in lipid composition could change the membrane fluidity and could result in defective cell division processes.

In this thesis, we have described several unknown proteins and their implications in the growth of the pneumococcus. The work presented can, in the future, help for development of antimicrobial compounds to fight pneumococcal infections.

Wetenschappelijke samenvatting

Het begrijpen hoe bacteriën groeien en delen is cruciaal om de veelvoudigheid van processen die deze organismen om ons heen reguleren te kunnen waarderen. Ook is het belangrijk en zelfs nodig om zo veel mogelijk informatie te verkrijgen over pathogene stammen om deze beter te kunnen bestrijden. *Streptococcus pneumoniae*, ook pneumokok genoemd, is een commensale bacterie die een serieuze pathogeen kan worden. De pneumokok is jaarlijks verantwoordelijk voor miljoenen doden doordat deze bacterie gemakkelijk ouderen en mensen met een verzwakt immuunsysteem kan infecteren. Omdat vaccinatie slechts deels effectief is en er veel antibioticaresistente pneumokokkenstammen zijn, is er een dringende behoefte aan nieuwe therapeutische doelwitten. *S. pneumoniae* is een grampositieve bacterie en is daarom verwant aan *Bacillus subtilis*. Toch zijn er fundamentele verschillen die laten zien dat ze niet zo nauw aan elkaar verwant zijn als vaak wordt aangenomen. Wat bekend is in andere organismen, is vaak voor de pneumokok nog een grijs gebied.

Belangrijke, onbeantwoorde vragen blijven hoe het geheel aan celdelingseiwitten de exacte mid-cellocatie in *S. pneumoniae* vindt, en hoe de celdeling synchroniseert met DNA-replicatie en chromosoomsegregatie. In andere, goed bestudeerde modelbacteriën (zoals *Escherichia coli* of *B. subtilis*) is het Min-systeem hoofdzakelijk verantwoordelijk voor het lokaliseren van het voornaamste celdelingseiwit FtsZ in het midden van de cel. Echter, hoe cellen de delingsstatus kunnen peilen en hoe dat leidt tot start van DNA-replicatie in deze organismen blijft tot nu toe onduidelijk en is het onderwerp van verschillende hypothesen. Aangezien zowel het Min-systeem als veel andere, geconserveerde mechanismen niet aanwezig zijn in *S. pneumoniae*, lijkt het erop dat er eigen ontwikkelde systemen zijn. Het identificeren van deze systemen en routes kan nieuwe, tot nu toe onbekende eiwitten aan het licht brengen die potentiële doelwitten kunnen zijn voor nieuwe medicijnen. Het zal zeker relevant zijn om de pijlen te richten op de basis, de kern van de celcycluseiwitten, omdat deze vaak betrokken zijn in essentiële processen en slechts in een deel van de bacteriën geconserveerd zijn. Ideale doelwitten zijn eiwitten die specifiek zijn voor *S. pneumoniae*, en essentieel voor de groei.

Verschillende methoden kunnen worden gebru ikt om nieuwe, essentiële bacteriële genen te identificeren. De meest gebruikte methode is Transposoninsertie-Sequencing (Tn-Seq). Deze methode werkt op basis van de insertie van transponeerbare elementen in het gehele genoom, om zo onderbrekingen te creëren in genen en operonen. De kwantificatie hiervan door middel van next-generation sequencing kan ons meer vertellen over of een gen overbodig is of juist essentieel. Deze methode leidt echter vaak tot een overschatting van essentiële genen en de experimentele validatie van de verkregen data kan langdurig zijn. Genen die

strikt noodzakelijk zijn, kunnen ook niet verder bestudeerd worden met Tn-Seq, omdat deze mutanten niet kunnen groeien. Tn-Seq studies die uitgevoerd zijn met *S. pneumoniae* suggereren dat ongeveer 350 genen essentieel zijn, waarvan velen een onbekende functie hebben. Om een betrouwbare methode te verkrijgen om genen die essentieel zijn bevonden vlug en gemakkelijk te analyseren, hebben we een induceerbaar systeem gemaakt dat gebaseerd is op CRISPR interference (CRISPRi). Terwijl transposoninsertie het open leesraam of het gen onderbreekt, resulterend in ofwel geen transcriptie ofwel afgebroken translatie, gaat CRISPRi uit van een inactieve vorm van Cas9, dat zich richt op de promotorregio van het beoogde gen en leidt tot geblokkeerde transcriptie. In **Hoofdstuk 2** hebben we een aantal bekende genen uitgeschakeld die betrokken zijn bij essentiële routes. Daarvan hebben we de groei, morfologie en het DNA verder geanalyseerd om zo een fenotype-depletiekaart te maken. Vervolgens hebben we ook alle genen die geen bekende functie in *S. pneumoniae* hebben, maar wel essentieel zijn volgens Tn-Seq studies, uitgeschakeld en de depletiefenotypes verder geanalyseerd en vergeleken met onze fenotypekaart. Deze aanpak maakte het voor ons niet alleen mogelijk om diverse genen te annoteren die eerder genegeerd waren of verkeerd geannoteerd werden door geautomatiseerde bioinformaticamethodes (bijvoorbeeld *murT* en *gatD*, beiden betrokken bij de biosynthese van peptidoglycaan) maar ook om twee nieuwe eiwitten te identificeren (TarP en TarQ) die beiden betrokken zijn bij de biosynthese van teichoïnezuren. Het gebruik van CRISPRi maakte het mogelijk om juist die genen waarvan de deletie lastig te bestuderen is te onderzoeken en demonstreerde de betrokkenheid van protease ClpX in de ontwikkeling van competentie.

Tussen de onbekende eiwitten die geclassificeerd zijn als betrokken bij DNA- / chromosoomreplicatie (ofwel waar CRISPRi-depletie leidde tot cellen zonder DNA en met vertraagde groei) hebben we ook het eiwit CcrZ gevonden. In **Hoofdstuk 3** demonstreren we dat CcrZ een nieuwe DNA-replicatieregulator is die de celdeling co-reguleert met de chromosoomreplicatie. In bacteriën is de belangrijkste initiator van DNA-replicatie DnaA verantwoordelijk voor het rekruteren van het DNA-replicatiecomplex op de specifieke startplek van de replicatie, de origin, maar er is weinig bekend over de verdere replicatie. In *S. pneumoniae* vindt DnaA-gemedieerde replicatie van begin tot beëindiging plaats in het midden van de cel. Hoe cellen bepalen om slechts één nieuwe replicatieronde per celdeling uit te voeren, is onbekend. We laten zien dat de voorspelde fosfotransferase CcrZ een interactie aan kan gaan met het belangrijke celdelingseiwit FtsZ, dat lokaliseert op de celdelingsplek, mid-cel. CcrZ blijkt essentieel te zijn voor DnaA-gemedieerde DNA-replicatie-initiatie, omdat de deletiecellen slecht repliceerden en er abnormale septa gevormd werden. Welbeschouwd is de coördinatie door CcrZ is een effectief systeem dat ervoor zorgt dat replicatie alleen op mid-cel plaatsvindt en dat een nieuwe ronde

van DNA-replicatie begint als CcrZ op de nieuwe delingsplek lokaliseert. Dit wijst op een sterke correlatie tussen de celdeling en de DNA-replicatie in *S. pneumoniae*.

In **Hoofdstuk 4** laten we zien dat de lipide-samenstelling cruciaal is voor de morfologie van de cel en het overleven van *S. pneumoniae*. Eerder was aangetoond dat de deactivatie van het eiwit PapP leidt tot sterke afname van de pathogeniteit van de pneumokok. Bij de deletie van *papP* zagen we morfologische defecten en afwijkende lokalisatie van de celdelingseiwitten FtsZ en FtsA. We stelden vast dat PapP een DHH-subfamilie-1-fosfatase is, die AMP maakt van pAp (fosfoadenosine-5'-fosfaat), een vetzuur-biosyntheseremmer. Deze verandering in lipide-samenstelling was direct verantwoordelijk voor de verandering in morfologie, wat duidt op een verband tussen de celdeling en de lipide-samenstelling van het membraan.

Het werk in dit proefschrift maakt de weg vrij voor de identificatie van nieuwe celcyclusregulatiemechanismen die wellicht geconserveerd blijken te zijn voor een breed scala aan bacteriën. De verkregen data kan ook relevant zijn voor toekomstig onderzoek naar nieuwe antibacteriële verbindingen en bijdragen aan het begrip van tot nu toe minder goed bestudeerde organismen.

6

Samenvatting voor de leek

Bacteriën zijn essentieel voor leven. Deze organismen zijn ongeveer 1µm (oftewel 1/1000ste van een millimeter) groot en dragen bij aan allerlei essentiële processen. Het bestuderen van de onderliggende biologie kan bijdragen aan een beter begrip van deze gigantische, maar microscopisch kleine wereld. Sommige bacteriën kunnen infecties veroorzaken. Daarom is het van belang om hun groei te stoppen en zo de vermeerdering en een erge invasie van de bacteriën in het lichaam te voorkomen. *Streptococcus pneumoniae* is een bacterie die normaal gesproken gevonden wordt in de keel van gezonde mensen, maar de bacterie kan een ziekmaker worden die leidt tot longontsteking of hersenvliesontsteking. Bij dit soort ontstekingen worden vaak antibiotica als effectieve middelen gebruikt. Deze over het algemeen synthetische moleculen inactiveren voornamelijk cruciale, essentiële eiwitten. Echter, meer en meer stammen worden resistent tegen verschillende antibiotica. Om nieuwe antibiotica te ontwikkelen is het cruciaal om de biologie van de pneumokok te begrijpen. Deze bacterie heeft de vorm van een rugbybal en deelt zich in het midden van de cel, de evenaar van de cel, door het samenknijpen van de cel tot twee nieuwe cellen. Hoe dit gebeurt, door middel van een speciaal "delingsmachientje" dat precies op de evenaar zit, snappen we eigenlijk nog niet zo goed. Daarnaast is het zo dat terwijl de moedercel langzaam twee dochtercellen maakt, ook het DNA (het chromosoom) zich rond de evenaar bevindt, en zich vermeerdert tot twee exemplaren voor de twee nieuwe dochtercellen. Dit proces wordt de replicatie genoemd. Deze celdelings- en replicatieprocessen zijn essentieel in de zin dat als één van deze twee mechanismen wordt geïnactiveerd, ook de pneumokok stopt met groeien. Een eiwit dat hierbij betrokken is, is daarom ook een ideale kandidaat voor een antibacterieel medicijn.

Op grote schaal fenotyperen voor het karakteriseren van onbekende eiwitten

Eiwitten zijn de producten van genen (bestaande DNA-sequenties) en de aanmaak ervan kan direct geblokkeerd worden op genniveau. Een manier om essentiële genen te vinden is willekeurig elk gen te inactiveren en te zien of ze al dat niet essentieel zijn (*S. pneumoniae* heeft ~2.000 genen). Deze methode heet Tn-Seq (wat staat voor transposoninsertiesequencing) en kan worden gebruikt om kleine stukjes DNA willekeurig in alle pneumokokgenen in verschillende cellen in te brengen, om op die manier de genen te inactiveren. Na het groeien van alle cellen met verstoorde genen, genaamd een 'bibliotheek', kunnen eigenlijk alleen de cellen overleven waarin slechts overbodige genen zijn geïnactiveerd. De genen die niet geïnactiveerd zijn, zijn dus essentieel. Door middel van deze techniek zijn er zo rond de 350 genen ontdekt die essentieel zijn voor pneumokokken.

Desalniettemin kost het valideren van de essentialiteit van deze genen met traditionele methoden, waarbij elk gen apart wordt verwijderd, veel tijd. Daarom

maken we gebruik van de CRISPRi techniek, die heel simpel en snel elk gen kan inactiveren (**Hoofdstuk 2**). We inactiveerden alle genen die essentieel bleken te zijn of waarvan de functie onbekend was. Daarbij keken we naar de groei en de vorm van elke mutant met behulp van de microscoop. Het fenotype, dus hoe ze er uit zien qua vorm en bijvoorbeeld hoe ze groeien, werd verder geclassificeerd om zo alles in beeld te krijgen in een specifieke "fenotypische kaart". Door het vergelijken van deze fenotypen van mutanten met fenotypen die al wel gelinkt zijn aan genen, waren we in staat om ook de functie van deze eerder onbekende genen te bepalen. Op deze manier vonden we dat twee eiwitten (MurT en GatD) betrokken waren bij het aanmaken van de celwand, een beschermende barrière van de cel. We vonden ook dat TarP en TarQ betrokken zijn bij de productie van teichoïnezuren, specifieke essentiële moleculen die verankerd zijn in de celwand.

Een ring die de celcyclus synchroniseert

Door middel van de screening uit **Hoofdstuk 2** hebben we ook een tot nu toe onbekend eiwit geïdentificeerd dat betrokken leek bij processen rondom het DNA. Dit eiwit hebben we CcrZ genoemd (Cell cyclus regulator Z) (**Hoofdstuk 3**). In een normale situatie moet *S. pneumoniae* er voor zorgen dat er slechts één chromosoom per cel is. Daarom moet de bacterie, als deze zich deelt tot twee nieuwe cellen, ook het DNA kopiëren op het goede moment en slechts één keer. Hoe een cel weet dat dit in gang gezet moet worden, wisten we nog niet, ook niet van andere bacteriën. We hebben nu dit coördinerende eiwit gevonden dat juist deze celdeling aan het kopiëren van DNA linkt. We vonden dat CcrZ ook lokaliseert op de evenaar van de cel, op de delingsplaats. In cellen zonder dit eiwit zagen we dat het kopiëren van DNA ernstig was verstoord. CcrZ kan dus kennelijk het startsein van deze DNA-replicatie activeren. Dit betrekkelijk simpele systeem zorgt er voor dat wanneer cellen beginnen met delen, de chromosoomreplicatie dan ook start tot een nieuwe ronde van celdeling.

De samenstelling van het membraan is cruciaal voor de vorm van de cel

Wanneer een cel deelt, produceert het meer celwand op de delingsplek voor het maken en "groeien" van twee nieuwe cellen. Er is een ongelofelijke hoeveelheid onderzoek gedaan om te begrijpen hoe de celwandsamenstelling de vorm van de cel beïnvloedt. Bovendien ligt er onder de celwand een lipidemembraan, een dubbele laag van vetzuren waar water onmogelijk doorheen kan. Zonder celwand verliest de cel zijn vorm en zonder membraan is er geen levende cel mogelijk, omdat dat nodig is voor de energieproductie (en voor nog vele andere eigenschappen). Daarom is het heel belangrijk om te begrijpen hoe veranderingen in de lipidesamenstelling de cel beïnvloedt. In **Hoofdstuk 4** hebben we een eiwit (PapP) gekarakteriseerd dat belangrijk is voor de aanmaak van die lipides. We hebben laten zien dat er zonder

dit eiwit vormdefecten waren en dat er een impact was op de celdelingsorganisatie. We concludeerden hieruit dat deze veranderingen van lipidesamenstelling ook de vloeibaarheid van het membraan veranderden en daarom defecten in het celdelingsproces veroorzaakten.

In dit proefschrift hebben we diverse onbekende en eerder onvolledig gekarakteriseerde eiwitten geïdentificeerd en bepaald hoe ze verwikkeld zijn in de groei en deling van de pneumokok. Dit werk kan in de toekomst bijdragen aan de ontwikkeling van antimicrobiële stoffen om zo een slag te leveren tegen pneumokokinfecties. Bovendien verbreedt dit ook onze kennis over essentiële processen in andere type bacteriën.

6

Résumé académique

Comprendre comment les bactéries se développent et se divisent est important pour évaluer la multitude de processus que ces organismes régulent autour de nous. Il est également nécessaire d'obtenir autant d'informations que possible sur les souches pathogènes, pour mieux les combattre. *Streptococcus pneumoniae* est une bactérie commensale qui peut devenir un pathogène grave. En effet, le pneumocoque est responsable de millions de décès chaque année car il peut facilement infecter les personnes agées, les personnes immunodéprimées ou en cas de surinfection. Étant donné que les moyens de vaccination ne sont que partiellement efficaces et que de nombreuses souches de pneumocoques sont résistantes à plusieurs antibiotiques, il y a donc un besoin urgent d'identifier de nouvelles cibles thérapeutiques. *S. pneumoniae* est une bactérie à Gram positif qui est fortement apparentée à *Bacillus subtilis*. Il présente cependant des différences fondamentales qui indiquent que ces deux organismes ne sont pas aussi liés que ce qui est généralement supposé. De nombreux mécanismes connus chez d'autres organismes se trouvent toujours dans une zone d'ombre pour le pneumocoque.

Parmi les questions les plus importantes restant à être élucidées, se trouvent celles de savoir comment le complexe de division cellulaire peut trouver son emplacement au milieu des cellules de *S. pneumoniae* et comment cet assemblage est synchronisé avec la réplication de l'ADN et la ségrégation des chromosomes. Chez d'autres bactéries modèles bien étudiées (par exemple *Escherichia coli* ou *B. subtilis*), le système Min est principalement responsable de la localisation de FtsZ, la protéine principale de division, au milieu des cellules. La manière dont les cellules peuvent détecter l'état de division et déclencher l'initiation de la réplication de l'ADN dans ces organismes, n'est cependant pas claire et est sujette à différentes hypothèses. Le système Min étant absent chez *S. pneumoniae*, tout comme de nombreux autres mécanismes « conservés » chez d'autres bactéries, il semble que le pneumocoque ait développé des systèmes qui lui sont spécifiques. L'identification de ces systèmes pourrait mettre en évidence de nouvelles protéines inconnues utilisables en tant que cibles thérapeutiques potentielles. Cibler des protéines du cycle cellulaire peut être pertinent, car ces processus sont souvent essentiels et sont parfois propres à chaque bactérie. Une cible idéale pourrait être une protéine spécifique de *S. pneumoniae* et qui, de plus, serait essentielle à sa croissance.

Différentes méthodes peuvent être utilisées pour identifier de nouveaux gènes essentiels bactériens. La méthode la plus commune est le séquençage d'insertion de transposons (Tn-Seq). Le Tn-Seq repose sur l'insertion d'éléments transposables partout dans le génome, afin de créer des perturbations de gènes / opérons. La quantification de ces insertions par séquençage peut nous indiquer si un gène

est négligeable ou essentiel. Cette méthode a cependant tendance à surestimer le nombre de gènes essentiels et la validation expérimentale des données obtenues peut être fastidieuse. Les insertions de Tn-Seq dans des gènes strictement essentiels ne peuvent pas être étudiées plus en détail, car les mutants ne pourraient pas se développer. Des études de Tn-Seq réalisées chez *S. pneumoniae* suggèrent que près de 350 gènes sont essentiels et que beaucoup d'entre eux ont des fonctions inconnues. Afin d'avoir une méthode rapide et fiable permettant d'analyser rapidement les effets de l'inactivation de chaque gène non essentiel, nous avons développé un système basé sur la modulation de l'expression des gènes (CRISPRi). Alors que l'insertion de transposons perturbe le cadre de lecture d'un gène, aboutissant à une interruption de la transcription ou alors de la traduction, CRISPRi s'appuie sur une Cas9 inactive ciblant la région promotrice du gène d'intérêt, bloquant ainsi complètement la transcription. Dans le **chapitre 2**, nous avons inactivé un ensemble de gènes essentiels connus, et analysé plus en détail leur croissance, leur morphologie et leur contenu en ADN pour créer une « carte phénotypique ». Ensuite, nous avons inactivé tous les gènes de fonction inconnue de *S. pneumoniae* qui avaient été annotés comme étant essentiels dans des études de Tn-Seq, et analysé leurs phénotypes pour les comparer à notre carte phénotypique. Cette méthode nous a permis d'annoter plusieurs gènes qui ont été ignorés ou mal annotés par des approches bio-informatiques automatisées (par exemple MurT et GatD, toutes deux impliquées dans la biosynthèse du peptidoglycane), mais aussi d'identifier deux nouvelles protéines (TarP et TarQ) impliquées dans la biosynthèse des acides téichoïques. L'utilisation de CRISPRi nous a également permis d'étudier des gènes difficiles à manipuler en raison de leur essentialité, nous permettant ainsi de démontrer l'implication de la protéase ClpX dans le développement de la compétence bactérienne.

Parmi les protéines inconnues que nous avons classées comme étant impliquées dans la réplication de l'ADN (leur inactivation entraînant des cellules sans ADN, associé à un retard de croissance), nous avons sélectionné la protéine CcrZ. Dans le **chapitre 3**, nous avons démontré que CcrZ est un nouveau régulateur de la réplication de l'ADN qui coordonne la division cellulaire avec la réplication chromosomique. Chez les bactéries, le principal initiateur de la réplication de l'ADN est DnaA. En effet, cette protéine est responsable du recrutement du complexe de réplication de l'ADN à l'origine de réplication. On ne sait cependant que peu de chose sur sa régulation au cours du cycle cellulaire. Chez *S. pneumoniae*, la réplication médiée par DnaA commence au milieu des cellules et continue à cet endroit jusqu'à la fin du doublement du chromosome. La façon dont les cellules peuvent sentir comment initier un nouveau cycle de réplication une seule fois par cycle cellulaire reste cependant inconnue. Nous avons montré que CcrZ peut interagir avec la protéine principale de division cellulaire FtsZ pour se localiser au site de division au milieu

des cellules. De plus, CcrZ semble être essentielle pour l'initiation de la réplication de l'ADN médiée par DnaA, car en son absence, les cellules étaient sous-réplicatives et formaient des cloisons anormales. Dans l'ensemble, la coordination par CcrZ est un système efficace pour garantir que la réplication se produit uniquement au milieu des cellules et qu'un nouveau cycle de réplication de l'ADN commence lorsque CcrZ est localisée au nouveau site de division. Cela indique une forte corrélation entre la division cellulaire et la réplication de l'ADN chez *S. pneumoniae*.

Dans le **chapitre 4**, nous avons montré que la composition lipidique est cruciale pour la morphologie cellulaire et la survie de *S. pneumoniae*. Il a été montré précédemment que l'inactivation de la protéine PapP réduisait fortement la pathogénicité du pneumocoque. En absence de *papP*, nous avons observé des défauts morphologiques et une localisation aberrante des protéines de division FtsZ et FtsA. Nous avons déterminé que PapP fait partie de la sous-famille phosphatase DHH 1, capable de produire de l'AMP à partir de pAp (phosphoadénosine-5'-phosphate), un inhibiteur de la biosynthèse des acides gras. En l'absence de PapP, le pAp s'accumule et entraîne une diminution de la biosynthèse des acides gras. Ce changement dans la composition lipidique étant directement responsable du changement de morphologie, indiquant un lien entre la division cellulaire et la composition lipidique de la membrane.

Les travaux présentés dans cette thèse ouvrent la voie à l'identification de nouveaux mécanismes de régulation du cycle cellulaire qui pourraient être transposés chez une grande partie des bactéries. Les données produites pourraient être cruciales pour orienter de futures recherches visant à mieux comprendre la biologie d'autres organismes moins étudiés.

6

Résumé non technique

Les bactéries sont essentielles à la vie sur terre. Ces organismes d'environ 1 µm de long (1/1000 millimètre) contribuent à toutes sortes de processus importants et leur étude peut nous aider à mieux comprendre ce monde microscopique qui nous entoure. Certaines bactéries pathogènes peuvent devenir infectieuses et il est donc nécessaire d'arrêter leur croissance afin d'éviter qu'elles ne se répliquent et par conséquent, d'empêcher une infection plus avancée. *Streptococcus pneumoniae* est une bactérie généralement présente dans la gorge des personnes en bonne santé, mais elle peut souvent devenir un agent pathogène et entraîner des infections graves telles que des pneumonies ou des méningites. Lors de telles infections, les antibiotiques sont principalement utilisés car ils sont très efficaces. Les antibiotiques sont souvent des molécules synthétiques, qui ont généralement pour effet d'inactiver des protéines essentielles nécessaires à la survie de la bactérie. Cependant, de plus en plus de souches bactériennes deviennent résistantes à de nombreux antibiotiques. Afin de trouver de nouvelles cibles pour les antibiotiques, il est crucial de comprendre la biologie de S. *pneumoniae*. Cette bactérie a une forme de ballon de rugby et se divise en son milieu, à « l'équateur » de la cellule, pour créer deux nouvelles cellules. On ne sait cependant pas encore exactement ce qui est responsable de la localisation de la machinerie de division au milieu de la cellule. Il est également important de garder à l'esprit que, lorsque que la cellule mère crée lentement deux cellules filles, l'ADN (formant un chromosome) est également dupliqué au milieu de la cellule. Chaque nouvelle copie du chromosome est ensuite tirée de part et d'autre dans les deux nouvelles cellules (formant la réplication de l'ADN). Ces processus de division cellulaire et de réplication de l'ADN sont essentiels, ce qui signifie que si une protéine à l'origine de l'un de ces mécanismes pouvait être inactivée, *S. pneumoniae* cesserait de se multiplier. Ce type de protéine s'avèrerait ainsi être une cible idéale pour le développement de nouveau médicaments.

Observer des défauts pour caractériser des protéines inconnues

Les protéines sont le produit de gènes (séquences d'ADN) et la production de ces protéines peut être bloquée directement au niveau du gène. Une façon d'identifier les protéines essentielles est d'inactiver aléatoirement chaque gène afin de de voir s'il est essentiel ou non (*S. pneumoniae* possède environ 2000 gènes). La méthode Tn-Seq (séquençage d'insertion de transposons) peut être utilisée pour insérer au hasard des petits fragments d'ADN dans tous les gènes du pneumocoque afin de les inactiver. Après avoir fait pousser chaque mutant (chaque cellule ayant un gène inactivé), seules les cellules avec des insertions dans des gènes négligeables (non-essentiels) survivent. Au contraire, les gènes sans insertion sont, par définition, essentiels. En séquençant l'ADN, il est possible de déterminer quels gènes ont été

inactivés, et donc d'identifier quels gènes sont essentiels. En utilisant cette technique, environ 350 gènes se sont révélés être essentiels chez le pneumocoque. La validation de leur essentialité prendrait cependant beaucoup de temps avec des méthodes traditionnelles, car chaque gène devrait être inactivé individuellement. À la place, nous avons utilisé la technique CRISPRi qui peut inactiver simplement et rapidement chaque gène (**chapitre 2**). Nous avons inactivé tous les gènes considérés comme étant essentiels dans la méthode Tn-seq et pour lesquels aucune fonction n'était connue. Nous avons ensuite examiné la croissance de chaque mutant et évalué la morphologie cellulaire à l'aide d'un microscope. Les phénotypes que nous avons obtenus (taux de croissance, forme cellulaire, *etc.*) ont été classés pour former une « carte phénotypique ». En comparant les phénotypes de ces mutants avec les phénotypes de gènes connus, nous avons pu extraire la fonction de certaines protéines inconnues. Par exemple, nous avons trouvé deux protéines (MurT et GatD) impliquées dans la fabrication de la paroi cellulaire (qui est la principale barrière de protection de la cellule), mais aussi TarP et TarQ, impliquées dans la production d'acides téichoïques, qui sont des composés essentiels, ancrés dans la paroi cellulaire.

Un anneau pour synchroniser le cycle cellulaire

En utilisant cette méthode, nous avons également identifié une protéine avec une fonction inconnue qui semblait impliquée dans la duplication de l'ADN, et l'avons nommée CcrZ (**Chapitre 3**). En temps normal, *S. pneumoniae* doit s'assurer que chaque cellule contient un seul chromosome. Ainsi, lorsque la bactérie se divise en deux nouvelles cellules, elle doit dupliquer son ADN au bon moment et une seule fois. On ne sait pas encore comment une cellule peut savoir que la division est sur le point d'avoir lieu et qu'elle doit dupliquer son ADN à cet instant précis, car aucun type d'activateur n'a été décrit chez d'autres bactéries. Pour la première fois, nous avons décrit ce type d'activateur : une protéine qui lie directement la division cellulaire à la réplication de l'ADN afin de coordonner la duplication du chromosome au cours du temps. Nous avons constaté que CcrZ est localisée au milieu de la cellule, au niveau du site de division. En son absence, nous avons observé que la réplication de l'ADN est considérablement réduite. Ainsi, CcrZ peut activer l'initiation de la réplication de l'ADN. Ce système assez simple garantit que lorsque les cellules commencent à se diviser, la réplication chromosomique commence et se poursuit jusqu'à un nouveau cycle de division (voir model Fig. 6e, Chapitre 3).

La composition de la membrane est cruciale pour la morphologie cellulaire

Lorsqu'une cellule se divise, elle produit davantage de paroi cellulaire sur le site de division pour créer et « faire pousser » deux nouvelles cellules. De nombreuses recherches ont été effectuées pour comprendre comment la composition de la paroi influence la morphologie cellulaire. Sous la paroi

cellulaire, se trouve la membrane lipidique. Sans paroi cellulaire, une cellule perdrait sa forme ; cependant sans membrane, il n'y aurait pas de vie car elle est essentielle pour la production d'énergie (et d'innombrables autres propriétés). Par conséquent, il est nécessaire de comprendre l'impact des changements dans la composition des lipides feraient à la cellule. Dans le **chapitre 4**, nous avons caractérisé une protéine (PapP) qui est importante pour la synthèse lipidique. Nous avons montré que lorsque cette protéine était absente, les cellules présentaient des défauts morphologiques et que la dynamique du site de division était impactée. Nous en avons conclu que des changements dans la composition lipidique pouvaient modifier la fluidité de la membrane et entraîner des processus de division cellulaire défectueux.

En conclusion, dans cette thèse, nous avons décrit l'identification de plusieurs protéines inconnues ou mal caractérisées et leurs implications. Les travaux présentés peuvent, à l'avenir, aider au développement de composés antimicrobiens pour lutter contre les infections à pneumocoques. En outre, cela élargit également nos connaissances sur les processus essentiels qui seraient intéressants à étudier chez d'autres types de bactéries.

6

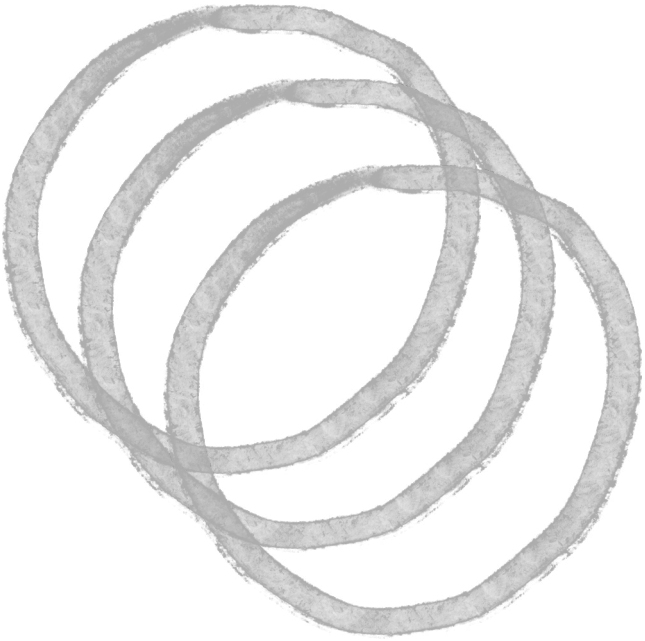

ACKNOWLEDGEMENTS

This part must be the most read chapter of every thesis ever produced. Even if some people would not be able to fully understand the different chapters or would not have the motivation to read through the entire book (I fully understand this), most of you will end up reading these lines. But why is that? In my opinion, it reflects a crucial aspect of a PhD thesis: people. Every working day as a PhD student can be roughly summarized as: holding a pipette and mixing liquids together. Although this seems to be simple repetitive gestures, it in facts helps us develop and sharpen our technical skills. Once every now and then, we can meet fellow scientists at conferences, lab meetings or any scientific events and discuss broad ideas which improves our overall knowledge. However, source for creativity and inspiration cannot be this easily described. These skills are improved within the PhD work environment and outside of it. These crucial abilities are also found in our surrounding environment, through art, hobbies, sport, *etc*. But most importantly, people. It doesn't really matter how hard a project can be, if someone next to you can give you a bit of ambition to pursue your objective. For this reason, there are many people that I would like to thank for contributing to this thesis.

A PhD training involves a lot of personal work and I was surprised how sometimes I could forget to stop for lunch, totally absorbed by what I was doing in the lab. After all, this is the way I see how a PhD should be: finding what you like through your work and getting a training out of it. However, the enthusiasm needs to start from somewhere, you cannot simply walk the door of a laboratory and start doing awesome stuff. There needs to be at first a push that motivates you to advance on your own. For this reason, I would like to thank **Jan-Willem** for doing an excellent job at giving so much enthusiasm. Even when a project is going well, you need to recharge the motivational batteries and every time I walked out of your office after short discussions, I was extremely motivated to continue the project. It is amazing to be able, every single time, to simply knock at your door with a question in mind and go out with a full new list of stuff to try. I will always remember our first meeting when you told me "I think you'll be OK, you have a good English", while I could barely order a pizza with my English. But for this reason, thanks for giving me the opportunity to do my PhD in your lab. I haven't seen any other lab like this one in term of people relationship and science. Moving an entire group to Lausanne was something that might appear quite tough, but you managed to still stay very available for all of us during this period and this resulted in a very smooth moving.

During my time in Groningen I was impressed to find the Molgen group very united and it offered a very ideal working environment. Thank you, **Oscar** and **Jan**, for being mainly responsible for this unity and thank you for the short discussions during the Monday meetings where your inputs were extremely valuable. I would like

to also thank the reading committee: **Prof. Tanneke den Blaauwen, Prof. Dirk-Jan Scheffers** and **Prof. Patrick Viollier** for evaluating this thesis and providing helpful comments.

Among the people that I met in Groningen, I want to address a special thank you to **Morten.** Beside always keeping me up-to-date about the French handball team beating the Norwegian team, you have always been present and very available for any specific and technical question. You taught me most of the techniques that I now use and I sincerely thank you for this. I will also always remember your support for my first half-marathon, where you brought us drinks all along the track and I believe that you ran more than we did on this occasion. **Robin**, I still feel sorry that we had to draw a red limit between my bench space and yours, and that sometimes my tip-boxes would go over it. I learned from it, and now try to keep my mess within its limit. More seriously, you showed me a lot about microscopy preparation, and I learned a lot about synthetic biology with you. I also had a really great time each time we went out together and your unique dance moves will always be remembered. **Katrin**, you also contributed a lot when I started, with teaching me a lot of different lab techniques and sharing what you had yourself learned before. Thank you also for picking me up on a tandem bike on my first day in Groningen. Although I couldn't reach the pedals, it was a fun ride! **Jelle**, I cannot remember how many times I walked in your office with a rather simple question and ended up discussing about it for half an hour. I learned a lot about how to think more broadly on a specific problem. I am also amazed by your scientific and general knowledge, and for this reason I would never have traded my spot in your team for pub-quizzes. Also thank you for organizing the game day at your place and for the cozy movie nights! **Rieza**, it was nice because we started our PhDs more or less at the same time and you could help me a lot with the PhD program related stuff. Important point, you were the first person to show me R and to explain me basic scripts, so I can only thank you for that. **Sebastiano**, thank you for your precious help on quite a hard project that I gave you. **Angel**, if you taught me something about Spanish people: they know how to eat. Thank you for all the excellent moments that we had, for sharing your literature with me, for the countless movie nights at your place, for being part of the best PV that Molgen has had, and most importantly for accepting to protect me with your badass sword as my paranymph.

I would also like to thank the people that I met in Groningen and who moved to Lausanne. **Renske**, you started your PhD one week earlier than I did and for this reason I always saw you as a kind of PhD sister. I cannot remember how many times I needed your support in and outside of the lab and you were always present for helping. Anytime I had to complain about something or just be happy about little things I knew I could always go to you and discuss about it, which was great. You also

integrated me in your music band and that was awesome for my creativity during my time in Groningen and I had a lot of fun. You also showed us around the most beautiful island of the Netherlands, I still cannot imagine the amount of sheep that I saw there. Thank you also for accepting the high responsibility that is to be my paranymph. I am pretty sure that **Doran**, you are secretly training her for sword fighting, so thank you for this. And also thank you for all the extensive discussions during which I learned a lot about microchip implants. **Arnau**, you speak your mind, and this is great because if something needs to be optimized in the lab, you will be one of the first ones to mention it. You were also the ideal roommate during almost a year in Groningen, thank you again to both you and **Marianna** for amazing diners. **Lance**, the lord of the rings. Thank you for reminding me every day which is the greatest country on the planet. You helped the entire lab a lot during the moving to Lausanne and you also helped me a lot with my moving! I really had a lot of fun every time we had a drink together but also in the lab for the most random discussions that one can imagine. Thank you also for your taste in music, this was great. **Xue**, I have no idea where you get your energy from. I always had the feeling you were working for three in the lab. You have a lot of scientific knowledge and always contribute to lab discussions, which is very valuable as you give precious input. You often amazed me because you dare a lot of things outside of the lab. Always the first one to say "I will try" to new adventurous things, food, sport, *etc*. and always offering your help. I stole by mistake your pink socks during Chinese hot-pot party in Groningen, and every time I see them it reminds me of that amazing evening. We will see if you get them back. **Stefano**, I learned a lot of Italian words by sitting in front of you in the office when you were unhappy with your computer. Thank you very much for all the help with our common project, you really did a lot. Also, without you, my nights would be quite uncomfortable, so thank you for delivering my bed. **Dimi**, I must admit that the lab feels maybe too quiet when you are not around. Thank you for often organizing brunches, apéros, *etc*. And thank you for our special tsipouro moments in Groningen.

Then there are the people that I met in Lausanne, and who constitute the Veening Lab 2.0 as I know it. First, **Jun**, thank you for setting up the lab so that we could all work when we arrived! You always helped a lot in the lab, never complaining when preparing buffers, media, *etc*. Even when it was not your turn. Of all the people in Lausanne, you were the only one joining every party, every barbecue, every apéro and I really enjoyed discussing with you. We also had the immense honor that you organized a tea ceremony and I will always remember it. So, thank you and **Nao** for this. **Paddy**, you were also among the first people here. I remember our first encounter on the campus months before you started and I was impressed by your energy, and you continue giving a positive energy to the lab, organizing plenty of things around. Thank you also for your exceptional music taste that really put me

in the right working mood in the lab. **Afonso**, before all, thank you for organizing this 18h-long Harry Potter marathon, and thank you for The Room. You are super involved in organizing activities for the group and with you I too often burst out laughing so much that I can't even drink my coffee. **Vincent**, if I need help with my analysis, whatever you are doing, you are always prioritizing it and trying to explain me what steps I should follow, thanks a lot for that. Also, when sometimes I get the feeling that the world around me gets a bit crazy and I need an honest opinion about certain topics I often go to you since you won't hesitate to say out-loud what many people think but don't dare to express. Thank you for that and thank you to **Bárbara** for amazing pastel de nata. **Monica**, without your help in the lab things would take so much longer. Thank you for keeping everything running smoothly and for the coffee breaks (even without coffee) where we can discuss a lot and empty my brain in a few minutes. **Julien**, you were my second Master student and I was "a bit" proud that you managed to stay for a PhD. You are always helpful and dedicated with anything that you start. You also taught me how to properly park a truck, I will always be grateful for that. **Liselot**, there is-e-lot of things to thank you for, the awesome adventures in South Africa, the crash course on how-to-rock-a-presentation, but most importantly, you have changed a whole generation with showing us how to save lunch food for the evening with your LiseBox. **Anne-Stephanie**, thank you for your help in the lab in Groningen and in Lausanne, I have the feeling that everything is much more organized and well labeled when you are around. Coincidence? **Jessica**, thank you for proofreading my French summaries, I was a bit rusty after these years. **Nienke**, thank you for your help with Dutch translation of the summaries.

During my project I also needed to learn some new techniques in Boston College, and I thank you **Tim van Opijnen** for helping me out. I would like to also thank **Christophe Grangeasse**, as you were the one that pointed me out Jan-Willem's lab at the first place.

The support for this thesis also comes from outside of the lab and for this I have to thank a few people. **Guillaume** and **Caroline**, merci pour m'avoir à rendu visite à Groningen et à Lausanne et pour votre support inconditionnel et pour m'avoir aidé avec la correction des résumés en Français. Ca mérite une chouille avec 3 Kg de son. **Živa** and **Jihed**, thank you for hosting me countless times in Amsterdam. **Alexis**, thank you for helping me with moving to the Netherlands and for always being open to discuss about my scientific crazy ideas. A big thank you to **Matheus** for designing the cover of this thesis and for giving me a lot of creative input during my time in Lausanne and thank you to **Natalia** for supporting his creativity (and mine) with awesome desserts.

Nina, hvala, da me vedno podpiraš in mi stojiš ob strani. During our time in Groningen you really helped me improve my canals swimming technique but also you motivated me to climb the tallest freestanding climbing wall in the world. Let's say I was not afraid. You also supported me all the way from Groningen to Lausanne, and I was extremely happy when you managed to stay here with me. Thank you for always being attentive when I talk about my days or about my project when I get a little confused. Exploring the Swiss mountains with you is also an undeniable source of inspiration, but also a lot of motivation for when I am back in the lab. **Tinko**, thank you for creating an ideal writing environment. Un grand merci à ma famille : **Maman, Jacques, Capucine, Béranger, Anne, Chantal, Isa, Papy, Tom, Marie** et **Eliott** pour votre support toutes ces années et pour votre aide avec les déménagements, pour m'avoir rendu visite plusieurs fois même si j'étais très loin et pour m'avoir donné un nombre incalculable de pots de confitures. Thank you to **Mojca, Fric** and **Urška** for your support and for always wondering how things are going with the science and in the lab.

There are many more people that I could thank, including all the successive students who were in the Veening Lab in the past years. During this PhD, I had very great working environments at the Molgen department in Groningen and at the DMF in Lausanne and I thank you all for helpeding me out during this 6-year journey and to make it memorable.

Acknowledgements

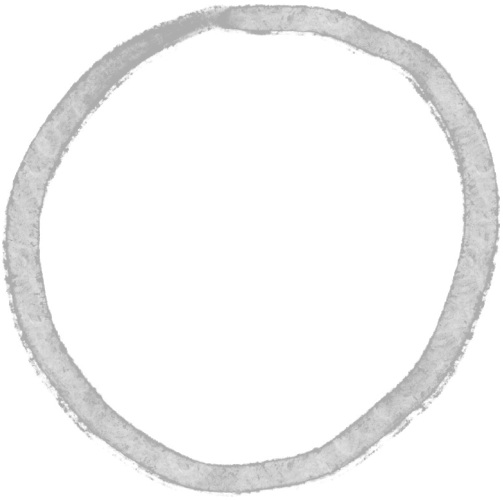

PUBLICATIONS OVERVIEW

1. Bojer, M.S., Wacnik, K., Kjelgaard, P., **Gallay, C.**, Bottomley, A.L., Cohn, M.T., Lindahl, G., Frees, D., Veening, J., Foster, S.J., et al. (2019). SosA inhibits cell division in *Staphylococcus aureus* in response to DNA damage. *Mol. Microbiol*. mmi.14350.

2. **Gallay, C.***, Sanselicio, S.*, Anderson, M.E., Soh, Y.M., Liu, X., Stamsås, G.A., Pelliciari, S., Raaphorst, R. van, Kjos, M., Murray, H., et al. (2019). Spatio-temporal control of DNA replication by the pneumococcal cell cycle regulator CcrZ. *BioRxiv* 775536.

3. Jensen, C., Bæk, K.T., **Gallay, C.**, Thalsø-Madsen, I., Xu, L., Jousselin, A., Ruiz Torrubia, F., Paulander, W., Pereira, A.R., Veening, J.-W., et al. (2019). The ClpX chaperone controls autolytic splitting of *Staphylococcus aureus* daughter cells, but is bypassed by β-lactam antibiotics or inhibitors of WTA biosynthesis. *PLOS Pathog*. 15, e1008044.

4. Kuipers, K.*, **Gallay, C**.*, Martínek, V., Rohde, M., Martínková, M., van der Beek, S.L., Jong, W.S.P., Venselaar, H., Zomer, A., Bootsma, H., et al. (2016). Highly conserved nucleotide phosphatase essential for membrane lipid homeostasis in *Streptococcus pneumoniae*. *Mol. Microbiol*. 101.

5. Liu, X., **Gallay, C.**, Kjos, M., Domenech, A., Slager, J., van Kessel, S.P., Knoops, K., Sorg, R.A., Zhang, J.-R., and Veening, J.-W. (2017). High-throughput CRISPRi phenotyping identifies new essential genes in*Streptococcus pneumoniae*. *Mol. Syst. Biol*. 13, 931.

6. Sorg, R.A., **Gallay, C**., and Veening, J.-W. (2019). Synthetic gene regulatory networks in the opportunistic human pathogen *Streptococcus pneumoniae*. *BioRxiv* 834689.

*shared first authorship